Selection effects in optical quasar surveys.

by

Crispin Julian Keable.

Doctor of Philosophy

University of Edinburgh

1987

This thesis has been composed by
myself, and consists entirely of
my own work except where indicated
otherwise in the text.

Acknowledgments.

There are many people without whom this thesis would not have been completed, and for whom I am very grateful. In particular, Cathy Smyth and Becky Jordan who both defused great discouragement at different times.

Lance Miller who kept me on the track particularly during the latter part of the work.

The SERC, and the worshipful company of Grocers, for their financial assistance.

The staff of the UK Schmidt telescope unit, whose excellent plate material and facilities are greatly appreciated. Also the staff of the COSMOS unit, in particular Harvey MacGillivray for all the data.

I also thank Sandro D'Odorico, and ESO, who provided useful data.

Other people who helped a great deal with useful discussions, ideas, and computer programs and whom I would like to thank are Stephen Beard, Russell Cannon, Roger Clowes, Clive Davenhall, David Emerson, Paul Mitchell, Malcolm Smith, and Sue Tritton.

Contents.

Chapter	0	Abstract.	1
Chapter	1	A review of quasar surveys.	2
	1.1	Why should one look for quasars?	2
	1.2	Survey methods.	4
	1.2.1	Completeness and Contamination.	5
	1.2.2	Radio and other non-optical survey techniques.	8
	1.2.3	Optical survey methods: photometric.	11
	1.2.4	Optical survey methods: spectroscopic.	13
	1.2.5	Optical survey methods: variability.	16
	1.3	Selection effects.	17
	1.3.1	Redshift effects.	18
	1.3.2	Line characteristic effects.	23
	1.3.3	Limiting magnitude effects.	24
	1.4	Conclusions.	27
Chapter	2	Quasar surveys in field 927.	29
	2.1	He eyeball survey.	33
	2.2	Automatic Quasar Detection prism survey.	35
	2.3	Other surveys in the field.	39
	2.4	Existing spectroscopy in field 927.	41
Chapter	3	New surveys: the AQD grens survey.	46
	3.1	Spectrum location: rationale.	47
	3.2	Spectrum location: procedure.	49
	3.3	AQD measurements and results.	53
	3.4	Reducing ESO spectroscopy: general.	54
	3.4.1	Spectral reduction.	56
	3.5	Results of ESO spectroscopy.	59

Contents (continued).

	3.6	Selection effects and completeness.	63
	3.7	Contaminants in the grens survey.	63
	3.8	Conclusions.	66
Chapter	4	New surveys: the UK Schmidt photometric survey.	69
	4.1	Schmidt direct plate material for the survey.	70
	4.2	COSMOS measurements of the plates.	73
	4.3	Threshold mapping and the generation of COSMOS parameters.	75
	4.4	Assessment of the COSMOS hardware upgrade.	76
	4.5	Plate calibration.	78
	4.5.1	Sources.	79
	4.5.2	Data reduction.	81
	4.5.2a	ESO CCD frames.	81
	4.5.2b	AAT service data.	84
	4.5.2c	INT CCD frames.	86
	4.6	Photometric errors.	89
	4.6.1	The intrinsic width of the stellar main sequence.	91
	4.7	Plate reductions.	93
	4.7.1	Pairing in the same colour.	93
	4.7.2	Calibrating the Schmidt datasets.	97
	4.7.3	Pairing datasets across colour.	100
	4.7.4	Star/galaxy seperation.	100
	4.7.5	Deblending.	103
	4.8	Results.	104
	4.8.1	The ultraviolet excess survey.	105
	4.8.2	The multi-colour survey.	109
	4.9	Conclusions.	115

Contents (continued).

Chapter 5		Relationships between surveys in the field.	117
	5.1	Comments on the He prism survey.	118
	5.1.1	Completeness	119
	5.2	Comments on the AQD prism survey.	122
	5.2.1	The larger AQD sample.	123
	5.2.2	The good AQD sample.	133
	5.3	A grens / photometric survey comparison.	136
	5.4	Multi-colour candidates.	138
Chapter 6		Conclusions.	142
	6.1	Construction of the final survey.	148
	6.2	Examination of the final survey.	150
	6.3	Future work.	152
	6.4	Evolution of quasars	155
		Appendix.	
		References.	

0. Abstract.

An investigation into the selection effects of optical quasar surveys is described. This is accomplished via the accumlation and comparison of optical quasar surveys of different types, which are then used to generate a survey free from selection effects.

A visual search and an automatic computerised search for quasars using U.K. Schmidt plates were already available in a single high galactic latitude field of 23 degrees^2.

An automatic search of a deep C.F.H.T. grens plate over 1 degree^2 in the centre of the field was undertaken. Slit spectroscopic observations were made of 26 candidates from this survey. These data allow conclusions to be drawn regarding the grens as a survey instrument.

An automatic photometric survey was also undertaken, using direct plates in the five wavebands U, J, V, R, and I from the U.K. Schmidt telescope. CCD frames were obtained in each of the wavebands from various sources, to allow calibration of data from the Schmidt plates. This has allowed the construction of a conventional ultraviolet excess sample, as well as a less conventional colour space density search generated sample.

Locating the various low dispersion spectroscopic survey candidates amongst the photometric survey data has brought to light various aspects of these surveys: in particular, the eye discovers a smaller surface density of candidates at most magnitudes. Secondly, the automatic prism plate search has significant progressive object losses brighter than the plate limit, which are subject to complex selection effects. Large numbers of galactic stars are mistaken for quasars because of peculiarities in their spectra seen at low dispersion. Also prism dispersion variations force a survey limit brighter than the plate limit. Colour synthesis from the prism plate works well at brighter magnitudes, unless spectra are saturated. The method is also subject to limitations due to poor spectrum signal to noise at fainter magnitudes.

Spectroscopy indicates that the automatic grens survey is complete, except for overlapped spectra. This is in part due to the linear dispersion of the transmission grating. The present survey is however subject to considerable contamination:- the reasons for this are examined and discussed. Conclusions drawn from examination of the grens sample colours are limited because the grens survey goes to a much fainter magnitude, over a limited area.

The photometric survey readily identifies objects which have peculiar colours, but a detailed examination of the properties of these objects must await further work.

Finally, a synthetic survey has been constructed, using all of the information available for each object. Redshift estimates were possible for about 30% of the 130 candidates - the higher redshift objects. Examination of the survey indicates that it is largely free from selection effects below a redshift of $z = 3.4$.

1. A review of quasar surveys.

1.1 Why should we look for quasars?

Recently, Hewitt and Burbidge (1986) have published a list of all known (to them) quasars - a total of 3574 objects. Why, then, has so much effort gone in to finding these objects over the last 23 years, and why should one search for new objects? The answers to both of these questions are quite involved, but I will try to give some sort of an answer to the first in this section, and to the second in the remainder of this chapter. Necessarily, the answers given mainly concern aspects relevant to the work undertaken in this thesis - a more comprehensive answer can be found in Weedman, 1986.

One of the first areas to excite interest, shortly after quasars' discovery, was that they were at such large redshifts, implying such high luminosities under the cosmological interpretation of redshifts, and were so unlike galaxies hitherto known, that many people questioned whether quasar redshifts really do have a cosmological interpretation. Despite the investment of large amounts of effort and resources (the Hewitt and Burbidge catalogue is testimony to this, as is the plethora of published material on the subject), this is about the only question which has received a definitive answer, and this only in the last few years (even now, remaining adherents of the noncosmological view press their views vigorously).

Briefly, Hutchings *et al.* (1984) and Gehren *et al.* (1984) have found galaxies at the same redshifts as many low redshift quasars,

Hutchings and Campbell (1983) have found tidal interactions between low redshift quasars and neighbouring galaxies, and Boroson, Oke and Green (1982) and Heckman *et al.* (1984) have found stellar absorption lines in galaxies associated with quasars, at the same redshift.

Ultimately, the study of quasars should provide better cosmological probes than have hitherto been available, but this cannot happen until such time as we understand the way in which quasars' luminosities evolve. Thus quasar evolution is one of the most fundamental questions in astronomy today, not just because of what we stand to learn about the quasars themselves, but because of what we might hope to gain from their use as tools for observational cosmology.

There is still a pressing requirement, then, for survey work to be done, because previous surveys have never managed to achieve a full coverage of the luminosity-redshift plane, and have been subject to various different selection effects. Analyses have therefore had to rely on results from surveys from different workers. For example Marshall, 1985, based his analysis on the surveys of Schmidt and Green, (1983) and his own spectroscopy of the Formiggini *et al.* (1980) survey. Although both are ultraviolet excess surveys, there are colour dependent transformations between the photometric systems used. The different interpretations allowed by the unpredictable effects of using surveys with different selection effects has generated a wide range of possible models for the evolution of the quasar luminosity function (eg. see Schmidt 1986 compared to Marshall, 1985, and Boyle *et al.* 1986).

Quasar clustering is also a subject from which many important questions may be answered. As with evolution, to reap the rewards one must first answer some thorny problems concerning quasar creation and the immunity of the survey from selection effects.

There are many other aspects of quasars which are interesting, of course, the investigation of which can be helped by new quasar surveys. Generally speaking the boundary conditions of the survey are less tight, because all that is required of the survey is that examples of objects are found in the relevant class. Quasars are used as probes, for example, in investigations of gravitational lensing (eg. Peacock, 1983) and in investigations of intergalactic absorption line clouds (eg. Sargent *et al.* 1980).

1.2 Survey Methods.

Active Galactic Nuclei (AGN) have been detected at all wavelengths where they have been looked for in the electromagnetic spectrum. The first, 3C273, was discovered by its radio emission by Schmidt (1963) (although one previously catalogued object, Ton 202, later turned out to be a quasar. It was located in a survey of blue stars by Iriarte & Charira (1957). A spectrum was obtained for this object in 1960 by Greenstein (Greenstein & Oke, 1970) but he misclassified it at that time as an old nova). However, it very soon became clear that many AGN are not bright at all wavelengths: indeed, ≈ 95% of quasars are undetected in radio surveys. In this section, I give a brief review of different survey techniques.

1.2.1 Completeness and Contamination.

Two of the most fundamental properties that any survey for AGN (or any other class of celestial objects) can have are those of completeness and contamination, so it is worth discussing them briefly here.

A survey can be said to be complete if, within some boundaries of angular extent and flux density, all of the objects in that class have been found. Three things are pertinent here:

a) it is valuable to retain this very simple definition of completeness, as it makes subsequent evaluation of the data and comparison with other surveys simple. Some authors have been tempted to include other bounds to their surveys (and so to their estimate of completeness), such as redshift, or equivalent width of the broad emission lines. These are really limitations of the survey technique, not of nature, and they should therefore be discussed separately as selection effects. The collected effect of all selection effects (and other non-detections due to sources of random noise within the survey) are then incorporated into the level of completeness.

b) One must be very sure that one has a clear understanding of the spectral and other properties of the class of object that one is looking for. Otherwise, there is always the possibility that there may be a large number of objects clumped just outside the selection criteria of the survey. This in practice is surprisingly difficult: if one understood all of the properties of the class one was looking for, what would be the point of looking for it? However it is encouraging to notice that there are no brand new types of quasars being discovered by other survey techniques such as variability, X-ray's or

radio. A proviso to this statement should be made, however. Recently, quasars have been discovered in the IRAS point sources catalogue (Neugebaur *et al.*, 1986) some of which have no previous optical identifications (Beichman *et al.*, 1986). Beichman *et al.* suggest that faint optical flux densities observed are due to obscuration by dust in the quasars' host galaxy, causing several magnitudes of optical extinction. Also, there are a few optically empty fields for IRAS point source identifications. It is unlikely that these will ever be a source of large numbers of new types of object, though, because one would expect to see some of them in the radio.

c) In practice, the flux density limit of the survey is often very hard to define accurately, and yet it is crucial to many of the questions that one would like to answer with a quasar survey. For example, one of the most interesting and vital questions a survey can address is that of evolution: Wampler and Ponz (1985) show how vital the survey limit is. I return to this subject in section 1.3 on selection effects, but briefly the things which make a survey limit hard to define are photometric errors - especially because it is unusual to have absolute spectrophotometry for a survey, and the inclusion of a broad emission line in a broad band magnitude can brighten that object into the survey. In addition, quasars are intrinsically variable (Hawkins, 1986), and as there is generally some time between when a candidate list is prepared and the survey is verified, some objects are likely to have varied enough to include or exclude them from the survey. These biases tend to operate in one direction, because of the rapidly increasing number of objects seen at increasing magnitudes, and because objects tend to be selected when they are at their brightest, if they are variable. Seeing also has a critical effect on the survey limit for slitless spectroscopy surveys - Osmer (1980) shows how easy

it is to be misled by plates of differing quality.

Finally, without spectrophotometry it is impossible to identify the effect that differing continuum slopes and redshifts have. A monochromatic limit must therefore refer to the rest frame spectrum of the quasar.

The other property of surveys mentioned here is that of contamination. Contamination is simply the accidental inclusion of classes of celestial objects other than those that the surveyor is looking for. This is typically caused by the survey method not discriminating precisely enough for the spectral properties of quasars. For example, emission line surveys locate all objects which have emission lines greater than some equivalent width. This can include emission line stars, and unwanted extragalactic objects such as extragalactic H II regions, LINER galaxies and Seyfert II nuclei as well as photographic junk such as emulsion blemishes and overlapped spectra. Another example are the ultraviolet excess surveys, which typically aim to locate objects with $U - B < -0.4$, and as a result cannot discriminate against white dwarfs, and some subdwarfs. The relative proportions of which classes are found depends on the magnitude limits of the survey - discussed by Green, Schmidt and Liebert (1986).

The other contributing factor to contamination is measurement error, which can accidentally modify the selection parameters of an object enough to cause it to be included in the sample.

The crucial difference between contamination and completeness is that

contamination can be eliminated from a sample by follow up spectroscopic work (which normally must be done anyway, to find the quasars' redshifts). So although it is very annoying, in that it is a waste of large telescope time to obtain spectra that are unwanted for the survey, it doesn't actually diminish the statistical validity of the survey. Completeness, on the other hand, refers to objects not included in the survey which should have been. This is more serious because the objects lost from a survey can only be subsequently recovered by doing a new survey. It is to this end that this work attempts to address the problem of completeness from optical surveys by using many survey techniques on the same survey area. Comparisons of different survey techniques in different parts of the sky are difficult, since it is not possible to deconvolve number density differences from the selection effects. In addition, there are large differences in the numbers of contaminating galactic stars which make comparisons of the same survey method in different areas difficult.

1.2.2 Radio and other non-optical surveys.

There are some very attractive features to the location of AGN at radio or other non-optical wavelengths, but also some insurmountable flaws. On the one hand, most galactic objects do not radiate at these frequencies, so it is comparatively easy to construct complete surveys at radio or other non-optical wavelengths. On the other hand, at most only ≃ 10% of optical quasars are detected as radio sources. Crucial here is the assumption that one makes about the radio objects: either one assumes that they form part of a continuous spectrum of objects

- in which case surveys of radio selected quasars could be used to derive luminosity functions applicable to all quasars, or else radio loud and radio quiet quasars are two distinct, though related, phenomena.

Many workers have followed Schmidt (1970), who introduced the radio to optical spectral index. On the basis of survey data then available, Schmidt suggested that this parameter is independent of optical luminosity or redshift. The implication is that there is a continuous distribution of quasar radio properties. Recent work, however, on the basis of newer survey data, suggests that this is not the case. Peacock, Miller and Longair (1986) were able to use a new optically selected sample (that of Schmidt and Green, 1983), from which they conclude that there are two classes of quasars - a radio loud class, which are the nuclei embedded in elliptical host galaxies (ie. the high redshift counterpart of giant radio galaxies), and a more numerous radio quiet class embedded in spiral host galaxies (the high redshift counterparts of Seyfert I galaxies).

Other evidence for this point of view has come recently from Fried (1986), who reviews high resolution imaging and spectroscopic surveys of low redshift quasars. He comes to the same conclusion as Peacock, Miller and Longair. For example, Hutchings, Crampton and Campbell (1984) found that there was evidence of spiral structure in 67% of optically selected quasars in their survey. Malkan (1984) concludes that radio selected quasars are generally located in ellipticals, also on the basis of an imaging survey.

It is unlikely that the problem divides as neatly as this in reality,

and indeed there is evidence already that a more complex picture will eventually have to be used. Stockton and MacKenty (1986), in an imaging survey of low redshift ($z < 0.5$) quasars, have found that $\simeq$ 25% have nebulosity caused by narrow band line emission, rather than a stellar continuum (suggestive of something other than a normal host galaxy). At lower redshifts, Heckman *et al.* (1986) have shown that giant radio galaxies are unlikely to be of a single type. They find that $\geqslant$ 25% of their objects show morphological peculiarities in the optical, while the rest are embedded in normal giant elliptical or cD galaxies. Be that as it may, it seems that the evidence is growing stronger for quasars actually to be divided into two classes in nature, as well as in our surveys.

It is also unlikely that new very deep radio surveys will reveal large numbers of quasars as sources. This is because the present generation of deep surveys (which go as faint as a few tens of μJy - Condon, 1984 and Windhorst *et al.* 1985) reveal large populations of faint, nearby star forming regions which become a basic source of confusion in using radio source counts to study quasar number counts, as well as many normal or near normal galaxies.

The detection rate for quasars in other parts of the spectrum is also very low compared to optical detections. The Einstein Satellite was used during its lifetime to survey about 100 square degrees, to a sensitivity of about $\simeq 10^{-13}$ ergs cm^{-2} s^{-1} at 2 KeV. This has yielded counts of $\simeq$ 1 quasar/square degree (Gioia *et al.* 1984, and Margon, Downes and Chanan, 1985). One important result from these surveys for the optical surveyor is that optical identifications show that no new types of optical quasars are found.

As with the radio selected quasars, detection of quasars in the X-ray region is interesting in its own right: they help to define the huge scope of the model that must be invoked to explain the quasar phenomenon. But because they are a special class they cannot be used to answer questions pertaining to all quasars, such as evolution, unless one is very sure indeed that one understands the relationship between the sub-class and the (optically selected) whole.

As far as the optical surveyor is concerned, then, one of the most important results to come from surveys at other wavebands is a negative one: no new types of optical quasars have been discovered which have different spectral properties to the ones already known. It therefore seems unlikely that there is a distinct class of 'obstinate' optical quasars, that all (for example) lie inside the stellar locus of colour-colour diagrams, and have redshifts which make their emission lines undetectable to slitless spectroscopy. This observation does not rule out the occasional obstinate object, of course! Nor does it rule out the possibility that surveys at other wavebands will preferentially select quasars from one or more optical sub-class.

1.2.3 Optical survey methods: photometric.

Very shortly after the discovery of quasars it was realised (mainly by Sandage, 1965, Sandage and Veron, 1965, and Sandage and Luyten, 1967) that quasars could be detected on the basis of their broad band colours. The spectral characteristics of most quasars are so different from most galactic stars that they are easy to identify. Many surveys have been published on this basis (Smith, 1984, gives a list). Most of

them make use of the property that lower redshift quasars are very blue in the U - B colour compared to most stars - which gives rise to the ultraviolet excess, or UVX, surveys. This is a very effective technique, since fairly small numbers of plates need to be scanned to produce the sample (an important consideration when most plate scanning was done by eye), and it is very unambiguous - the only problems one has are close to the survey limits, where photometric errors scatter objects which should be too faint into the survey more frequently than scattering objects which should be in the survey, out (because the number-flux density relation is steep).

However, this method has two major drawbacks: firstly, at redshifts higher than $z \simeq 2.2$, the Lyman-α emission line enters the B bandpass. There is also normally what is effectively a continuum drop from the red to the blue side of this line due to the Lyman-α 'forest' of absorption lines. These effects combine to redden considerably the U - B colour of normal quasars, so at these higher redshifts the method is insensitive.

Secondly, hot white dwarfs and hot subdwarfs also have an ultraviolet excess, and so are included in the sample. The apparent magnitude distribution of these objects is quite different, so there will be quite different contamination levels at different survey magnitudes. Green, Schmidt and Liebert (1985) show that the quasar apparent magnitude distribution is by far the steepest, and so should dominate the number counts by $B \simeq 19$. However, the contaminants can only be identified through follow up spectroscopy.

Recently, fast flying spot microdensitometers have been built (see

MacGillivray and Stobie (1984) for a description of the COSMOS machine, or Kibblewhite *et al.* (1983) for the APM machine) which have enormously enhanced the possibilities for broad band optical surveys. These machines can digitise an entire sky limited UK Schmidt plate (containing, at high galactic latitude, some few x 10^5 celestial images) in ≃ 6 hours, retaining only photometric, astrometric and some morphological information. This has greatly improved photometric surveys, which are now no longer confined by the patience of the surveyor (but by the generosity of the telescope-time allocation committee!) as to how many plates can be scanned. As a result, many plates in one band can be used to reduce photometric errors and eliminate spurious images (eg. satellite trails, asteroids, bits of dirt on the emulsion and emulsion flaws as well as large scale background variations caused by a plate processing or hypersensitization error). Also, many more broad band magnitudes can be incorporated into the survey giving a much larger range of colours than the original (U - B) or (U - B), (B - V) colours used in UVX surveys. Stars can then be confined in this 4 or 5 dimensional multicolour space to a narrow locus. The rest of the multidimensional volume is searched for stellar objects. In this way it is possible to overcome the redshift limitations of the UVX surveys described above. Only rather exceptional quasars with colours that simulate a stellar spectrum will then be lost from the survey.

1.2.4 Optical survey methods: spectroscopic.

The broad, strong emission lines observable in the spectra of most quasars at most redshifts has meant that they are relatively easy to

discover using low dispersion slitless spectroscopy. Smith, 1978 and 1981, reviews this topic extensively. The first time quasars were located using this method was the identification of emission lines in the spectra of previously known quasars by Hoag and Schroeder (1970). Since then, many slitless surveys have been undertaken - a list is given in another review by Smith, 1984. In particular, the use of an objective prism with the UK Schmidt telescope has proved extremely useful in locating large numbers of quasars (see, for example, Clowes *et al.* (1980) and Clowes and Savage (1983)). Unfortunately visual searches are very susceptible over areas as large as those of a UK Schmidt plate to the effects of the wandering attention of the surveyor, and to unintentional modifications in the selection criteria. The method is also constrained by the fact that the emission line which is most strong in the spectrum of most quasars (the Ly-α/N V combination) can only be seen at a limited band in redshift. Other difficulties are mentioned in section 1.3 on selection effects. Thus, the most commonly used photographic emulsion, IIIaJ, has limited sensitivity for quasars of $z < 1.7$ (where Ly-α is to the blueward of the emulsion cutoff at λ = 3200 A, but other weaker lines such as C IV and C III] etc. may be visible), a good sensitivity for quasars with $1.7 < z < 3.2$ (where Ly-α is in the passband of IIIaJ) and a very low sensitivity for quasars of $z > 3.2$ (where Ly-α is redder than the emulsion cutoff of IIIaJ at λ = 5400 A). In addition, it is <u>very</u> efficient between $1.7 < z < 2.4$, where both Ly-α and C IV are in the IIIaJ bandpass. As with the photometric surveys, the development of fast microdensitometer machines has allowed these searches to be done automatically - for example the Automatic Quasar Detection package of Clowes (1984) and Clowes, Cooke and Beard (1983), and the Prism Reduction System of Hewett *et al.* (1985). These

systems have gone a long way to reduce the uncertainty associated with searches done by eye, but are of course still limited by intrinsic difficulties associated with the technique, such as the discontinuous redshift coverage mentioned above, and other selection effects described later in section 1.3. It is also possible, using slitless survey plates, to identify spectra with peculiar colours: the portions of the spectrum corresponding to the U and the B passbands (for the IIIaJ emulsion) are identified, and a U - B colour is constructed. This goes some way towards addressing the decreased sensitivity of emission line searches to quasars of redshifts $z < 1.7$. It is only possible, though, to construct this one colour. Thus it is not possible to recreate the full information advantage of using many broad band magnitudes.

Other photographic emulsions, sensitive to redder wavelengths, are less useful than IIIaJ for slitless spectroscopic work. Older emulsions such as IIaD have a coarser grain size and are not hypersensitized and so are not as sensitive. IIIaF has the problem that its spectral response varies with wavelength, so a slitless spectrum can show what looks like an emission line, but is actually an artefact of the emulsion sensitivity. Figure 1.1 shows the spectral response functions of the IIIaJ and IIIaF emulsions, illustrating this point. IIIaF prism plates are usually taken using a filter which attenuates flux below $\lambda = 4850$ Å.

Slitless surveys can also be done using a grism or grens (the former is a grating/prism combination, the latter is a grating/prismatic lense combination). These instruments have been mounted on 4m telescopes, and so can survey up to two magnitudes fainter than the 1.2m UK

Schmidt. However, the survey field of view is as a result smaller - typically less than or equal to 1 square degree. Surveys done with these instruments are harder to automate, because some objects contain more than one image:- the main dispersion element is a transmission grating, so brighter objects typically have a zero, first and second order images.

1.2.5 Optical survey methods: variability.

The variability of quasars is not only interesting in its own right, it can also be used as a search technique for optical quasars. Many quasars vary by $\simeq 1$ magnitude or more, and as no correlation between variability and redshift has ever been found (Cristiani, 1986) this method has been suggested as a means of overcoming the redshift biases of other optical survey methods. Once variable stars have been eliminated from the survey (easily done as most of the galactic stars vary over a short timescale and are periodic) virtually all of the sample objects are found to be quasars on subsequent slit spectroscopy. Hawkins (1986) has searched for objects which vary by > 0.35 magnitudes in a Schmidt field. He is somewhat unclear about the actual level of incompleteness, but it is clear that many quasars do not vary by this much, and are therefore missed. It is possible that the same drawbacks hold for variable quasar samples as for radio samples (mentioned earlier: section 1.2.1). The main problem with variable quasar selection is that not enough variable quasars are known to make firm statements about their selection effects: it is stated that there is no correlation with redshift only because variable quasars are found across a broad band of redshift, yet the same is

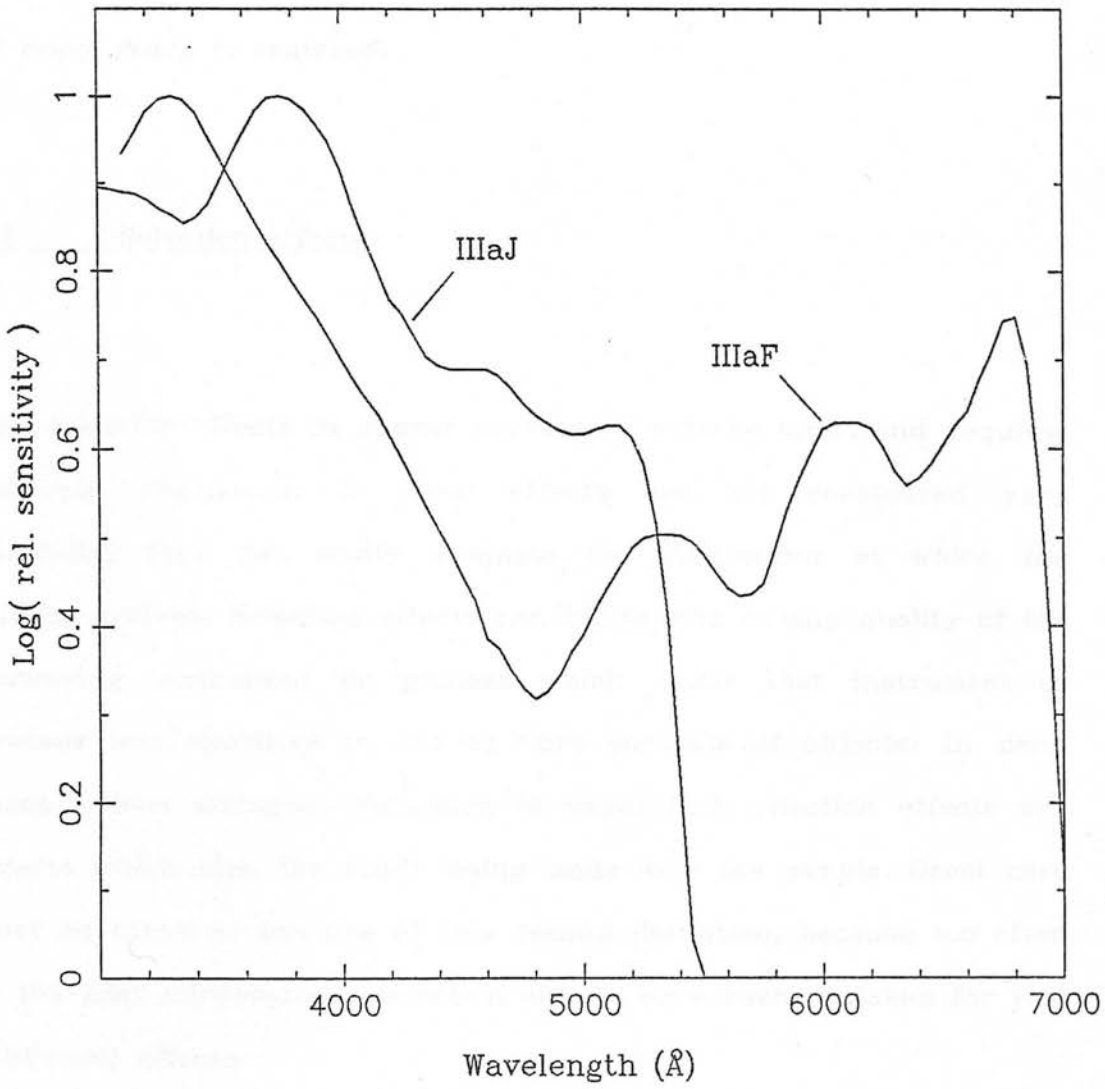

Fig 1.1 Sensitivity curves of photographic emulsions commonly used for prism plates as a function of wavelength. A filter is normally used with IIIaF cutting off below λ = 4850Å.

true of emission line surveys, and few would deny that these have redshift selection effects. The key point is that variable quasars are hard to find because one must make many observations/epoch (to reduce photometric errors) over many epochs, and a maximum baseline of many years is required.

1.3 Selection effects.

The selection effects in quasar surveys is a large topic, and requires separate discussion. If these effects are not considered very carefully, they can easily dominate the conclusions at which the survey arrives. Selection effects can be defined as any quality of the surveying instrument or process which makes that instrument or process less sensitive to one or more subclass of objects. In many cases a less stringent definition is valid: that selection effects are effects which bias the study being made with the sample. Great care must be taken in the use of this second definition, because too often in the past unrecognized selection effects have been mistaken for real (physical) effects.

Some selection effects have already been mentioned in section 1.2 but I will mention again all effects pertaining to optical quasar discovery (for example: that all quasars are not detected as variables is not strictly a selection effect; some quasars may not <u>be</u> variable. However, variability is itself a selection effect in other discovery techniques: section 1.3.3). Broadly, I will divide this section into redshift effects, line characteristic effects, and flux density or luminosity effects. I

will further subdivide these categories as to survey method, but it must be remembered that some selection effects are not as easily classifiable as this, and so there is some overlap between sections.

1.3.1 Redshift effects.

The most complex of these is for prism surveys. Firstly, as has been mentioned, the strongest line in the quasars' spectrum is the Lyman-α/N V combination. This is the most easily detected, then, in quasars whose redshifts are between $z \simeq 1.7$ and $z \simeq 3.4$, where it is in the 'window' defined by the atmospheric cutoff at ≃ 3200 Å and the cutoff of the IIIaJ emulsion at 5380 Å. This does not mean that quasars are undetectable as emission line objects outside this range. Other lines are easily detectable in some quasars' spectra, but there must be some loss of sensitivity, varying in a complex way, as lines of different strengths go in and out of the redshift window at lower redshifts. For example, more confidence would be given to a quasar candidate at $z \simeq 1.2$ if C IV and C III] were both seen at low signal to noise, than a quasar at $z \simeq 0.5$ showing an Mg II line at the same signal to noise and in the same place on the spectrum as the C III] line, or another quasar at $z \simeq 1.2$ in which one of the carbon lines is intrinsically weaker. All that can really be said is that one must be aware of likely incompleteness at these lower redshifts. It is true that candidates can be identified on the basis of UV excess in their prism spectrum, and indeed prism surveys routinely classify candidates by the detection method: emission line, UV excess and others. But there are problems with these candidate selection procedures - see chapter 5. The extent of this incompleteness can only be quantitavely assessed

when one has redshifts for a truly complete survey of the same region as the prism survey.

Related to this is an effect first noticed by Savage (1978). This is that prism surveys suffer because resolution decreases rapidly with increasing wavelength. Table 1.1 shows dispersions for the two objective prisms of the UK Schmidt telescope. Values for dispersion are given in Å/mm. Values for the dispersion 1 prism came from Nandy *et al.* (1977), and for the other dispersions from Cannon *et al.* (1982). This effect is obviously greatest for the low dispersion prism, but tempered if more than one line is seen in the spectrum. This is a difficult effect to quantify, but Savage (1978) notes that lines of equivalent width less than 50 Å could not be detected with certainty beyond about 4600 Å (ie. Ly-α for quasars $2.8 < z < 3.4$, or Mg II for quasars $0.6 < z < 0.9$) on prism 1.

Hazard and McMahon (1985) find it impossible to locate emission lines at wavelengths longward of 6000 Å on IIIaF plates because the rapidly increasing prism dispersion produces a strong enhancement of the continuum flux per mm., making lines unidentifiable (in many cases

Table 1.1: UK Schmidt prism dispersions.

Dispersion → / Line ↓	1	2	3	4
Hϵ (3970 Å)	1852	955	630	470
Hγ (4340 Å)	2440	1260	830	620
Hβ (4861 Å)	3470	1788	1180	881
Hα (6563 Å)	8088	4167	2750	2052

they note the spectrum saturates). This effect is presumably also at work on the IIIaJ prism plates.

Prisms other than prism 1 have not been used extensively in quasar survey work, because ≈ 2 magnitudes are lost from the limiting magnitude when the medium dispersion prism (dispersion 3) is used, and more if both prisms are used - ie. dispersions 2 and 4 (Savage *et al.* 1985 has looked at objects in deep CCD sequences on plates in good seeing with the different prism combinations to obtain these numbers).

A grism or grens survey is likely to suffer from some of the same selection effects as a prism survey, except that because the dispersion element is a transmission grating, the dispersion is virtually linear and so the lines are equally detectable at all wavelengths (except for the wavelength dependence of the emulsion response).

The main redshift selection effect for UV excess surveys has already been mentioned: at redshifts greater than $z \approx 2.2$, Ly-α enters the blue passband, and the 'Ly-α forest' of absorption lines at wavelengths shortward of Ly-α both conspire to stop the object showing an UV excess.

Finally, the situation as far as multicolour surveys is concerned is quite complex. It is possible that a particular quasars' spectrum, if seen at a different redshift, would lie inside the stellar locus. But some combinations of line width and continuum slope, as they are redshifted, never will. So for every multicolour survey, there is likely

to be some level of incompleteness, difficult to quantify. The importance of this is affected by how many colours are used in the survey, and the quality of the photometry - a larger number of colours reduces the percentage of multidimensional volume occupied by the stellar locus. Improving the quality of the photometry in either a UVX survey or a multicolour survey helps by reducing the volume of colour-colour space occupied by the stellar locus, and reducing the number of interesting objects misplaced into the the stellar locus. It should be remembered that this process cannot be continued indefinitely, as photometry is improved. Ultimately, there are a number of physical effects which can shift stars in the solar neighbourhood of a particular spectral type away from the zero-age main sequence on an H-R diagram. These effects are duplicity, metallic abundance, rotation and ageing, and can result in substantial broadening of the main sequence on two colour plots ($\approx$ 0.4 magnitudes). The effects are described in more detail and quantified in section 4.6.1.

The position of quasars in multicolour space is much harder to define. A quasars' spectrum as observed over the optical bandpass is essentially a power law continuum with a set of broad ($\approx$ 1000's of km s^{-1}) and a set of narrow ($\approx$ 100's of km s^{-1}) emission lines superimposed. However, the continuum power law index α can vary over $-0.5 < \alpha < -1$ for most quasars, where the power law is defined $f_\nu \propto \nu^\alpha$. A thermal component to the continuum is also sometimes seen. The emission lines' equivalent widths' can vary over at least a decade, which can modify a broad band magnitude by up to a magnitude (Wampler and Ponz, 1985). In addition, as many as 10% or more quasars may have broad absorption lines (Hazard *et al.* 1986),

which can be up to 65 000 $km.s^{-1}$ wide. This has a dramatic and unpredictable (while the redshift remains unknown) effect on broad band magnitudes, scattering these object from their anticipated positions in colour space. As all these possible differences are redshifted, clearly it is extremely difficult to predict average values for broad band colours, and so localize where on a colour - colour diagram objects of a particular redshift will lie. Several authors have tried, using an 'average' quasar spectrum, to plot a quasar locus on colour - colour diagrams. The spectrum is convolved with the broad band filter profiles for different redshifts, and so a simulated set of broad band magnitudes is obtained for each redshift. Cheney and Rowan-Robinson (1981) constructed an average quasar spectrum on the basis of published spectra, whose locus was plotted on U - B vs. B - V diagrams. Objects such as this could be located at virtually all redshifts using their selection criteria - it only goes as red as $U - B \geq -0.4$ at $z = 2.5$, and even here some UV excess surveys such that of Boyle *et al.* (1985) would pick it up. On the other hand, Dunlop *et al.* (1986) use their spectrum of the high redshift, narrow lined object 1351 - 018 to show that it would lie inside the stellar locus at $2.7 < z < 3.0$, and for $z > 3.5$. Indeed other high redshift objects recently discovered are much redder than Cheney and Rowan-Robinson suggest (Shanks, Fong and Boyle (1983), and Hazard and McMahon (1985)). The conclusion is, then, that without a better understanding of the different elements of quasars' spectra and redshift, it will be impossible to predict with any confidence where objects 'should' lie in colour - colour space. All that can be done is locate all objects at low density locations in colour colour volume.

1.3.2 Line characteristic effects.

A major line characteristic selection effect has been mentioned already: low dispersion slitless spectroscopic surveys can only identify emission lines of greater than a limiting equivalent width. The limit depends on the dispersion of the instrument, but is typically ≈ 50 Å (Hazard *et al.* 1986) for prism 1 of the UK Schmidt. In addition, though, objective prism surveys suffer from non-linear dispersion reducing the instruments' sensitivity to emission lines at higher wavelengths. There is also more continuum flux/unit distance on the spectrum at higher wavelengths in prism spectra, so they can more easily become saturated.

If strong, broad, lines are redshifted into a broad band magnitude, they contribute to the photometry in this band. Clearly, then, to define the quasar luminosity function independently of redshift effects, spectrophotometry must be obtained for the whole survey to define narrow band rest frame magnitudes.

It is rare that surveys have such precise spectrophotometry a) because it is expensive in telescope time, and b) because a narrow band magnitude is required at the rest wavelength - normally surveys cover such a range of redshifts that the required wavelengths cannot be seen through the atmosphere, and K corrections must be used with all their associated problems. Wampler and Ponz (1985) estimate that for $z \simeq 2$, strong Ly-α and C IV lines can increase the apparent brightness of a faint quasar by a factor of two.

1.3.3 Limiting magnitude effects.

These are probably the most insidious, because they are the hardest selection to deal with.

First of all, it is crucial to remember the importance of accurately defining where the survey cutoff is in apparent magnitude. This is because, to use the survey to try to understand evolution means that the survey must be used to construct luminosity functions at different redshifts. An error in locating the sample cutoff yields errors in the quasar space density calculations, and so produces errors in the derived luminosity function. The problem here is that the cutoff of the survey is often very hard to find, because of some of the intrinsic properties of surveys. Photometric errors and variability are obvious sources of difficulty, but also (as shown in chapter 5) strong lines are visible in low dispersion spectra to very faint magnitudes. So there is a gradual tail off in quasar number counts towards fainter magnitudes, as only stronger line objects are found. In photometric surveys, the survey limit is a function of colour. Each broad band magnitude has a plate limit of its own, which means that the overall survey cutoff is actually colour dependant. Ultimately, of course, the survey limit must be a limit of luminosity. Wampler and Ponz (1985) have shown that because absolute magnitude is a function of redshift, and the limit as actually measured is one of apparent magnitude, the survey limit is redshift dependent: objects at low redshifts are easily discovered that are fainter than what must be defined to be the survey limit.

Photometric errors and variability also generate a selection effect

which is independent of the survey cutoff. The number counts of quasars increase very rapidly with increasing apparent magnitude (eg. Green, Schmidt and Liebert, 1986) so small photometric errors (whether they are measurement errors or intrinsic variability) change the slope of the number-flux density relation. This is because more objects are scattered from fainter to brighter magnitudes than vice versa. This effect, first discussed by Kron (1980) can happen at all magnitudes, but is likely to be worst at fainter magnitudes, because photometric errors increase with increasing magnitude.

Variations in seeing, plate sensitivity and sky brightness are all of crucial importance for the detection of emission lines on slitless spectrum plates. Osmer (1981), in his analysis of the Curtis Schmidt survey (Osmer and Smith, 1980) shows that there are variations of up to factors of four in the numbers of objects found from plate to plate, and the seeing and other variations from plate to plate can account for all of the variation.

This effect can have complex consequences: He (1986, private communication) searched two UK Schmidt prism plates by eye (the results of this search are included in this thesis). The plates UJ5839P and UJ5846P were both searched because they have perpendicular dispersion directions, so that a pair of overlapped spectra could be identified as such, rather than being misinterpreted as an emission line object. If known quasars are inspected on both plates, however, it is immediately apparent that the seeing for UJ5839P is considerably worse than that for UJ5846P - lines easily seen on the latter are hard to detect on the former. It is unfortunately not clear what effect this might have on the survey, as information as to which plate a

candidate came from was not recorded.

Stronger lined objects are easier to identify on slitless spectrum plates than weak lined ones. Clowes (1981) has shown that this is a function of magnitude: weaker lined objects fall below a rising line equivalent width detectability threshold as they get fainter. This can make the survey limit hard to identify: very strong lined objects are still easy to locate for an object that is more than a magnitude below the nominal plate limit. This effect is illustrated in figure 5.8.

Incorrect choice of the quasar continuum slope can also cause substantial error. Ultimately, a survey would measure the emitted flux at some standard wavelength (since a bolometric magnitude is impossible). However, if the survey is over a broad range of redshifts, this may not always be observable, and so one must make the measurements at some other wavelength and make K-corrections. If the continuum slope is badly estimated, this can lead to large errors in calculations of the space density of quasars. For example, Wills and Lynds (1978) who note that their choice of 1 for the optical spectral index is from a wide range of observed indices, and will have a strong effect on their calculated V/V_m. Also Wampler and Ponz, (1985) who note that a change in continuum slope of 0.5 leads to a change in any space density estimate of a factor of two, at $z = 2$.

In addition, quasars can be lost from any survey of photographic plate material because of blemishes, emulsion flaws or bits of dirt in the measurement phase of an automatic survey. Some methods are more susceptible to this effect than others - for example, there are many junk images on grism or grens plates caused by scattered light

from the grating and zeroth order diffraction images. This is not a problem for most survey applications, however, because the objects lost are lost at random, and so do not modify the statistical conclusions to which the sample is put. Objects 'gained' (ie. spuriously included in the survey) are eliminated when the survey is confirmed with slit spectroscopy.

1.4 Conclusions.

The arguments of this chapter are briefly summarized in this section. Searches for quasars in the optical are still vital because it is in this passband that most quasars are seen. Surveys done in the optical so far are not free from selection effects, which are numerous and can easily override the conclusions of the surveyor.

There is still no real alternative to the use of photographic plates as a detection medium. The advantage gained from the use of a linear electronic detector (a CCD) still cannot outweigh the photographic advantages of reasonable sensitivity, large information storage ability, durability and rapidity. This is only true where the photographic data can be put onto a quantitative basis with the use of a plate digitisation device. Were CCD's of a larger format to be constructed, the photographic advantage would probably be lost because of the time saved by the surveyor in the reduction of CCD data.

Although to some degree there can be said to be an information trade-off between the additional sensitivity of direct plates compared

to the additional spectral information of prism plates, for the purposes of surveys required for cosmology this is largely negated by the much more severe selection effects at work in prism surveys. This topic is addressed further in this thesis. Partially as a result of this, quasar surveys continue to need confirmation by slit spectroscopy from large telescopes.

Probably the best way of changing this balance is the use of a low dispersion grism with a linear CCD detector. The grism dispersion would have to be sufficient to identify major stellar features, and the CCD size would have to be sufficient to allow it to compete with plates, after such inequalities as calibrating the plate, and the ease of reduction of the CCD data, have been taken into account.

2. Quasar surveys in field 927.

Evidently, as seen in chapter 1.3 on selection effects, optical survey techniques are plagued with difficulties. But equally evidently, it depends very much what one is hoping to achieve with the survey as to how important this is. If, for example, one wishes to study the properties of individual objects, then no statistically complete or representative sample is required. Any survey will do, as long as it locates objects of the desired type, and as long as statements about all quasars are not then made. Even if the object is to look at quasars as a class, it may be possible to use a survey which has selection effects, as long as one is confident that they do not have a bearing on the aspect of quasars that one is looking at. For example, it is quite legitimate to use a prism survey to search for clusters. This is because even though the survey will have many, complex selection effects in redshift, if a cluster is found at some redshift, it will be a valid detection because the whole survey has the same sensitivity at that redshift. One must be extremely careful, however, before one makes statements about the clustering of quasars at other redshifts on the basis of the cluster detected. The danger here is that one normally does not know the full extent of the selection effects on a survey, because they depend on the intrinsic properties of quasars, which remain obscure (otherwise one would not need to do the survey). This is a circular problem.

There is a final class of problems, which require that selection effects are kept to the minimum and are well understood. These are problems dealing with the statistics of all aspects of all quasars, or the

statistics of one aspect which cannot be decoupled from selection effects. Problems in these classes include quasar evolution, and the luminosity function. The former requires coverage of the whole redshift-luminosity plane, and the latter requires knowledge of luminosities at a particular redshift. A survey which meets these requirements - which minimized all selection effects that cannot be eliminated, and which understood those that remain, has proved elusive, and is the object of this thesis. Probably the best available to date are those of Schmidt and Green (1983) and of Boyle *et al.* (1985), extended in Boyle (1986). However, both surveys have serious deficiencies. They are both UVX surveys, and so limited in their redshift coverage. As a result the coverage of the Hubble diagram for both surveys is limited. In addition, Schmidt and Green's survey has a bright magnitude cutoff, while Bolye's survey has poor photometry, and varying candidate selection limits. Wampler and Ponz (1985) emphasise the difficulties of drawing firm conclusions from surveys with poor photometric cutoffs. However, the great advantage of both of these surveys is that they both have complete slit-spectroscopic identifications for all objects.

So it would be nice to have a survey which overcame these limitations, ie. that meets the following criteria:

- it should be deep enough in apparent magnitudes to have good representation at all luminosities.
- it should not be limited, or have sensitivity variations, in redshift space.
- finally, it should have good enough photometry to reduce flux density selection problems near the boundary of the survey (and, of course, so as not to modify the luminosity function).

The candidates thus generated must then be spectroscopically observed, in order to pick the real quasars from other candidates, to find accurate redshifts for all of the quasars, and to obtain continuum slopes for all of the quasars, in order to be able to do K corrections on them. In practise, these demands are very hard to meet. The first phase of candidate selection must be done using optical survey methods, because large numbers of quasars do not radiate in other passbands, and it is not clear that the reason for this is uncorrelated with the things that a survey is useful for: the three dimensional spatial and luminosity distribution. Unfortunately, optical selection mechanisms have many selection effects which are hard to calibrate and/or eliminate (section 1.3).

In addition, the final phase is likely to require large numbers of slit spectra. This should not be too extravagant of telescope time given the recent development of multi-object slit spectrographs at many telescopes, assuming the spectra thus obtained can be reliably flux calibrated.

The only practical way to carry out the survey phase of such a program is to use many optical survey techniques on the same field. That is the rationale behind this thesis. In an attempt to generate such a survey, UK Schmidt field 927 was chosen. This is because the field centre, at 10^h40^m +5°00', is at high galactic latitude (b = 52°) - a requirement for quasar surveys to reduce contamination with galactic stars, and absorption due to galactic gas and dust. It is also close to the equator, so that it is available to telescopes in both hemispheres. It has thus been possible to collect objective prism and direct broad band plates from the UK Schmidt telescope at the Siding

Spring Observatory in Australia, and grens plates from the Canada-France-Hawaii telescope in Hawaii.

This plate material has allowed the following surveys of the field to be compiled:

1) An 'eyeball' survey of the objective prism plates. This survey is presented and used in this thesis by permission of Mr. He (private communication, 1986), who did the survey.

2) An automatic survey of the same plates. This survey was done by Dr. Clowes (private communication, 1986) who gave permission for its inclusion in this thesis.

3) An automatic survey of the grens plate.

4) An automatic UV excess survey of the direct broad band plates.

5) An automatic multicolour survey of 5 colour broad band plates.

Surveys 3, 4 and 5 were undertaken by the author, and are not included in this chapter as they are described in more detail in chapters 3 and 4.

The reasons for the apparent duplication of effort in the surveys are the following:

- Automatic surveys of prism plates are still relatively untested. Therefore comparison of its results with a relatively well understood method (eyeball searches of the same plates) is useful.

- Apparent duplication between the prism plates and the grens survey is not real, because survey limits on the prism plates are $15.5 \leqslant B_J \leqslant 19.8$, while on the grens plate limits are $18 \leqslant B_J \leqslant 22$. On the other hand, plate area for the prism plate is 25 square degrees compared to 1 square degree for the grens plate. Selection effects are

also different, because of the linear grating dispersion.

- The rationale for doing a UV excess survey, as well as a multicolour one which contains UV information is explained more fully in section 2.3, but briefly it is done because multicolour surveys are new, and it is therefore easier to compare the UV excess survey with existing surveys, and use the knowledge gained to help to understand the other colours.

2.1 He eyeball prism survey.

Schmidt field 927 has been searched visually by Mr. He, from the Peking Normal University. He used a light table and travelling microscope to search the prism plates UJ5839P & UJ5846P over 25 square degrees. The two plates have their dispersion directions perpendicular to each other, so by searching both plates it is possible to identify and eliminate overlaps, and check the reality or otherwise of emission features (emulsion blemishes and other defects can look very like emission lines if unfortunately placed). Plate UJ5846P is actually significantly better than UJ5839P, which adds to the uncertainty of defining the survey limit (discussed further below). UJ5839P has an exposure time 10 minutes longer, so spectra of about equal faintness can be seen on both plates, but the seeing was evidently worse for this plate, as objects which have known emission lines are easier to identify on UJ5846P.

He selected 731 candidates, on the criteria of ultraviolet excess and displaying an emission line. The candidates were graded into five

classes, 1, 2, and 3 for the emission line objects, and 4 and 5 for the ultraviolet excess. He (1986, private communication) expects the reliability of the classes to be about 100% (class 1), 80% (class 2), 50% (class 3), 50% (class 4), and 20% (class 5). In order to define as complete a sample as possible, one must include the large numbers of objects in classes 3 and 5. Table 2.1 shows the breakdown by class of the survey. The large contamination rate for the high probability UV excess class 4 is quite understandable for this selection criterion because various classes of galactic stars show ultraviolet excess, such as white dwarfs and blue subdwarfs (see Boyle, 1986, who reports a 50% contamination rate in a broad band survey of UVX objects, and Green, Schmidt and Liebert (1986) who have published number counts of all UVX objects).

On the basis of follow up spectroscopy of another He survey, Smith (1986, private communication) says that classes 3 and 5 do not include as many quasars as He indicates. Smith believes that by ignoring these two classes, the completeness of the survey will not be substantially affected, while the contamination will be hugely

Table 2.1: He survey: numbers of candidates.

Class	No. of candidates
1 (100% pr.)	11
2 (80% pr.)	49
3 (50% pr.)	179
4 (50% pr.)	140
5 (20% pr.)	352

reduced. On this basis, I propose to ignore classes 3 and 5. Hereafter, then, the 'eyeball survey' includes only those objects in classes 1, 2, and 4.

2.2 Automatic Quasar Detection prism survey.

The Automatic Quasar Detection system (AQD) is a software package designed by Clowes (1984) & Clowes *et al.* (1983) specifically to overcome the difficulties associated with searching objective prism or other low dispersion slitless spectrum plates by eye. This system was designed specifically to handle data produced by the COSMOS machine at the R.O.E. in its 'mapping' mode (see MacGillivray and Stobie, 1984 for a description of COSMOS). Mapping mode data is essentially the raw transmission value pixel data over the whole plate. It is only normally used for work with prism plates, as the data produced is enormously bulky compared with image analysis mode (I.A.M.) data (details are given in chapter 4): 12 magnetic tapes per Schmidt plate for mapping data versus 1 magnetic tape per plate for I.A.M. data Dr. Clowes processed the data for this field, using prism plate UJ5846P and direct plate J9952, and kindly provided the survey for this project. Plate measurement for this survey took place before the COSMOS hardware upgrade from 8-bit to 14-bit digitisation in 1984, so the survey could be improved by doing it again (an assessment of the effects of this increase in dynamic range is made in section 4.4), but time constraints have made this impossible. Pixel size for this survey was a 16μ spot size and a 16μ step size. A brief description of the AQD system is given here, which is relevant also to chapter 3, an AQD

search of a CFHT grens plate.

After the plate has been measured, the data is processed offline with the COSMOS analyser (Stobie, 1986), to yield in the resulting I.A.M. parameter catalogue a list of the locations of the spectra (table 4.2 gives a list of the I.A.M. parameters) - if prism dispersion is in the 'X' direction, the emulsion cutoff position of the spectrum is given by IYCEN, the Y centroid, and XMIN, the minimum image value in X.

This list is then paired with the I.A.M. data from the direct plate of the same field. The reason that a direct plate is required is so that overlapped spectra can be geometrically identified (from direct plate positions and knowledge of the dispersion direction), and because accurate positions of the spectrum emulsion cutoff are required for extraction of the spectrum and subsequent wavelength calibration of spectral features, as well as being useful for star/galaxy separation. The prism plate positions were found not to estimate the cutoff position well because they are a function of object brightness and object colour. Overlapped spectra are thrown away at this stage, but the star/galaxy separation information is kept for a later stage, because known quasars can have extended images on UK Schmidt plates if they are at low redshifts.

The positions are used to extract small rectangular boxes of pixels around each object, typically 8 x 128 pixels for Schmidt prism plates. This considerably cuts down the bulk of the data. Next, a file of 1 dimensional intensity spectra is constructed, by adding together rows of pixels which are parallel to the spectrum, to the corresponding element of the following row. The transmission values are converted

into intensities as described by Clowes *et al.* (1980). In addition, a continuum is fitted to each spectrum by using a digital filter, and a noise spectrum similar to the noise expected is generated. The software then searches these spectra for features associated with quasars' spectra (such as emission lines, ultraviolet excess, and broad absorption lines), and an output catalogue is generated of all objects selected.

The principle selection method is emission line location. A minimum signal / noise ratio is specified by the user at the outset, and any spectra showing lines of peak value (compared to the typical noise size calculated at this point) more than this are identified as emission line candidates. In this survey, the s/n ratio specified was 8. For UVX candidate selection, two broad band filters are defined, and the corresponding magnitude found. In this survey, the 'U' filter was defined as pixels 36 - 51 inclusive ($\simeq$ 3490 A - 3815 A) and the 'B' filter was defined as pixels 12 - 24 inclusive ($\simeq$ 4170 A - 4660 A). Pixel numbers refer to the distance from the closest unit pixel to the emulsion cutoff. Spectra are selected when the colour so defined exceeds a specified limit - for this survey, objects whose $U - B < +0.4$ (remember that these colours are not real Johnson U and B, and so the criterion is not the normal $U - B < -0.4$) were selected.

For field 927, this selection process produced a total of 3492 candidate spectra over 25.4 square degrees. Of these, 2152 objects were detected on the basis of emission lines, 752 objects were detected as having a UV excess, and 558 satisfied both criteria. This is obviously an unrealistically large number: $\simeq$ 137/square degree brighter than $B_J \simeq 20$, compared to Boyle's (1986) estimate of 15

quasars/square degree, or 16/square degree allowing for Boyles estimate of his incompleteness (≃ 10%).

The source of the contamination is galactic stars of particular spectral types, which can mimic the quasar features being looked for on low dispersion spectra. In order to identify these objects and thus create a catalogue of high probability quasar candidates, Dr. Clowes has adopted the following procedure (adopted using the results of slit spectroscopy on surveys of other fields, and through trial and error): firstly, objects with unusually wide or off-centre spectra are thrown away. This effectively cuts out bright stars and bright galaxies. After this, the survey contains 2604 objects, of which 1795 were selected by emission line alone, 574 by UV excess alone, & 235 using both selection procedures. I shall call these 2604 the 'larger AQD sample' and use only them in comparisons with other surveys etc. as it is very unlikely, from inspection of the objects lost, that any genuine quasars have been lost in cutting down the catalogue in this manner. There are still 103 candidates/square degree, ie ≃ 85% contamination.

Next, a grade number is assigned to each candidate. This is built up by the addition of an integer for 'good' quasar features, and the subtraction of one for 'bad' features. 'Good' features are:

1) Stellar, under star/galaxy separation on the direct plate.
2) Selected by emission lines.
3) Selected by UV excess.

'Bad' features are that the object shows a stellar feature, defined in the following way. Some spectra show what is interpreted by AQD to be an 'emission line' peak in the region 25 < line < 31, where the numbers are numbers of pixels from the emulsion cutoff. This

corresponds to the stellar continuum between the broad Hβ and Hγ absorption lines seen in hot white dwarfs. Becuase these lines are broad and deep, they can mimic an emission line when seen at low dispersion. Finally, a value between 0 and 1 is added to the grade on the basis of the strength of the spectrum's strongest emission line, relative to the continuum magnitude at the position of the line.

This grade number was used to cut the larger AQD sample down again to 264 objects, all of which have an emission line, and 123 of which were also selected by the UV excess criterion. These objects are referred to as the 'good AQD sample' hereafter. These are all extremely high probability candidates - Clowes estimates ≃ 80% to be quasars on the basis of slit spectroscopy of another survey. However, this procedure obviously adds redshift selection effects, making the survey less complete. This is because quasars in the redshift band $2.0 < Z < 2.2$ would have their Ly-α/N V shifted into the 'stellar feature' band, and so would be weighted down for selection.

2.3 Other surveys in the field.

Other surveys in field 927 were carried out by the author, and are described more fully in chapters 3 and 4. Briefly, for the sake of completeness, they are mentioned here.

i) A ≃ 0.75 square degree survey in the centre of the Schmidt field, down to a limiting magnitude of $B_J \simeq 22$. This was done using a CFHT grens plate, which was then searched using the automatic quasar detection of Clowes (1984) & Clowes *et al.* (1983). AQD had to be

modified to measure this type of plate.

ii) An ultraviolet excess survey. This was done using UK Schmidt direct plates in U and B_J, measured by COSMOS over ≃ 24 square degrees. Four U and three B_J plates were used, to reduce photometric errors. This survey has limiting magnitudes, defined by the worst plate in the appropriate colour or the limit of available calibration, of $B_J \simeq 20.8$ and $U \simeq 20.4$.

iii) A multicolour survey. This was done using COSMOS measurements in five colours, U, B_J, V, R, & I. Each colour has at least three plates, to reduce photometric error and to eliminate rubbish such as emulsion blemishes, satellite trails and meteors, as well as checking for the presence of field effects.

Surveys ii) and iii) are classed as different, above, for the following reasons: firstly, because many quasar surveys have been done by looking for UV excess objects. In order to make comparisons with them it is sensible to make the distinction. The only reason that people in the past <u>have</u> done UV excess surveys is because of data handling limitations - until recently, most surveys were done by plate searching by eye, and so only a few plates could be searched. Secondly, the blue data reaches fainter magnitudes than the multicolour data for the types of objects being looked for. This is because many faint, blue objects are below the survey limit for the redder colours. They are, however, still perfectly well detected in the U and B_J. It is therefore a waste of information to throw them away. Finally, the UV data covers a larger area than the 5-colour data, because the multicolour survey had to be 'drilled' around bright stars. This is because of the peculiarities of the IVn emulsion plates, used for the I colour. For further details of these surveys, refer to

chapter 4.

A search for variable objects in the field could not be included in this thesis, due to the difficulty in obtaining plates over a sufficiently long epoch change. Such plates would already have had to exist, because the timescale of a PhD. is not long enough (Hawkins (1986) has plates over 7 years). However, objects which do show variability on the shorter timescales of the multicolour survey (1983 - 1986) will presumably be picked up, because their variability will in general contribute to their peculiar colours. Hawkins detects variability at about the 0.35 magnitude level, while the photometric survey has errors smaller than this. There is of course no guarantee which way this effect will shift the object, but in general it should shift objects away from the stellar locus.

2.4 Existing slit spectroscopy in field 927.

A total of 39 quasars have slit spectroscopy in field 927, and of these all but three have reliable redshift measurements. They were discovered in a variety of different programs, including telescope time awarded to this project. I list their positions, redshifts, the source of the measurements, and the method of discovery in table 2.2.

Because they all come from different programs, slit spectroscopy has been obtained for these objects with no well defined goal. The different workers each had their own goals for obtaining these data. I give here a brief description of the intentions of the researchers. The

objects obtained by Mr. He were in a program of spectroscopy of different fields he had searched, in order to try and understand the properties of his visual surveys. That of D'Odorico were obtained during the commissioning run of a new faint object spectrograph, EFOSC, which was the instrument used by the author and D'Odorico (chapter 3 gives details). Oke and Cannon objects (several of their spectra are of the same objects as spectra from He, but are attributed to the latter as He has higher resolution spectra) are part of an unpublished UVX survey. Clowes and Robertson are engaged in a study of close pairs of quasars, and sources 6 and 7 were obtained by the author and collaborators as part of this program. All objects not obtained by the author are included with the kind permission of the respective individuals who did the spectroscopy, except for the 4C radio sources, published by Lynds and Wills (1972).

Although the spectra do come from such a wide variety of different programs, they still make an invaluable contribution to the understanding of the surveys in this work, particularly to the multi-colour survey, where there is little experience from other workers.

The object at $10^h39^m41.3^s$ +4°47'30" shows faint nebulosity on the POSS survey plates, and would therefore historically be classified as a Seyfert I. It seems somewhat arbitrary to make this distinction, given for example the detection of galaxy light in quasar images by Hickson and Hutchings (1987) and Hutchings *et al.* (1984) and the similarity of the quasar and Seyfert luminosity functions (Weedman, 1986).

Although it is unusual to find Seyferts at such high redshifts, this is surely simply because of the difficulty in observing such objects, because they are faint. Using the assumptions that $q_o = 0.1$ and $H_o = 75$ km.s^{-1}.Mpc^{-1}, the absolute magnitude of this object is $M_B = -22.1$. This places it firmly on the Seyfert I side of the somewhat arbitrary boundary of $M_B = -23$ between quasars and Seyferts adopted by Schmidt and Green (1983).

Another interpretation for objects such as this comes from Stockton and MacKenty (1986), Boroson, Persson and Oke (1985) and Boroson and Oke (1984) who have detected spatially resolved emission line nebulosity around quasars up to redshifts of $z = 0.5$. Stockton and MacKenty state that in some of these objects, the emission from one line can dominate the total surface brightness over a wide band filter. They make the observation that many of their survey objects are in groups of galaxies, and so it is interesting to note that there is a group of faint galaxies surrounding this one.

Figure 2.1 is a histogram of the redshifts of the confirmed objects. The three objects which do not have a redshift were put into the first bin. This diagram shows marked differences from others of this sort (eg. especially those of Hewitt and Burbidge, 1986) - there are fewer high redshift ($z > 2.0$) objects than one would expect, especially given that most slit spectroscopic effort has come from slitless prism plate surveys (Hewitt and Burbidge find the histogram strongly peaked at $z \approx 2.0$ for such surveys). But no significance can be attached to this because a) small number statistics and b) only part of the grens area is complete (see chapter 3) - other objects have slit spectra more or less at random.

Table 2.2: Known quasars in field 927.

Ra (1950)	Dec (1950)	Z	source	discovery method	B_J
10 38 30.7	+4 35 11	2.404	1	em. line	20.04
10 38 38.9	+4 6 21	0.928	1	em. line	18.87
10 38 39.7	+5 29 26	1.249	1	em. line	19.62
10 38 48.6	+4 10 31	1.410	1	em. line	18.02
10 40 31.8	+3 57 7	0.854	1	UVX prism	18.08
10 41 15.0	+4 54 3	0.556	1	em. line	19.35
10 41 33.6	+5 47 20	2.092	1	em. line	17.95*
10 42 16.7	+4 8 38	0.213	1	UVX prism	17.16*
10 42 43.0	+5 40 44	-	1	UVX prism	18.65
10 42 52.6	+4 50 50	0.294	1	UVX prism	18.92*
10 43 37.3	+3 52 13	1.480	1	UVX prism	18.95
10 44 20.8	+5 57 40	1.223	1	em. line	18.28
10 44 40.4	+6 7 50	0.888	1	em. line	18.26
10 44 57.4	+5 40 46	1.306	1	em. line	-
10 45 24.6	+5 38 1	1.244	1	em. line	19.39
10 40 0.5	+5 7 37	3.27	2	em. line	21.4**
10 41 54.0	+5 34 44	1.92	3	UVX prism	-
10 38 40.9	+6 25 59	1.270	4	radio	16.19*
10 46 56.5	+5 21 25	1.115	4	radio	19.37
10 33 40.5	+3 34 50	1.513	5	UVX / em.	18.56
10 41 31.3	+3 30 36	0.267	5		-
10 32 29.6	+6 17 13	0.245	5	UVX	18.74
10 35 12.9	+4 18 17	1.085	5	UVX / em.	17.82
10 35 8.5	+4 18 9	-	5	UVX	19.43
10 34 5.8	+5 23 41	BL Lac?	5	UVX	19.25
10 34 5.9	+5 25 15	1.061	5	UVX / em.	19.27
10 38 38.0	+5 28 19	2.76	5	UVX / em.	19.59
10 41 22.2	+4 54 10	2.41	5	UVX / em.	18.60
10 43 21.8	+6 40 14	0.429	5	UVX	19.06
10 43 16.5	+6 40 25	1.507	5	UVX / em.	17.88
10 46 48.0	+4 29 11	1.37	5		20.11
10 47 46.6	+5 1 30	1.3	5	UVX / em.	19.56
10 40 48.1	+4 38 2	2.33	6	em. line	18.92
10 38 59.6	+5 1 47	1.83	7	em. line	19.57
10 39 7.7	+5 3 31	1.96	7	em. line	20.17

Table 2.2 (continued)

Ra (1950)	Dec (1950)	Z	source	discovery method	B_J
10 39 15.1	+4 59 15	1.53	7	em. line	19.60
10 39 24.3	+4 57 37	1.97	7	em. line	20.32
10 39 36.9	+4 41 44	1.63	7	em. line	19.81
10 39 41.3	+4 47 30	0.419	7	em. line	19.40*
10 39 50.2	+4 42 54	2.20	7	em. line	20.15

Sources.

1. Spectroscopy obtained by He, X.T. (1986, private communication)
2. " " " D'Odorico, S. (1985, priv. communication)
3. " " " Cannon, R.D. & Oke, J.B. (1986, private communication)
4. 4C radio sources, Lynds & Wills (1972)
5. Spectroscopy obtained by Clowes, R.G. & Robertson, G. (1985/86, private communication)
6. Spectroscopy obtained by Cannon, R.D., Clowes, R.G., Keable, C.J. (1984)
7. Spectroscopy obtained by D'Odorico, S. & Keable, C.J. (1986)

Notes.

* - identified as galaxies morphologically.

** - photometry from J10128 only.

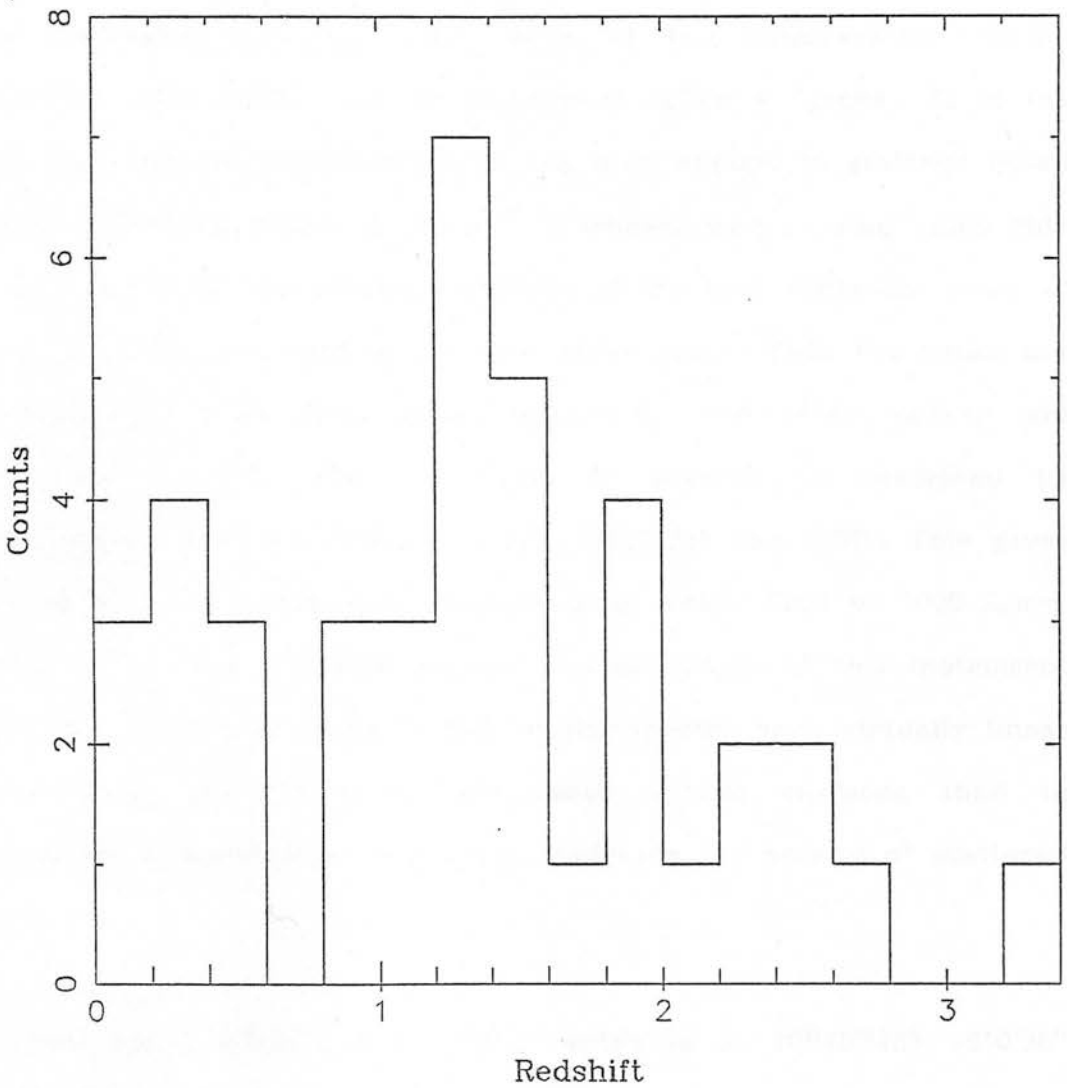

Fig 2.1 The redshift distribution of all objects with measured redshift in field 927.

3. New surveys: The AQD grens survey.

This survey, undertaken by the author, is an automatic search of a low dispersion spectrum plate taken at the Canada-France-Hawaii telescope (the CFHT) with an instrument called a 'grens'. It is the first time that an automatic search has been applied to grating- based slitless spectrum plates. A grens is a transmission grating ruled onto a prismatic lens: the prismatic element of the lens shifts the point of zero coma from the zero to the first order image. Thus the optics are optimized for the first order spectrum, and other orders are essentially useless. The instrument in question is described by Richardson (1979) and Fouere *et al.* (1982) for the CFHT. This gives low dispersion spectra with dispersions of either 2000 or 1000 Å/mm. over a field of ≈ 1 square degree. The advantage of this instrument over say a grism or prism is that a) the spectra have virtually linear dispersions, and b) there are fewer optical surfaces than in equivalent systems such as a grism, reducing the amount of scattered light.

A deep plate, A3057, whose plate centre is at $10^h40^m45^s$ +5°0'38" (1950) (the field centre of the UK Schmidt field 927) was obtained from C.D. Impey (private communication, 1984). This plate is a 2^h exposure on hypersensitized IIIaJ emulsion, using the 'green' grens (2000 Å/mm) in good seeing (≈ 1").

A filter, gg395, was used to cut off the spectra at wavelengths shorter than 3950 Å. This has the disadvantage of eliminating the ultraviolet part of the spectrum, but was considered necessary in

order to reduce spectrum crowding in the field. The instrument has limits of 18 < B < 22 with this configuration, and as brighter images have a zero, a second, and sometimes negative order images as well as the useful first order, image confusion can be a problem. There is also a certain amount of scattered light from the very bright images on the plate. Plate 3.1 shows a section of the grens plate, and plate 3.2 shows the comparable section of the prism plate UJ5846P.

3.1 Spectrum location: rationale.

The biggest difference between automating grens plate searches and prism plate searches is that of spectrum identification and location. This is because spurious images on the grens plate are not just the large noise peaks that come above the threshold level, as they are for the prism plates. As has been mentioned, there are genuine photographic images on the plate, that are useless and must be located and eliminated before the required spectra can be extracted from the plate. Spectrum location has been discussed in section 2.2, but clearly the same approach cannot be adopted for the grens: one cannot obtain direct plates from the same instrument (to yield spectrum positions) because the instrument itself acts as the field corrector. Any direct plates would have to be taken with a different corrector, giving a plate with different field distortions. One must therefore face the following choice: either the images can be used directly, and a software system is built to use image information (such as ellipticity, asymmetry, centre of gravity etc.) in order to detect the first order images (similar to the system built by Borra *et*

Plate 3.1 This plate shows a part of the grens plate CFHT3057. The segment shown has been magnified ≈ 5.1 times from the 13.64"/mm. plate scale of the CFHT. As a result, this segment shows 7.4' x 5.1'.

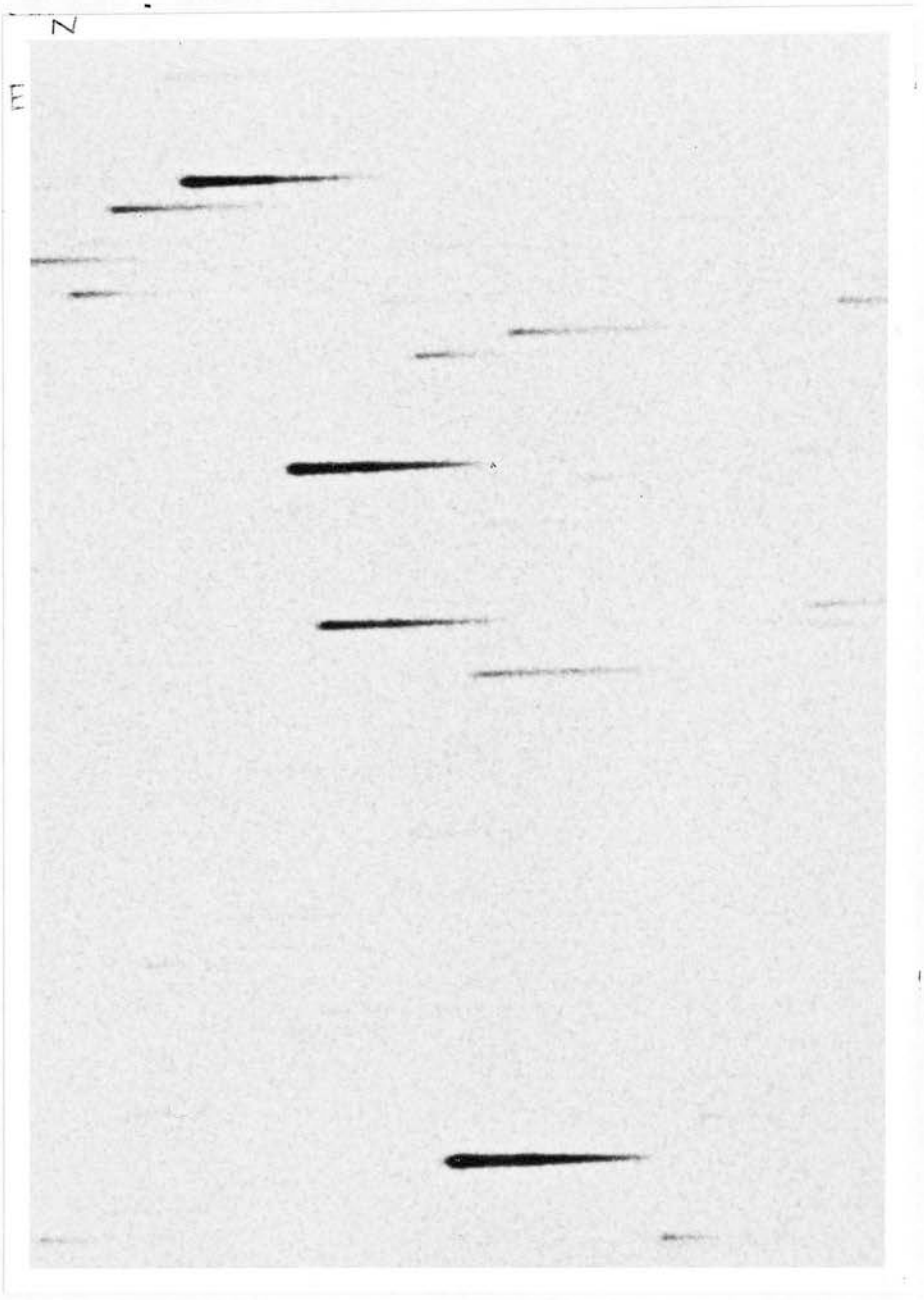

Plate 3.2 This plate shows the same area of sky as plate 3.1 It is taken from the UKSTU prism plate UJ5846P, magnified some 24.9 times to bring it to the same scale as plate 3.1 from the Schmidt plate scale of 67.14"/mm.

al. 1987), or else a direct plate from another instrument is used, and a software system is built to map the field distortions from one instrument to those of the other.

On consideration and inspection of the plate, I decided on the latter approach. This is because of several convenient factors in its favour: a system to discriminate between orders would have to be very sophisticated, as there is a considerable amount of overlap between order characteristics. For example, a strong emission line on a faint continuum may look very similar to a zeroth order image. A second order image can look very like a first order image, and amongst the brighter images, the zeroth, first and second order images can be connected by scattered light.

Also, the project already had excellent direct plate material in the field, of comparable depth, from the UK Schmidt telescope. An advantage of using such a plate is that because only the central square degree of a 36 square degree plate would be needed, the Schmidt data is essentially without field distortions over this small area. As a result, I used the centre of plate J9952, which visual inspection showed to be about the same depth as the grens plate.

The central part of the COSMOS IAM data was extracted and used. As has been mentioned before (in section 2.2), it is not possible to calibrate magnitudes from this plate (without great difficulty) because stars only two magnitudes above the plate limit are saturated, and there is a severe background variation across the plate caused by processing or hypersensitization error. However, this does not affect object location. This plate was used because it was the first very

deep plate obtained for the field from the UK Schmidt. As a result, if calibrated magnitudes are quoted for this survey, they are obtained by location of the object in the photometric survey (described in chapter 4).

3.2 Spectrum location: procedure.

All catalogue handling for the project was done using the HAGGIS database handling system, except for plotting programs and transformation programs mentioned here, which were written by the author to operate on HAGGIS catalogues.

The object must be to map all Schmidt plate objects onto the corresponding positions that they would have had, had they been through the grens without refraction. That is, the object is to find the zeroth order image positions for all objects, even though fainter objects have no zeroth order images. From here, the first order spectrum is easy to find, as the emulsion cutoff of IIIaJ (5380 Å) in the first order spectrum is just a linear offset from the zeroth order position, a distance measured by the grens designers to be 1522 μm to the wavelength cutoff at 5380 Å (Richardson, private communication, 1984).

First of all, as with a Schmidt prism plate, the grens plate was measured by the COSMOS measuring machine to produce mapping mode (MM) data, over the whole plate. The COSMOS step size was 16 μm, and the spot size was also 16 μm. This dataset is simply the raw

transmission value and pixel information as measured by the COSMOS machine. Then, the data were processed with the COSMOS analyser (Stobie, 1986) in order to obtain Image Analysis Mode (IAM) parameters (table 4.2 lists these parameters).

In order to connect the two datasets, the Schmidt X,Y position data was first transformed linearly to the CFHT plate scale: the Schmidt plate scale is 67.14"/mm. and the CFHT plate scale is ≈ 13.64"/mm., so the Schmidt X,Y positions were multiplied by 4.92.

The easiest objects to identify in the CFHT dataset are the zeroth order images, as they are a distinctly different shape from other images (round, rather than elongated) and they all have the same image profile (that of the seeing disk, apart from distortions from the optics). Thus, my strategy was to identify these images, so that they might be equated with the corresponding Schmidt image, allowing the plate distortions to be mapped. Firstly, a histogram of object ellipticities (actually UMINAX/UMAJAX), figure 3.1 shows that most objects are very elongated. Everything with ellipticities e > 0.6 were chosen, yielding a list of 482 objects. On visual inspection of objects in this list on the plate, only ≈ 50% proved to be genuine zeroth order images. The remainder were due to stray bits of scattered light, emulsion scratches (one of the analyser's faults is that it breaks very long objects into a succession of small images) and blemishes, and areas of extreme background variation. These last are produced when the background curvature is so great as to cause the COSMOS background measurement procedure (which assumes little background curvature over a scale length of < 128 pixels) to make mistakes. Thresholding then takes place using this badly estimated background,

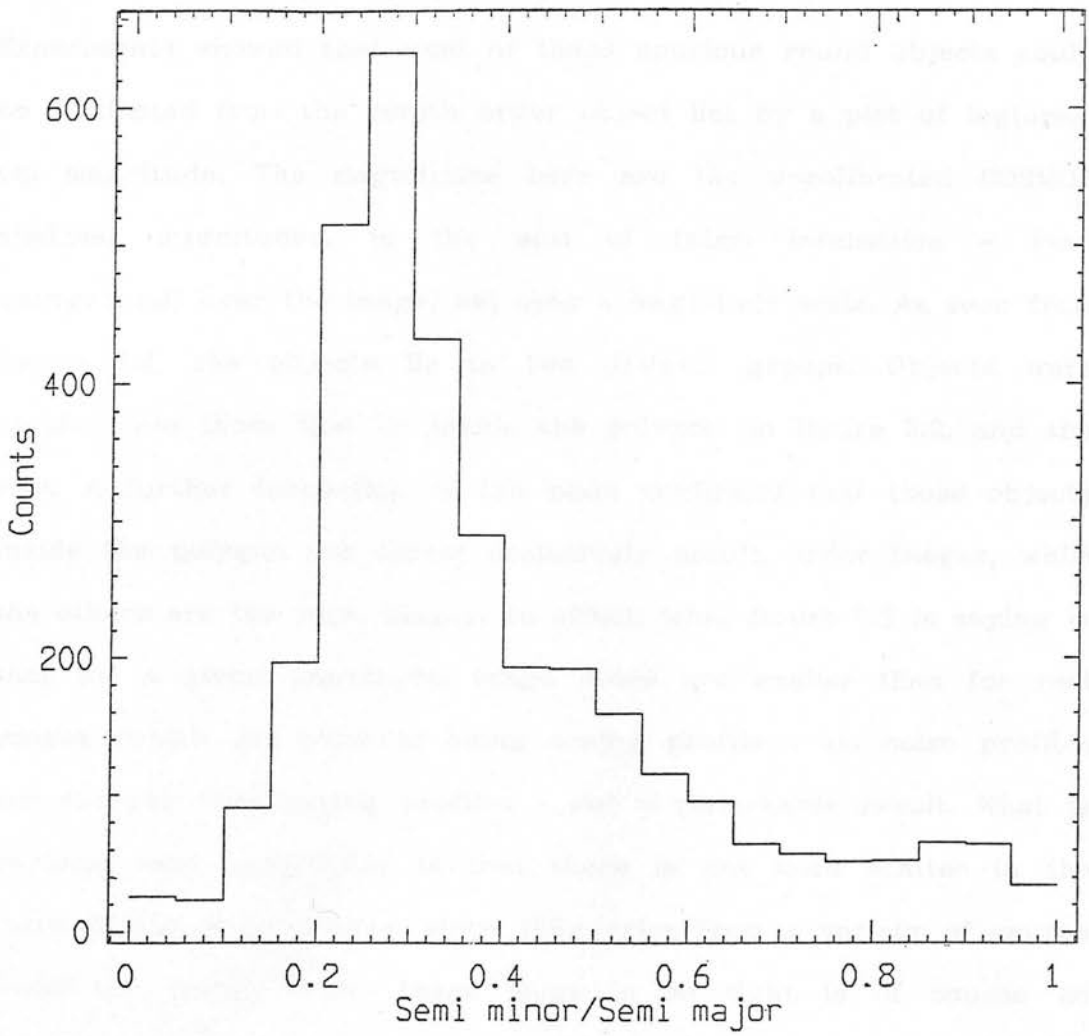

Fig 3.1 Object ellipticities on grens plate CFHT3057. All objects with $\frac{\text{semi-minor axis}}{\text{semi-major axis}} \geq 0.6$ were chosen as being the zeroth order images. Other more elongated objects contain the first and other order images.

and large numbers of sky noise peaks are identified as images. This effect is extremely localized, however, to the area around the step wedge and the guide probe.

Experiments showed that most of these spurious round objects could be eliminated from the zeroth order object list by a plot of log(area) vs. magnitude. The magnitudes here are the uncalibrated COSMOS analyser magnitudes, ie the sum of (pixel intensities - local background) over the image, set onto a magnitude scale. As seen from figure 3.2, the objects lie in two distinct groups. Objects were divided into those that lie inside the polygon on figure 3.2, and the rest. A further inspection of the plate confirmed that those objects inside the polygon are almost exclusively zeroth order images, while the others are the junk images. In effect, what figure 3.2 is saying is that for a given magnitude, image areas are smaller than for real images (which are close to being seeing profiles). Ie. noise profiles are sharper than seeing profiles - not a remarkable result. What is perhaps more remarkable is that there is not more scatter in the locus of the noise images, since they arise from a variety of causes (that the zeroth order image locus is so tight is of course no surprise). Be that as it may, a list of 224 zeroth order images was produced with positions spread evenly across the plate.

The next step was to match these objects to the corresponding objects in the Schmidt direct plate data set. Again, adopting a 'computational Occam's razor', I visually cross-identified some ten or so images, and after locating them in the two datasets calculated the average linear translation and rotation required for the (CFHT plate scale) Schmidt plate positions. This transformation was applied to all

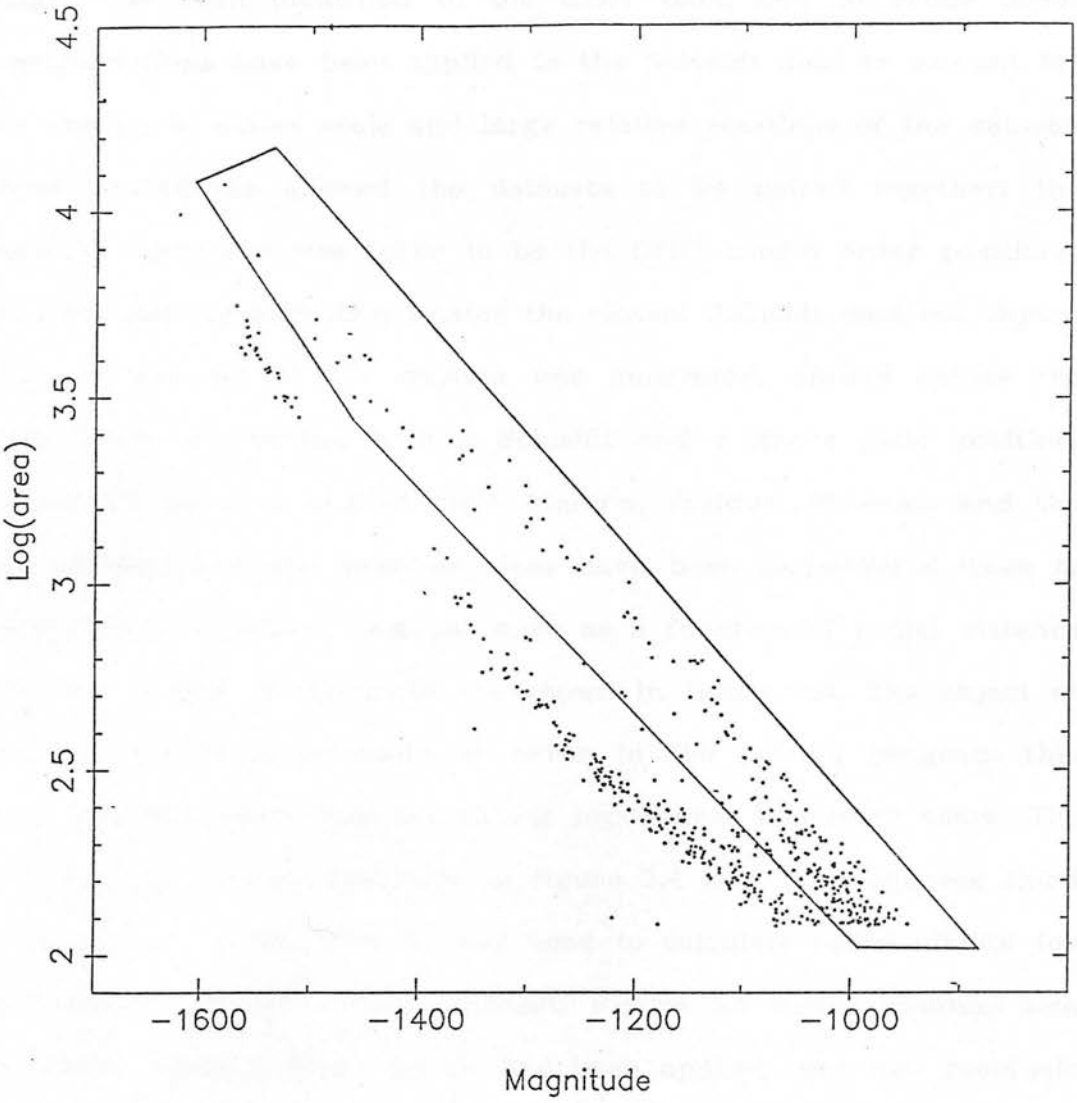

Fig 3.2 Plot of Log(area) as a function of magnitude, for all grens plate objects with $\frac{\text{semi-minor axis}}{\text{semi-major axis}} \geq 0.6$.
Inspection of the plate showed that objects within the polygon are zeroth order images. Others are junk images.

of the objects in the Schmidt data set.

To recap, then, the position so far is that a) a set of zeroth order images has been identified in the CFHT data, and b) crude linear transformations have been applied to the Schmidt data to account for the change in plates scale and large relative rotations of the dataset. These procedures allowed the datasets to be paired together: the 'master' object list was taken to be the CFHT zeroth order positions, then the pairing algorithm locates the closest Schmidt data set object. Thus a data set of 177 objects was generated, spread across the plate, each one having both a Schmidt and a grens plate position. Figure 3.3 shows a plot of plate location, residual direction and the size of the residuals (residual sizes have been magnified 8 times to make them visible),and residual sizes as a function of radial distance from the centre of the plate are shown in figure 3.4. The object at $X \approx 100$, $Y \approx 35$ is evidently an error in the pairing program: this point was eliminated from the fitting procedures discussed below. The line running through residuals in figure 3.4 is a least squares third order polynomial fit. This fit was used to calculate radial offsets for each member of the Schmidt dataset. Figure 3.5 shows residual size vs. radial distance after the fit had been applied, and new residuals are plotted in figure 3.6, this time magnified by 24 times. There is still plainly a 'pincushion' distortion, suggestive of a parabola. Another least squares fit was made, this time to a parabolic, and again each object in the Schmidt dataset was shifted according to its position, by the amount dictated by the fit. Once more, residuals are shown in figure 3.7 as a function of radial distance. The rms differences are now ≈ 0.03 mm, or ≈ 2 pixels. Although this procedure has not given an accurate emulsion cutoff position (2 pixels $\approx$ 60 Å),

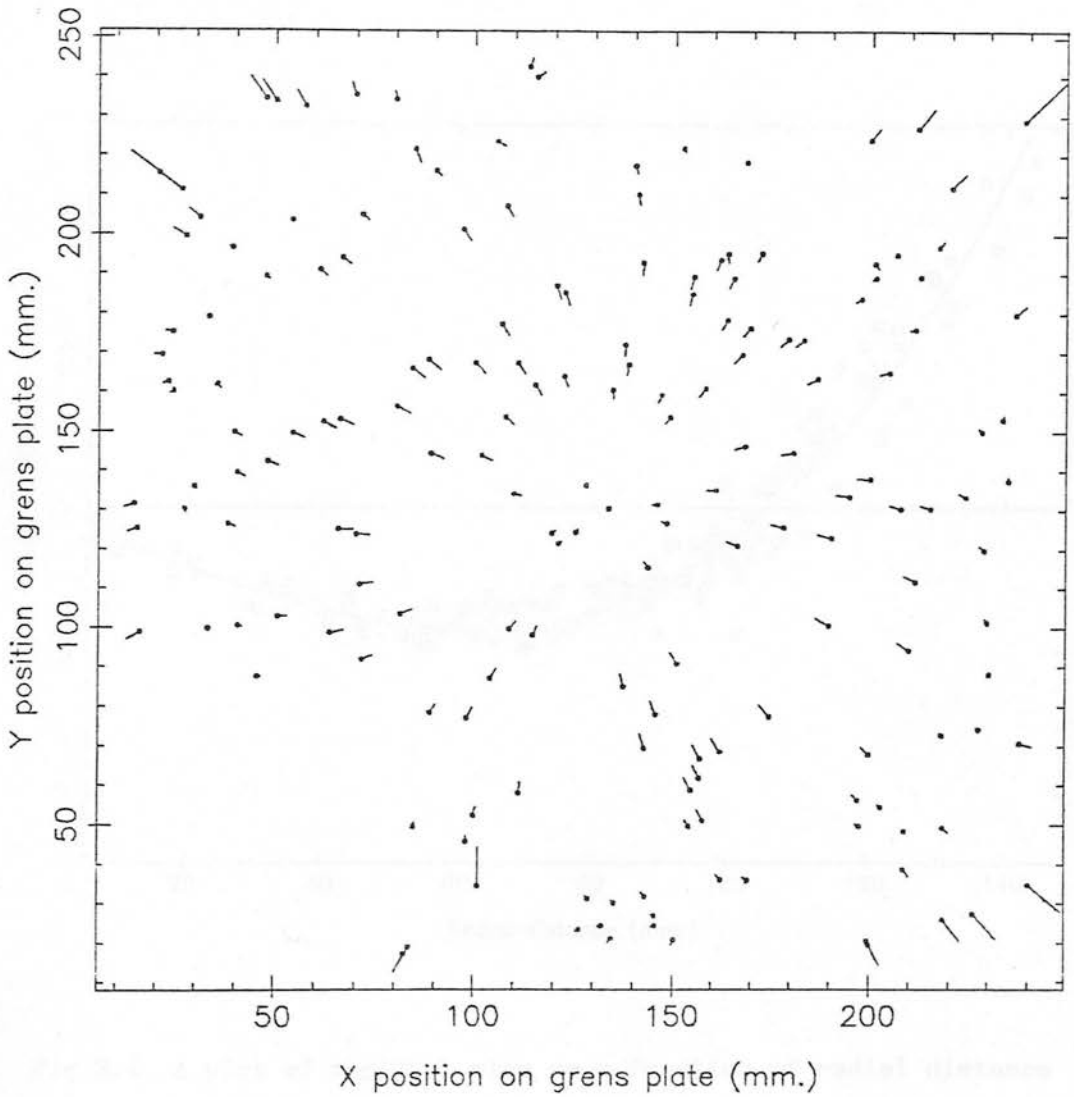

Fig 3.3 A plot of plate residual from the UKST plate position to the CFHT grens plate position as a function of position on the grens plate. Direct plate positions have been crudely corrected for the change in plate scale and different measurement orientations. Residual sizes are magnified 8 times. The bare area at lower left is the position of the step-wedge on the grens plate. Occaisional points not following the typical local are bad pairs.

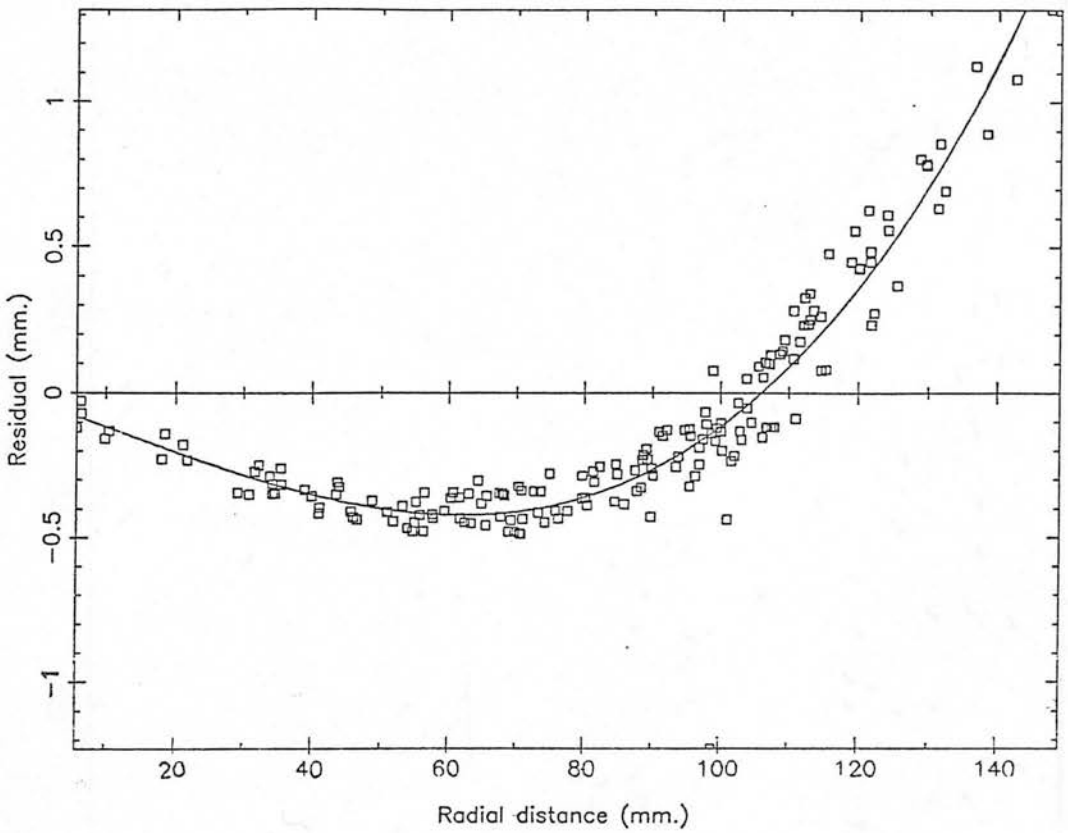

Fig 3.4 A plot of residual size as a function of radial distance from the centre of the plate. Line fitted is the least squares best fit 3rd order polynomial. Radial corrections on the direct plate could be calculated from this fit, and were applied to all objects.

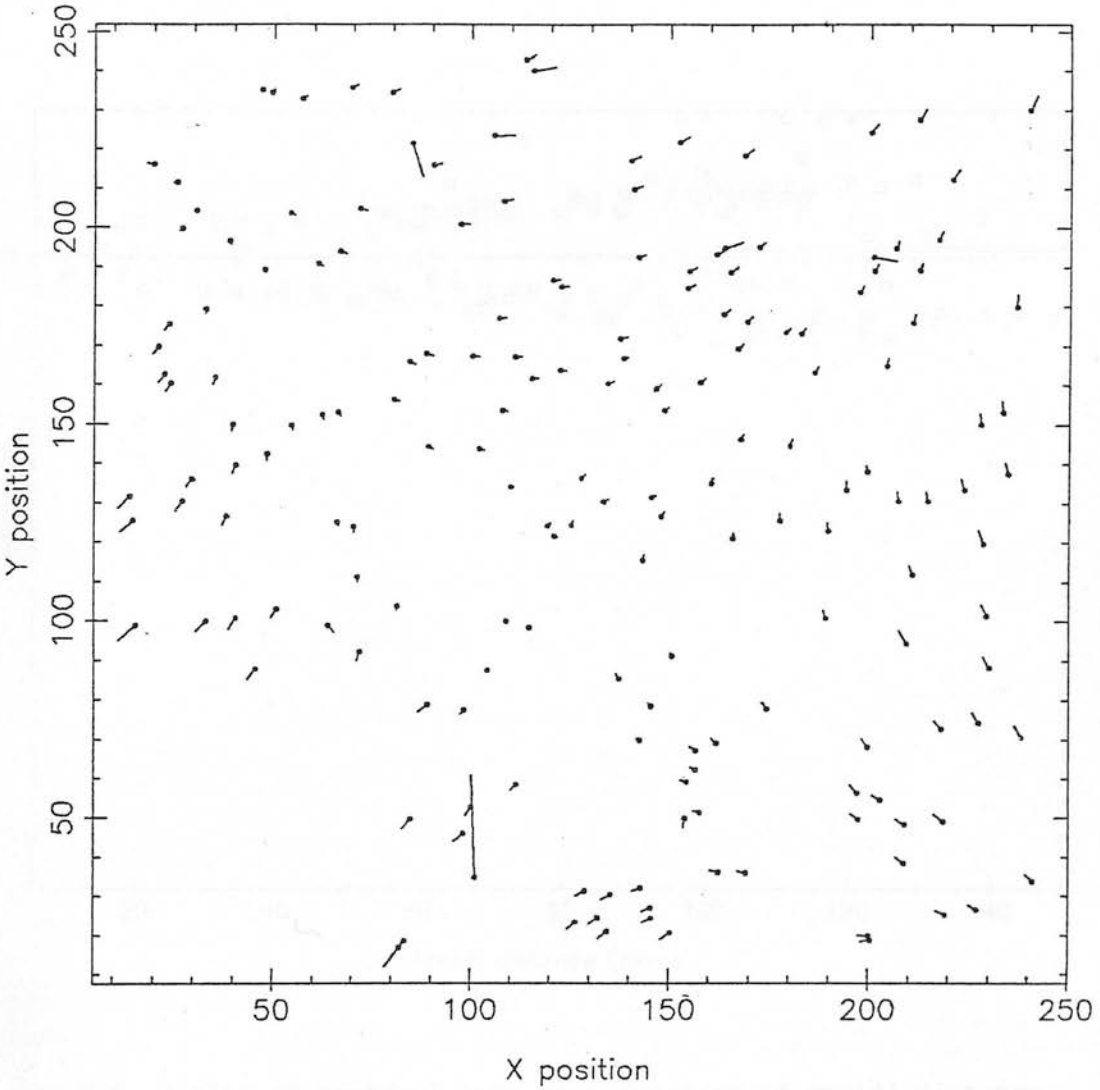

Fig 3.5 A plot of plate residual from the UKST plate position to the CFHT grens plate position as a function of plate position, after radial transformation of the UKST positions. Residual sizes are magnified 24 times As in fig 3.3, points not following typical local are bad pairs.

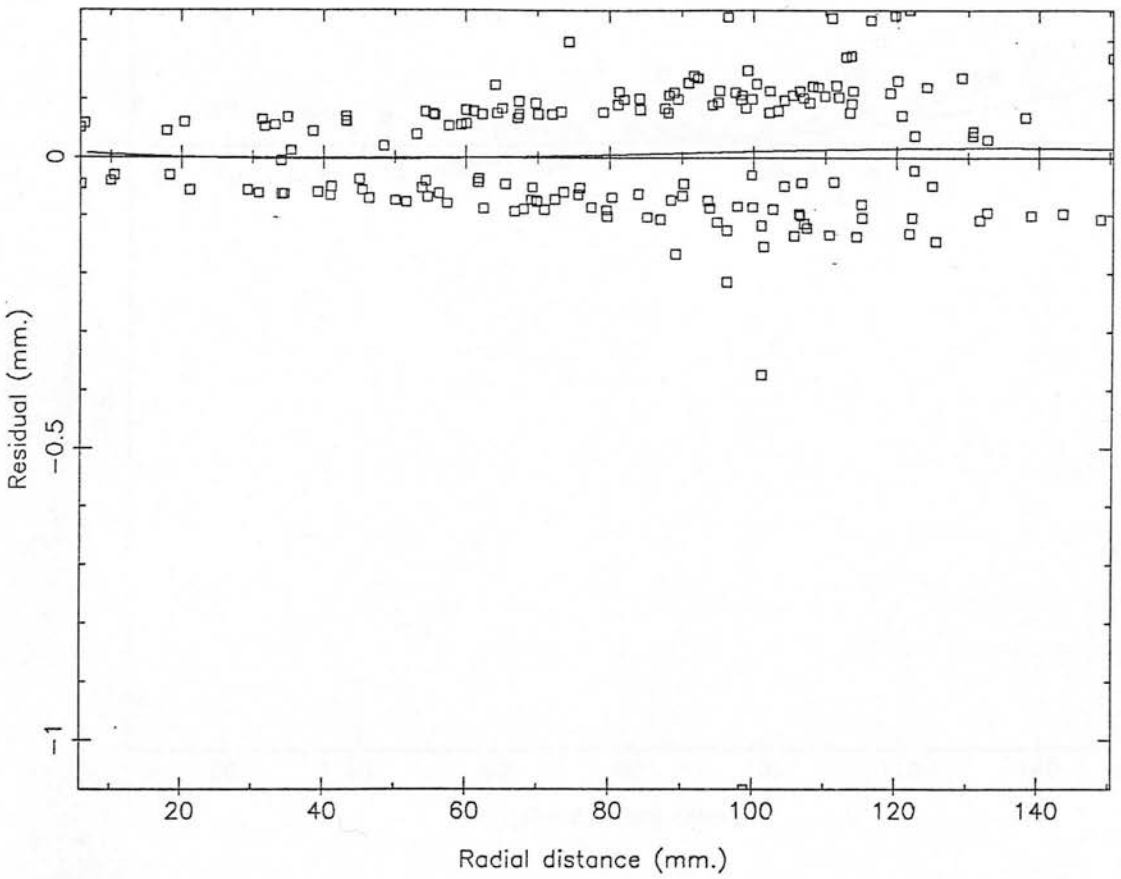

Fig 3.6 A plot of residual size as a function of radial distance from the centre of the grens plate, after the best fit 3rd order polynomial had been applied.

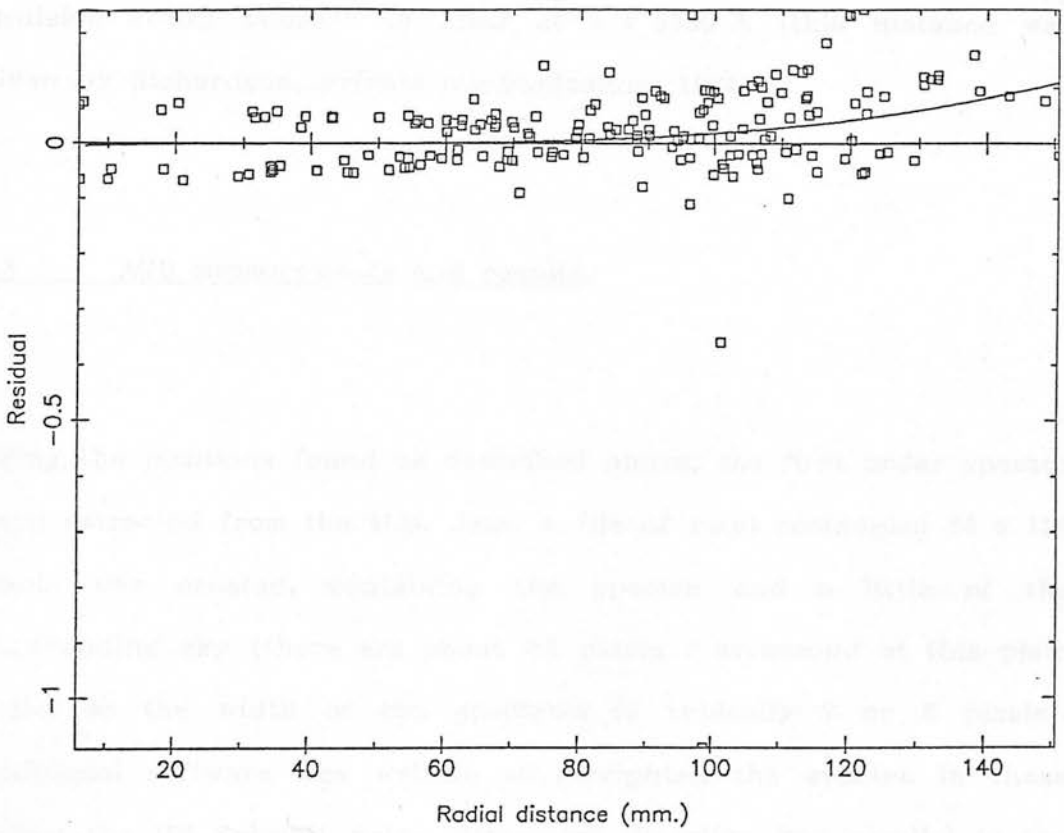

Fig 3.7 A plot of residual size as a function of radial distance from the centre of the grens plate after applying a least squares best fit to the direct plate dataset.

it is sufficiently accurate to locate the first order spectra. This was judged to be of sufficient accuracy, because AQD does not require an accuracy greater than this in order to work. The final positional transformation, then, was just the 144 pixel = 2304 μm required to move in the dispersion direction from the zeroth order image to the emulsion cutoff position of IIIaJ at λ = 5380 Å (this distance was given by Richardson, private communication, 1984).

3.3 AQD measurements and results.

Using the positions found as described above, the first order spectra were extracted from the M.M. data. A file of pixel rectangles 24 x 128 pixels was created, containing the spectra and a little of the surrounding sky (there are about 4.6 pixels / arcsecond at this plate scale, so the width of the spectrum is typically 7 or 8 pixels). Additional software was written to straighten the spectra in these boxes: the UK Schmidt prism dispersion direction lies parallel to the plate edge, but this is not true for the CFHT grens, and spectra may be up to 5° away from being parallel to the plates' edge.

This data was then run through the AQD software (described in section 2.2), looking for emission lines and a red excess (the software fits a continuum from the emulsion cutoff position, so if there is an emission line close to the cutoff, it will not be found. It can, however, be found by placing a synthetic filter just short of the cutoff, and creating a 'red excess' colour with another filter further down the spectrum).

A total of 112 candidates were inspected by eye on the grens and direct plates to weed out visually obvious galaxies, emulsion blemishes and overlaps (as well as quasars which had already been identified). This left a total of 76 spectra, which are shown in figure 3.8.

A total of 5 quasars were already known in the field of the grens (see table 2.3): all except one (lost in the scattered light from a bright star) were relocated in the grens survey, and are included in figure 3.8 - quasars with slit spectra have a dot next to the identification number.

Photometry for the survey has become available from the photometric survey (chapter 4). In order to obtain photometry for the faintest possible objects in the survey, the deepest J plate (J10128) was used, which has been calibrated to $B_J = 21.3$. A histogram of the magnitudes of survey candidates is presented in figure 3.9. In this figure, objects fainter than the limit of J10128 are given the bright limit of $B_J = 21.3$.

3.4 Reducing ESO spectroscopy.

In this section, I describe spectroscopic data taken during an observing run in February, 1986, the methods employed to reduce the data and the results obtained.

Three nights of observing time were awarded by the European Southern Observatory in collaboration with S. D'Odorico to obtain

10 41 24.774 04 50 25.80

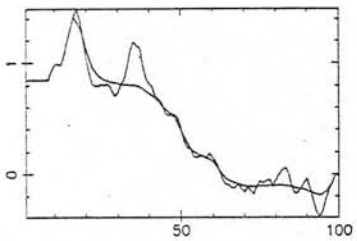

453 Fig 3.8.1

10 41 22.964 04 37 55.16

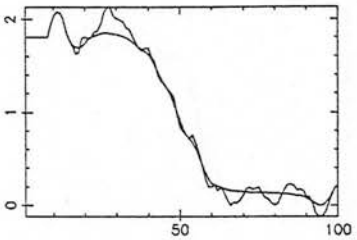

602 Fig 3.8.2

10 41 21.784 04 46 05.39

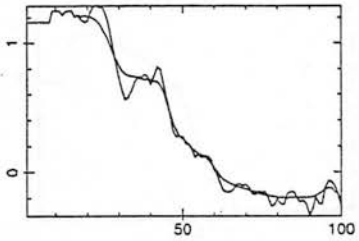

625 Fig 3.8.3

10 41 22.194 04 54 10.22

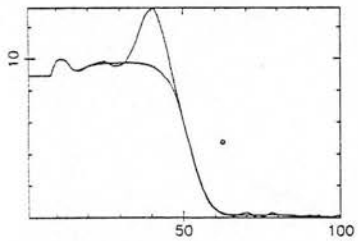

•663 Fig 3.8.4

10 41 07.349 04 37 42.19

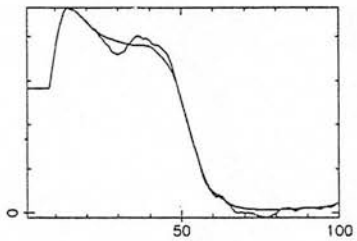

786 Fig 3.8.5

10 41 13.457 04 57 23.86

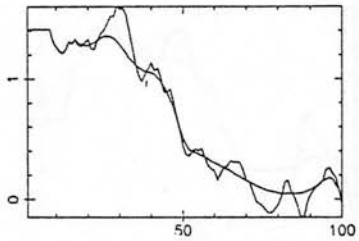

836 Fig 3.8.6

10 41 03.434 05 02 29.30

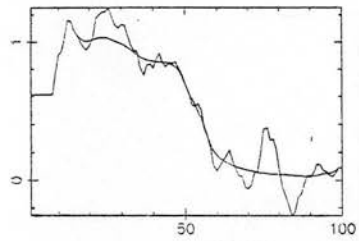

1105 Fig 3.8.7

10 41 03.985 05 03 24.08

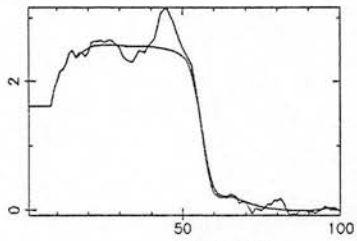

1107 Fig 3.8.8

10 40 48.098 04 38 02.82

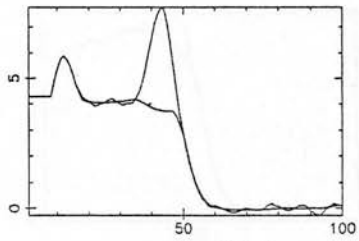

•1318 Fig 3.8.9

10 40 51.068 04 39 47.22

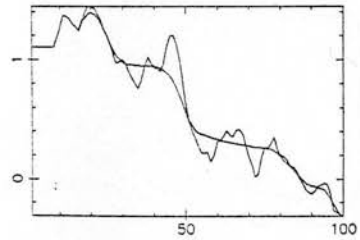

1320 Fig. 3.8.10

10 40 50.416 04 43 30.67

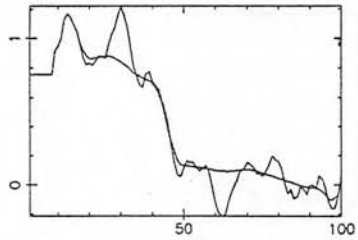

1329 Fig 3.8.11

10 40 39.174 04 50 17.76

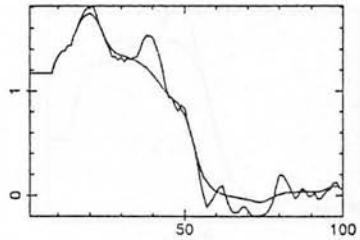

1691 Fig 3.8.12

10 40 37.547 04 53 20.77

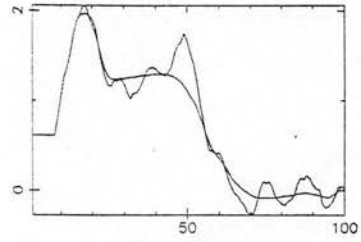

1701 Fig 3.8.13

10 40 41.049 04 56 52.18

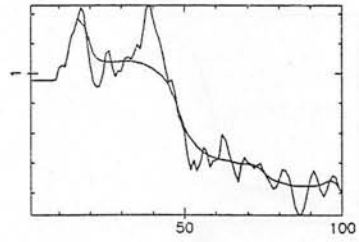

1730 Fig 3.8.14

10 40 34.203 04 36 53.45

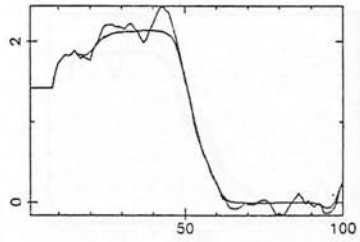

1946 Fig 3.8.15

Fig 3.8 One dimensional plots of the grens plate candidates, located by AQD. Plate dispersion is linear, with λ=5380Å cutoff at the lefthand end and λ decreasing to the right. Dispersion is roughly linear at 2000Å / mm., so pixel 50 = 4100Å. Number left of fig. number is object id. Id's underlined were observed at ESO (cf. figs 3.10 - 3.33). Id's with dot are quasars.

10 40 36.570 04 43 03.93

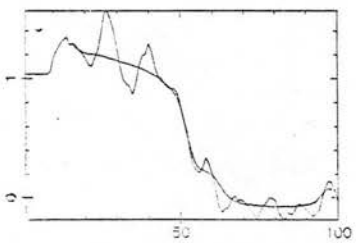

1984 **Fig 3.8.16**

10 40 33.944 04 59 23.81

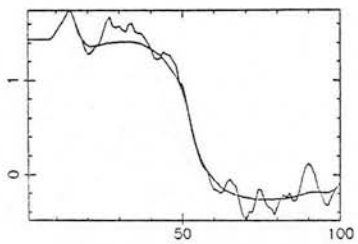

2091 **Fig 3.8.17**

10 40 24.984 04 48 24.74

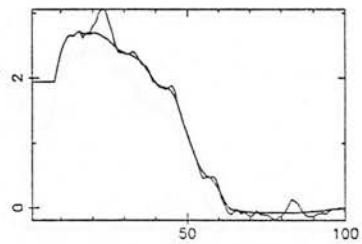

2281 **Fig 3.8.18**

10 40 26.509 05 08 07.55

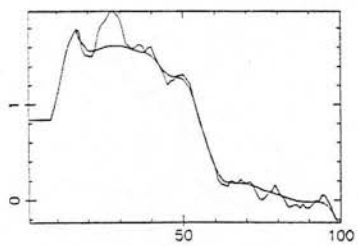

2357 **Fig 3.8.19**

10 40 11.546 05 04 23.03

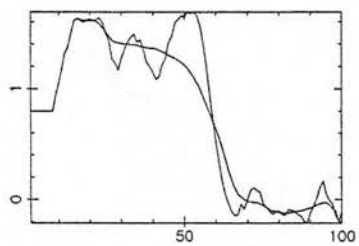

2528 **Fig 3.8.20**

10 40 18.296 05 11 04.81

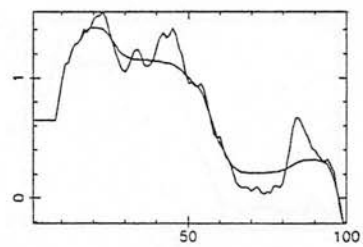

2540 **Fig 3.8.21**

10 40 10.077 05 16 20.04

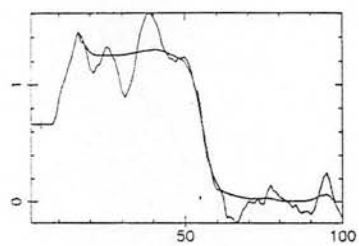

2556 **Fig 3.8.22**

10 40 10.264 05 18 03.59

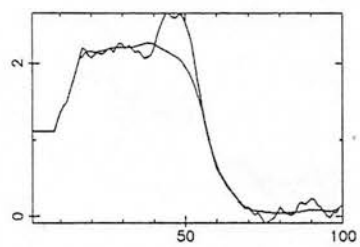

2562 **Fig 3.8.23**

10 40 08.697 04 37 07.72

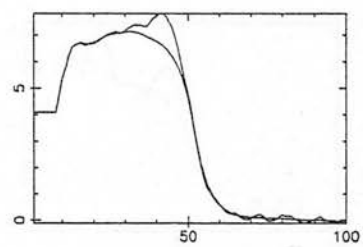

2628 **Fig 3.8.24**

10 40 02.569 04 47 45.15

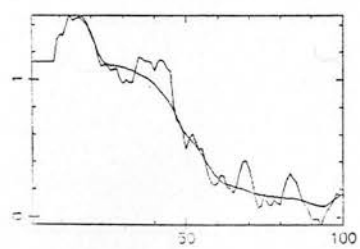

2660 **Fig 3.8.25**

10 40 03.838 04 51 24.34

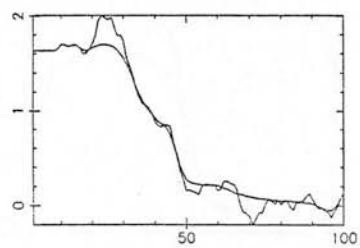

2676 **Fig 3.8.26**

10 40 02.572 04 56 12.29

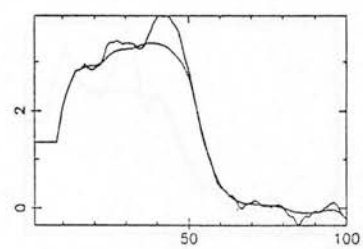

2693 **Fig 3.8.27**

10 40 03.140 05 08 59.09

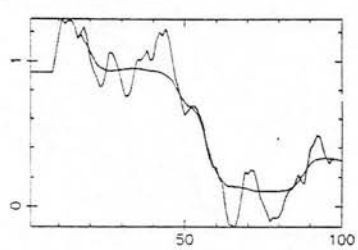

2769 **Fig 3.8.28**

10 40 02.887 05 16 09.09

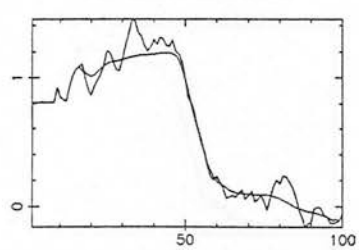

2794 **Fig 3.8.29**

10 40 05.989 05 17 28.33

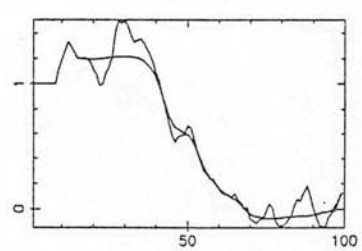

2802 **Fig 3.8.30**

Fig 3.8 (continued).

10 39 55.940 04 38 08.58

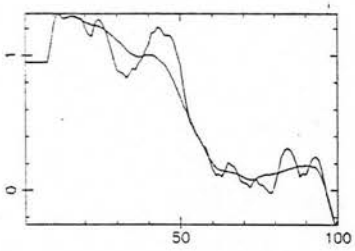

2864 **Fig 3.8.31**

10 39 53.776 05 02 09.03

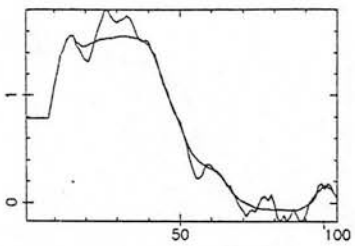

2942 **Fig 3.8.32**

10 39 59.137 05 09 10.72

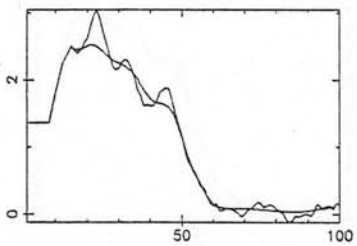

2964 **Fig 3.8.33**

10 39 57.294 05 16 55.57

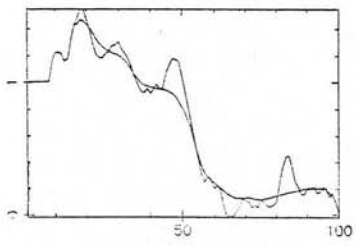

2992 **Fig 3.8.34**

10 39 57.261 05 20 13.49

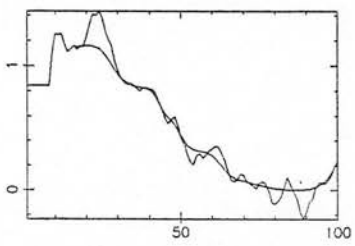

3005 **Fig 3.8.35**

10 39 50.206 04 42 54.21

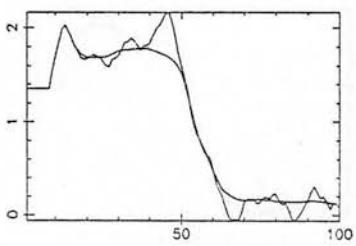

• 3074 **Fig 3.8.36**

10 39 43.184 05 09 37.96

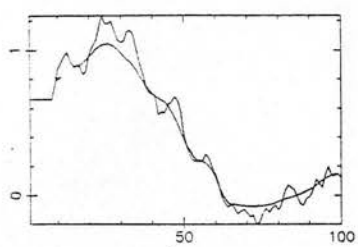

3151 **Fig 3.8.37**

10 39 44.344 05 10 48.86

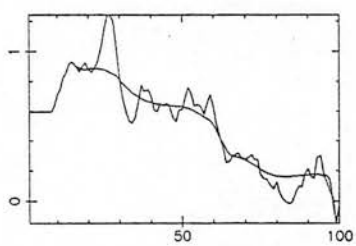

3155 **Fig 3.8.38**

10 39 41.951 05 12 06.87

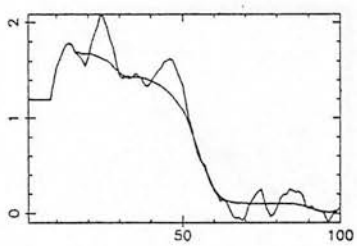

3160 **Fig 3.8.39**

10 39 36.886 04 41 43.88

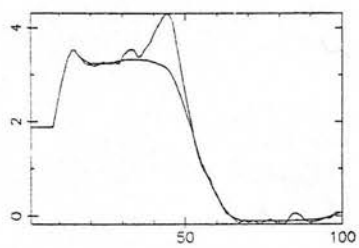

• 3283 Fig 3.8.40

10 39 41.305 04 47 30.50

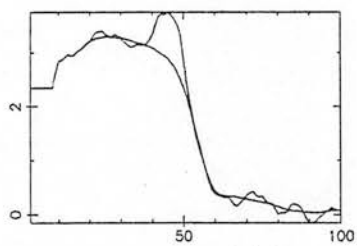

• 3302 Fig 3.8.41

10 39 40.623 04 52 18.24

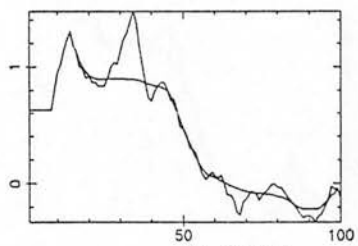

3309 Fig 3.8.42

10 39 38.643 04 55 15.17

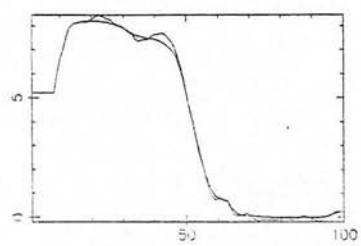

3321 Fig 3.8.43

10 39 40.036 05 18 35.06

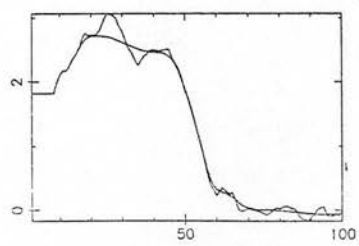

3380 Fig 3.8.44

10 39 32.192 04 50 37.50

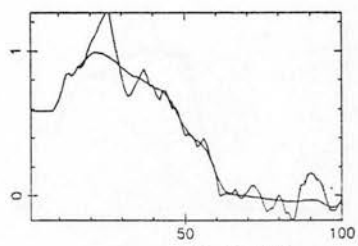

3466 Fig 3.8.45

Fig 3.8 (continued).

10 39 31.430 04 54 20.48

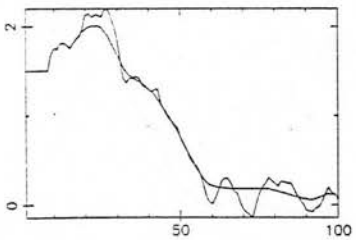

3472 Fig 3.8.46

10 39 24.322 04 57 36.94

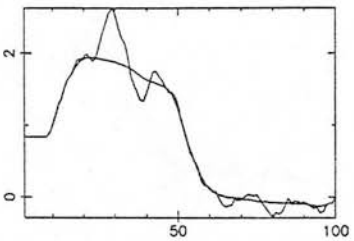

•3481 Fig 3.8.47

10 39 30.188 05 16 54.77

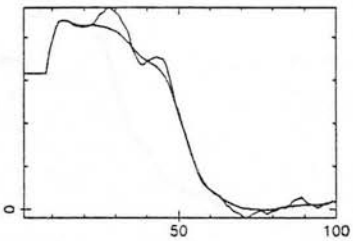

3547 Fig 3.8.49

10 39 25.853 05 18 33.71

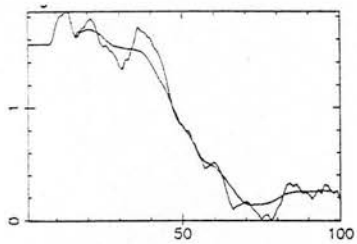

3552 Fig 3.8.50

10 39 16.431 04 55 40.32

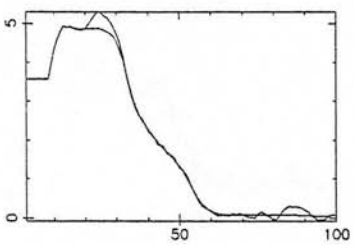

3667 Fig 3.8.51

10 39 15.120 04 59 15.52

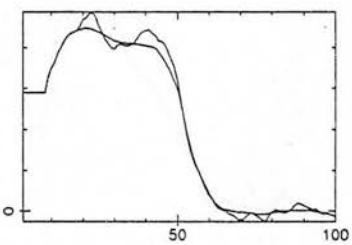

•3681 Fig 3.8.52

10 39 22.657 05 06 02.92

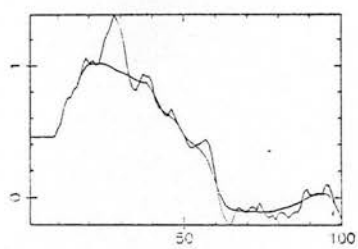

3707 Fig 3.8.53

10 39 19.231 05 11 19.77

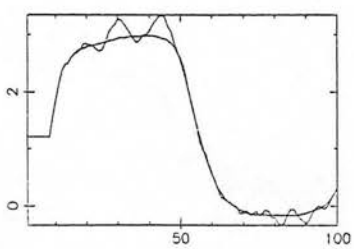

3720 Fig 3.8.54

10 39 17.464 05 17 44.14

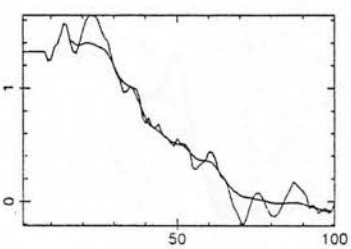

3741 Fig 3.8.55

10 39 17.297 05 17 52.92

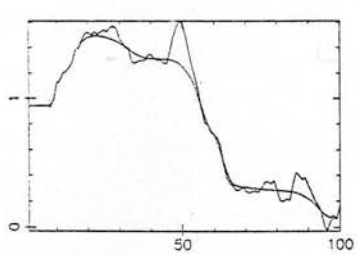

3742 Fig 3.8.56

10 39 11.520 04 36 43.80

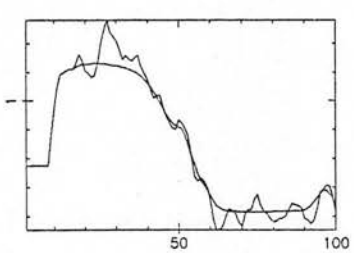

3799 Fig 3.8.57

10 39 05.933 04 39 40.09

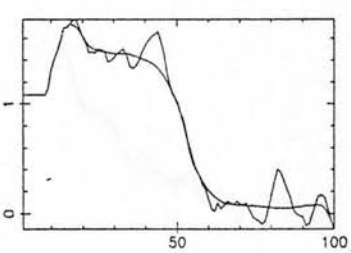

3822 Fig 3.8.58

10 39 07.615 04 46 10.60

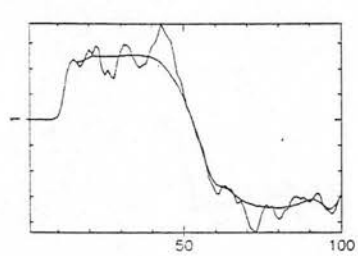

3849 Fig 3.8.59

10 39 07.684 05 03 31.32

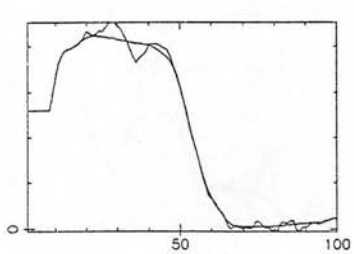

•3915 Fig 3.8.60

10 38 59.655 05 01 47.06

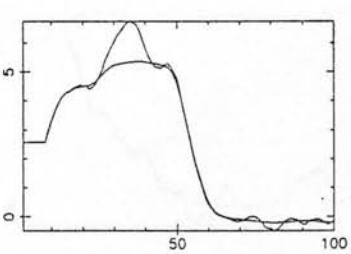

•4096 Fig 3.8.61

Fig 3.8 (continued).

10 38 55.813 05 11 27.00

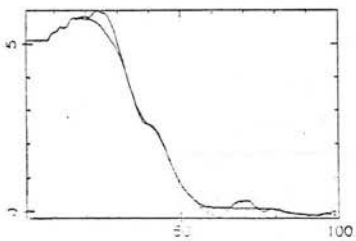

4121 Fig 3.8.62

10 39 01.219 05 13 59.20

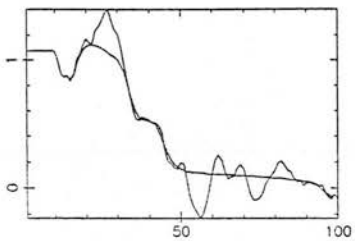

4127 Fig 3.8.63

10 38 58.032 05 15 42.71

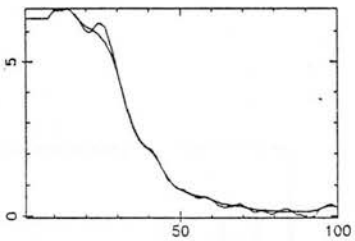

4128 Fig 3.8.64

10 39 02.576 05 17 57.91

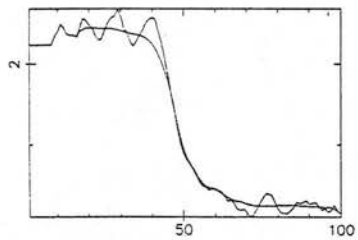

4139 Fig 3.8.65

10 38 55.209 05 10 50.22

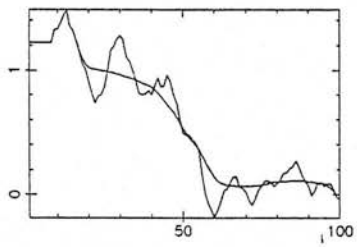

4292 Fig 3.8.66

10 38 45.544 04 38 16.31

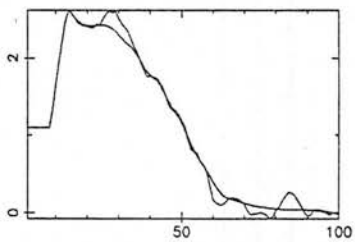

4379 Fig 3.8.67

10 38 44.951 04 44 08.13

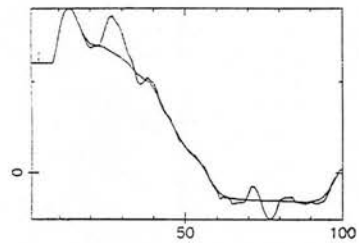

4395 Fig 3.8.68

10 38 37.689 05 03 52.98

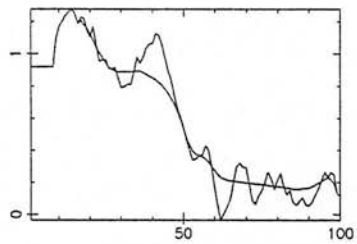

4457 Fig 3.8.69

10 38 45.095 05 14 38.90

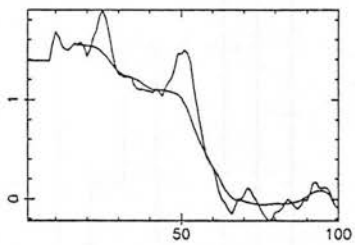

4494 Fig 3.8.70

10 38 34.660 04 44 18.38

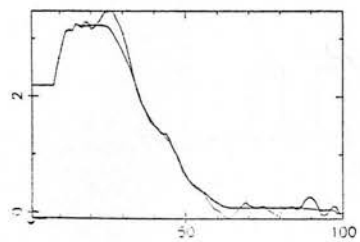

4582 Fig 3.8.71

10 41 11.100 04 40 05.25

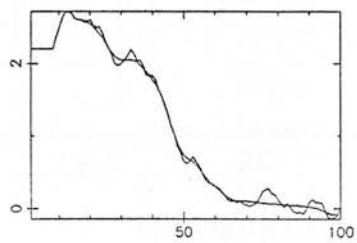

792 Fig 3.8.72

10 40 59.622 04 49 14.83

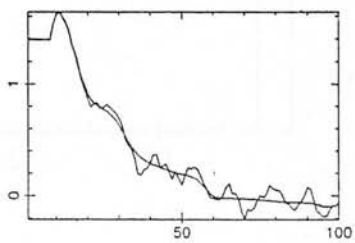

1042 Fig 3.8.73

10 40 00.464 05 07 37.02

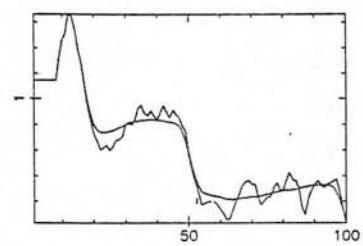

• 2765 Fig 3.8.74

10 39 29.096 04 50 28.33

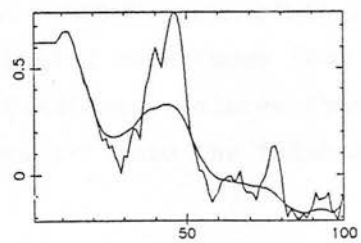

3465 Fig 3.8.75

10 38 41.128 05 14 52.63

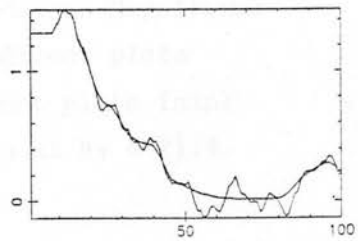

4496 Fig 3.8.76

Fig 3.8 (continued).

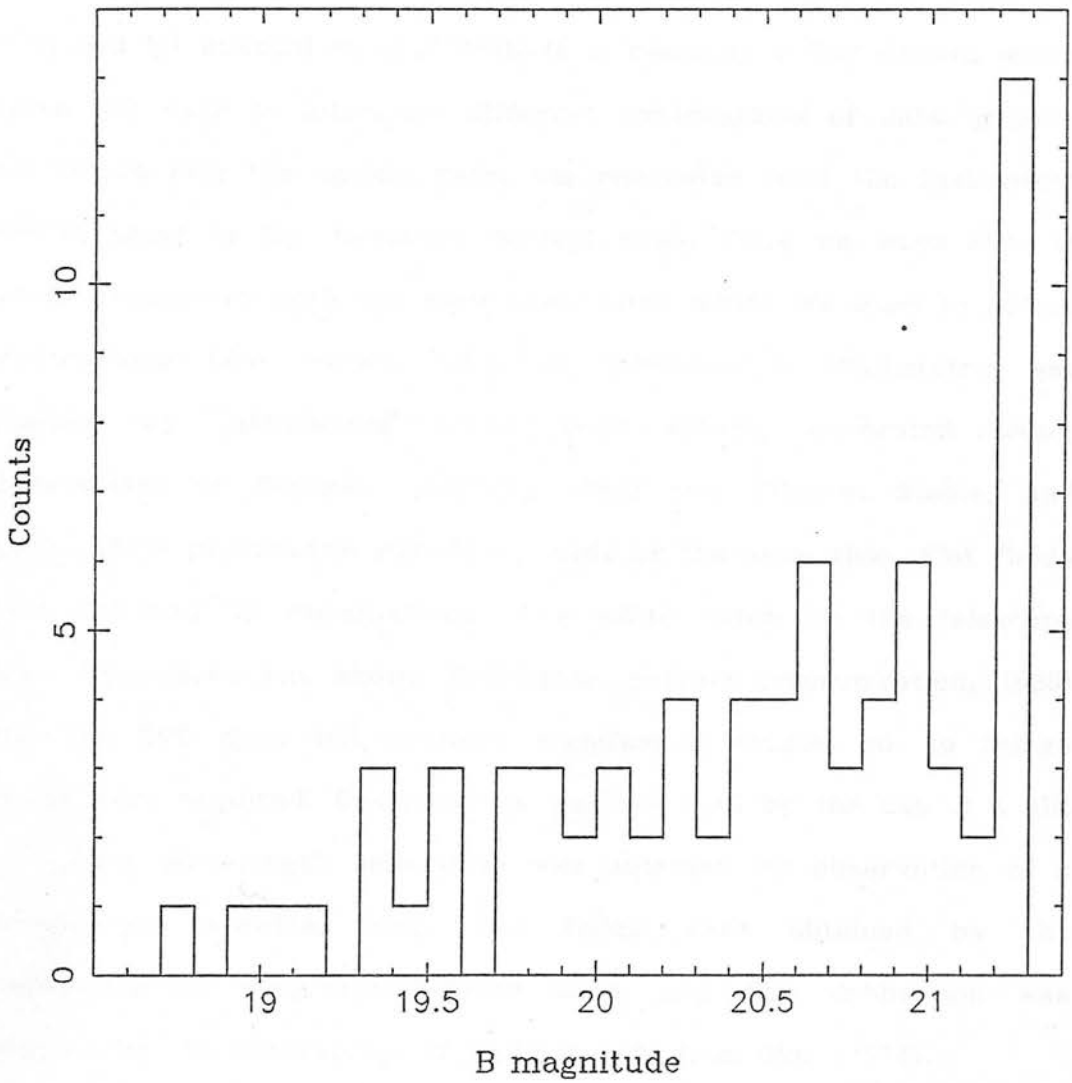

Fig 3.9 Histogram of CFHT grens plate candidates. Magnitudes are calibrated magnitudes from UKS direct plate J10063. Candidates fainter than direct plate faint limit were put into the faintest bin at B_J = 21.4.

spectroscopy of the candidates selected from the grens survey. The time was on the ESO 3.6m telescope at La Silla, Chile. The instrument used for spectroscopy was the recently developed EFOSC (ESO Faint Object Spectrograph and Camera) CCD camera. This instrument is described by Buzzoni *et al.* (1985). It is basically a CCD camera which allows the user to introduce different combinations of slits, grisms, and filters into the optical path, via commands from the instrument control panel in the telescope control room. Thus we were able to obtain photometry with the same instrument which we used to obtain spectroscopy (see section 4.6.4, on photometry). Photometry was obtained by introducing broad band filters, calibrated using observations of E-region (Graham, 1982) and Gilmore, Stobie, and Sagar (1985) photometric standards made at the same time. Flat fields were obtained by observations of a white patch on the telescope dome. Experience has shown (D'Odorico, private communication, 1986) that the CCD does not produce significant fringes, so no fringe frames were required. Spectroscopy was obtained by the use of a slit and grism. Wavelength calibration was obtained by observation of a helium/argon spectral lamp, flat fields were obtained by the observation of a quartz halogen lamp, and flux calibration was obtained by the observation of white dwarfs from Oke, (1974).

The slit/grism combination used was a 1.5" slit with the B1000 grism: this is a low dispersion (850 A/mm) grism sensitive from 3600 A - 8000 A. The camera pixel size is 30 μ (= 0.675"), so a slit width of 1.5" (chosen because seeing is typically 1" at La Silla) corresponds to $\simeq$ 2.5 pixels. Resolution, therefore is $\simeq$ 65 A (= 850 x 0.03 x 2.5).

This low resolution was judged to be the best compromise in obtaining as many observations from the run as possible, while still allowing identification of spectral features, and the calculation of quasar redshifts.

Objects were selected for observation on a 'next closest object' basis (because the ESO 3.6m can offset small distances very accurately), in order that we should observe as many candidates as possible. Integration times were kept to 600 seconds for all objects, yielding a signal to noise of ≈ 5 for object 9 (one of the faintest objects in the survey) - adequate for identification of spectral features and redshift calculation.

A total of 26 objects were observed, out of a total of 61 in the survey. 6 objects are quasars, 4 are narrow lined objects with spectra typical of LINERS or Seyfert II galaxies, 13 are galactic stars, and 3 remain unidentified at this low resolution.

3.4.1 Spectral reduction.

All spectra were reduced using the STARLINK FIGARO spectral reduction package. The procedure followed for the reduction of all spectra was the following:

- The raw data frame was subtracted of the principally DC bias component added electronically to the CCD image.
- Any cosmic ray events were removed from the frame by interpolation perpendicular to the dispersion direction. Single or double bad pixels were thus removed, and no other blemishes were

found on the frame close to the spectrum (there is a bad line caused by a dead readout pixel in the CCD, but it is parallel to the dispersion direction and close to the edge of the frame, so it could safely be ignored).

- Experiments showed that flat fielding was not necessary. After flux calibration, a spectrum that had been flat fielded was identical within the noise to the same spectrum that had not been flat fielded. The difference is that the instrument sensitivity function defined to flux calibrate the spectrum in the un-flat fielded case has the CCD flat field component convolved with the actual instrument sensitivity.

- Spectra were then extracted from the 2-d frames, and sky subtracted. This was done by first extracting a segment of the frame perpendicular to the dispersion direction. This cross section could be used to find the location of both edges of the spectrum, and to determine which parts of the slit were suitable for use in sky subtraction (occasionally, faint objects accidentally fell on the slit). Thus, the spectrum was extracted from the frame by adding all rows perpendicular to the dispersion between spectrum edges. Two sky spectra were also obtained for each spectrum, one from either side of the spectrum, as close as possible without including light from the object or another faint object. The sky spectra were added, and the composite sky spectrum (after normalizing to the amount of sky flux per row in the object spectrum) was subtracted from the object spectrum. Normally, no residual sky emission features were visible in the object spectrum.

- Next, the spectrum was wavelength calibrated. This was done using calibration observations of a helium/argon discharge tube. The helium/argon line centres were fitted with a fifth order polynomial to the actual (laboratory) line wavelengths. The polynomial thus derived

was used to rebin the object spectra, such that the resultant spectrum was in bins of equal wavelength and flux is conserved. Using this polynomial to rebin the arc line spectrum itself, gave a fit to lab. values with rms errors < 1 Å for 14 lines fitted between 3800 Å and 9600 Å. More than one calibration spectra were taken during the observations, but polynomial fits were found to be virtually identical, and so only one was used for all spectra. This is reasonable, since the usual cause of wavelength calibration variations is thermal variations in an imaging tube - which of course has little bearing on a cooled CCD camera.

- Spectra were corrected for atmospheric effects using atmospheric extinction measurements made at ESO. At the same time, airmass correction was performed.

- Flux calibration was only carried out on interesting (ie. emission line) objects. It was carried out using observations of white dwarf calibration stars (Oke, 1974). A synthetic spectrum of the calibration star was created from Oke's published data. This was used to define an instrumental response function, by comparison with the observations made at the telescope. The object spectrum is then calibrated by multiplying it by the instrumental response. Tests (performed by using the instrumental response defined from one standard to calibrate observations of another, which was then compared to its published spectrum) showed that a), flat fielding the original frame made no difference to the calibrated output - the instrumental response function is modified - and b) because the grism efficiency is falling rapidly at wavelengths longer than ≃ 7000 Å, signal to noise of spectra become extremely poor at these wavelengths, and so object spectra were clipped above this value.

- Finally, an attempt was made to correct the spectra of interesting

(again, emission- line) objects for the effects of atmospheric absorption, as there were lines seen in the red ends of all spectra. The method used was to interpolate across these features in the spectrum of an object whose spectrum is known to be flat in this wavelength regime (in this case an early star). The interpolated spectrum is then divided by the original stellar spectrum, yielding a spectrum which is 1.0 everywhere except where the absorption lines occur. This coefficient spectrum is used to multiply the object spectrum. Unfortunately, because the sensitivity of the grism is changing rapidly towards the red end, this correction procedure was not completely satisfactory. As a result, atmospheric absorption features can still be seen in some spectra.

3.5 Results of ESO spectroscopy.

As has been mentioned before in section 3.3, objects were selected from the grens plate on the naive assumption that selection criteria would be similar to those of the UK Schmidt prism plates. This assumption was necessary because I had had no previous experience of spectral classification using this instrument, and none was readily obtainable within Britain. In particular, this is the first attempted implementation of a machine search of such plates. There are, however, significant differences between grens and prism, such as the absence of ultraviolet on the grens plates, the linear dispersion, and the difference in plate scales. Although it is obvious that these differences exist, it was less clear before the search how these effects might modify search criteria. As a result, the similar search

criteria used (barely modified from prism plate searches) produced a high contamination rate in the selected sample. This would be easy to reduce in further spectra of grens selected samples using the slit spectra obtained for this thesis.

It is not likely that the completeness rate of the sample will be affected by this effect, as objects were preferentially included rather than rejected, as it was appreciated that the effect would be at work (the selection criterion and sample are discussed in more detail in section 3.3).

However, for efficient use of the telescope time, candidates were classified into self-similar groups, so that if several members of a group proved to be objects of one type, other members of the group could be treated accordingly (ie. dropped from the candidate list if they turned out to be galactic stars). Otherwise, candidates were observed on a next nearest basis, as it was found that offsetting the telescope over short distances was extremely accurate, and no additional tweaking of positions was required.

A list of objects is given in table 3.1, and grens spectra are shown with the appropriate EFOSC spectrum in figures 3.10 - 3.35. Object 1329 is not included in these figures because an unfortunate data corruption means that only an uncalibrated spectrum of the object still exists. It is a flat, featureless spectrum and thus the feature seen on the grens spectrum, figure 3.8.11 must be dirt on the plate. As is easily noticed (object 2281, figures 3.8.88 and 3.18), plate defects can appear to be convincing emission lines in a grens spectrum. This could be avoided with the use of two cross dispersed

Table 3.1: Results of ESO spectroscopy.

I.D.	RA (1950)	Dec (1950)	B_J	remarks
453	10 41 24.8	+4 50 26	20.95	unidentified - narrow lines?
602	10 41 23.0	+4 37 55	20.67	star - none
1042	10 40 59.6	+4 49 15	21.14	star - none
1320	10 40 51.1	+4 39 47	20.77	LINER/SyII (0.26)-[OII],Hβ, [OIII],Hα
1329	10 40 50.4	+4 43 31	21.26	star - none
1691	10 40 39.2	+4 50 18	20.48	HII/stbst (0.13) - [OII],HB, [OIII],Hα
1946	10 40 34.2	+4 36 53	20.18	star B0 - A. Hβ,Hα
2281	10 40 25.0	+4 48 25	20.01	unidentified
2660	10 40 2.6	+4 47 45	21.25	star - none
2676	10 40 3.8	+4 51 24	20.82	star M1 - A. TiO
2693	10 40 2.6	+4 56 12	19.90	star early - A. Hγ,Hβ
2864	10 39 55.9	+4 38 9	20.94	LINER/SyII (0.40)-OII],Hγ,Hβ, OIII]
3074	10 39 50.2	+4 42 54	20.33	qso (2.2) -Lyα,SiIV,CIV,CIII]
3283	10 39 36.9	+4 41 44	19.77	qso (1.63) - CIV,NIII],CIII], MgII
3302	10 39 41.3	+4 47 30	19.53	Sy I (0.418) - OII],Hγ,Hβ, [OIII],MgII
3309	10 39 40.6	+4 52 18	20.94	star - none
3321	10 39 38.6	+4 55 15	19.11	star09 - A. Hβ,Hγ
3465	10 39 29.1	+4 50 28	21.08	unidentified
3472	10 39 31.4	+4 54 21	20.67	star - none
3481	10 39 24.3	+4 57 37	20.27	qso (1.97) - OIV],NIV],CIV, CIII]
3667	10 39 16.4	+4 55 40	19.77	star K3 - A. TiO,CaI
3681	10 39 15.1	+4 59 15	19.72	qso (1.53) - CIII],CIV,MgII
3799	10 39 11.5	+4 36 44	20.92	star - none
3822	10 39 5.9	+4 39 40	20.59	star - none
3915	10 39 7.7	+5 3 31	20.32	qso (1.96) - OIV,CIV,CIII]
4096	10 38 59.7	+5 1 47	19.55	qso (1.83) - CIV,HeII,NII], CIII],MgII

Notes. remarks are formatted - id. (redshift) - lines
Id. numbers as in figure 3.8.Stellar absorption lines are preceeded with 'A.' Lines seen on grens plate spectrum are underlined.

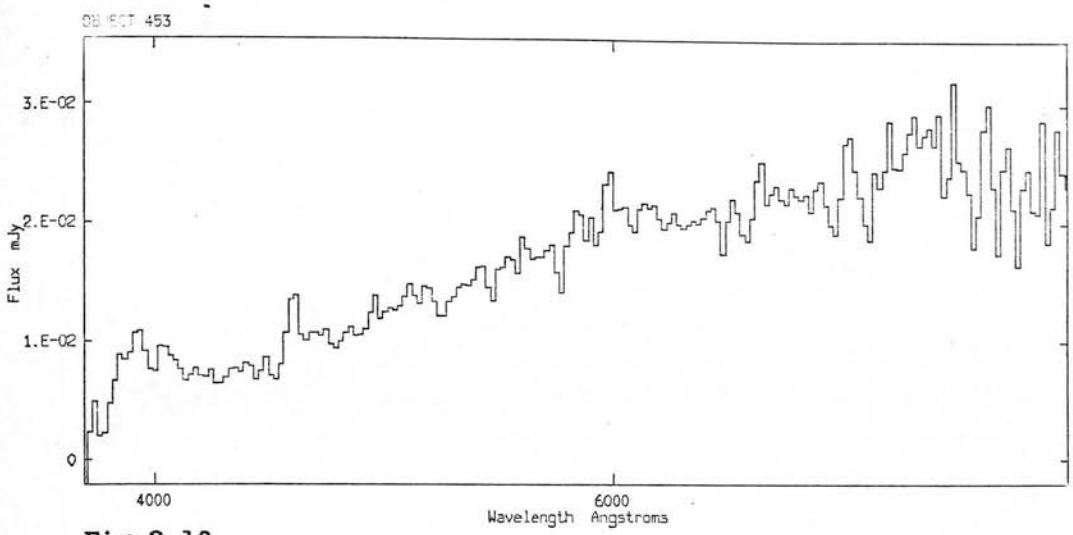

Fig 3.10

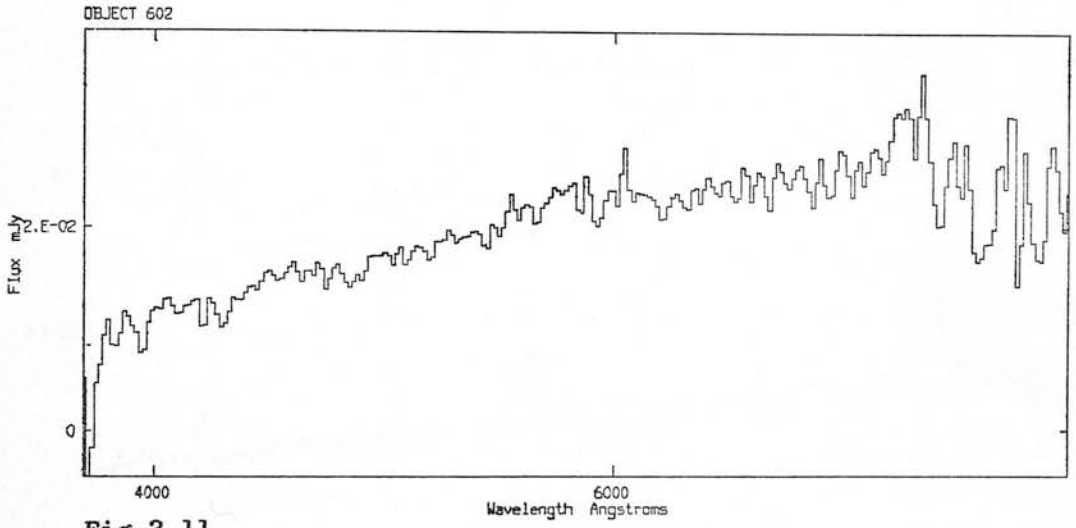

Fig 3.11

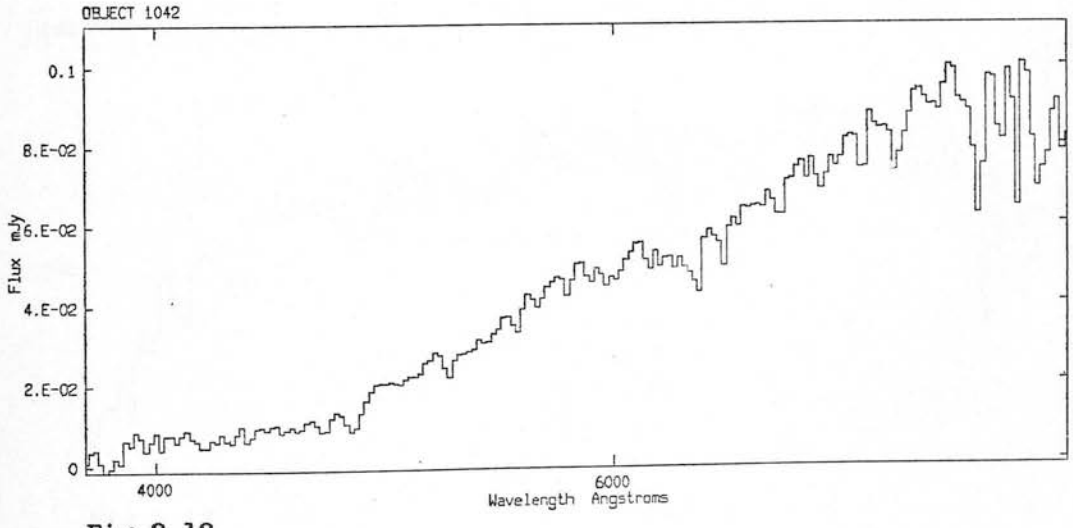

Fig 3.12

Figs 3.10 - 3.12 Slit spectra of objects observed at ESO.

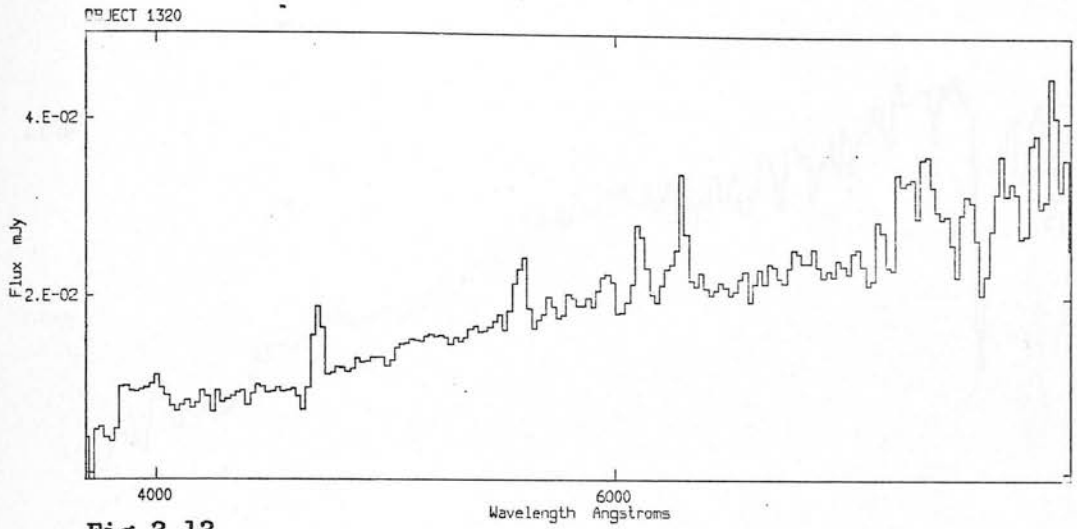

Fig 3.13

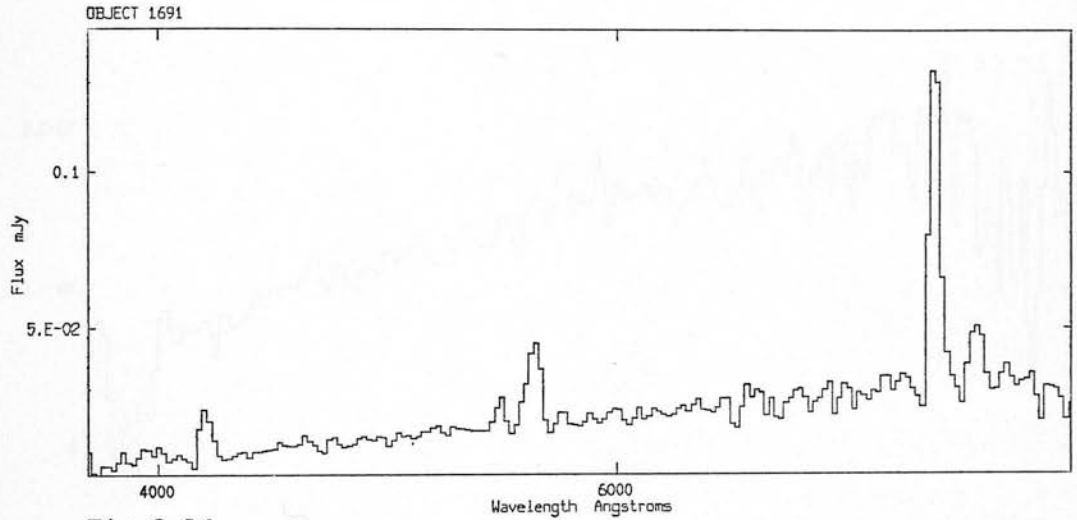

Fig 3.14

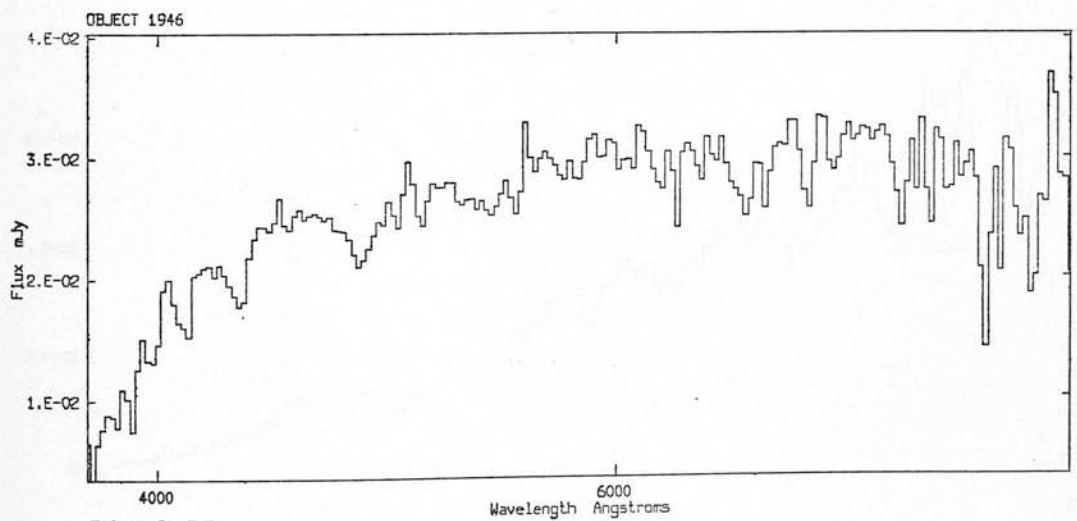

Fig 3.15

Figs 3.13 - 3.15 Slit spectra of objects observed at ESO.

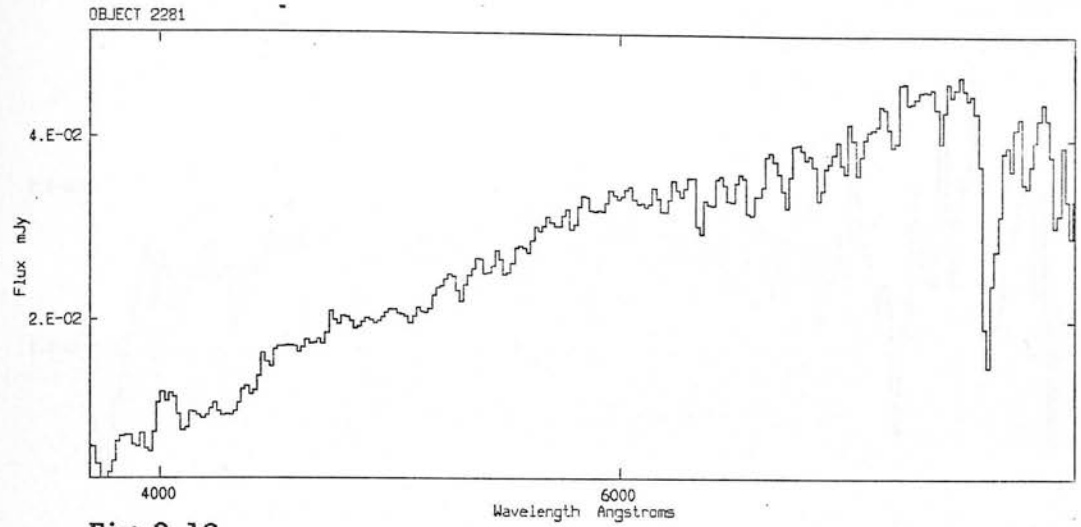

Fig 3.16

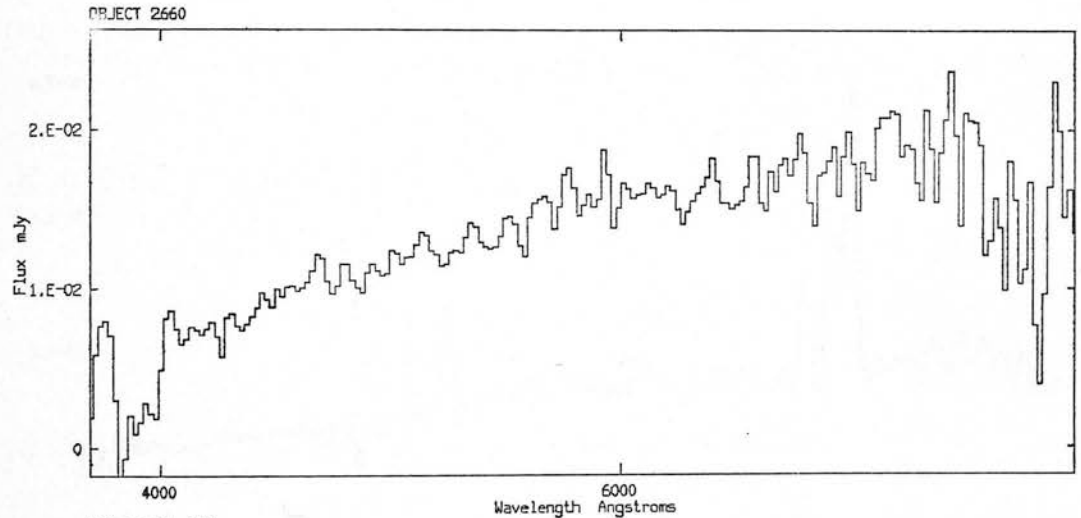

Fig 3.17

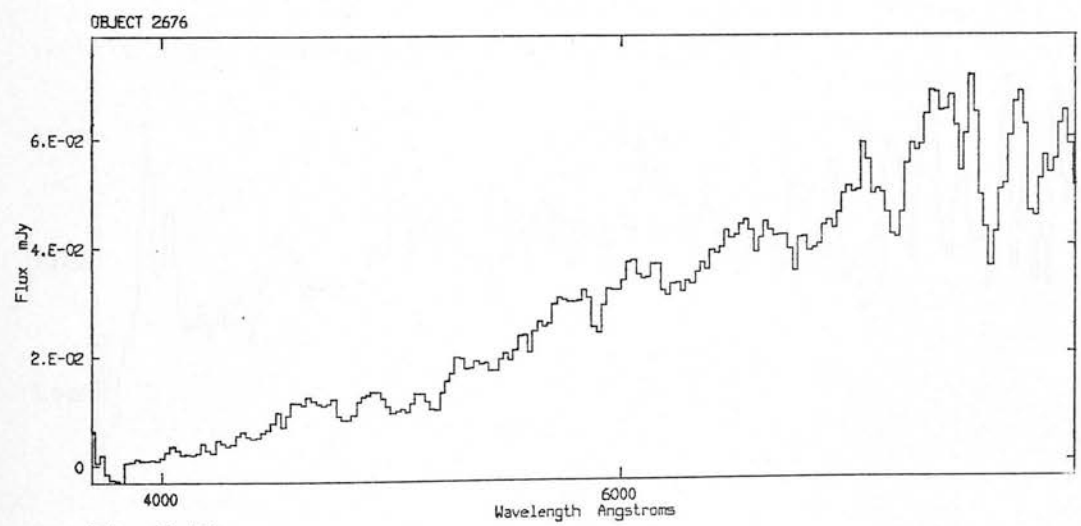

Fig 3.18

Figs 3.16 - 3.18 Slit spectra of objects observed at ESO.

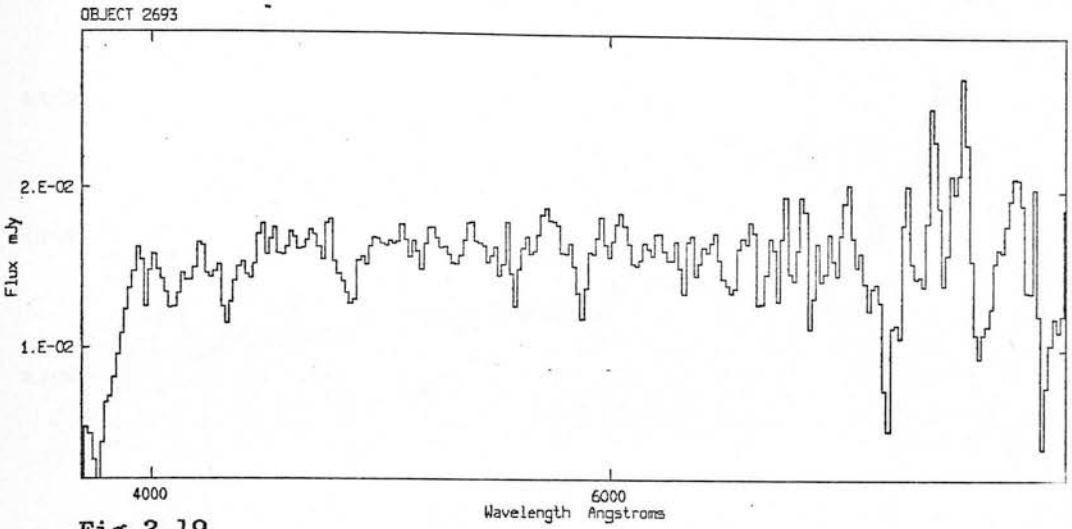

Fig 3.19

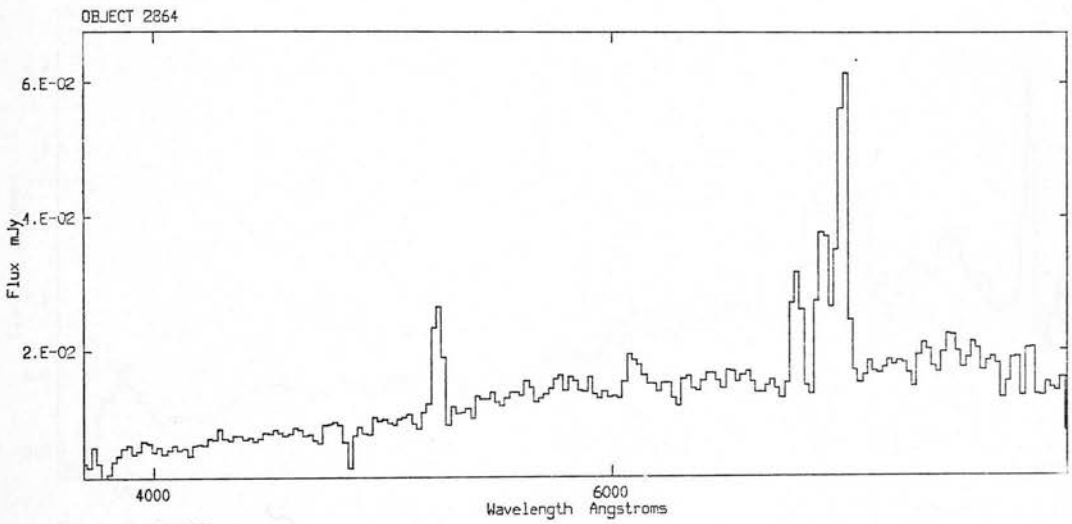

Fig 3.20

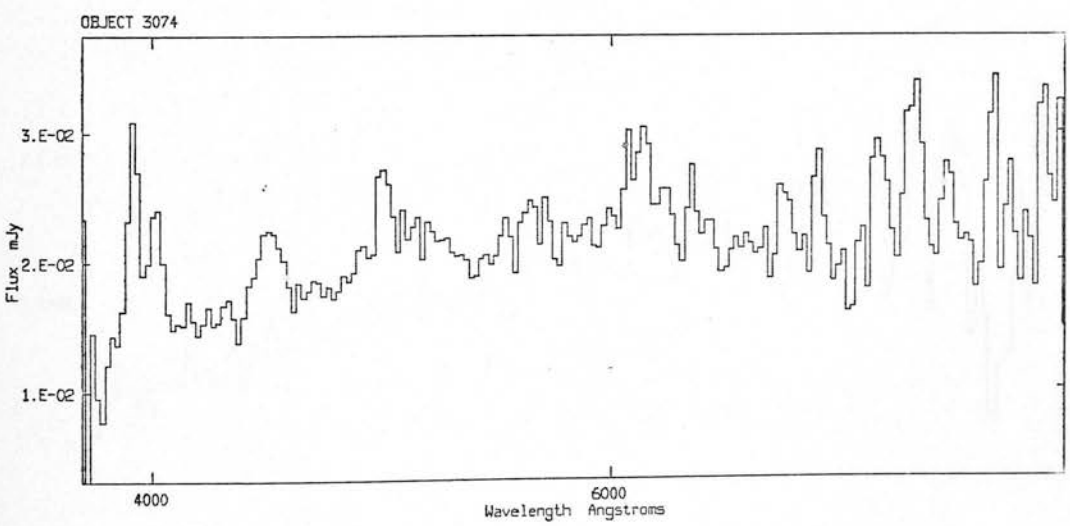

Fig 3.21

Figs 3.19 - 3.21 Slit spectra of objects observed at ESO.

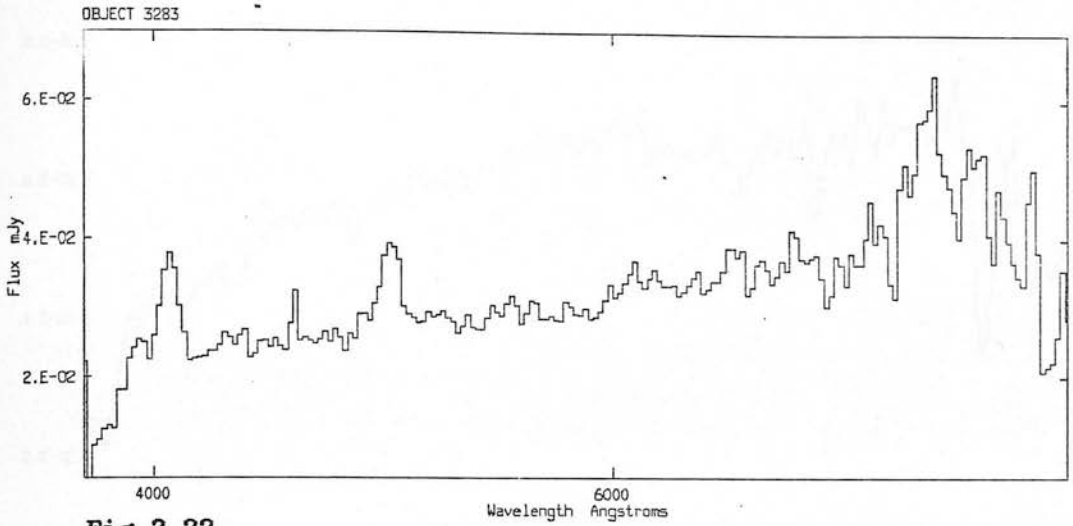

Fig 3.22

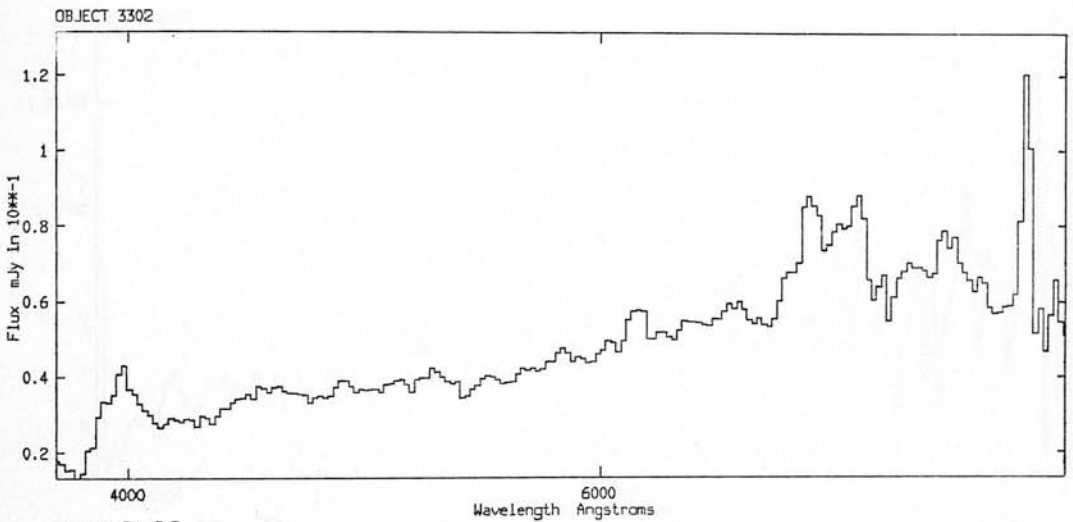

Fig 3.23

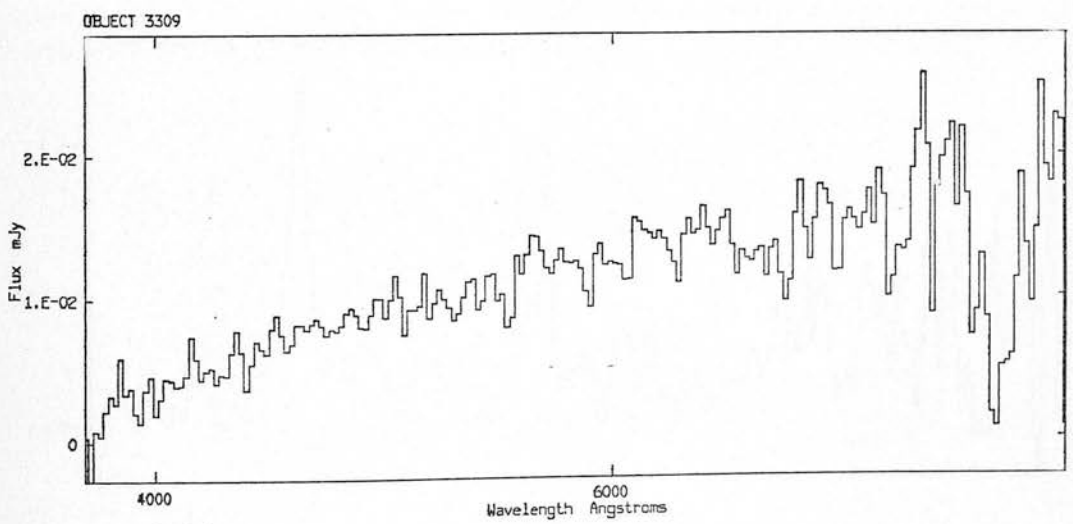

Fig 3.24

Figs 3.22 - 3.24 Slit spectra of objects observed at ESO.

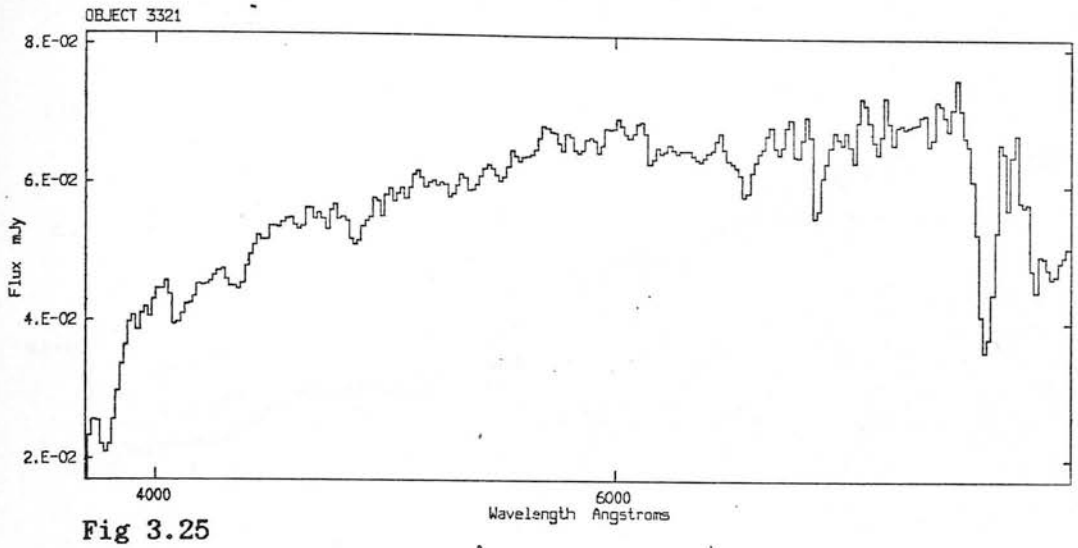

Fig 3.25

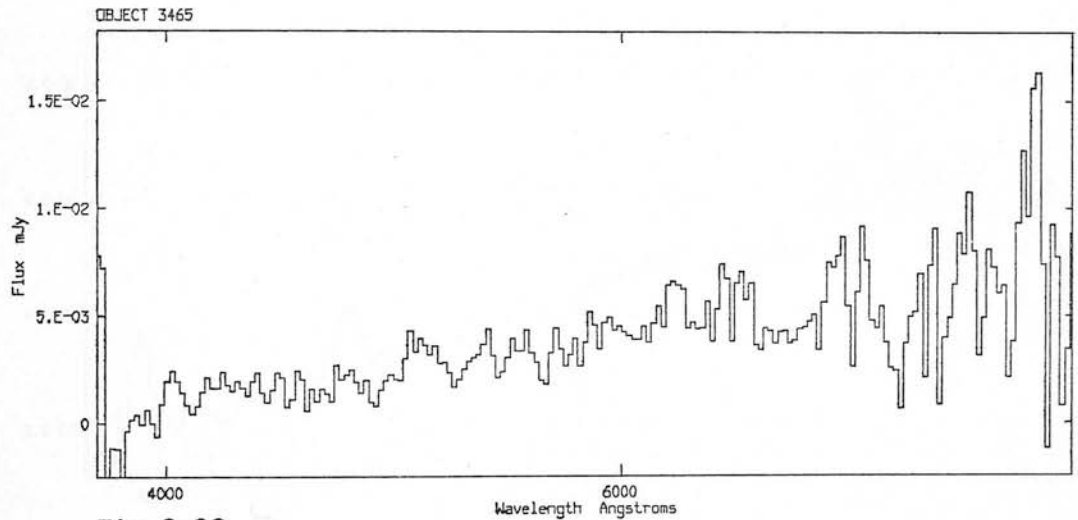

Fig 3.26

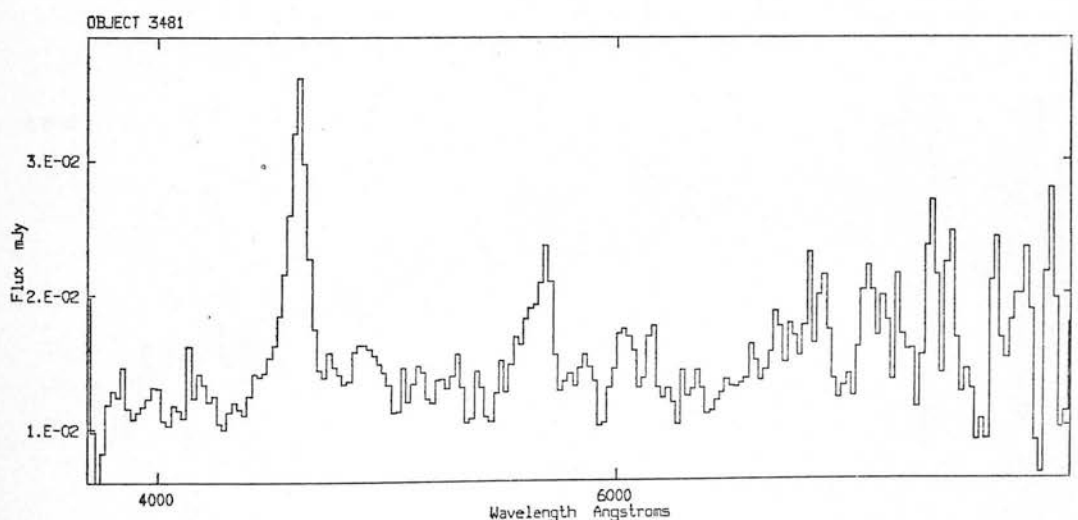

Fig 3.27

Figs 3.25 - 3.27 Slit spectra of objects observed at ESO.

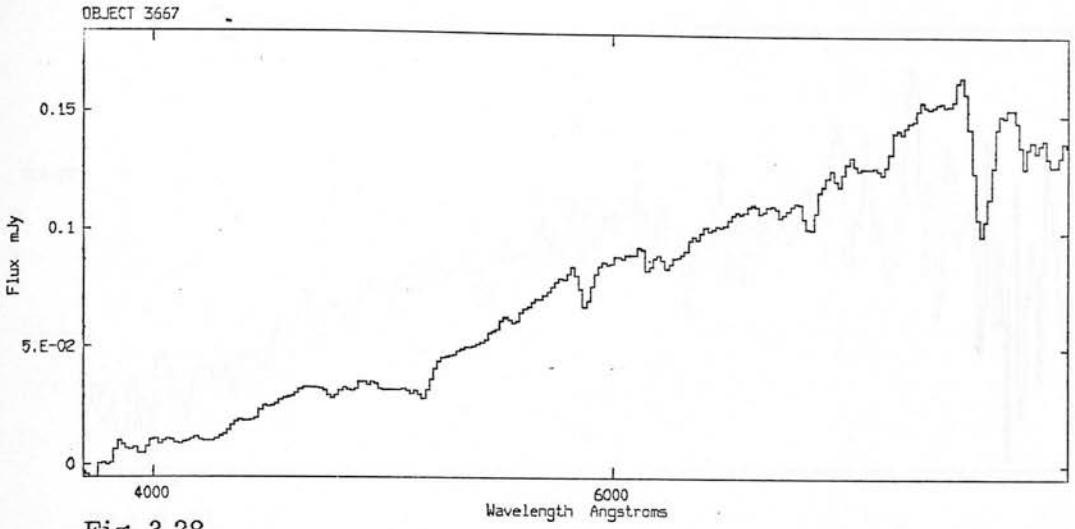

Fig 3.28

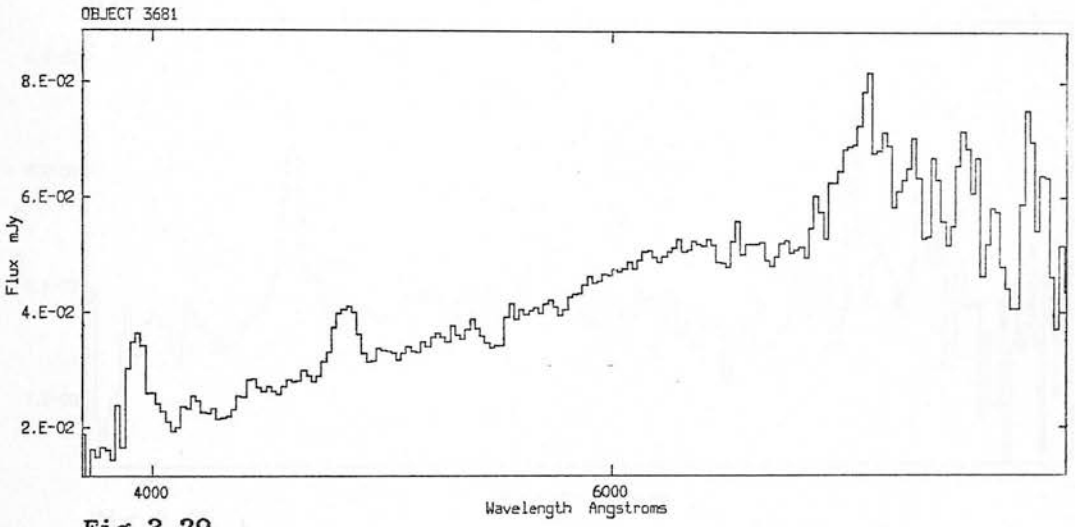

Fig 3.29

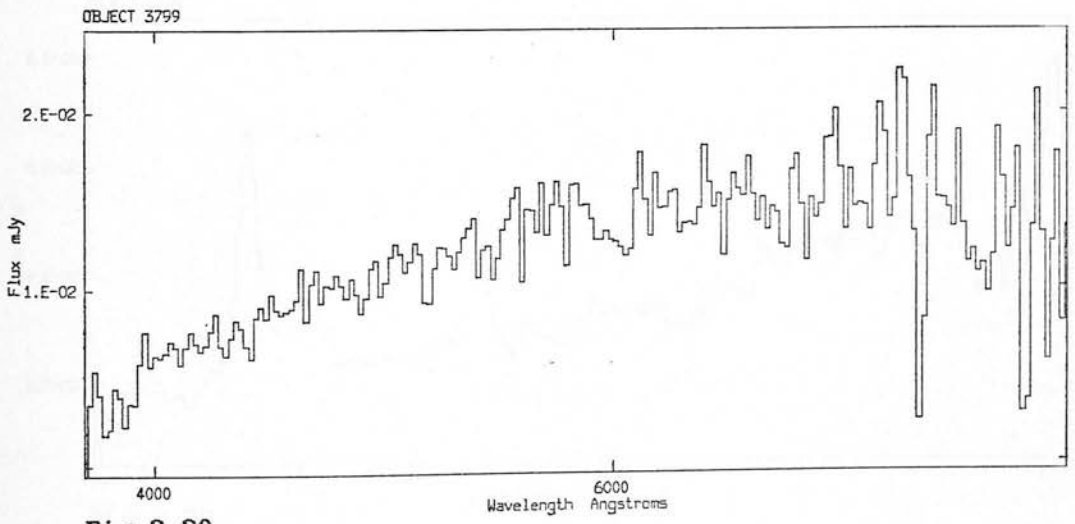

Fig 3.30

Figs 3.28 - 3.30 Slit spectra of objects observed at ESO.

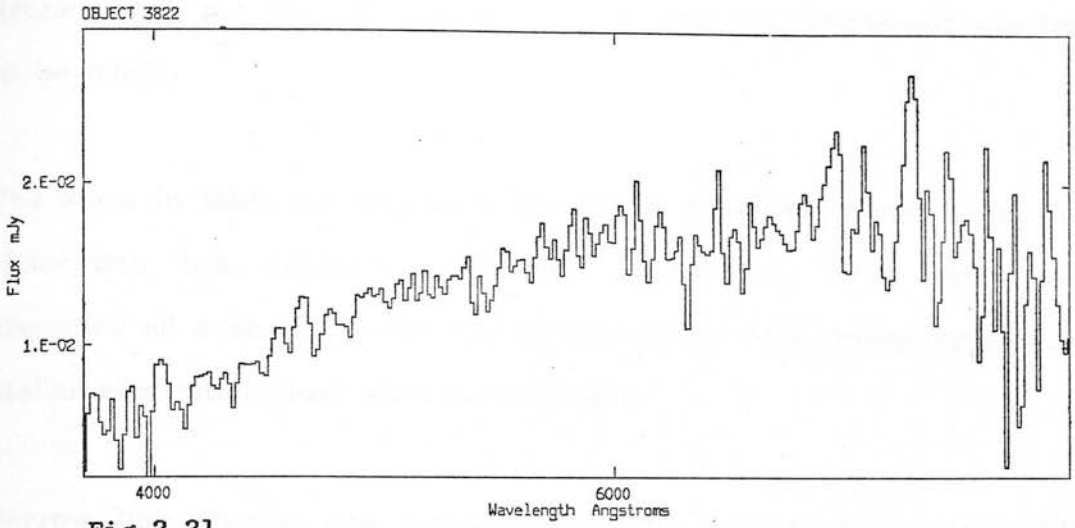

Fig 3.31

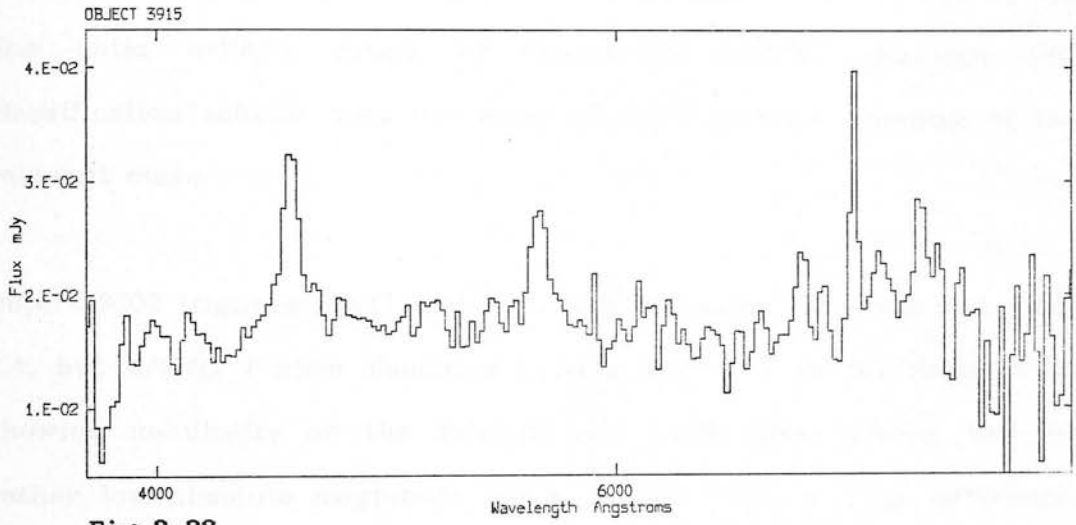

Fig 3.32

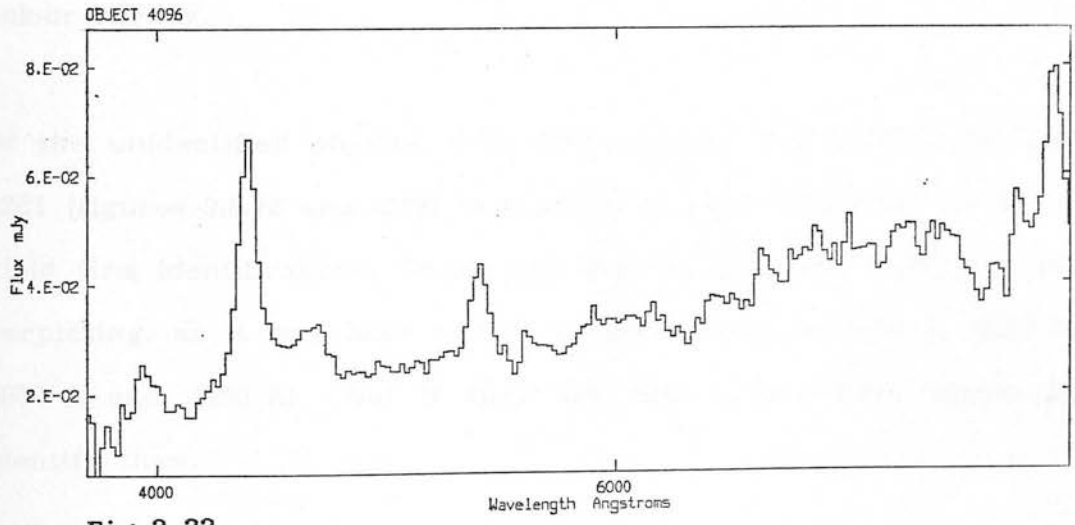

Fig 3.33

Figs 3.31 - 3.33 Slit spectra of objects observed at ESO.

grens plates per field (which would also allow the overlapped spectra to be used).

The stars in table 3.1 only have identified spectral classes when the absorption line systems are readily identifiable. Other stars are classified as such under the assumption that in this configuration the stellar absorption lines were unresolvable.

Narrow line objects are divided into being either extragalactic HII regions, starburst nuclei, Seyfert II or LINERS on the basis of the line ratio criteria given by Osterbrock (1985), although this classification scheme does not apply to all published examples of the relevant class.

Object 3302 (figures 3.8.41 and 3.23) was discussed in detail in section 2.4, but briefly I have classified it as a Seyfert I on the basis of its showing nebulosity on the Schmidt and POSS direct plates, and its rather low absolute magnitude for a quasar. This is a bit arbitrary, and its colours and so forth are used in assessment of the colour colour survey.

Of the unidentified objects, both 3465 (figures 3.8.75 and 3.26) and 2281 (figures 3.8.18 and 3.18) have signal to noise ratios too low to yield firm identifications. Object 453 (figures 3.8.1 and 3.10) is a bit perplexing, as it may have narrow emission lines (at 3930 A, 4030 A, 4600 A and 5980 A) but if they are real I have been unable to identify them.

3.6 Selection effects and survey completeness.

The inclusion of object 1691 in the grens survey is due to the discovery of the O III] (3727) line in the grens spectrum (see figures 3.8.12 and 3.14). This is a narrow line: the EFOSC spectrum has a full width at half maximum of < 3 pixels, ie unresolved using the 1.5" EFOSC slit: all that can be said is that the grens can identify emission lines at least 4500 $km.s^{-1}$ wide. However, narrow line objects show line widths which are typically a few hundred $km.s^{-1}$, so it is reasonable to suppose that the grens can identify all objects that show a classical quasar broad line region, as long as they are in the redshift window of the instrument (3950 Å $< \lambda <$ 5400 Å). Unless line strengths in the broad line region evolve very rapidly (recent evidence of the spectra of high redshift optically selected quasars makes this unlikely - Schmidt, Schneider and Gunn, 1987), all quasars should be detectable between $0 < z < 3.5$ - the latter is where Ly-α is redshifted redward of the grens passband. At redshifts lower than $z \approx 2$ many possible emission lines are detectable - confirmed objects show no bias to preferential Ly-α detection.

3.7 Contaminants in the grens survey.

The level of contamination amongst those objects spectroscopically observed in the survey is clearly very high ($\approx$ 60%). The reason for this is that this is the first time such a survey has been undertaken automatically. The only body of experience available was that obtained

from searches of the UK Schmidt prism plates. Thus candidate location was done with the expectations of the prism survey in mind. However, with the prism plates it is possible to improve the contamination level (see section 2.2), and with the experience gained here a similar improvement should be possible.

Three serious causes of contamination are identified here, all of which can be eliminated in a subsequent survey. The first of these effects is exemplified in figures 3.8.42 and 2.24 of object number 3309 in the survey. What appears to be a prominent emission feature in the grens spectrum turns out to be nothing at all in the slit spectrum. The feature in the grens spectrum could be caused by dirt on the emulsion, or by stray images from another object (either a bit of scattered light or a faint zeroth order image). This is quite a serious problem, causing the mistaken inclusion of four or five objects. These spurious objects could be eliminated from the survey easily by the inclusion of another plate, cross dispersed to the first. It would then be unlikely that bits of dirt would lie in the same place on the spectrum of the same object, and spectra would not lie in the same relationship to one another, so problems with stray bits of light or zeroth order images would disappear. Processing two plates would have the added advantage that objects would not be missed underneath the spectra of bright stars.

The second class of spurious objects identified are hot white dwarfs (spectral type DA, from Oke 1974). These are picked up as having an emission line, because their broad, Balmer series absorption lines Hβ and Hγ are both resolved on the grens spectrum and AQD identifies an 'emission line' between these lines. Examples are objects 1946

(figures 3.8.15 & 3.15), 2693 (figures 3.8.27 & 3.19), 3321 (figures 3.8.43 & 3.25) and 3822 (figures 3.8.58 & 3.31). Clearly, software could identify these, and eliminate them. There is not likely to be a problem of confusion between these and real quasars at redshift $z = 2.78$ (which puts Ly-α in the same position as the spurious line) because a second spurious line is generated between the Hγ and the filter cutoff (or presumably Hε). The objects are very blue, and so the cutoff is sharp. Hence the AQD continuum following routine does not follow the spectrum closely, and an emission line is identified.

The third effect to be identified causes the spurious inclusion of late type main sequence stars. Examples of these are objects 602 (figures 3.8.2 & 3.11), 2676 (figures 3.8.26 & 3.18), 3667 (figures 3.8.51 & 3.28), and 3799 (figures 3.8.57 & 3.30). The reason for the inclusion of these objects is the broad TiO band at $\lambda = 5165$ Å (Pritchet and Van den Bergh, 1977) and the objects' late type, ie red colour. This means that the spectrum continuum falls away to the blueward of the absorption band. This causes the AQD software to identify an emission line at $\lambda \approx 4840$ Å. Clearly, these objects could also be identified by software after location by AQD, but it is difficult to see how to avoid generating a selection effect against genuine quasars at $z \approx 3$ (where Ly-α lies at this wavelength) - especially if the quasar has a strong Ly-α forest, causing a sharp continuum drop. Otherwise it may be possible to distinguish between these and real quasars by the careful definition of a colour, with two synthetic magnitudes spanning the continuum drop.

Had these processes been applied to this survey, some ten to twelve objects which were observed at ESO would not have been. This would

bring contamination from its ≈ 60% level to < 20% (without another plate, it is difficult to know which objects to include in the first category). This is clearly a substantial and worthwhile improvement.

3.8 Conclusions.

The CFHT grens and AQD is clearly a very powerful combination for locating quasars. Although the ESO spectroscopy produced a contamination level of ≈ 60%, it is clear from the preceeding section that this could be reduced to ≈ 20% - a substantial and worthwhile improvement. However, it should be stressed that this is dependant on the use of a second cross-dispersed plate. If this is not available, it would not be possible to reduce the surveys' contamination to better than ≈ 45%.

More importantly, it is demonstrably less effected by selection effects than Schmidt slitless prism plate surveys. The (re)discovery of the object at z = 3.27 (figure 3.8.74) shows that there is not a problem with identifying lines close to the emulsion cutoff - prism plates have increasing difficulty due to dispersion changes, an effect discussed in section 1.3. It is also interesting to note that five out of six of the new discoveries of quasars are at redshifts z < 2.2, ie. the discoveries were not due to the identification of the broad Lyα / NV blend, but of weaker lines such as CIV (1549), CIII] (1909), and MgII] (2798). In addition, the discovery of narrow lined object indicates that there is no difficulty in resolving weak or narrow lines - in fact the increasing loss of candidates with weaker lines at fainter apparent

magnitudes seen in prism surveys (discussed in section 1.3 and again in section 5.2) is certainly not a problem on the grens plate at magnitudes brighter than B_J = 20.97. This is the faintest magnitude at which a narrow lined object was detected. The survey is therefore complete, for quasars less than about z = 3.3. This can be said with confidence (only for quasars that show broad emission lines) because there is no redshift band which does not have a broad line shifted into the grens spectrum. Occasional objects in this regime may have been lost due to the large amount of scattered light generated by bright stars in the field, but this could be remedied with the use of a cross dispersed plate. Thus the survey is statistically complete to a magnitude of $B_J \approx 21$, and possibly fainter. The only objects lost will be due to scattered light, which is statistically unimportant (in that the sample is not biased).

The objects observed at ESO can be used to predict number counts of quasars expected in the whole of the grens survey. Candidates for observation were selected on a 'next nearest' basis, ie. statistically at random (since no ad hoc quality factor was introduced). Thus the probability of finding a successful candidate is 7 / 23 = 0.30 (7 excludes the Seyfert I, since these numbers are to be compared with the numbers generated by other surveys, but includes a previously known quasar in the ESO spectroscopy area since it would have been observed by the criteria, and thus discovered. The 23 excludes the 3 unidentified objects). This is just a binomial distribution type of problem, so the expected number of successful candidates over the whole survey is 22.5 ± 3.97.

In order to make comparisons with other studies, account must be

taken of the area surveyed. All objects over ≈ 0.20 degrees^2 were observed at ESO, and if object numbers are limited to those whose $B_J \leq 20.5$, a total of 34.8 ± 5.4 quasars per degree^2 are expected.

This compares to Boyle, 1986, who gives 26.31 ± 1.90 for $B_J \leq 20.5$. Remember, though, that Boyles' survey is insensitive for $z > 2.2$, and he estimates an incompleteness of 10%. This is likely to be an underestimate, since Hewitt and Burbidge (1987) find ≈ 26% of all objects have $z > 2.2$. Anyway, the predicted number of quasars found on the grens agrees to within 1 σ with the best estimates available at this magnitude.

4. New surveys: UK Schmidt photometric survey.

The ideas behind a photometric survey are discussed in detail in section 1.2.4. This chapter describes the survey itself: the data used, the calibration required, and the reduction procedures adopted. Finally, a list of quasar candidates is drawn up. Although the survey is divided into two parts, a UV excess and a five colour, this makes no difference to most of the plate reductions - only to final selection criteria. As a result, most of this section applies to both surveys. The project was awarded PATT telescope time from the UK Schmidt to obtain deep sky limited plates in the survey passbands, U, B_J, V, R, and I. Several plates were in fact obtained in each colour. These plates were measured using the COSMOS measuring machine, and data were analysed using STARLINK facilities at Edinburgh. Catalogue handling was done within the HAGGIS database processing package, which was written at the ROE while this project was underway. When changes to the software were needed, they were made as necessary to implement new facilities, and to increase execution speed for frequently used programs. All new programs were written to conform to the HAGGIS data format, as it forms a convenient framework within which it is possible to pair plates, perform arithmetic operations on parameters, and select subsamples of the dataset.

All of the plates required calibration, for which CCD frames were obtained from the ESO 3.6m, the AAT, and the INT. The CCD frames are calibrated into the Kron-Cousins photometric system - the U, B, and V colours originally come from Johnson and Margon (1953), and the R and I colours were developed by Cousins (1980a and 1980b) and

Bessell (1979). However, it ultimately proved impossible to use this system for the photographic photometry. This is because some objects close to the survey limit have a well defined magnitude in one waveband, but are below the plate limit in another band - as a result they cannot be calibrated because no colour correction can be defined. It would be a gross waste of information to throw these objects away, so instead the CCD photometric standards were transformed from the Kron-Cousins into the 'natural' photographic colours of the Schmidt, before calibration was performed. Colour equations have been deduced from standard star observations for the Schmidt by Blair and Gilmore, (1982).

4.1 Schmidt direct plate material available for the survey.

Altogether, a total of 24 deep, sky limited plates were available to or were taken for the survey. These plates are listed in table 4.1. The emulsions and filter combinations used to define the wavebands are listed below, and plots of normalized sensitivity for the photographic wavebands are shown in figure 4.1.

U	emulsion: IIIaJ	3200 - 5380	}	3200 - 3900
	filter: UG1	3200 - 3900	}	
J	emulsion: IIIaJ	3200 - 5380	}	3950 - 5380
	filter: GG395	3950 →	}	
V	emulsion: IIaD	3200 - 6500	}	4950 - 6500
	filter: GG495	4950 →	}	

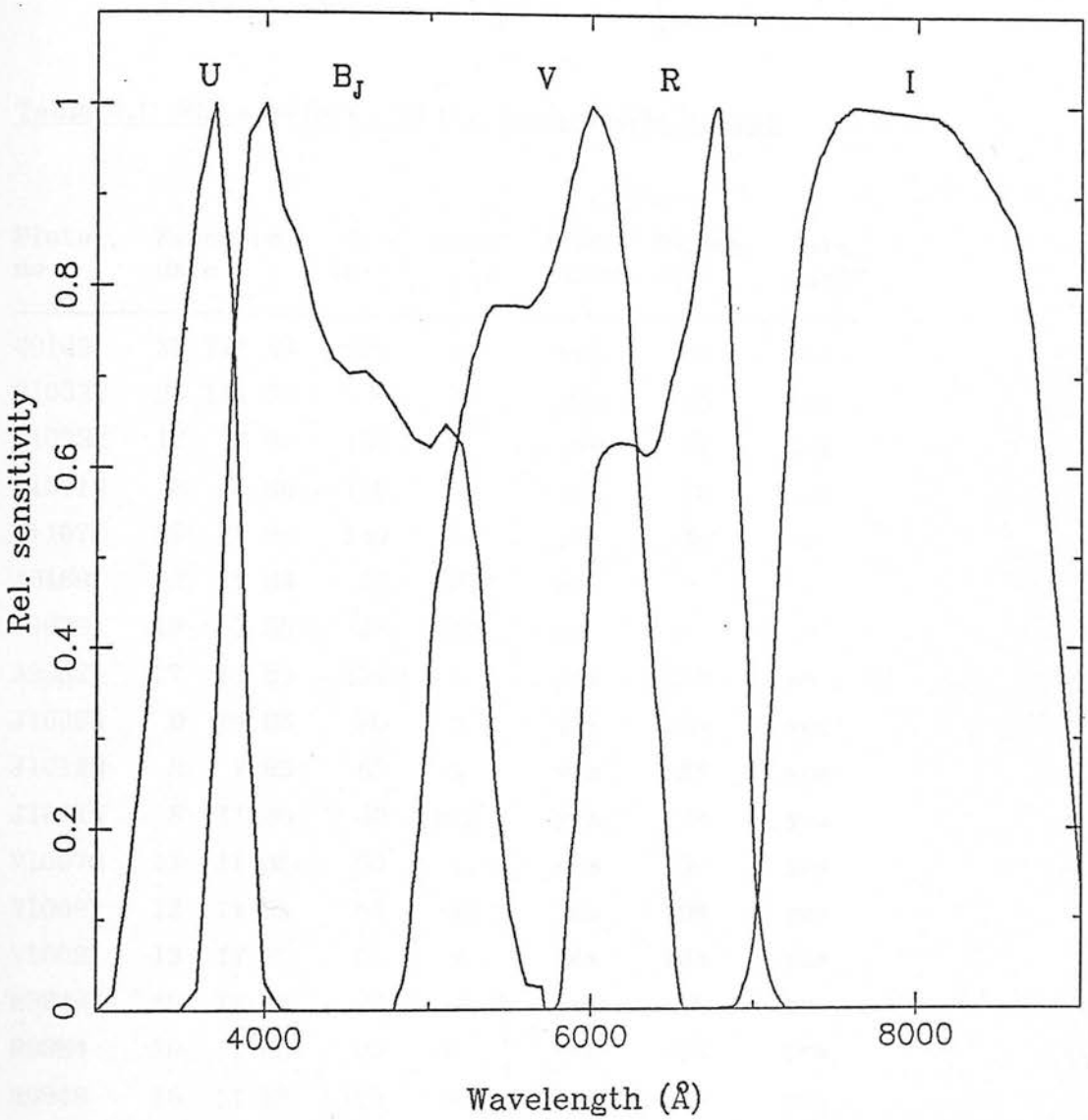

Fig 4.1 Photographic filter and emulsion sensitivity curves.

R	emulsion: IIIaF	3200 - 6900	6300 - 6900
	filter: RG630	6300 →	
I	emulsion: IVN	6700 - 9000	7150 - 9000
	filter: RG715	7150 →	

Table 4.1: Plate material in the photometric survey

Plate no.	Exposure date	Time (min)	Qual -ity	Meas -ured	Thresh -old	Data used?
U9140	28 III 84	180	αT	yes	5%	yes
U10032	26 III 85	186	αI	yes	5%	yes
U10082	12 IV 85	180	α	yes	5%	yes
U10719	8 II 86	180	αT	yes	7%	yes
U11076	29 IV 86	180	αI	yes	6%	no
J9169	2 IV 84	60	BEI3	no	-	-
J9879	18 I 85	90	βID	no	-	-
J9952	27 II 85	100	α	yes	20%	no
J10063	9 IV 85	90	α	yes	5%	yes
J10128	8 V 85	60	α	yes	5%	yes
J10715	8 II 86	80	BI3	yes	7%	yes
V10070	11 II 85	60	α	yes	9%	yes
V10081	12 IV 85	60	αI	yes	9%	yes
V10091	13 IV 85	60	α	yes	10%	yes
R9248	29 IV 84	90	αD	yes	5%	no
R9884	20 I 85	90	α	yes	5%	yes
R9949	26 II 85	120	αI	yes	5%	yes
R10067	10 IV 85	111	γTI	no	-	-
R10071	11 IV 85	110	α	yes	5%	yes
I10045	30 III 85	90	αE	yes	5%	yes
I10060	8 IV 85	75	αE	yes	5%	no
I10129	8 V 85	25	βF	yes	10%	no
I10766	19 II 86	90	BI4	yes	5%	yes
I10900	20 III 86	90	BEI3	yes	5%	yes

For a more comprehensive discussion of the Schmidt telescope, the

emulsions and the filters used, see the Schmidt telescope handbook (1983).

Column 4 of table 4.1 shows the grade assigned to each plate by the observer at the telescope. This quality control factor is also described in more detail in the UKSTU handbook, and is slightly arbitrary for non ESO/SERC survey plates, as it is assigned by observers who are under instructions not to spend so much time on non-survey programmes. Essentially, however, it gives some indications of the plate quality. Grades A, B, C, . . . are given to survey plates (in order of decreasing image or plate quality), and non survey plates α, β, γ, . . . Here, α normally covers survey grades A and B. Sometimes, however, when more time is available at the telescope, it is possible to give a non survey plate a survey type grade. The following letters refer to different types of imperfection or blemish: I for images > 40 μ, T for trailed images, E for emulsion blemishes on the plate, D for an overexposed plate, and F for a fogged plate.

Plates were selected for measurement by COSMOS on the basis of this grade, and a visual inspection of the plate. This was not always an adequate filter, and sometimes plates had to be rejected later, when some peculiar effect became apparent in the COSMOS data. At the premeasurement stage, plates were only rejected if a large proportion of the images were affected, or it seemed unlikely that COSMOS would be able to measure it very well. For example, if the images are slightly trailed the effect on COSMOS magnitude measurement is not great, and so the data can be used (so U9140 and U10719 were used). If on the other hand the plate is overexposed, many of the images will be saturated, or if there is a processing error giving large scale

background variations, then plate calibration becomes a problem (so J9952 and R9248 could not be used).

4.2 COSMOS measurement of plates.

The COSMOS machine is a fast, flying spot microdensitometer, and is described in detail by MacGillivray and Stobie (1984). It is possible using this machine to digitise an entire Schmidt plate in a few hours. All plates in the survey were measured with a 32 μ spot size, and a 16 μ step size. This setup is a compromise between pixel size and measurement time - the pixel size means there is about 1 pixel per arcsecond for the Schmidt platescale of 67.14"/mm (in fact none of the plates have seeing as good as one second) - and is intended to reduce the effects of emulsion noise.

Subsequent on-line processing of the data reduces the raw pixel information into parametrized information for each object, pertaining to astrometry, photometry and morphology. This process is referred to as the 'COSMOS analyser', and the software suite is described in Stobie (1986). There are 20 parameters per image (except in the new de-blended data, discussed in section 4.7.5). The parameter details are given in table 4.2.

Shortly after the start of this part of the project, in mid 1984, the COSMOS machine hardware was upgraded from its original 8-bit digitisation (256 transmission levels) to 14-bit digitisation (16384 transmission levels). This upgrade was carried out with the intention

of improving the dynamic range available to the machine, and in consequence the accuracy of the parameters (Beard, 1986, private communication). The parameter errors had been measured

Table 4.2: COSMOS parameters

Param. name	Description	Units
RA	Right Ascension	Hours (1950)
DEC	Declination	Degrees (1950)
XMIN	X min. of image	0.1 μ
XMAX	X max. of image	0.1 μ
YMIN	Y min. of image	0.1 μ
YMAX	Y max. of image	0.1 μ
AREA	Image area	Pixels
IMAX	Max. intensity over sky	Arbitrary rel. intensity
COSMAG	COSMOS magnitude	
ISKY	Sky intensity at image centroid	
IXCEN	Weighted X centroid	0.1 μ
IYCEN	Weighted Y centroid	0.1 μ
UMAJAX	Unweighted semi-major axis	0.1 μ
UMINAX	Unweighted semi-minor axis	0.1 μ
UTHETA	Unweighted orientation	degrees
IMAJAX	Weighted semi-major axis	0.1 μ
IMINAX	Weighted semi-minor axis	0.1 μ
ITHETA	Weighted orientation	degrees
CLASS	Star/galaxy separation	unfilled
IDSEQ	Sequential i.d. number	

under the 8-bit digitisation by Hewett (1983), but as a consequence of the upgrade (all plates for this programme were measured with 14-bit

digitisation), the parameter errors had to be re-measured to assess the efficacy of the upgrade (section 4.4).

4.3 Threshold mapping and the generation of COSMOS parameters.

As has been mentioned, if COSMOS were to simply output the transmission value of every pixel, vast quantities of data would be produced (measuring 250 x 250 mm^2 with 16 μm pixels gives $\approx 2.4 \times 10^8$ pixels, or $\approx 4 \times 10^5$ blocks of storage space on a VAX!) - quite unwieldy, and virtually impossible to deal with more than one plate at a time. As a result, the machine instead deduces a local background before measurement proper begins, and then writes out only those pixels which are a fixed percentage level above the background (the 'threshold cut'), and which are associated with enough other super-threshold pixels to generate an image more than the 'area cut'. Subsequently, software in the analyser (Stobie, 1986) calculates the COSMOS parameters. Specifically, a magnitude

$$\text{COSMAG} = -2.5 \times \log(\Sigma(I - I_{sky}))$$

is calculated, where the summation is over all intensity values I in an image which are above the threshold level, and I_{sky} is the local sky background intensity. This is divided by the local sky background value, to give a 'magnitude' measurement brighter than the sky. One of the main difficulties of this method of magnitude estimation (for stellar images) is that the machine is essentially measuring an

isophotal magnitude - the percentage of flux lost is therefore correlated with magnitude. This is the principle reason why, to say anything meaningfully about COSMOS faint image photometry, images must be calibrated using CCD images or something similar. Of course, at bright magnitudes, other effects become increasingly important in making the COSMAG/real magnitude relationship non-linear, such as photographic saturation, a limited dynamic range in COSMOS, diffraction spikes and ghosts. These effects are of little concern here, because this programme is only concerned with the fainter objects.

4.4 Assessment of the COSMOS hardware upgrade.

In order to understand the changes made in the upgrade from 8-bit to 14-bit digitisation levels, the central 2 square degrees of plate J10063 were scanned twice in succession for this project. COSMOS had the same setup characteristics on both occasions (ie. the same threshold and area cuts), so comparison of the two datasets should yield instrumental errors. HAGGIS was used to pair the two data sets such that each object in the output dataset had two measurements per parameter. The objects were then binned into magnitude bins of 0.1 magnitude, and the standard deviations for every parameter of these bins were calculated. These values are plotted in figure 4.2. These diagrams can be compared to diagrams in Hewett, (1983), who plotted similar diagrams in 1982 (his figure 3.15) for the 8-bit digitisation incarnation of COSMOS.

The magnitude diagrams show a significant improvement: $\sigma_8 = 0.04$,

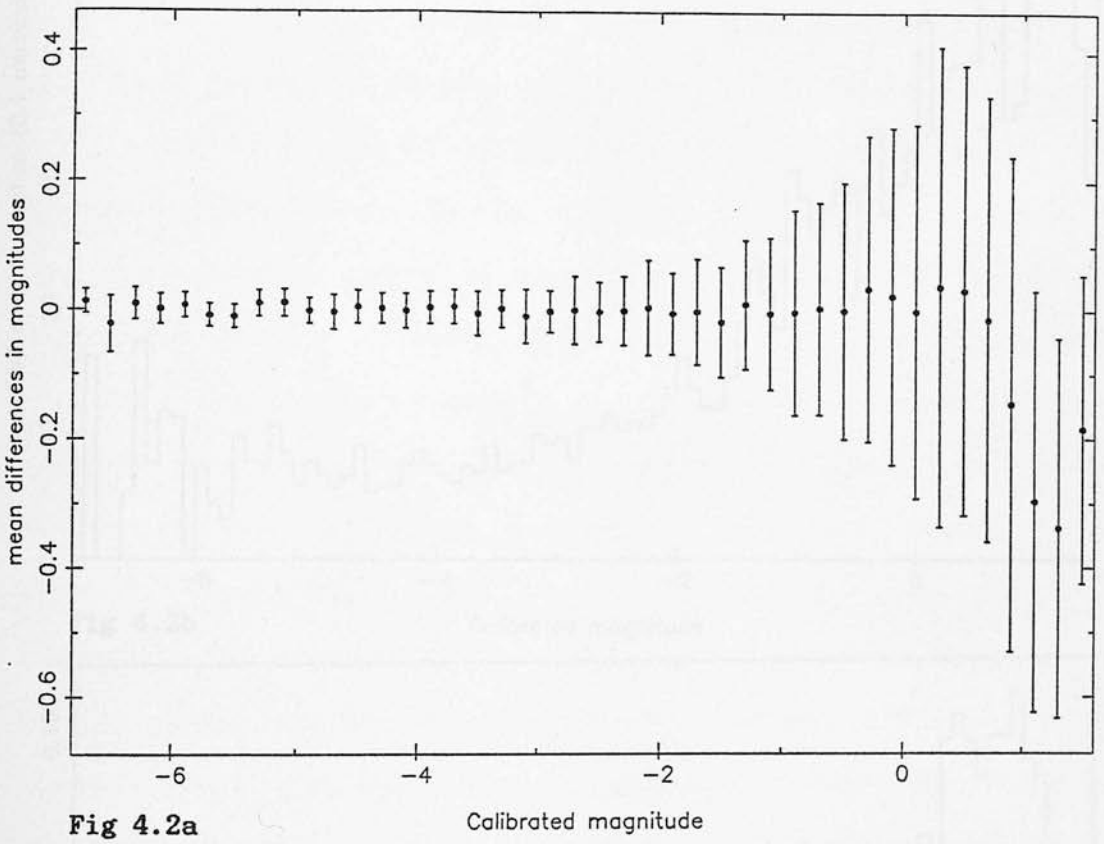

Fig 4.2a

Fig 4.2 RMS errors for COSMOS I.A.M. parameters as a function of COSMOS magnitude. The data are averages from repeated measurements of 2 degrees^2 in the centre of J10062.

a) Mean difference in magnitude vs. COSMOS magnitude.

b) Error in position vs. COSMOS magnitude.

c) Error in log(Area) vs. COSMOS magnitude.

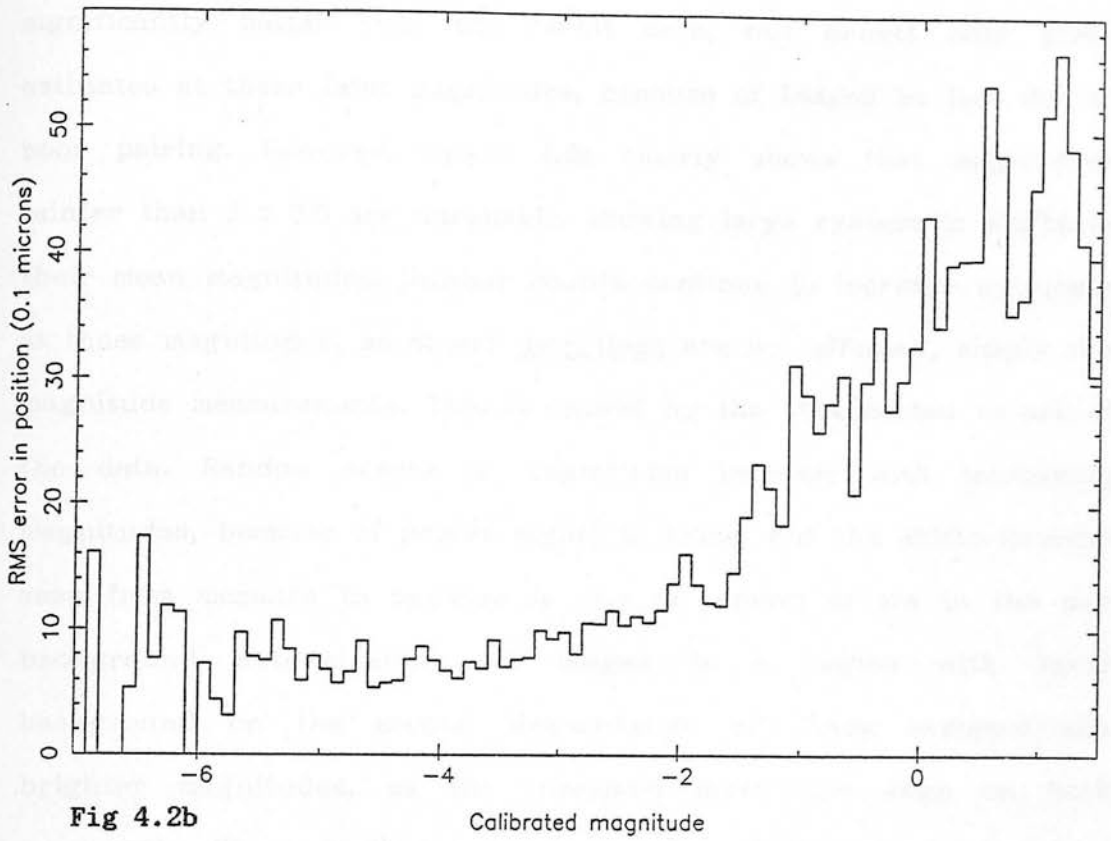

Fig 4.2b

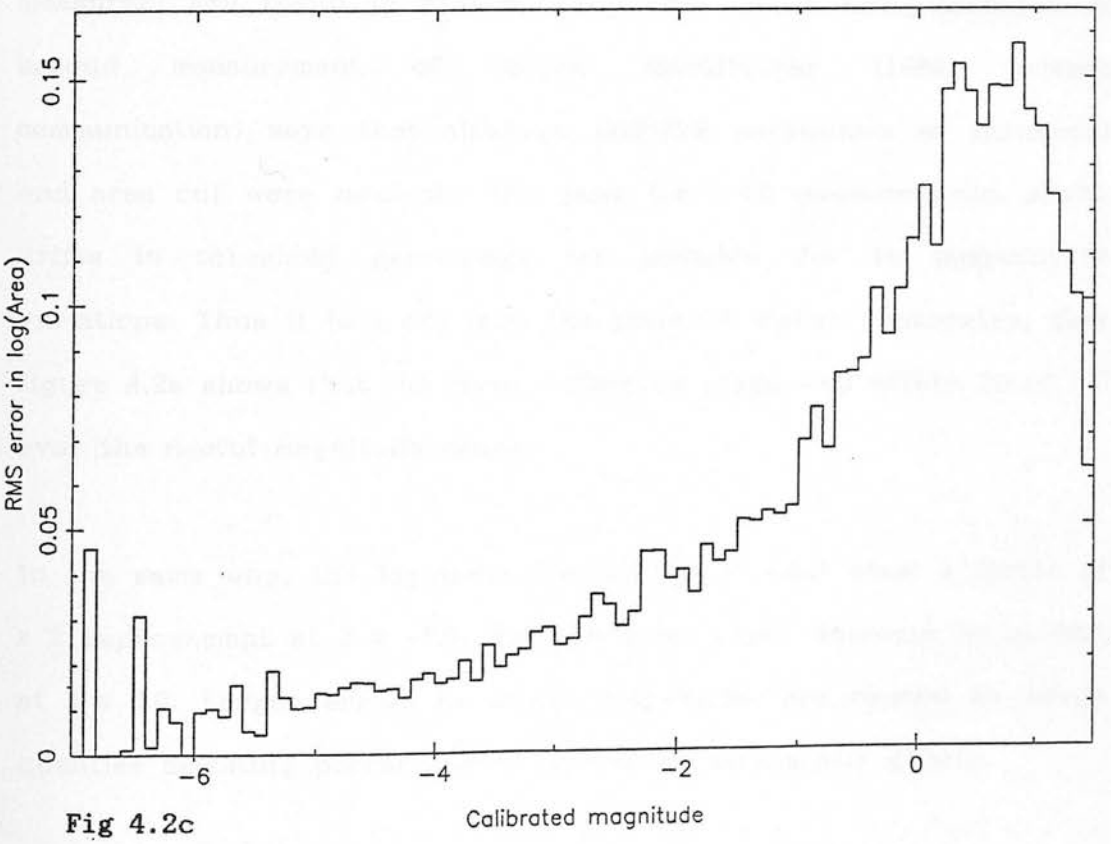

Fig 4.2c

σ_{14} = 0.025 at J = -4.0 ($B_J \approx 17$). At fainter magnitudes, however, the situation is less clear. At J = 0.0 ($B_J \approx 21.5$) the 8-bit data seems significantly better than the 14-bit data, but Hewett only gives estimates at these faint magnitudes, because of images he lost due to poor pairing. However, figure 4.2a clearly shows that magnitudes fainter than J = 0.0 are unreliable, showing large systematic shifts in their mean magnitudes. Number counts continue to increase uniformly at these magnitudes, so object detections are not affected, simply the magnitude measurements. This is caused by the thresholded nature of the data. Random errors in magnitudes increase with increasing magnitudes, because of poorer signal to noise, but the shifts-in-mean seen from measure to measure is due to random errors in the sky background determination: all images in a region with lower background on the second measurement will have systematically brighter magnitudes, as the threshold level (the same on both measures) will result in systematically more pixels being included in second measurement of images. MacGillivray (1986, private communication) says that although COSMOS parameters of threshold and area cut were nominally the same for both measurements, slight drifts in threshold percentage are possible due to temperature variations. Thus it is good, from the point of stellar photometry, that figure 4.2a shows that the mean difference stays well within 1σ of 0.0 over the useful magnitude range.

In the same way, the log(area) errors (figure 4.2c) show a factor of $\approx$ 2 improvement at J = -4.0, but the same slight decrease in quality at J = 0.0. Larger errors at bright magnitudes are caused by image qualities becoming poorer due to diffraction spikes and ghosts.

RMS errors in position are enhanced over all magnitudes, as can be seen in figure 4.2b.

These parameters are the most crucial for the photometric survey: the positions to determine plate to plate pairs, the magnitudes to determine colours, and log(area) and ellipticity to eliminate galaxies. The magnitude and position errors are smaller than errors introduced from other effects: the positional errors of $\approx 1\ \mu$ correspond to < 0.1" at Schmidt plate scales - but with seeing typically 1.5", COSMOS measurement errors can never cause image confusion. Also larger, systematic effects are at work (see section 4.7.1) due to differential refraction or errors in COSMOS astrometry.

COSMOS magnitude errors are small compared to calibration errors (section 4.6) and intrinsic photographic errors (ie. Poisson photon counting statistics and errors associated with the photographic emulsion - see Furenlid, 1978)

4.5 Plate calibration.

A search of the literature revealed that there are no published photometric sequences in the UK Schmidt 927 field. As a result, sequences had to be obtained in order to calibrate the plates. Deep sequences were needed, as the Schmidt plates go as faint as $B_J = 21.5$, so telescope time was sought for CCD photometry. This section describes the sequences obtained, and the reduction procedure adopted. The most general photometric system is that of

Cousins (1980a- and 1980b) based on the old Johnson system (Johnson and Morgan, 1955), for which many calibration standards are available (Graham, 1982, Landolt, 1983, and Stobie, Gilmore and Sagar, 1985). This is the system adopted here. No attempt has been made to calibrate the galaxy magnitudes, which as a result must be excluded from the survey. It should be pointed out here, that the magnitudes ultimately used are slightly modified, for reasons given in section 4.7.2.

4.5.1 Sources.

Photometric calibration was carried out using CCD frames in which there was a high incidence of stellar objects in the CCD field. Visual inspection of the Schmidt plate gave a number of different field centres, and photometry was obtained for as many of these as possible. The requirement for the CCD field centres was to obtain a large number of stellar objects close to the centre of the Schmidt field, and then individual CCD fields close to the edge of the Schmidt field. This is so that a sequence could be fitted to the Schmidt data with no danger of large scale field effects, using the data at the centre, then field effects could be identified, by comparison with the edge fields. Only three complete sets were eventually obtained, details of which are given in table 4.3.

The ESO frames were obtained while doing spectroscopic confirmation of grens survey objects. INT frames were kindly provided by Dr. R.D. Cannon, who took them while engaged on a photometry project of his own, and the AAT frames were part of a service data request.

Table 4.3: Photometry obtained

Telescope	Date	Field (1950)	Colours
ESO 3.6m	Feb. '86	10 39 15 +4 59 15	B, V
"	"	10 39 41 +4 47 30	B, V
INT	Mar/Apr86	10 39 15 +4 59 15	U, R, I
"	"	10 39 41 +4 47 30	U, R, I
AAT service	Jan. '86	10 33 11 +2 52 34	U, B, V, R, I

CCD chips used at all three telescopes were of a similar type: a thinned, back illuminated RCA chip of 320 x 512 pixels. The physical size of the pixels is 30 μm^2, giving the following frame sizes for the different telescopes: the ESO 3.6m frame size was 3.6' x 5.8', the INT frame size was 3.9' x 6.3', and the AAT frame size was the smallest at 2.6' x 4.2'.

Both fields at 10^h39^m lie close to the centre of the Schmidt field 927, and together provide about 40 calibration points in R, and about 23 points in U. This number varies somewhat because of the different plate limits of plates within the same photometric band.

The magnitude distribution of the calibration points is good over the range of interest for calibrating the Schmidt plates. The actual range of the data points can be seen by reference to the calibration curves, shown in figure 4.9.

The AAT service field is in one corner of the Schmidt field, though some one degree away from either of the closest edges to avoid vignetting effects in the Schmidt plates. This field provides an additional 12 calibration points in R, and 5 additional calibration

points in U. It is also intended as a check on large scale plate variations in the Schmidt field.

4.5.2 Data reduction.

All data were reduced using the STARLINK FIGARO 2-d reduction package. With this software system, it is possible to do all operations of bias subtraction, frame division, defringing and photometry required. Occasionally, as special needs arose, new pieces of software were implemented. For example, the bias frame subtraction procedure was largely automated, and the weighting function in the aperture photometry routine was modified.

4.5.2a ESO CCD frames.

The bias level is essentially a constant over the CCD frame. This was subtracted from object frames, calibration frames and flat fields. Dark current frames were obtained, but after bias subtraction negligible dark current was found, so no dark current subtraction was done. Flat fields in B and V were normalized to one. Object frames and calibration frames were then divided by flat fields of the appropriate colour. Data frames were then checked for field flatness by collecting statistics in small areas of the chip containing no celestial objects or blemishes. These tests show that small scale variations (measured by the standard deviation of the area) does not change appreciably across the chip in either B or V. Large scale variations (as measured by the change in local mean) are smaller than 1% over most of the

chip in both B and V. There was a more significant difference close to one corner of V fields, but this area of chip is small and no measurements were made close to it. However, field variation that was found, was non-random. This was caused by the dramatic field vignetting which occurs in the EFOSC instrument (due to a design error), when a filter is in place. Because the effect was so small, it was not worth attempting to eliminate it. It is, therefore, a source of error.

Calibration frame data taken at ESO were field F867-8 (from Stobie, Gilmore and Sagar, 1985) and field E5 (from Graham, 1982). The F867 field was more useful, as it is a CCD observation of many stars, tied to the E region standards, which could provide a check for colour effects. Grahams E regions are six or seven photoelectric observations over about 1 degree^2. The photometric accuracy of the E-regions is about the same as that of Stobie, Gilmore and Sagar, but because Graham used a photoelectric photometer, it was only possible to obtain one or two standards per CCD frame. It was far more productive, therefore, to use the Stobie, Gilmore and Sagar frames.

Aperture photometry was carried out using a synthetic, weighted aperture of 8 pixels diameter (5.4"). Radial profiles (figure 4.3) show that at this distance from an objects' centre, the profile is indistinguishable from the sky background. Instrumental magnitudes, M_I, are calculated to be :

$$M_I = -2.5 \log(\Sigma w_i I_i - \Sigma w_i I_{sky})$$

where the summation is over all pixels in the aperture. The I_i's are

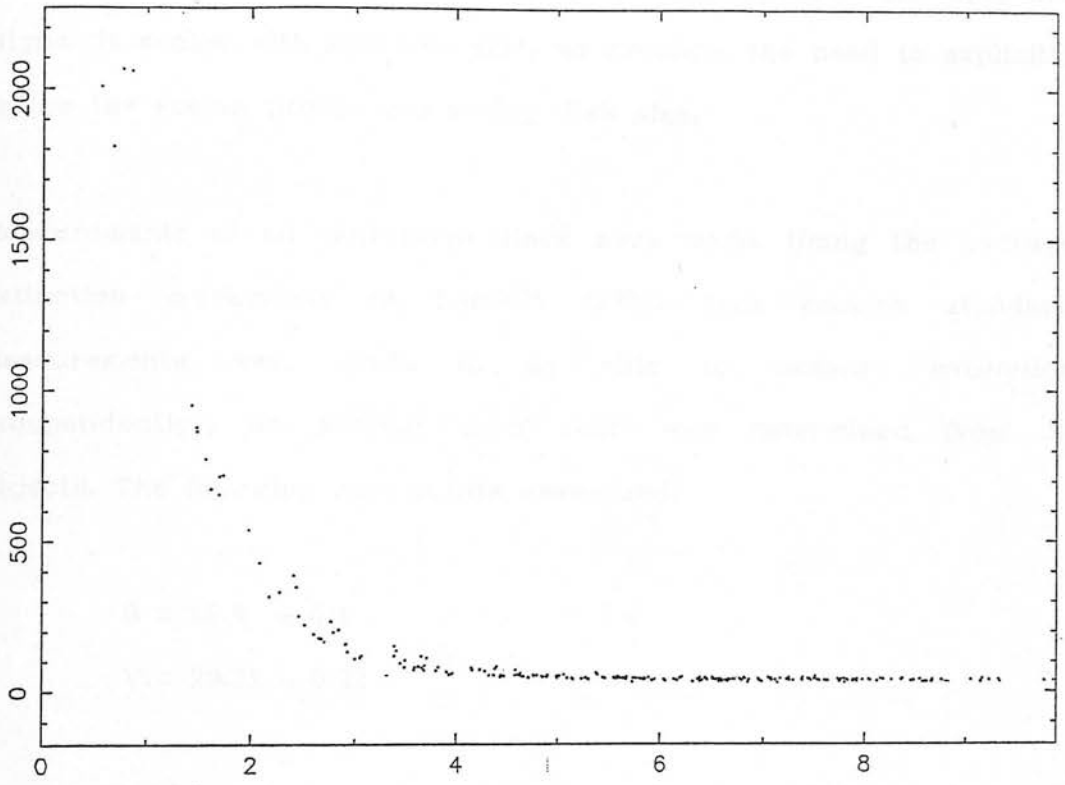

Fig 4.3 A radial profile from one of ESO calibration frames. Data are number of counts versus radial distance in pixels from the centroid of the object. The object is quite indistinguishable from the sky by pixel 4 from the centre, so the choice of this as the aperture size is reasonable.

measured intensities in the aperture, and I_{sky} is the mean sky intensity in an annulus surrounding the object, calculated after exclusion of bad pixels. The w_i form a weighting function, which is flat topped and slopes gently away from unity towards the aperture edges. It scales with aperture size, so avoiding the need to explicitly define the seeing profile and seeing disk size.

Measurements of all calibration stars were made. Using the average extinction corrections of Landolt (1983) (not enough standard measurements were made to be able to measure extinction independently), an average zero point was determined from all objects. The following zero points were used:

$$B = 28.8 \pm 0.1$$

$$V = 29.32 \pm 0.02$$

which are normalized to an arbitrary exposure time of 5 seconds. A colour relationship was looked for using these standard measurements (figure 4.4) but any relationship is smaller than the errors.

As a result, the object stars were measured, and the following calibration equations were used to obtain real magnitudes from measured values:

$$B = 28.84 - M_I - k_b X$$

$$V = 29.32 - M_I - k_v X$$

Where M_I = instrumental magnitude (defined above).

X = airmass

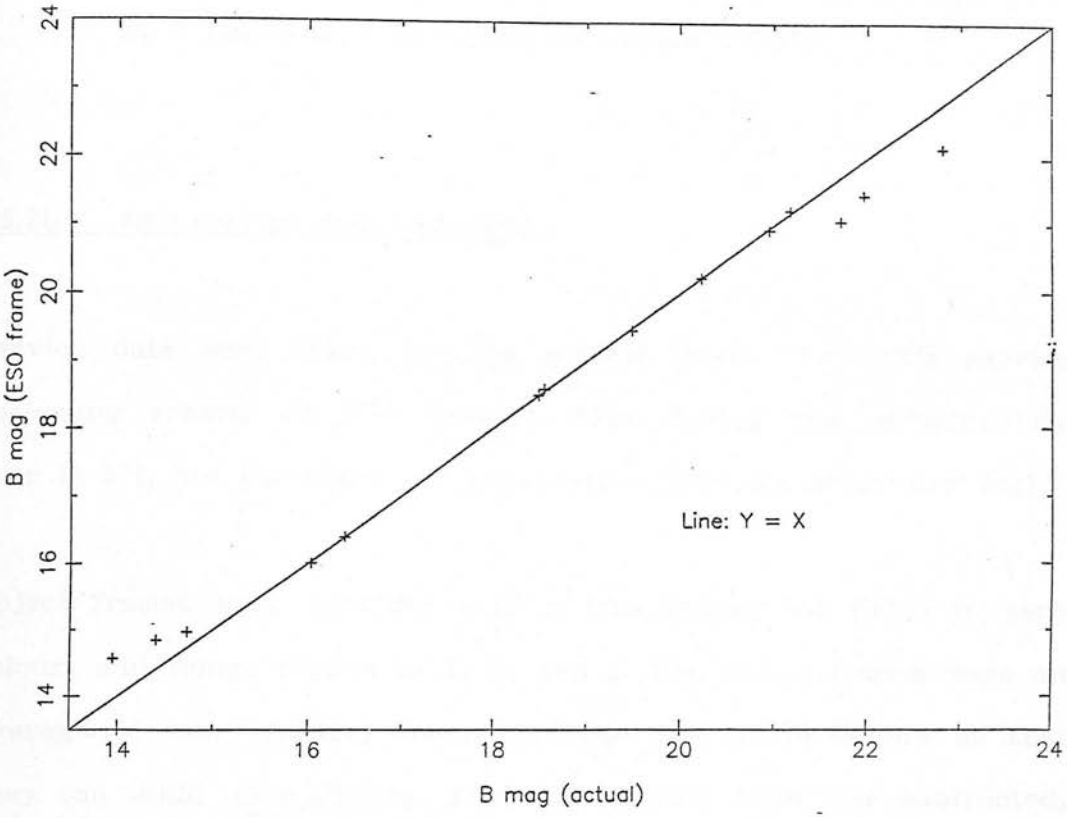

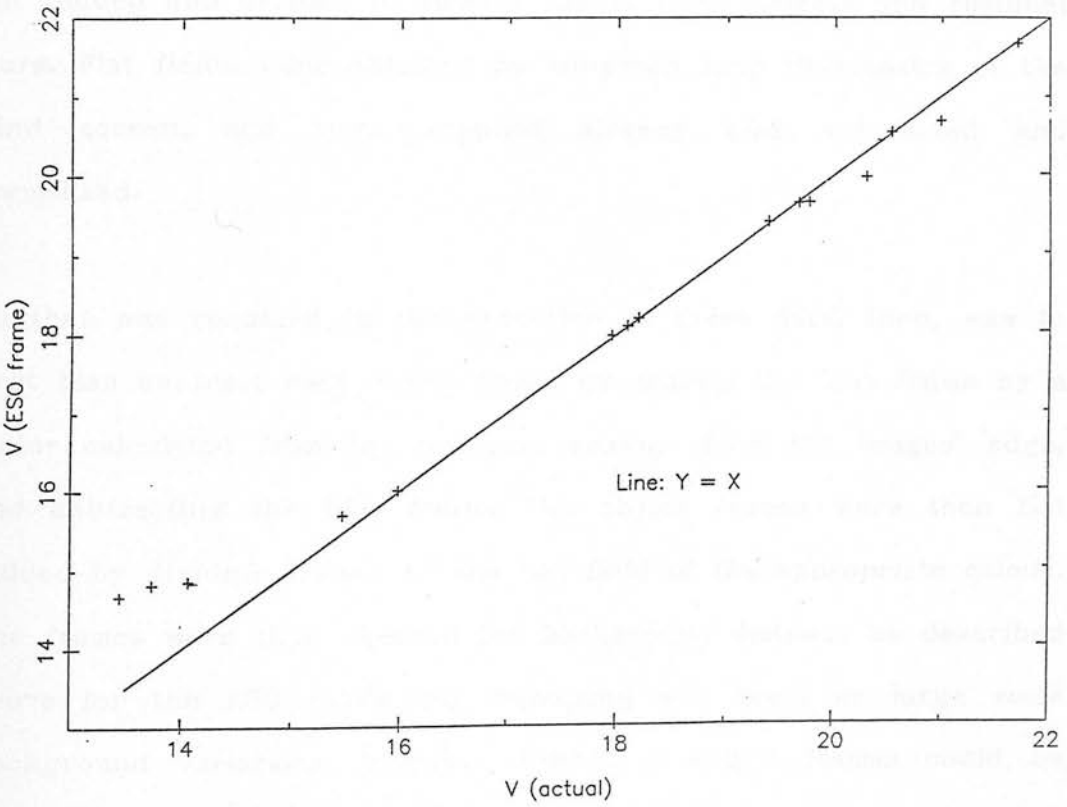

Fig 4.4 Measured magnitudes from F867 standards versus published magnitudes for both the B and V bands used at ESO. The average zero point (excluding bright saturated objects) and extinction correction have been used. Any colour relation would show as a deviation from the plotted line.

k_b = Landolts' B extinction correction = 0.283

k_v = Landolts' V extinction correction = 0.172

4.5.2b AAT service data reduction.

Service data were taken for the project under the AAT's service observing scheme on 14th January 1986. Seeing was unfortunately poor (≈ 3"), but the night was photometric (from the observers' log).

Object frames were provided with a bias frame, flat fields in each colour, and fringe frames in V, R, and I. The fringe frames were an average of many frames, donated to the AAT by observers so that they can build up a library. They had already been bias subtracted, flat fielded and cleaned to remove cosmic rays, defects and residual stars. Flat fields were obtained by tungsten lamp illumination of the wind screen, and were supplied already bias subtracted and normalized.

All that was required in the reduction of these data, then, was to first bias subtract each object frame by scaling the bias frame by a factor calculated from the overscan region along the images' edge, and subtracting the bias frame. The object frames were then flat fielded by dividing frames by the flat field of the appropriate colour. The frames were then checked for background flatness as described above for the ESO CCD's. No vignetting was seen, or large scale background variations. Finally, the V, R and I frames could be defringed.

Fringes are caused by the narrow emission features in the night sky background, which can produce interference patterns when incident on a thinned, back illuminated CCD chip (whose thickness is only of the order of the incident light). The effect is worst in the red, because longer red wavelengths are more comparable to chip thickness, and because there are strong atmospheric lines in the red. For these frames, fringes were noticeable in the V, R and I. To remove the fringes from the object frames, then, an area of the object frame was chosen which contained no objects. The mean of the fringe frame is then calculated in this area, which is subtracted from the frame. A scaling factor is then calculated, which will minimize the noise on subtraction of the object frame by the scaled fringe frame. In all cases, the fringe frame subtraction was performed such that any residual fringes were smaller than 1% of the size of the background.

The AAT also provide calibration equations, which are based on standard star observations taken of Landolt (1983) and Graham (1982) standards. Observations were taken throughout the night to yield the zero point correction and airmass terms, but colour terms and cross terms were based on data collected at the AAT over the preceeding months. These equations were generated using a synthetic aperture which integrates all light to a radius of 24 pixels. The equations are given below:

$$U = 21.690 - 2.5\log(ADU/T) - 0.56X + 0.07X(B-V)$$

$$B = 23.576 - 2.5\log(ADU/T) - 0.27X + 0.15(B-V) + 0.01X(B-V)$$

$$V = 23.197 - 2.5\log(ADU/T) - 0.13X + 0.05(B-V) - 0.04X(B-V)$$

$$R = 23.201 - 2.5\log(ADU/T) - 0.13X - 0.07(V-R) + 0.05X(V-R)$$

$$I = 21.844 - 2.5\log(ADU/T) - 0.08X + 0.02(R-I) - 0.01X(R-I)$$

Here, ADU = sum of sky subtracted pixels within aperture.

T = exposure time in seconds.

X = airmass.

Although most of the red colour and cross terms are negligible, all were used as the zero point calculations included them. The FIGARO aperture photometry program was modified in order to make final object photometric measurements, excluding a weighting function and including these equations.

4.5.2c INT CCD frames.

For the reduction of INT CCD frames, I followed a similar procedure to that used for the ESO and AAT frames. Dark current frames, taken at the time of observations, showed that there was negligible dark current, so no corrections were needed for dark current. First, the bias level was subtracted from each frame. No separate fringe frames were available - the flat fields were taken of the night sky at twilight, in the (mistaken) belief that the chip did not produce fringed images. As it turned out, the V, R and I science frames all had significant fringes. The key point here is whether the fringes at twilight scale in intensity at the same rate as the night sky background (which is what is being measured by the flat fields). If they do, then the fringes will divide out of object frames in the same operation as the flat fielding (although the objects themselves are not flat fielded correctly - see below). If they don't, then some fringing

pattern will remain after flat fielding. In this case, dividing by a normalized flat field did eliminate all traces of the fringes in the background of the V and R science frames, but still left significant residual fringes in the I band. This problem was overcome by constructing an artificial flat field from the sky limited object frames. All of these were used (ten, from the whole run), so that there were ten sky limited values for each pixel. After normalizing the frames, the median of these ten values was found for each pixel (the mode should really be used, but is much more computationally extravagant). The value so calculated for each pixel should have any traces of object flux removed (unless one is unlucky enough to have objects on the same region of chip in a large number of frames), and so is used at the appropriate location in the output frame. A flat field is thus produced which has the sensitivity variations caused by the chip and optics, and fringes scaled to the same ratio above the background as those on the science frames.

Dividing science frames by this flat field takes out the sensitivity variations of the chip, and since the fringes have been appropriately scaled, in the background regions they disappear. It must be remembered, though, that fringes are not a sensitivity variation: they are effectivly additive. Thus, dividing by fringes scaled by the appropriate factor will free background areas from fringes, but any fringes on objects are scaled by the wrong factor. This is a source of measurement error, then, for both sky flats and atrificial flats. It is the best flat fielding that can be done unless frames free from atmospheric fringes are available (ie. dome flats).

Throughout the observing run, observations of calibration standards

from Landolt (1983) were made. These provided a check on the photometric quality of the night, and were then used (again using Landolts' average extinction measurements) to determine average zero point corrections and colour equations for each band.

Zero points found are given in table 4.4, and colour equation fits are shown in figure 4.5. When this had been done, program object stars could be measured, and used for the photometric calibration of the Schmidt plates.

Table 4.4: INT zero points.

Band	Zero point
U	22.71 ± 0.09
B	25.97 ± 0.08
V	25.72 ± 0.05
R	25.67 ± 0.05
I	24.77 ± 0.04

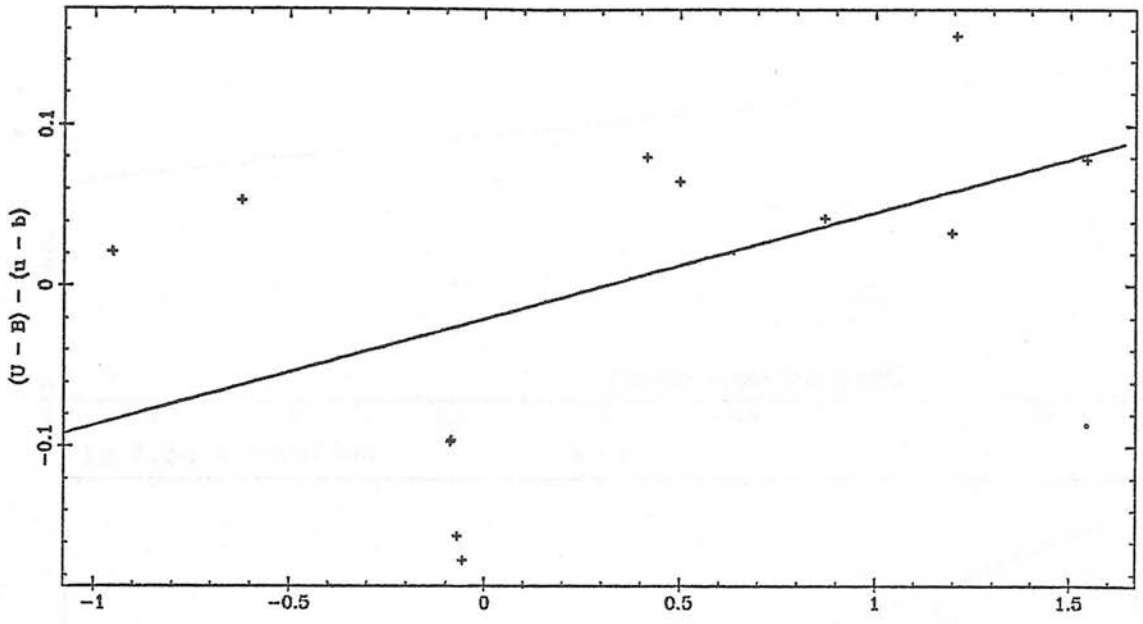

Fig 4.5a U equation

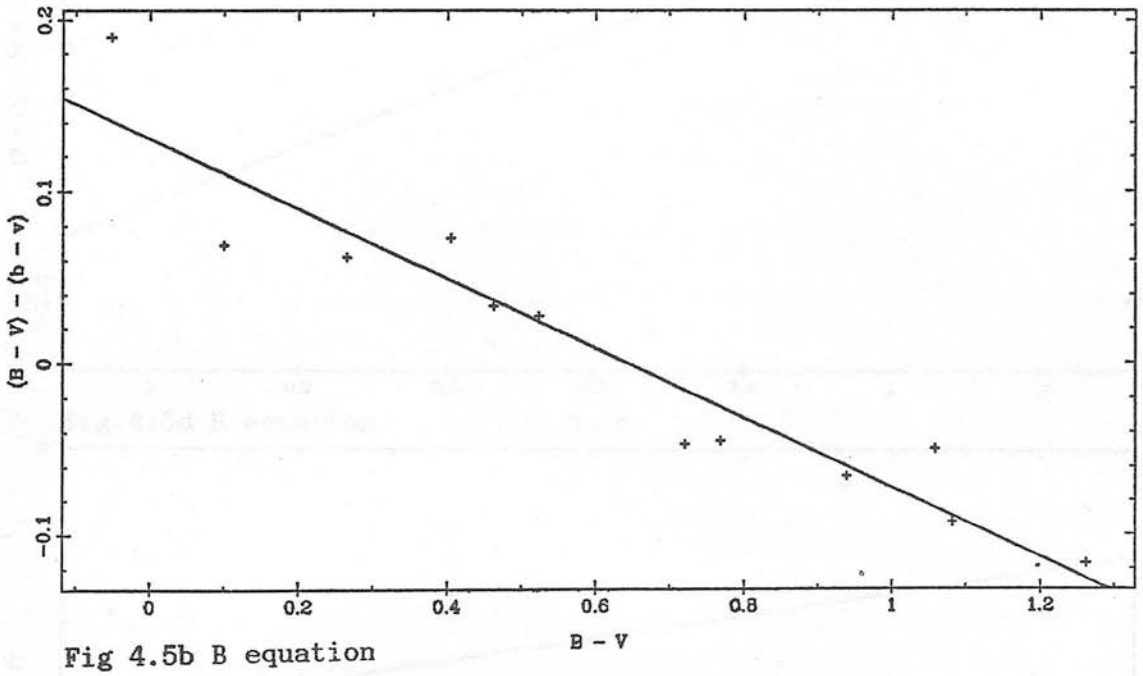

Fig 4.5b B equation

Fig 4.5 Colour equations derived for the INT CCD data. Lines drawn are least squares best fit straight lines to the data points, which are measurements of Landolt standards. Upper case values are those measured. Lower case are from Landolt. Only the 'B' equation was applied to the data.

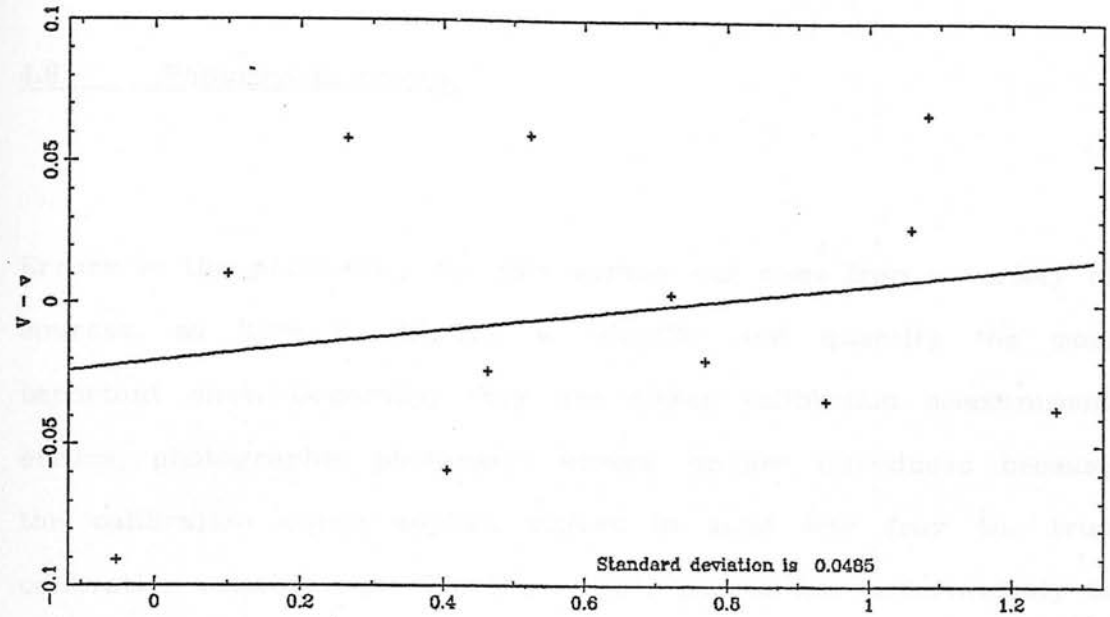

Fig 4.5c V equation

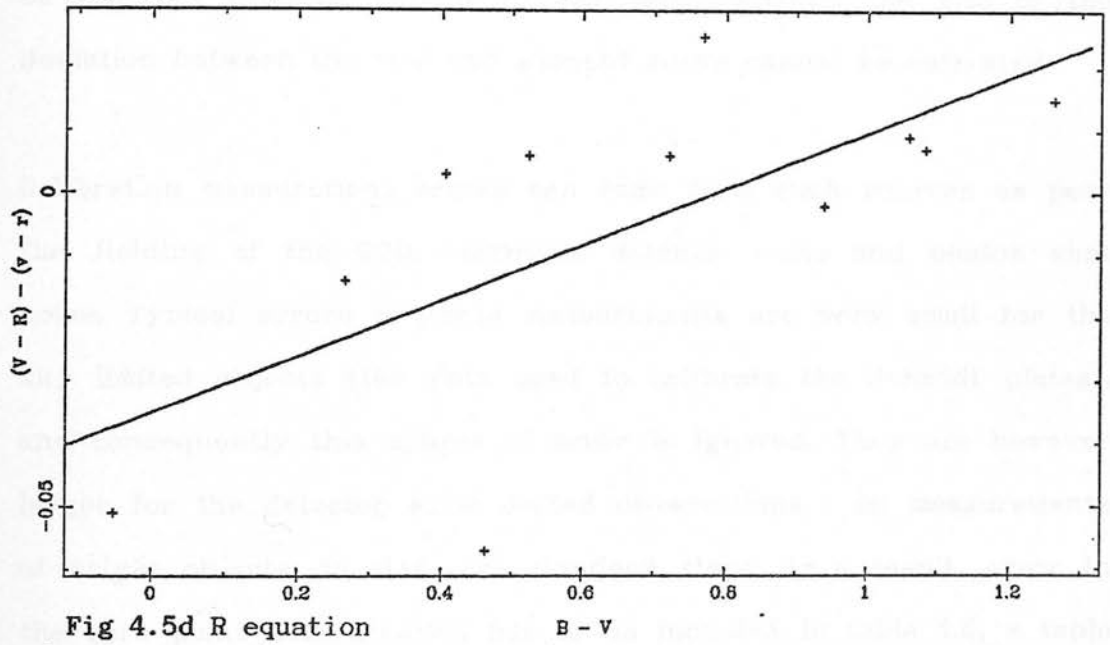

Fig 4.5d R equation

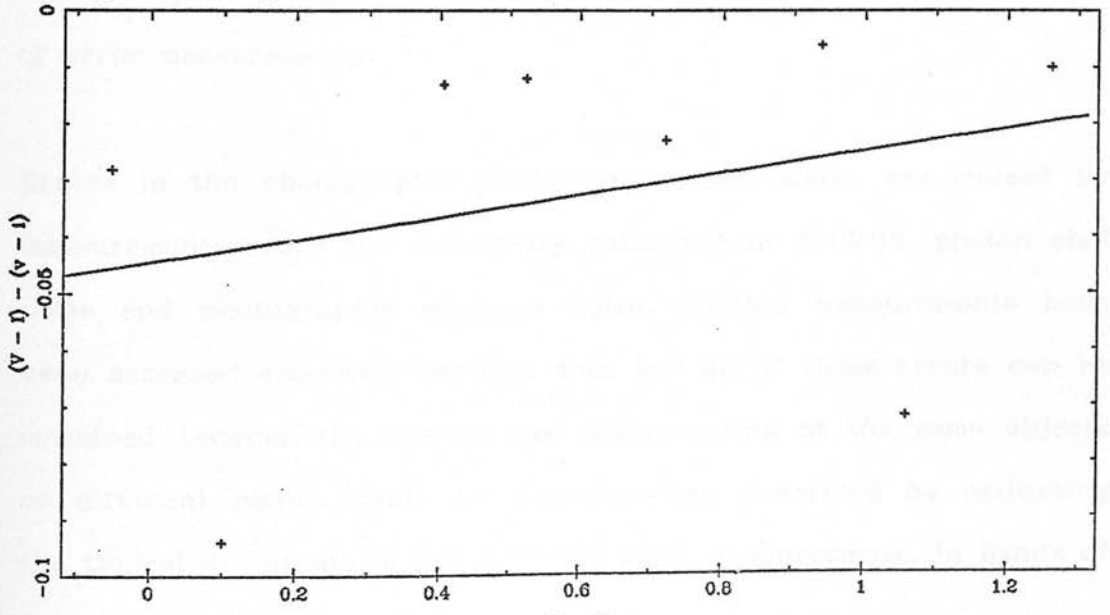

Fig 4.5e I equation

4.6 Photometric errors.

Errors in the photometry for this survey can come from a variety of sources, so here I will try to identify and quantify the most important ones. Generally, they are either calibration measurement errors, photographic photometry errors, or are introduced because the calibration curve applied differs in some way from the true calibration relationship. This third error source has unfortunately to be ignored, because without further measurements, the size of the deviation between the real and adopted curve cannot be estimated.

Calibration measurement errors can come from such sources as poor flat fielding of the CCD, electronic detector noise and photon shot noise. Typical errors in these measurements are very small for the sky limited objects (the data used to calibrate the Schmidt plates), and consequently this source of error is ignored. They are however larger for the detector noise limited observations - ie. measurements of bright objects, in this case standard stars. As a result, error in the zero point determination has to be included in table 4.5, a table of error measurements.

Errors in the photographic photometry measurements are caused by measurement errors and sensitivity variations in COSMOS, photon shot noise and photographic emulsion noise. COSMOS measurements have been assessed elsewhere (section 4.4), but all of these errors can be combined because the survey has measurements of the same objects on different plates. Table 4.5 was therefore generated by estimating the typical deviations in the different plate measurements, in bands of

magnitude, after the exclusion of galaxies - section 4.7.4. So, no account is made of the effect of variable objects, which is assumed to be small.

Table 4.5: Photographic photometry errors.

Magnitude → / Band ↓	15	17	18.5	20	zero point	no. of plates
U	0.112	0.091	0.095	0.099	0.09	4
B_J	0.047	0.060	0.074	0.096	0.02	3
V	0.403	0.315	0.302	0.214	0.05	3
R	0.063	0.092	0.083	0.165	0.02	3
I	0.082	0.096	0.131	-	0.03	3

A general picture emerges from this table, confirming ones knowledge of the emulsions and calibration process: generally, errors are likely to be larger at fainter magnitudes, but at bright magnitudes they are also bad because of COSMOS induced field effects, which are worse at bright magnitudes, and because there are fairly few calibration points here, and also because the curvature of the calibration curve is high at bright magnitudes. It is more important for the survey to get the calibration curve right at fainter magnitudes, so the fitting process (section 4.7.6) concentrated on this.

Also, the different emulsions show their differences: the V band, which uses the old medium grain size IIaD emulsion compares badly with the bands which use the modern higher quantum efficiency fine grained emulsions.

4.6.1 The intrinsic width of the stellar main sequence.

Ultimately, the photometric candidate selection technique will not be dominated by photometric accuracy but by intrinsic physical mechanisms that broaden the stellar zero-age main sequence on H-R diagrams. It is therefore of interest to try to evaluate these, and see what contribution to the broadening might be expected from the different effects.

The 'best' colour-magnitude diagrams (best in the sense of having the tightest main sequence locus) come from observations of globular clusters - eg. Richer and Fahlman (1986), who have measured a dispersion of 0.01 magnitudes at V = 21.7 - the limiting accuracy of their photometry. This can only show what little effect the broadening mechanisms described below have on globular clusters, since the situation is very different in the solar neighbourhood.

There are four broadening mechanisms which have a substantial role to play in broadening the solar neighbourhood zero-age main sequence locus.

Firstly duplicity. It is well known that about 50% of stars in the solar neighbourhood are doubles - see for example van de Kamp (1971). Clearly, unless the individuals of a pair happen to be well matched in spectral type, the temperature difference between the members will produce an observed object of unusual colours. It is not clear what the distribution of mass ratios is, it is not possible to say how large this effect is. Presumably pairs with very large mass difference will also be very different in luminosity, and therefore it is pairs of

moderate difference that would cause the problem.

Secondly, differing metallic abundances can substantially shift the positions of stars of a particular spectral type on two-colour or H–R diagrams - see for example Wildey *et al.* (1962) who show that shifts of 0.14 magnitudes are typical in stars of the same spectral type, due to line blanketing effects.

Thirdly, a stars' rotation can change its position on the zero-age main sequence. The size of the change depends not only on the rotation velocity but also whether it is seen pole-on or equator-on. Stritmatter (1969) gives a theoretical explanation for this effect.

Finally, unlike stars in a globular cluster, stars in the solar neighbourhood are likely to have a considerable spread in ages, and so some stars will have evolved away from the zero-age main sequence. Iben (1967) has calculated the theoretical width of the main sequence due to evolution to be 0.2 magnitudes

Iben (1967) has also estimated that the contributions to main sequence broadening are about the same from abundance differences, rotation and evolution, so allowing the same contribution from duplicity brings the combined estimate from all of these effects to be about 0.4 magnitudes, or a typical width of 0.55 magnitudes in two colour diagrams. These estimates can only be a very rough indication at best - the observational measurements are poor or lacking. But never the less, the photometric errors calculated in the last section are fairly small, in comparison to this intrinsic width. Rare errors ($> 3\sigma$) are comparatively large and can still scatter objects out of the stellar

locus.

4.7 Plate reductions.

4.7.1 Pairing plates in the same colour.

Pairing of the COSMOS datasets was carried out using the HAGGIS pairing facility. Because it took ≈ 2 hours of CPU time on the VAX 11/780, and many pairing operations were required, the HAGGIS program was modified. Tests performed by Dr. Miller (private communication, 1986) revealed that writing out the paired datasets consumed the most CPU time, so that it was only necessary to modify the output section of the HAGGIS program. The rest of the program remains unaltered. This saved about 1 hour of CPU time per pairing operation, without changing the operational algorithm of the program at all.

The pairing operation that is performed is a simple matching of two coordinates. COSMOS provides astrometry for every object on the plate, as two of the IAM parameters (see table 4.2). This is done by searching standard star catalogues, and identifying catalogue stars in the dataset. Astrometric accuracy is estimated by the COSMOS team to be at worst ≈ 2" (MacGillivray, private communication 1986). As the x,y positions on the plate could in principle vary from measurement to measurement, and are quite likely to change from plate to plate of the same field, I decided to use this astrometric information for the pairing. The pairing program must be presented with a 'primary'

dataset and a 'secondary' dataset. Each object in the primary is inspected, to see if one of the secondary dataset objects lies within a specified tolerance of the primary object. For each pair found, a new object is created in the output dataset. It is also possible to retain information about any remaining unpaired objects in either dataset, so that checks can be performed to deduce whether pairing was satisfactory. If more than one secondary dataset object lies within the tolerance box of a primary object, or if two or more primary dataset objects have the same secondary object within their tolerance boxes, the pair with the shortest separation is chosen and written to the output catalogue, and this fact is noted and reported to the program user. That this operation is performed correctly is of crucial importance, because if under some circumstances the wrong object is chosen then the output dataset will contain an object with peculiar colours - just what is being searched for. As the number of objects being looked for is probably no more than 1% of the total dataset, it would be fairly easy to swamp the objects selected with legitimately odd colours if incorrect pairings are made in the pairing process. As the pairing program was fairly new when the project was started, it seemed wise to perform independent checks to those the program author had made. As a result, the first catalogues paired were grids of test points. The secondary dataset was a similar grid pattern to the primary, but offset from the corresponding primary object by various amounts. In this way, several small faults in the pairing program were located, which the author of the pairing program kindly fixed. In particular, the number of multiple matches found was not correctly recorded, and sometimes if a secondary object lay close to the edge of a primary tolerance box, a pair was not found due to mistaken rounding error handling in the pairing code.

Next, the optimum pairing tolerance was found. This was done by pairing the same two datasets (two of the V plates) together with varying error box size. Plots could then be made of tolerance size versus the number of pairs, and tolerance size versus number of multiple matches found (figure 4.6). It is seen that at about 3", the number of pairs found flattens dramatically, and at the same tolerance size the number of multiple matches starts to increase very rapidly. This result is fairly reasonable, because the seeing disc size is typically ≈ 1.5", and astrometric errors are of the same order. If there are systematic effects in the astrometry program, they are likely to be cause by badly measured catalogue positions. Since all of the programme plates are of a similar epoch, systematic effects are thus likely to be the same on different plates.

However, Dr. Miller (private communication, 1986) discovered that there sometimes <u>are</u> systematic effects of up to ≈ 1" from plate to plate in the same colour. These are likely to be caused by varying atmospheric refraction from plate to plate - no special zenith angle was specified with the plate requests, so they are at different angles. This effect can be corrected be selecting the brighter images (although not the <u>very</u> bright ones, which have poor positional accuracy due to a relatively large area of saturated emulsion at the centre of the image, and the different centroids of different image components) on both plates. ≈ 40000 images were used, which could then be paired with confidence using a much larger than usual tolerance size (5") without including many multiple pairs. The positions from both the primary and secondary databases were retained, and this dataset was used to locate and correct any substantial errors that were found. Dr. Miller has written a program

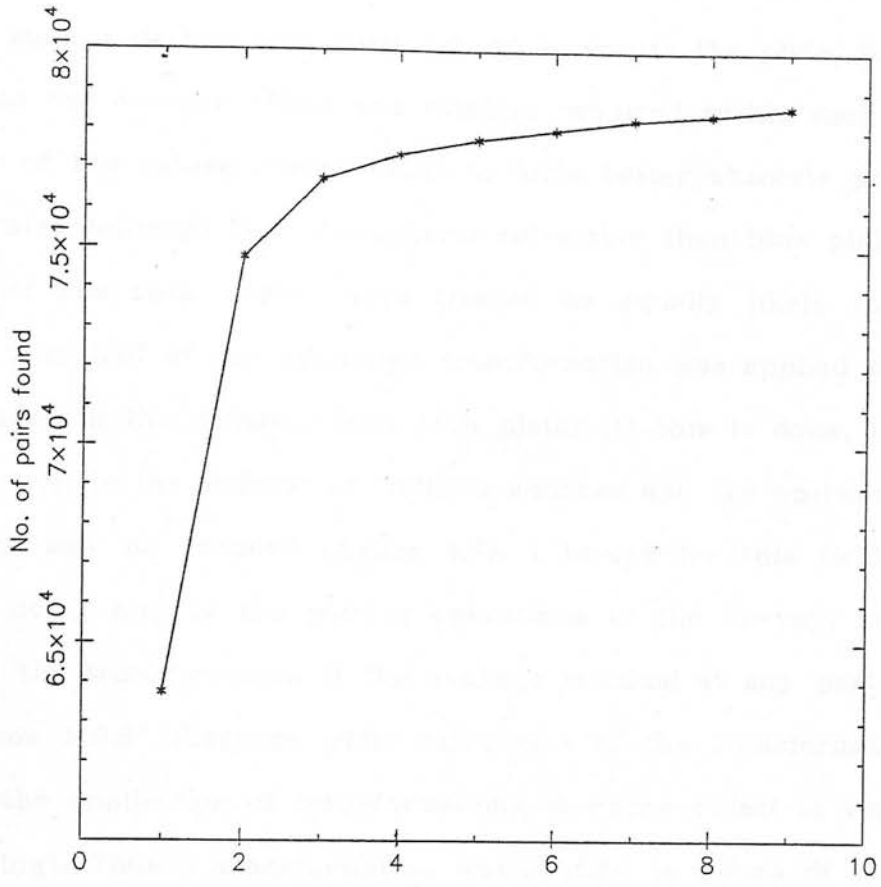

Fig 4.6a

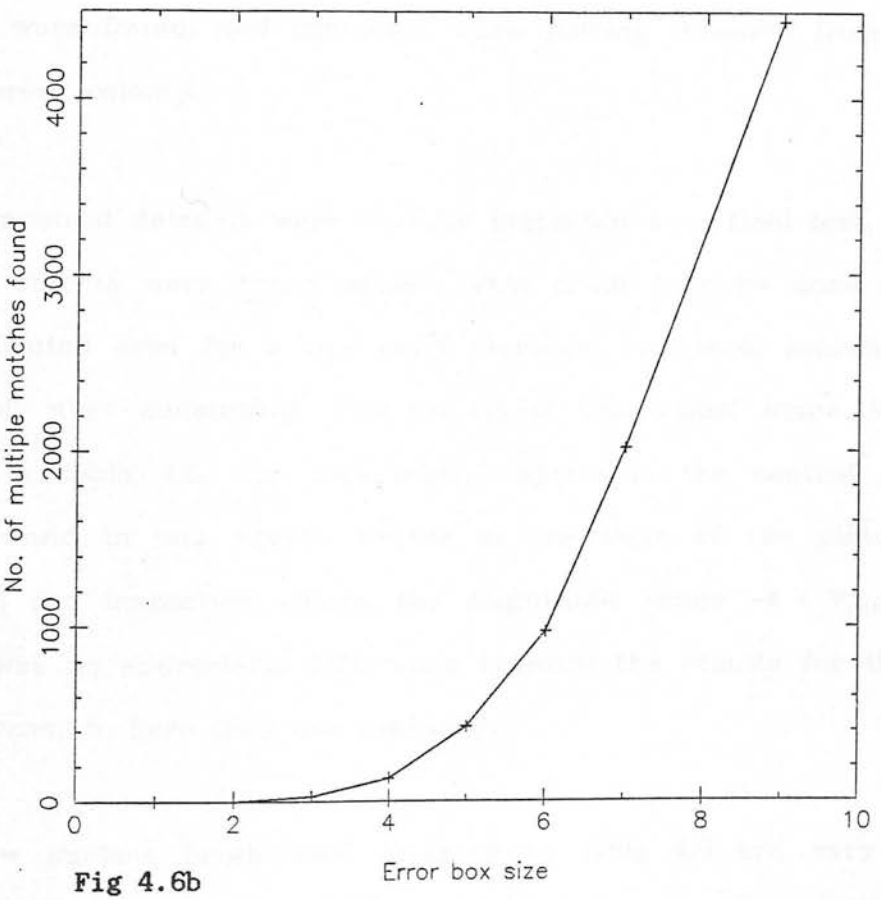

Fig 4.6b

Fig 4.6 Optimum error box sizes. Tolerance box sizes are in arcseconds.
a) Number of pairs found vs. tolerance size.
b) Number of multiple matches found vs. tolerance size.

to bin such a dataset into small sub areas across the plate, and then calculate the average offset and rotation required within each bin. If neither of the datasets were likely to have better absolute positions, (red plates undergo less atmospheric refraction than blue plates, but plates of the same colour were treated as equally likely to be in error) then half of the calculated transformation was applied to all of the images in the datasets from both plates. If this is done, there is a reduction in the number of multiple matches and the optimum error box size may be reduced (figure 4.7). I looked for this field effect before doing any of the pairing operations in the survey, but only applied the transformation if the average residual at any part of the plate was > 0.5" (because while calculation of the transformations is quick, the application of transformations to every object is very time consuming). Thus a transformation was applied to plates of the same colour only occasionally, but sometimes fairly large effects (up to ≈ 1.5") were found, and corrected when pairing datasets from plates of different colours.

Next, unpaired datasets were visually inspected as a final test, to see if real objects were being missed. This could only be done over a fairly limited area for a few plate pairings, as visual searches are extremely time consuming. The results of the visual inspection are shown in table 4.6. For this table, objects in the central square degree, and in one square degree at the edge of the plate were selected for inspection within the magnitude range $-4 < V_{COS} < -2$. There was no appreciable difference between the results for the two plate areas, so here they are combined.

The 'low surface brightness' category in table 4.6 are very faint,

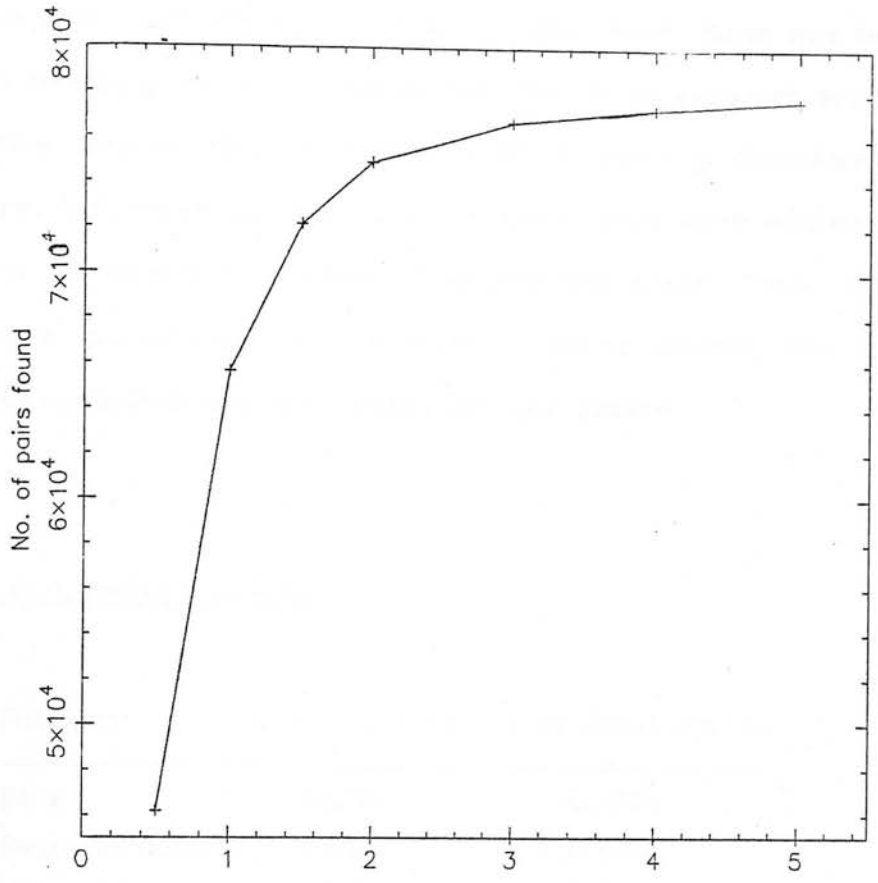

Fig 4.7a

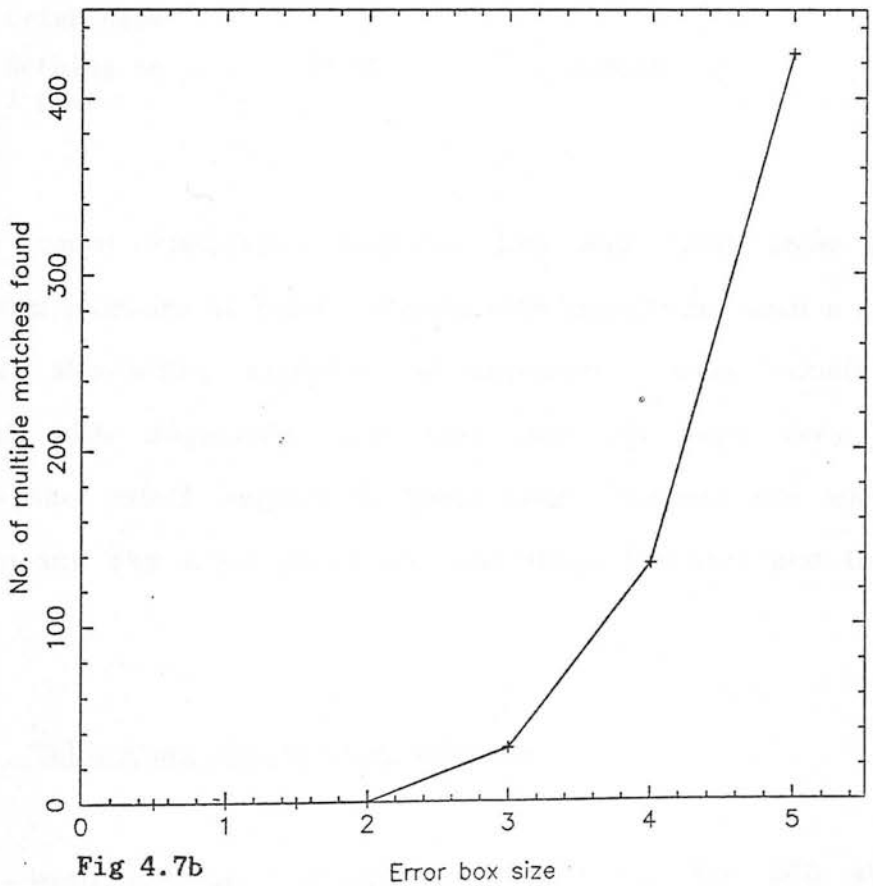

Fig 4.7b

Fig 4.7 Optimum tolerance size after linear transformation.
a) Number of pairs vs. tolerance size (arcseconds).
b) Number of multiple matches vs. tolerance size (arcseconds).

fuzzy objects, virtually undetectable on one plate. Some are brighter, and are probably unpaired due to astrometric or centroid errors. The distinction between these and those marked 'pair' is therefore a little arbitrary, but those marked as pairs are a little more stellar, and so likely to be unpaired because of astrometric error. Table 4.6 shows that as a percentage of the total numbers paired, the numbers remaining unpaired are very small, for any reason.

Table 4.6: Unpaired objects.

Category	$-4 < V_{cos} < -2$	% of total paired
Pair	10.8%	0.002%
Emulsion flaw	13.0%	0.002%
Asteroid	8.7%	0.001%
Low surface brightness	30.4%	0.004%
Nothing on 1 plate	37.0%	0.005%

Number count histograms (figures 4.8a and 4.8b) show steadily increasing numbers of paired objects with magnitude, until a cutoff is reached. Meanwhile, numbers of unpaired objects remain fairly constant with magnitude until they start to grow very rapidly towards the cutoff magnitude. These large numbers are where the emulsion and sky noise peaks are just above the area and threshold cuts.

4.7.2 Calibrating the Schmidt datasets.

As has been mentioned before, in section 4.1, the CCD standard

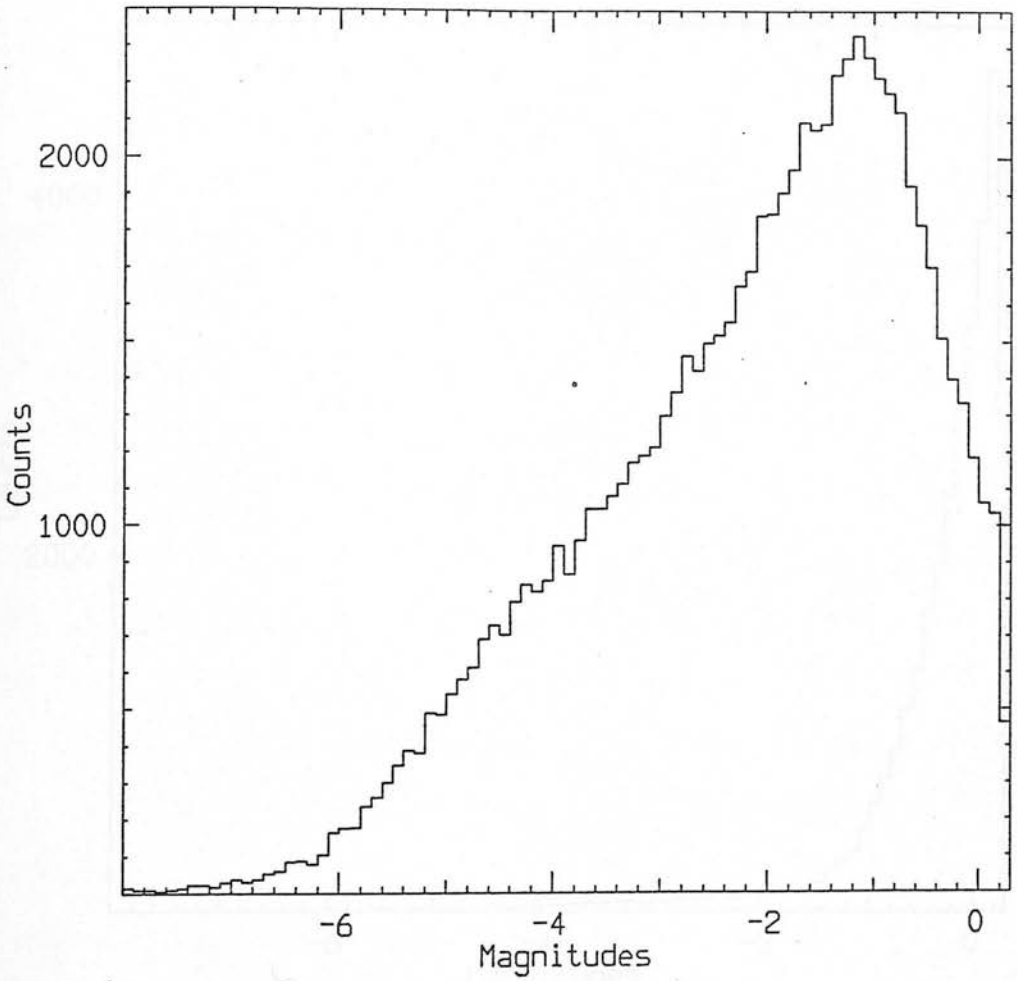

Fig 4.8a The total number of pairs fount after linear transformation as a function of COSMOS magnitude. The data are for the pairing operation between V10091 and V10081, which required transformation under the criterion described in the text.

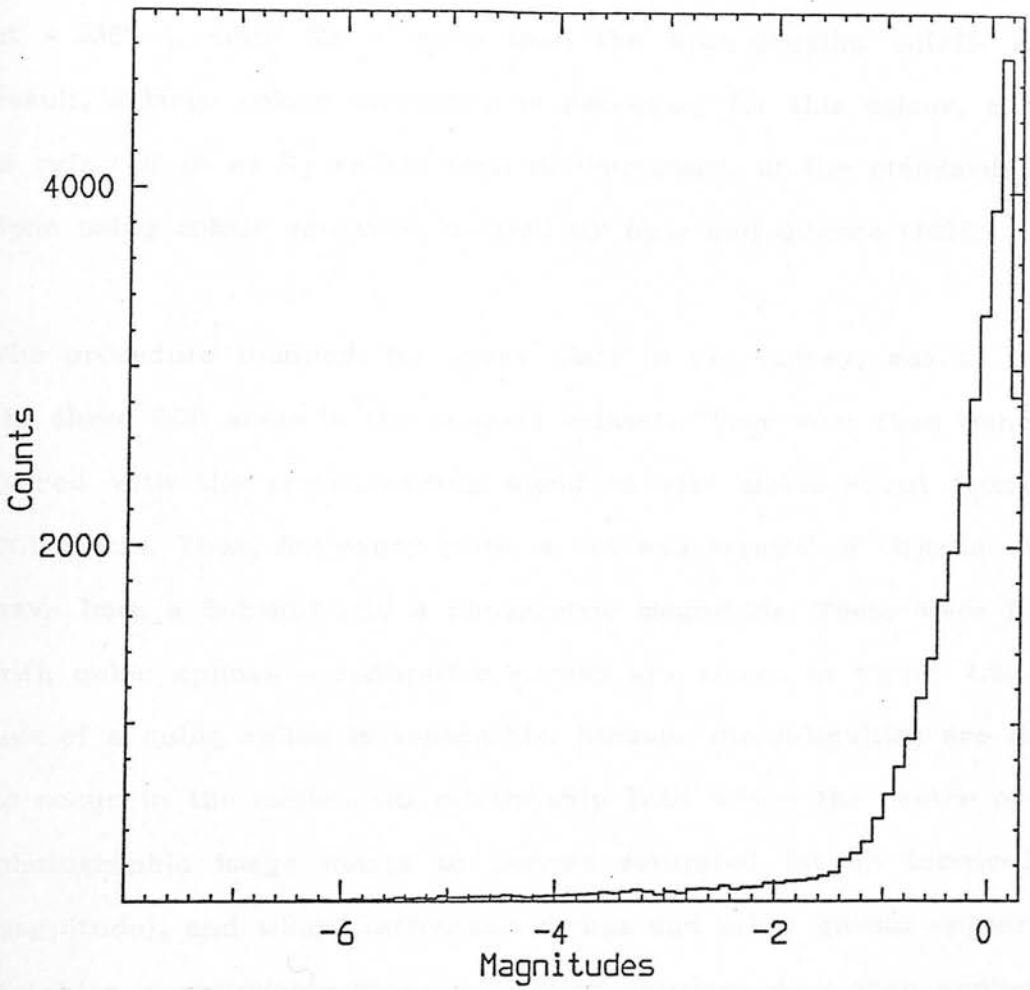

Fig 4.8b The total number of unpaired objects as a function of COSMOS magnitude. The data are from the same pairing operation as those for figure 4.6a.

magnitudes were converted into the 'natural' Schmidt photometric system before use. The main difference is in the B passband - the red end of the Schmidt B passband is defined by the IIIaJ emulsion at ≈ 5380 A, some 600 A more than the Kron-Cousins cutoff. As a result, a large colour correction is necessary for this colour, and so is referred to as B_J rather than B. Conversion of the standards was done using colour equations derived by Blair and Gilmore (1982).

The procedure followed, for every plate in the survey, was to locate the three CCD areas in the Schmidt dataset. These were then manually paired with the corresponding standard star measurement from the CCD frame. Thus, for every plate, a list was created of objects which have both a Schmidt and a photometric magnitude. These were fitted with cubic splines - calibration curves are shown in figure 4.9. The use of a cubic spline is reasonable, because discontinuities are likely to occur in the calibration relationship both where the centre of the photographic image starts to become saturated (at an intermediate magnitude), and where diffraction spikes and other ghosts appear (at brighter magnitudes). These calibration relations were then applied to every object in the Schmidt dataset, except for those whose Schmidt magnitude lay above or below the ends of the spline fit. Thus it is ultimately the calibration relation which defines the survey cutoff at faint magnitudes, as in all cases there were objects on the plate fainter than the faintest calibration objects. Faint magnitude cutoffs are given in table 4.7. At brighter magnitudes, the survey cutoff is defined by the presence of ghosts and diffraction spikes in the images. These tend to introduce errors in the spline fit, because discontinuities between image characteristics are sharp, and there are only a small number of brighter calibration points. As a result, bright

Fig 4.9a U9140

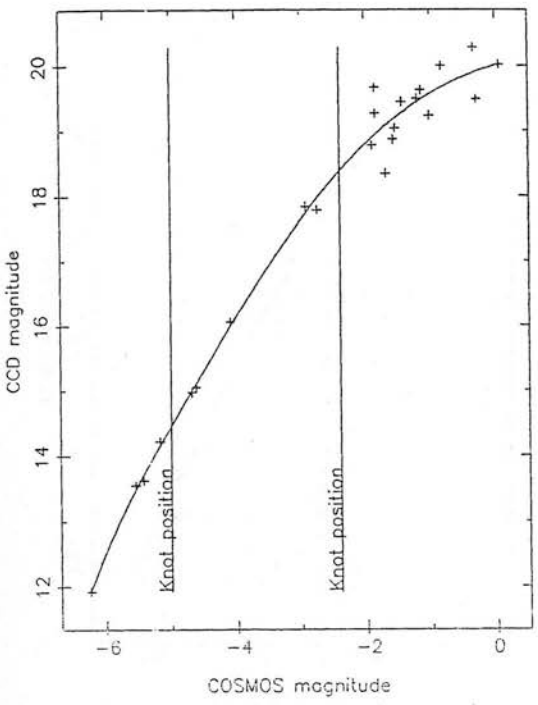

Fig 4.9b U10082

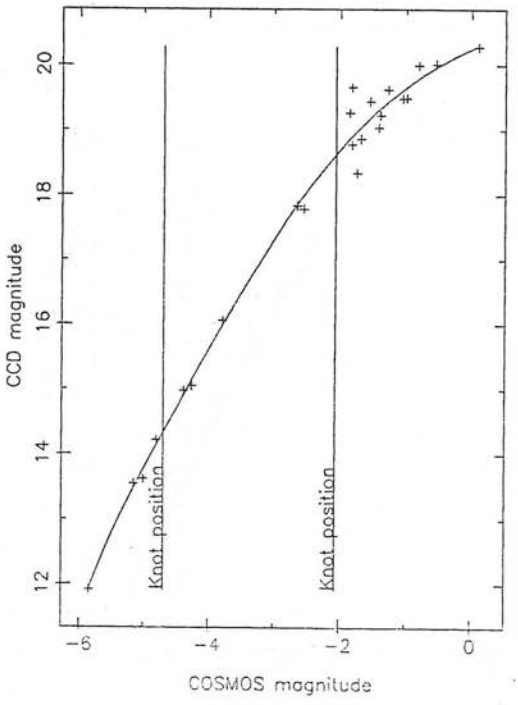

Fig 4.9c U10032

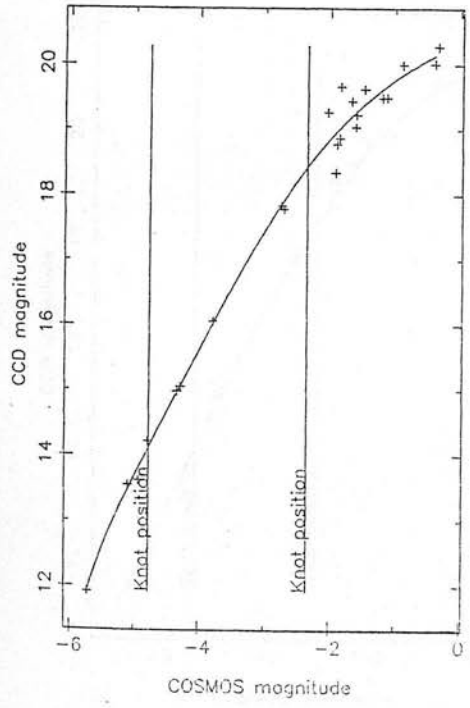

Fig 4.9d U11076

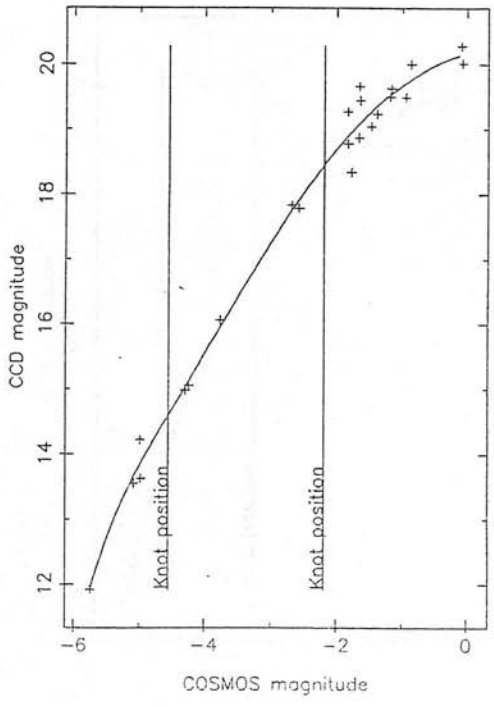

Fig 4.9 Calibration curves, showing calibrated CCD magnitudes as a function of COSMOS magnitude, and the best fit cubic spline.

Fig 4.9e J10063

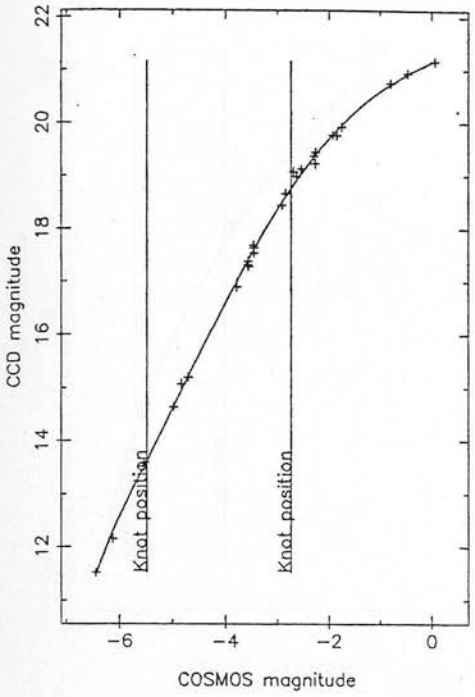

Fig 4.9f J10128

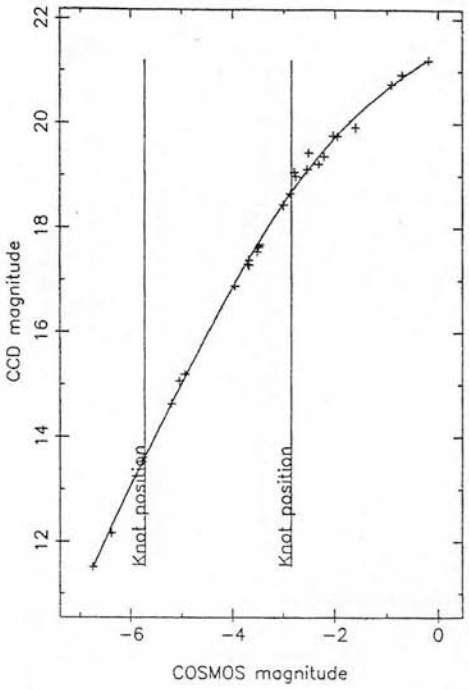

Fig 4.9g J10715

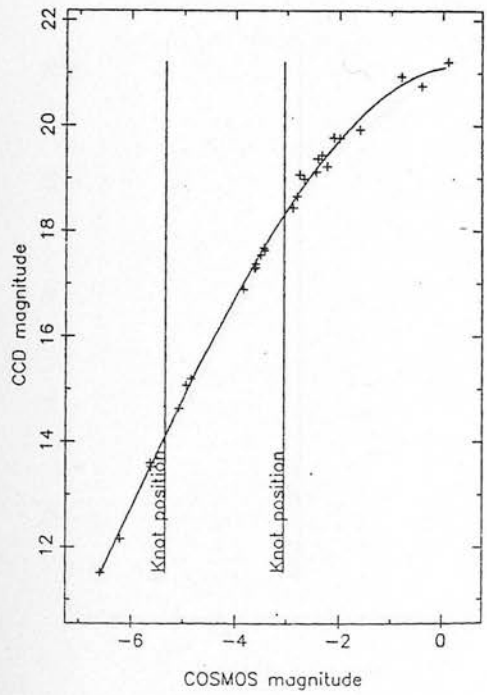

Fig 4.9h V10070

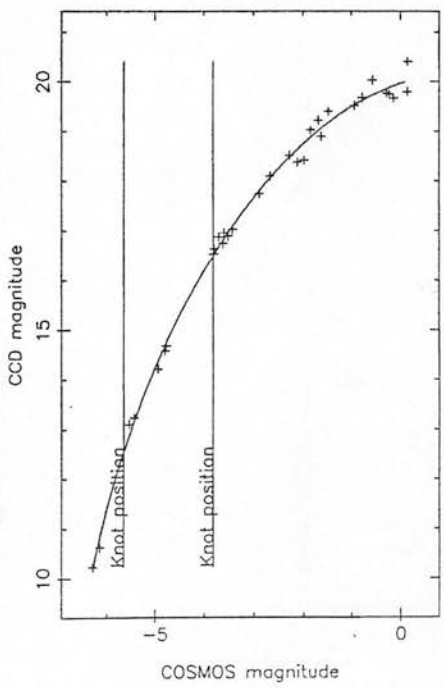

Fig 4.9 (continued)

Fig 4.9i V10081

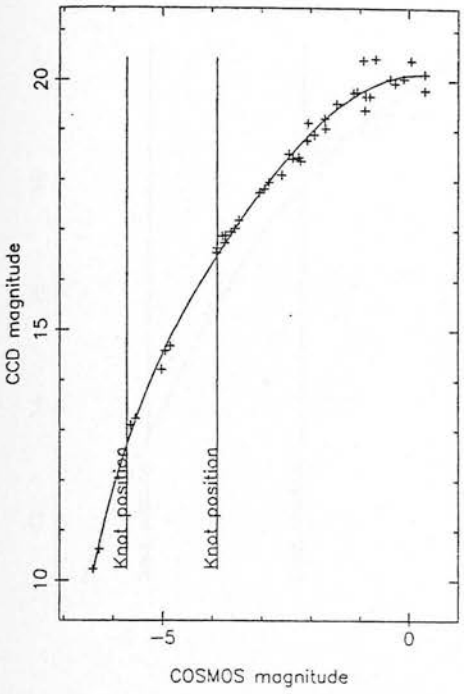

Fig 4.9j V10091

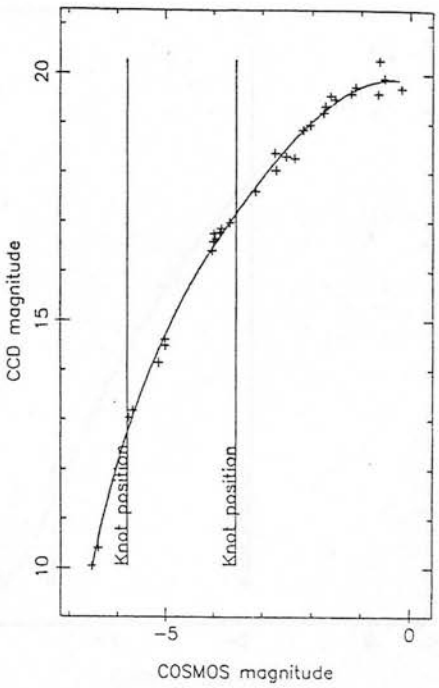

Fig 4.9k R9949

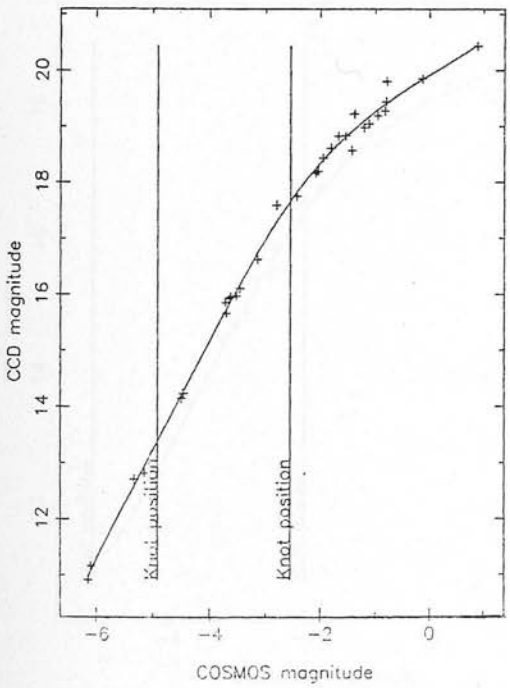

Fig 4.9l R9884

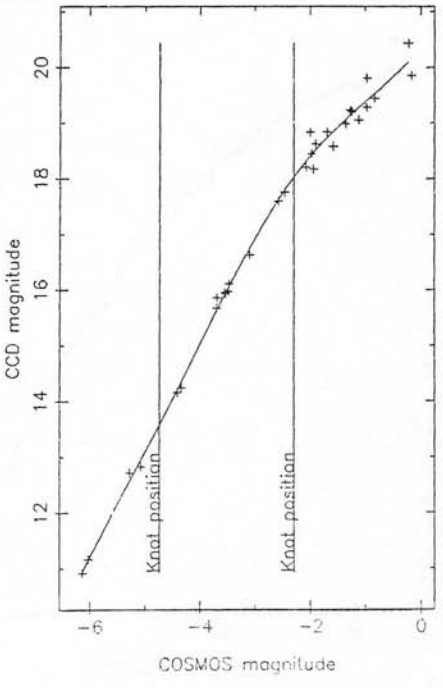

Fig 4.9 (continued)

Fig 4.9m R10071

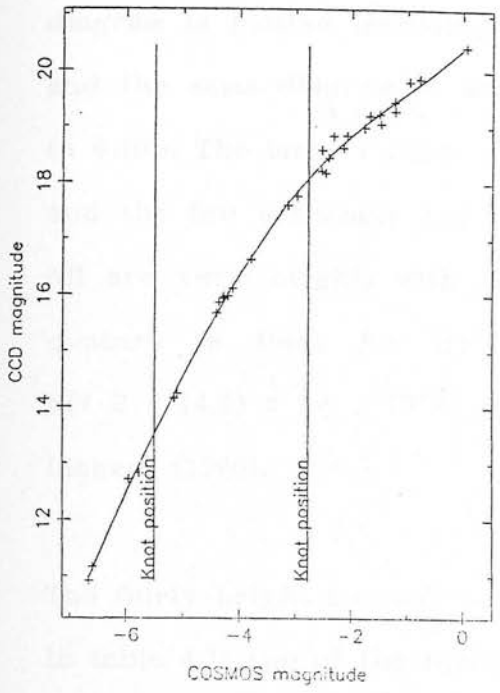

Fig 4.9n I10045

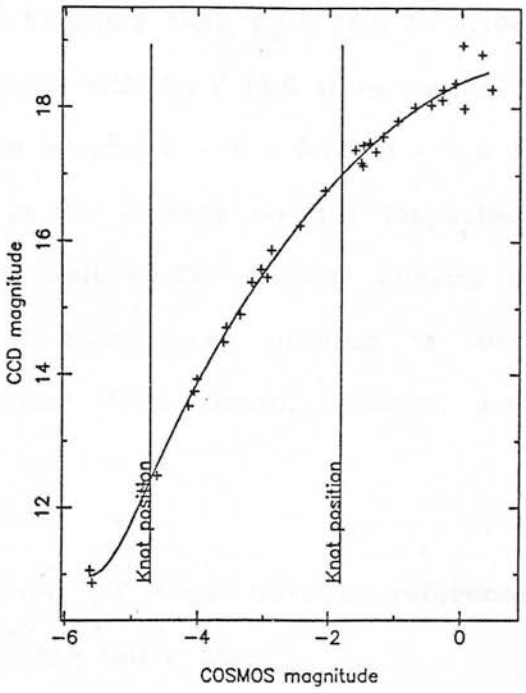

Fig 4.9o I10766

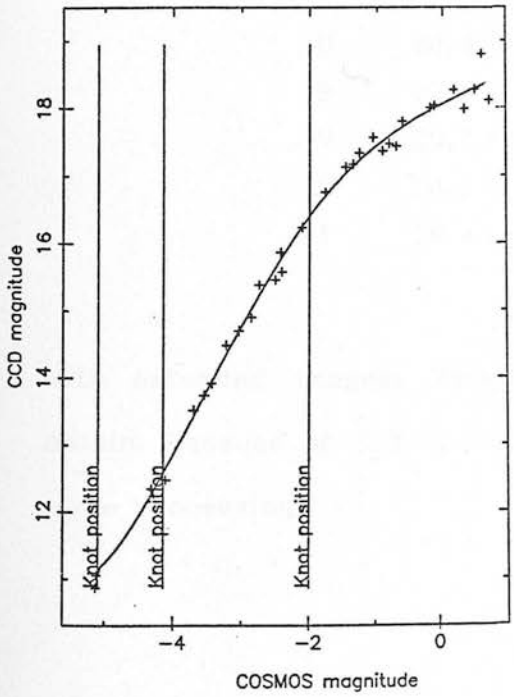

Fig 4.9p I10900

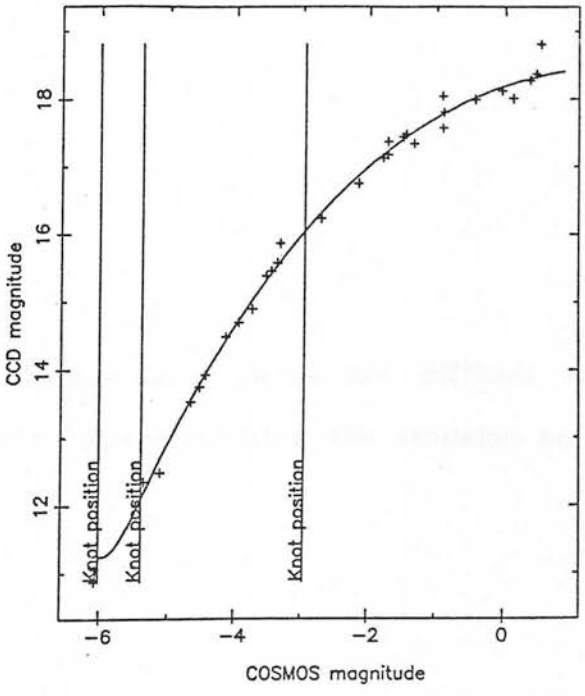

Fig 4.9 (continued)

objects ($B_J \leq 14$) are calibrated badly, and so have peculiar colours. This is demonstrated in figure 4.10, in which a U - B vs. B - V diagram is plotted including objects brighter than $B_J = 14.5$ in 4.10a, and the same diagram in which objects with $B_J < 14.5$ were excluded in 4.10b. The large number of objects around U - B = 0.75, B - V = 1, and the few extremely red objects in U - B were visually inspected. All are very bright, with diffraction spikes. The number density of quasars is tiny, for $B_J < 14.5$, of course, so nothing is lost. $N(< B = 14.5) = 1.8 \times 10^{-3}$ per degree^2 from Green, Schmidt and Liebert (1986).

The fairly bright I cutoff shown in table 4.7 is explained by reference to table 4.1: two of the three I plates are fairly poor,

Table 4.7: Faint magnitude cutoffs of the photometric survey.

Band	Magnitude
U	20.4
B	21.5
V	20.1
R	20.1
I	18.4

with extended images. Very high quality I plates are difficult to obtain, because of difficulties with hypersensitizing the emulsion and plate processing.

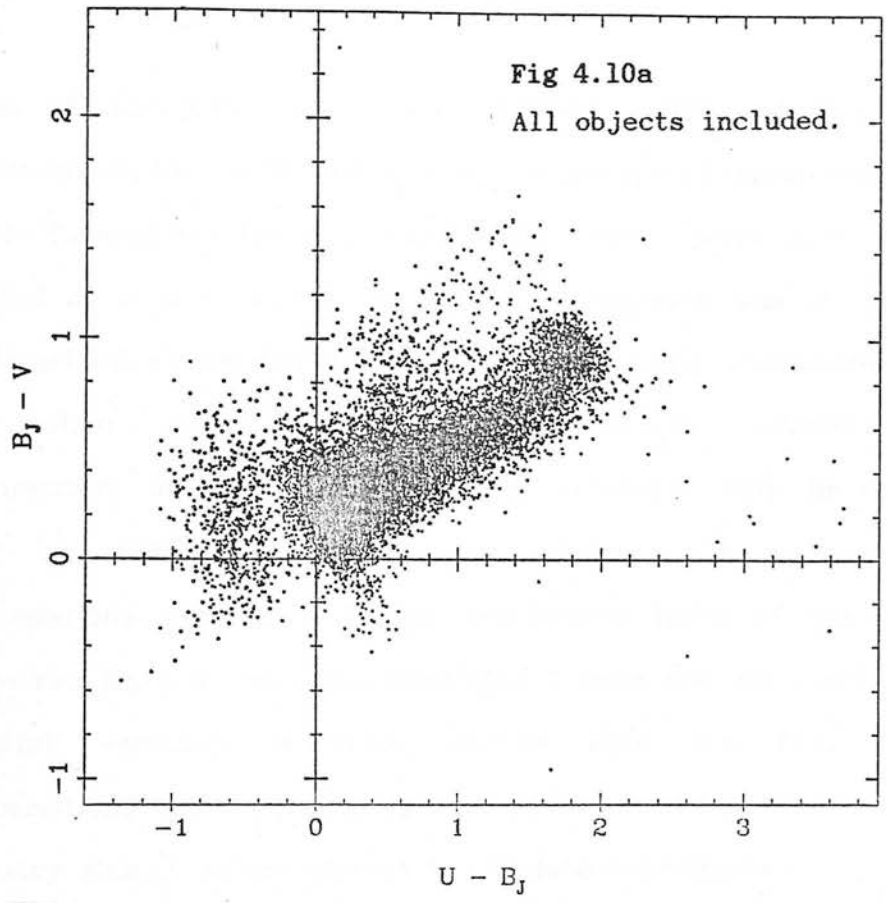

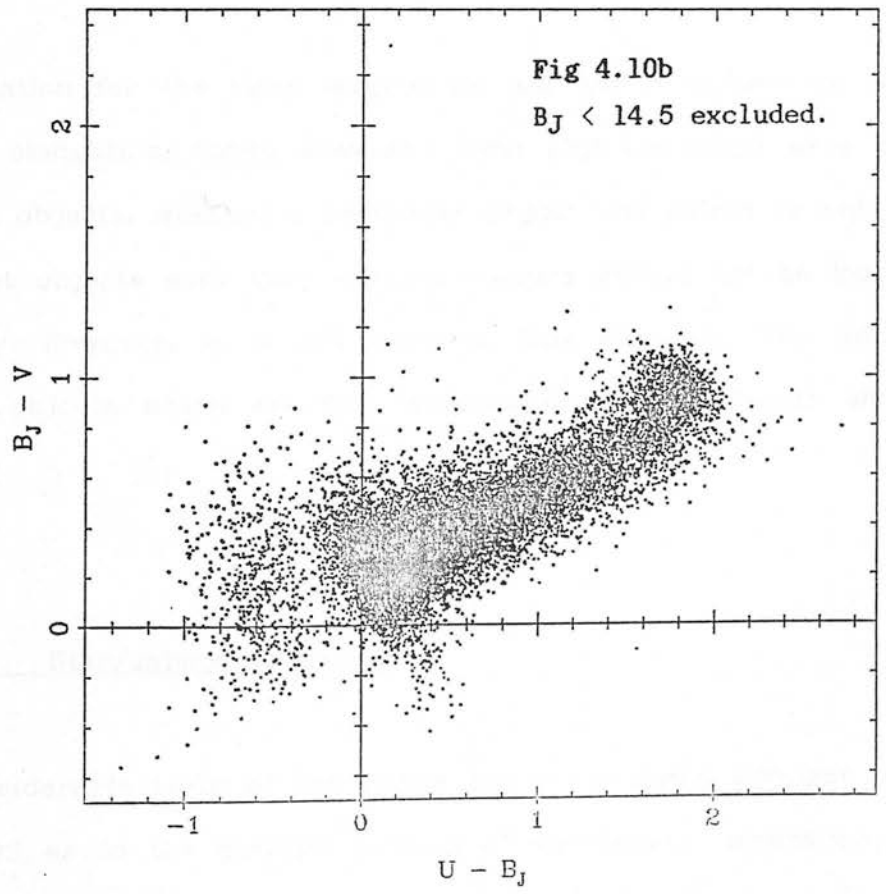

Fig 4.10 Two colour plots, showing $U - B_J$ vs. $B_J - V$. Magnitudes used are averaged over all plates in the band, after calibration.

4.7.3 Pairing datasets across colour.

Datasets of different colours were paired together at the earliest opportunity, so that a catalogue might be generated containing all the available information for each object. Spurious objects could then be discarded at a later stage. The pairing procedure was the same as that described in section 4.7.1, with the following extensions: in all cases, when pairing datasets of different colours, linear transformation of the coordinates was required. This is evidently caused by differential atmospheric refraction. As a result, all transformations were made to the astrometric frame of the R band, because red light is refracted least (the I band was not used because the IIIaF emulsion is much deeper than the IVn, and so transformations are more reliably defined to the R band) and so the R astrometry should be the closest to absolute coordinates.

Information for the mean magnitudes and other parameters (such as image elongation, image area and local sky intensity) were retained for all objects, whether a particular object was paired or not. This is so that objects with very extreme colours should not be lost to the survey. However, it is not clear at this time how the information about objects which are not represented in all datasets should be used.

4.7.4 Star/galaxy separation.

A considerable body of experience has accumulated amongst users of COSMOS as to the optimum method of star/galaxy separation. Hewett

(1983), Prestage (1985), Miller (1986, private communication) and Collins (1986, private communication) have all put considerable time and effort into this problem. As a result, I have adopted the single easiest adequate approach, based on their experience, with only a small amount of checking to ensure that my expectations were met. In fact, as noted by Prestage (1985), looking for stellar images is far easier than looking for galaxies, because most selection criteria actually divide single stars from 'other objects', rather than galaxies. This 'other objects' category contains galaxies, some overlapped objects, and elongated images, such as meteors, while the single stars are a well defined reference point in IAM parameter space. As a result, separation in log(area) vs. magnitude plots (after excluding very elliptical or elongated images, where an image was of sufficient area to reliably use ellipticity information) seemed the most productive. Plots of these parameters reveal a well defined stellar locus, with the galaxies a distinct distance away. The gap gradually grows smaller with increasing magnitude, until the two loci merge at about $B_J = 19$. This selection procedure breaks down at bright magnitudes, but the brighter images had already been rejected (discussed above). The only remaining questions were which area and magnitudes to use, and how to do the separation. Plots in figure 4.11 show different combinations of a) $\log(A_1)$ vs. M_{u1}, b) $\log(A_1)$ vs. M_1, c) $\log(A_a)$ vs. M_a where A_1 is the area from the deepest plate in the band, A_a is the average area from all plates, M_{u1} is the uncalibrated magnitude from the deepest plate, M_1 is the calibrated magnitude from this plate, and M_a is the mean (calibrated) magnitude from all plates in the band. Inspection of these plots led to the use of $\log(A_a)$ vs. M_a for the separation, since the gap between the two loci is visible to fainter magnitudes on this diagram.

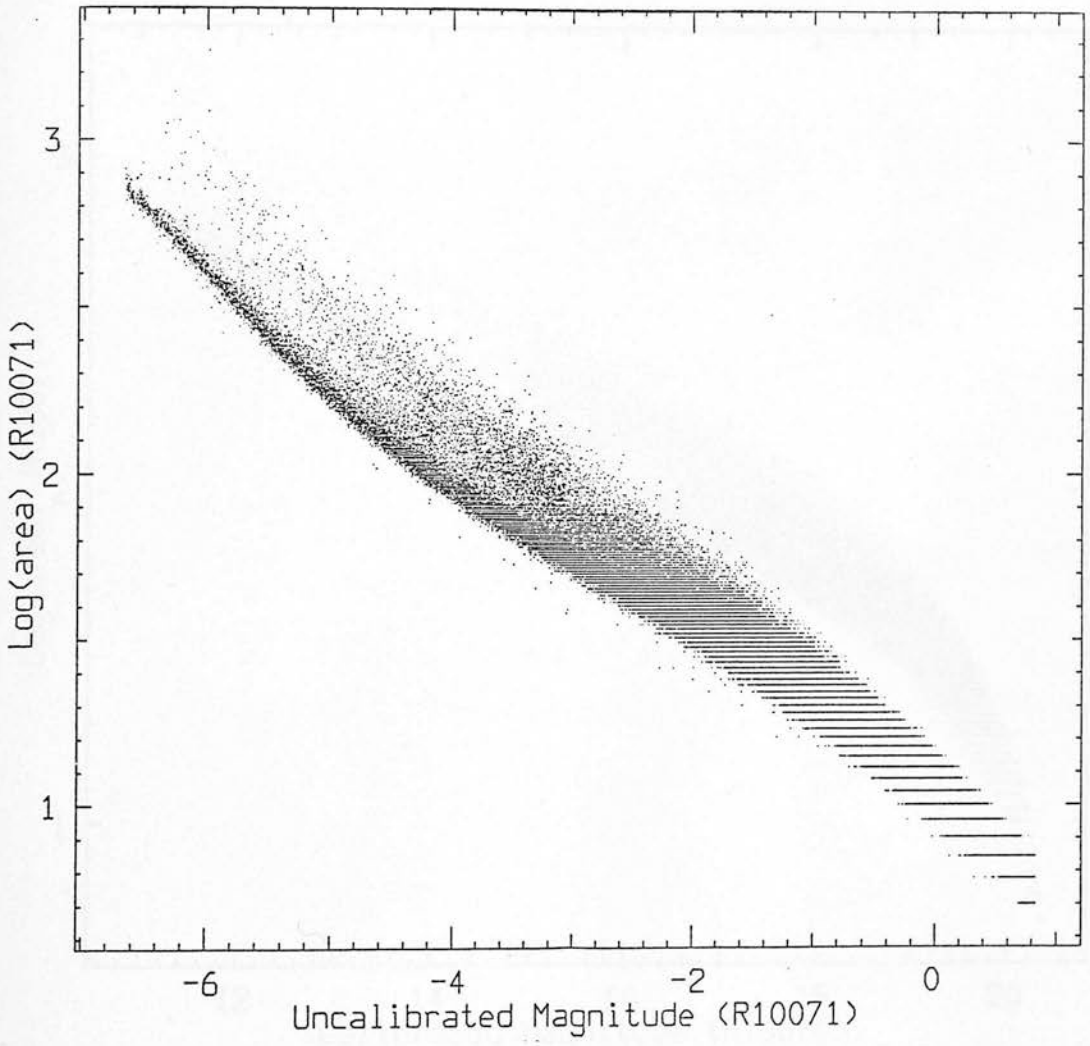

Fig 4.11a Star / galaxy seperation: Log(area) as a function of COSMOS magnitude. Both area and magnitude are from the best plate in the R band, R10071.

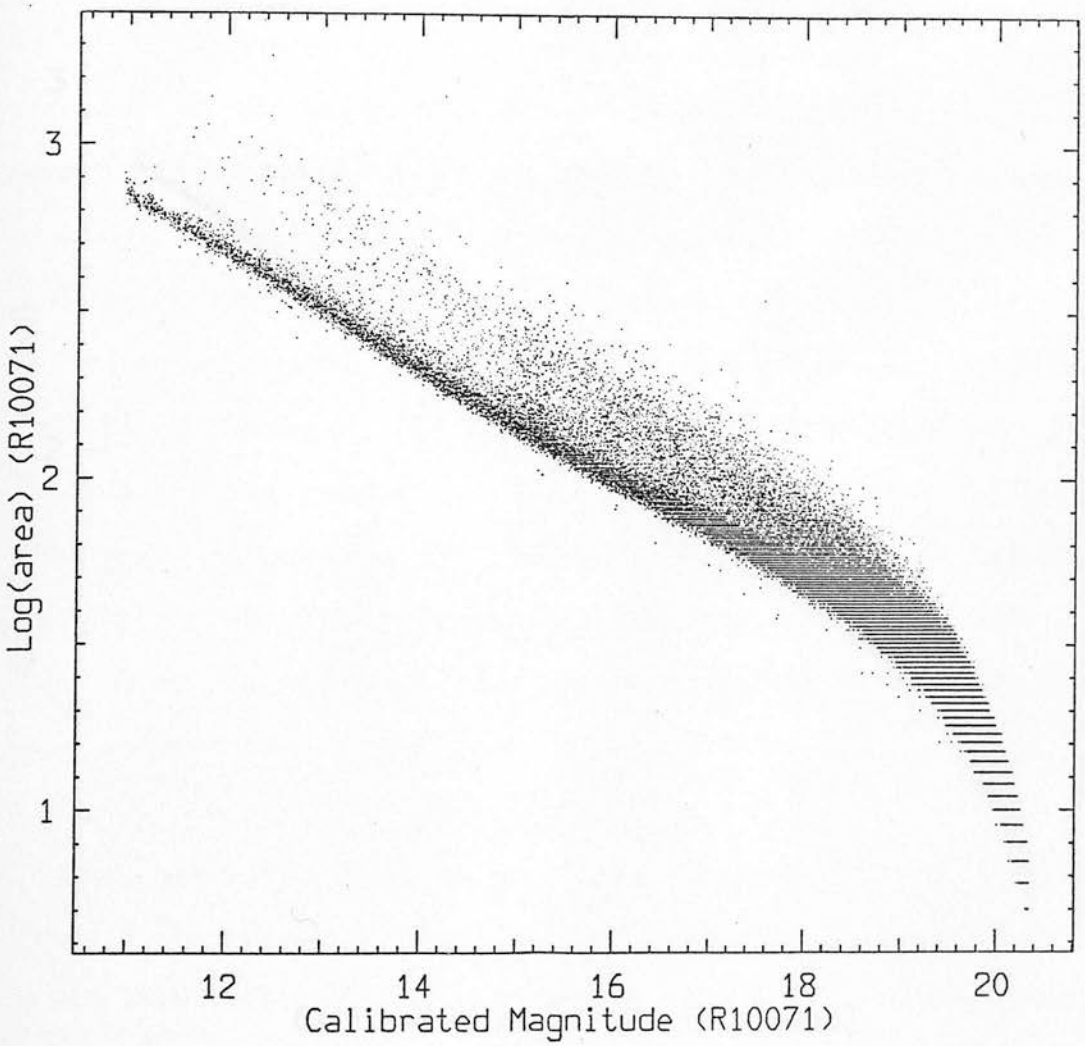

Fig 4.11b Star / galaxy seperation. Log(area) as a function of calibrated magnitude. As in 4.9a, both area and magnitude come from plate R10071.

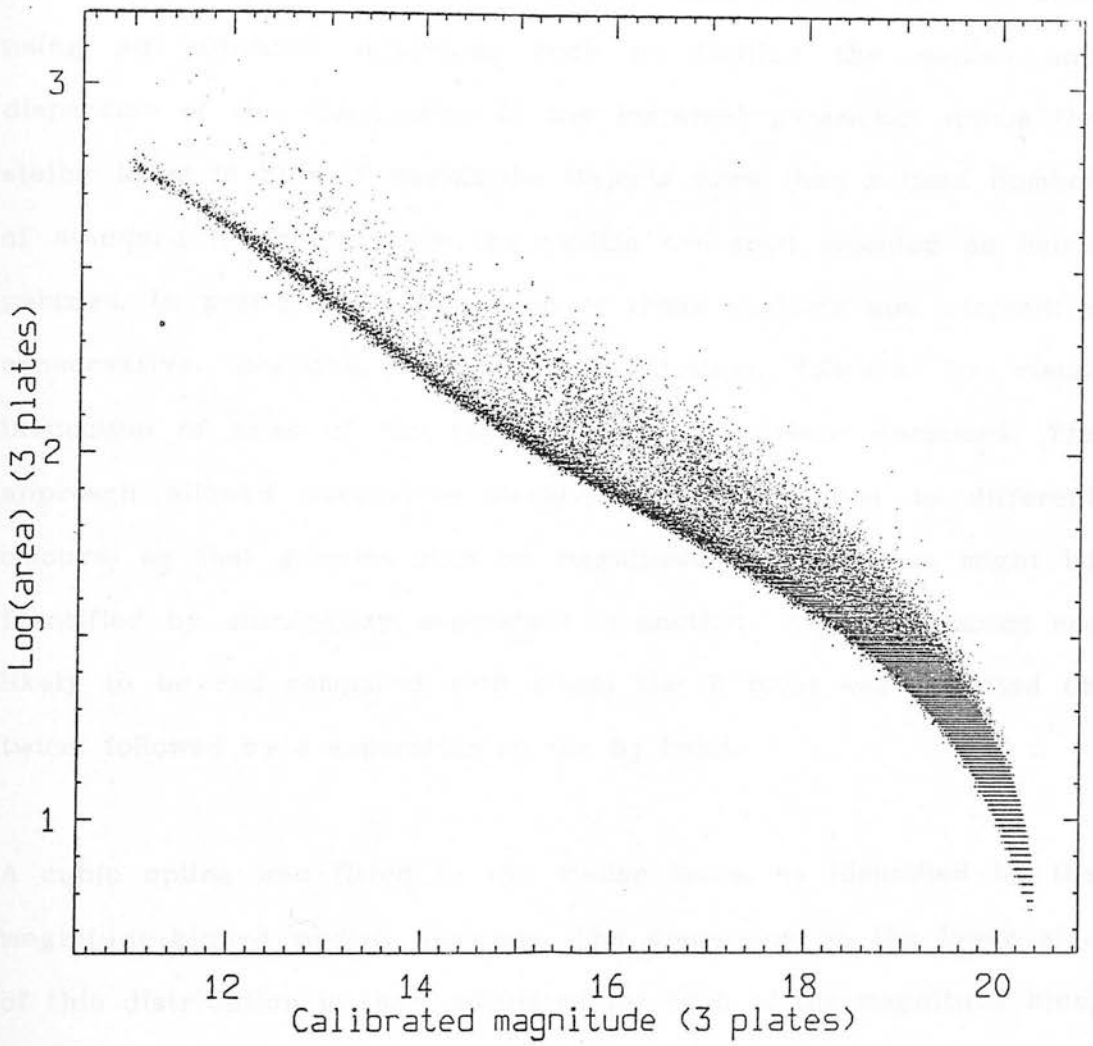

Fig 4.11c Star / galaxy seperation: Log(area) as a function of calibrated magnitude. Here, both areas and magnitudes are averaged values from all plates in the R band: plates R10071, R9949 and R9884.

Two possible methods of separating objects in the stellar locus from galaxies were considered. The region containing stars may be defined interactively, using eye classification of a sub-set of the objects to define the boundary. Alternatively, the classification can be done using an automatic approach, such as finding the median and dispersion of the distribution of the log(area) parameter across the stellar locus in bins of magnitude. Objects more than a fixed number of standard deviations from the median are then rejected as being galaxies. In practice, a combination of these methods was adopted: a conservative, iterative, automatic classification, followed by visual inspection of some of the rejected objects between iterations. The approach allowed successive iterations to be applied to different colours, so that galaxies with no magnitude in one colour might be identified by star/galaxy separation in another. Because galaxies are likely to be red compared with stars, the R band was operated on twice, followed by a separation on the B_J band.

A cubic spline was fitted to the stellar locus, as identified by the magnitude-binned median positions. The dispersion on the lower side of this distribution is then calculated for each of the magnitude bins, and finally every object further away than 2σ on the upper side in that bin is marked as a galaxy. Figure 4.12 shows the number counts of the objects found in this way. It can be seen that fainter than R = 18.8 there is a sharp loss in the numbers of galaxies found - about the point where the two loci of figure 4.9c meet. This is confirmed with reference to figure 4.13, which shows a Log(area) vs. magnitude plot for the selected objects, and the two tracks indeed coalesce at about R = 18.8.

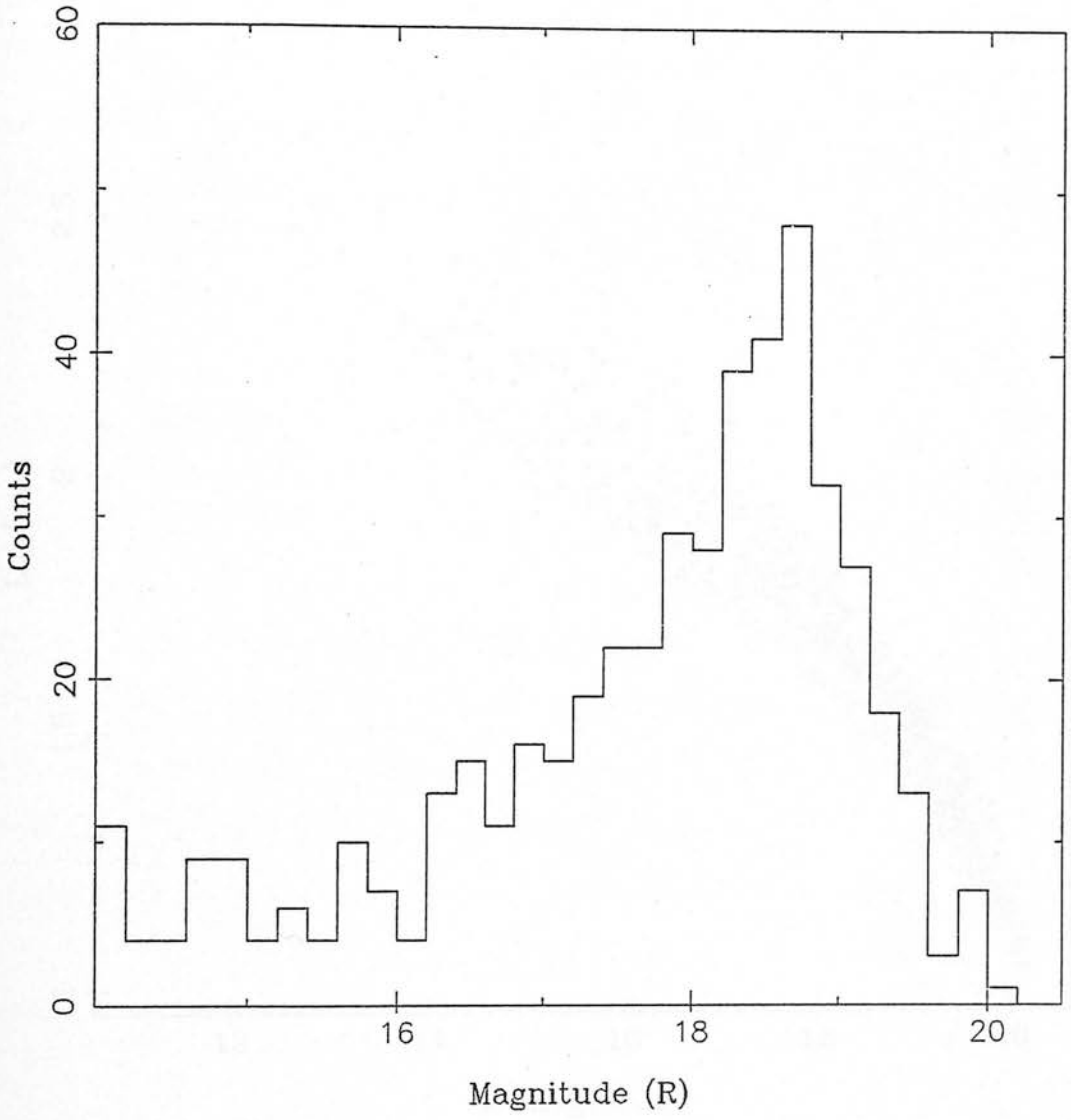

Fig 4.12 Number counts of galaxies in the central square degree, as a function of calibrated R magnitude.

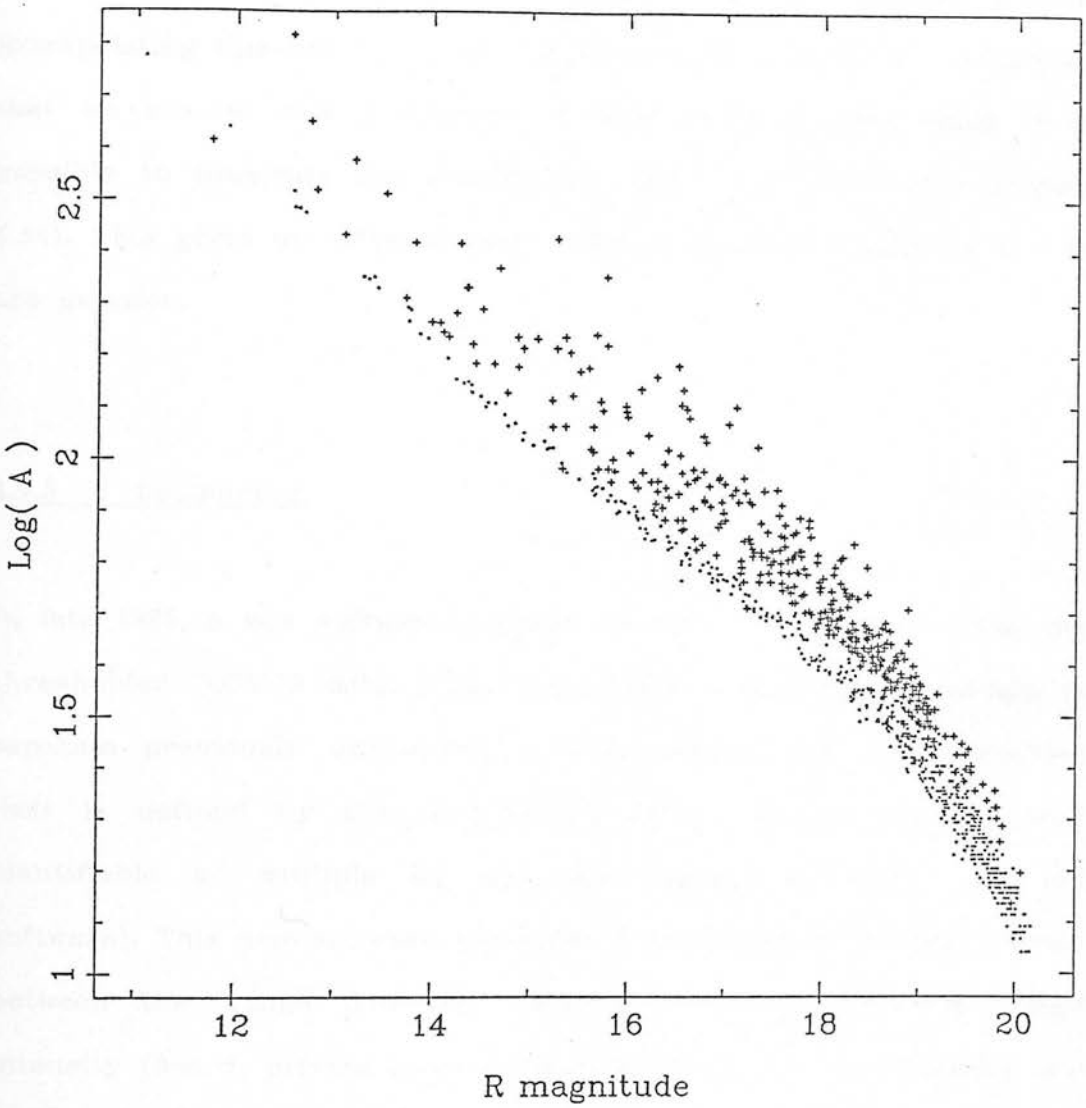

Fig 4.13 Log(area) as a function of calibrated R magnitude, showing 1 object in every 400 in the catalogue. Points are classified as stars, and plus signs are classified as galaxies.

The numbers of galaxies remaining at fainter magnitudes can be estimated using the assumption that brighter than R = 18.8 all galaxies are being found and discarded from the star list. A straight line can then be fitted to this brighter part of the distribution. Extrapolating this line to fainter magnitudes of interest, and assuming that we see no new population of faint stars at this point it is possible to integrate the distribution above the fitted line (figure 4.14). This gives an estimate that ≈ 60% of all objects seen at R = 19 are galaxies.

4.7.5 Deblending.

In late 1986, a new software package became available to analyse the thresholded COSMOS data. This incorporates a deblending package, to separate previously unresolved multiple images (the IAM resolution limit is defined by the thresholding level, and so images easily identifiable as multiple by eye are unresolved under the old software). This new software generates 8 intermediate threshold levels between the 'image detection' threshold and the maximum image intensity (Beard, private communication 1986). If the image breaks into 2 or more images under one of these re-thresholdings, a multiple image is signalled and IAM parameters are calculated for the sub-images. It was not possible to use this software on all of the plates in the survey, because they would all have had to be remeasured, and a considerable extra allocation of computer resources would have been necessary. As an alternative, in order to locate the faint multiple images not found by star/galaxy separation (a multiple image is likely to have peculiar colours, so its identification and

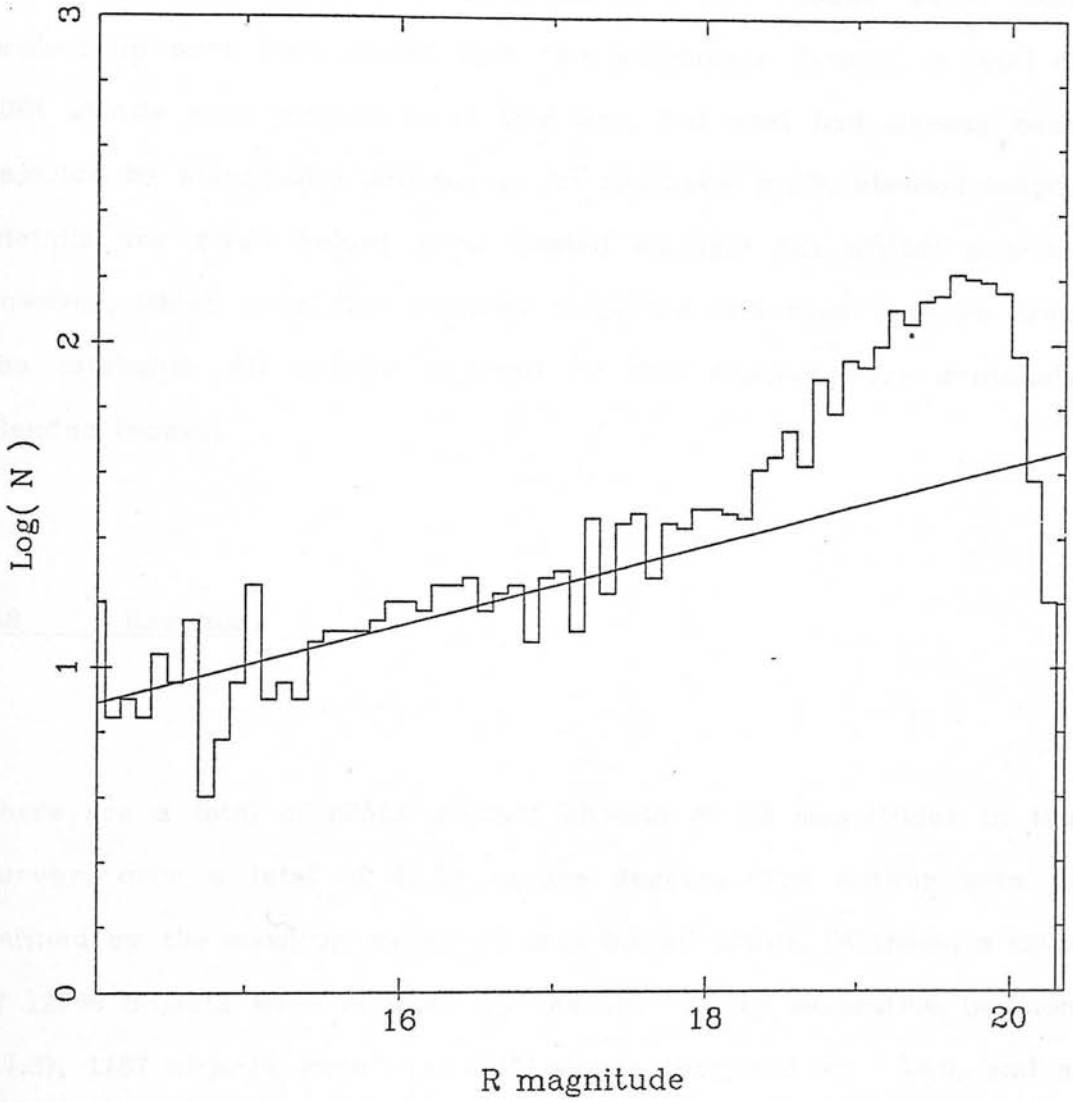

Fig 4.14 Log(counts) as a function of calibrated R magnitude, for all objects in the central square degree of the plate after star/galaxy seperation has taken place. Also shown is the least squares best fit line to the data from $14 < R < 18.5$ used to predict numbers of galaxies remaining in the catalogue.

elimination from the survey is very desirable) just one - the deepest R plate, R10071 - was re-measured using this software (which had been optimized for faint blends by putting the re-thresholding levels fairly close together, fairly close to the sky. Images which were broken up were then paired with the multicolour dataset. A total of 2084 blends were discovered in this way, but most had already been rejected by star/galaxy separation. An additional ≈ 500 blended images (details are given below) were located amongst the stellar objects, however, which were first visually inspected and then rejected from the catalogue. All objects rejected by this process were genuinely blended images.

4.8 Results.

There are a total of 82561 distinct objects of all magnitudes in the survey, over a total of 23.68 square degrees. The survey area is defined by the maximum measured area for all plates. Of these, a total of 12066 objects were rejected by the star galaxy separation (section 4.7.3), 1187 objects were rejected because they had $B_J < 14.0$, and a further 512 were identified and rejected as blended images (section 4.7.4). The remaining 68796 objects are broken down in table 4.8.

As has been discussed before (in section 2.4) the survey has (somewhat arbitrarily, from the viewpoint of the data) been divided into an 'ultraviolet excess' part and a 'multicolour' part. This was done mainly to allow comparisons to be drawn between this work and those of other authors. The only real difference between the two

Table 4.8: Numbers of stellar object in the photometric survey.

Magnitude	Number
U	18506
B_J	46002
V	41061
R	62733
I	39864

surveys is that from the catalogue described, all objects with both a U and a B_J magnitude were copied to another catalogue, which contains a total of 17766 objects. The remaining catalogue, as described below, was drilled of areas around bright stars.

4.8.1 The ultraviolet excess survey.

This survey is compiled from all objects from which a $U - B_J$ colour could be calculated. It therefore includes all those objects which have both a U and a B_J. There are a total of 17766 objects in these categories, of which some 877 have a $U - B_J < -0.4$ - the conventional cut made in $U - B_J$. This is not actually the same criterion as for example that used by Green, Schmidt and Liebert (1986), because the B band is not the same. The difference, however, is a function of colour and therefore cannot be applied to very blue objects which have no V. Colour dependent differences are in fact fairly commonplace between surveys in the literature.

Figure 4.15 is a colour - colour plot of $U - B_J$ vs. $B_J - V$ for all objects with these colours. Marked on the plot are the mean colours

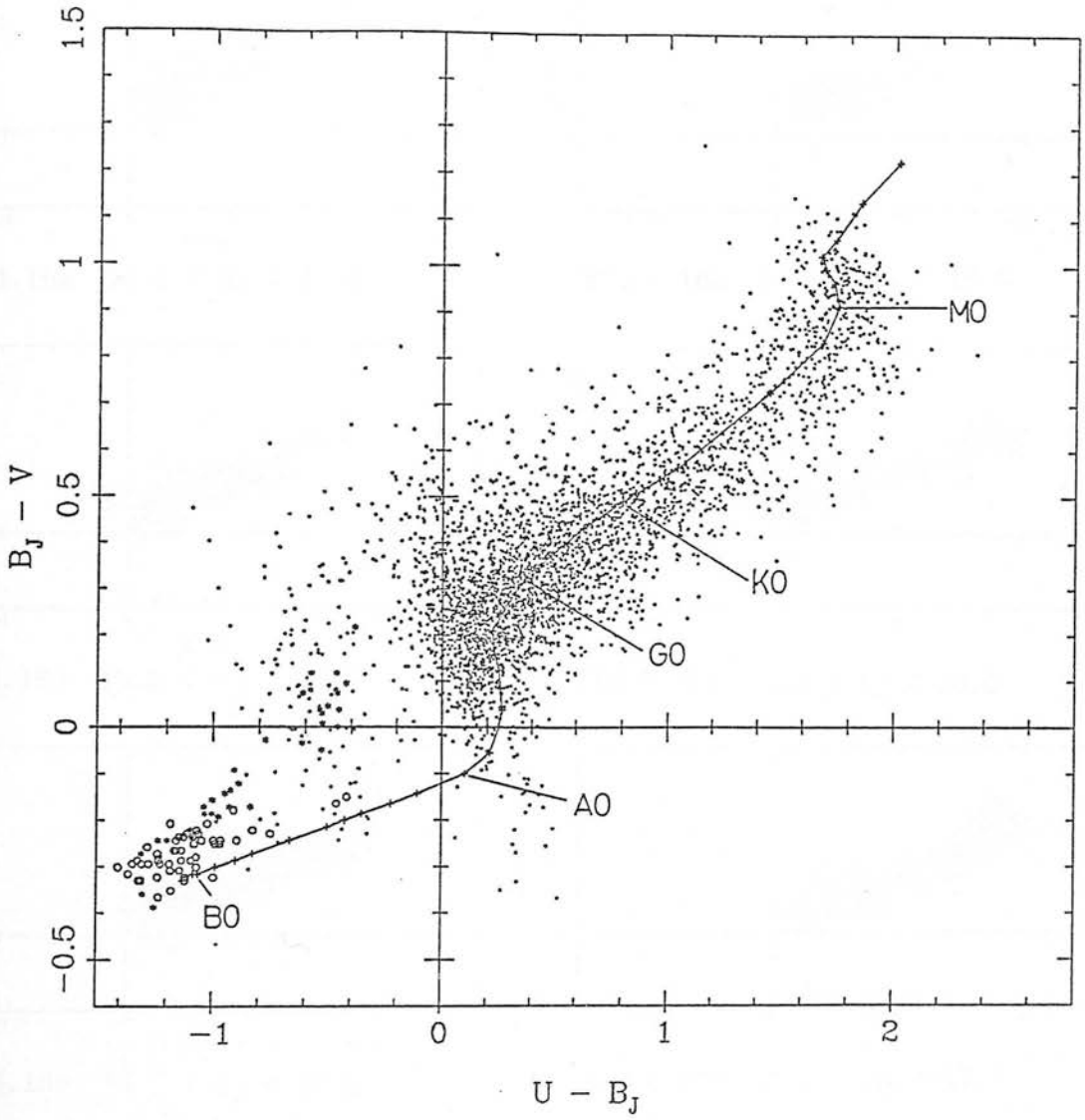

Fig 4.15 $U - B_J$ vs. $B_J - V$. Data shown are 1 object in every 5 which are above the survey limits in all magnitudes. The line overplotted runs along average main sequence colours, from Johnson, 1966 - transformed to the Schmidt colour scheme. Open circles are the positions of some of the subdwarfs, and stars are the positions of some of the hot white dwarfs taken from Green, Schmidt and Liebert, 1986.

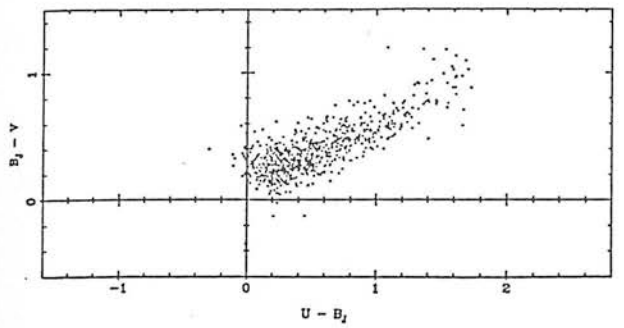

Fig 4.16a $14.5 < B_J < 15.0$

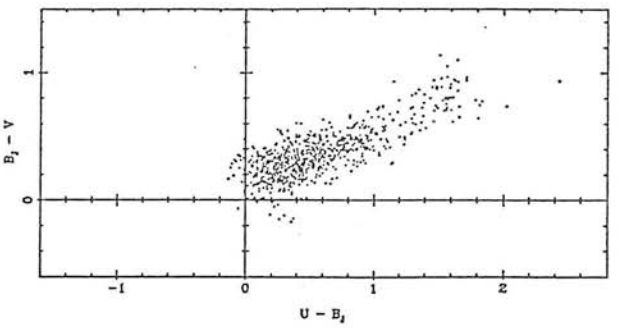

Fig 4.16b $15.0 < B_J < 15.5$

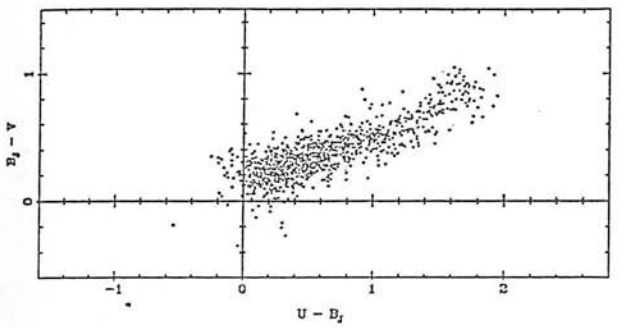

Fig 4.16c $15.5 < B_J < 16.0$

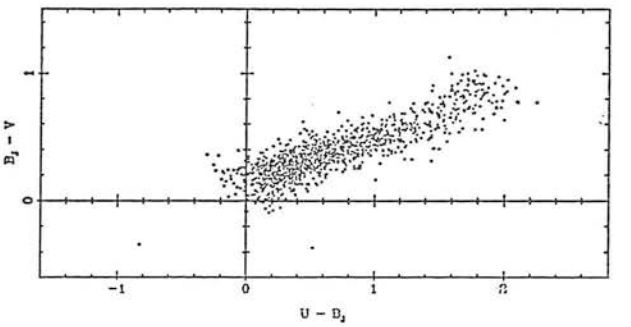

Fig 4.16d $16.0 < B_J < 16.5$

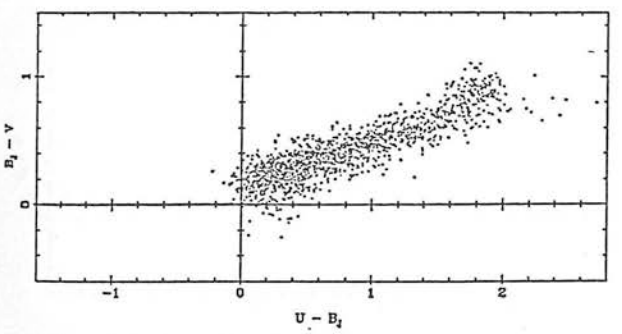

Fig 4.16e $16.5 < B_J < 17.0$

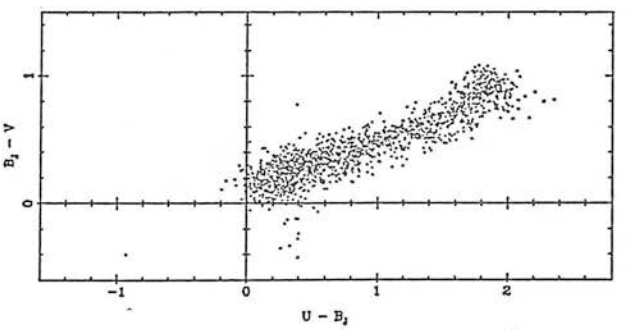

Fig 4.16f $17.0 < B_J < 17.5$

Fig 4.16 Plot of $U - B_J$ vs. $B_J - V$, binned in half magnitude interval bins of B_J.

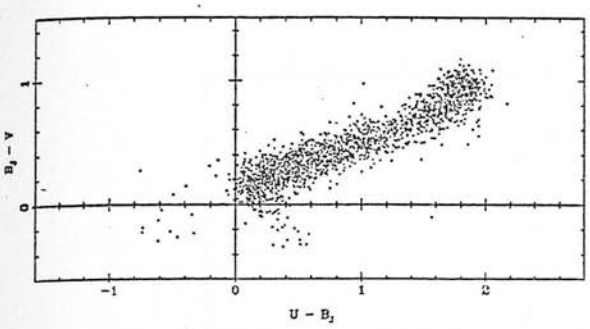

Fig 4.16g $17.5 < B_J < 18.0$

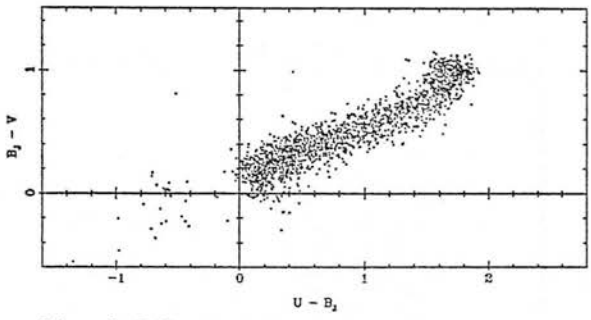

Fig 4.16h $18.0 < B_J < 18.5$

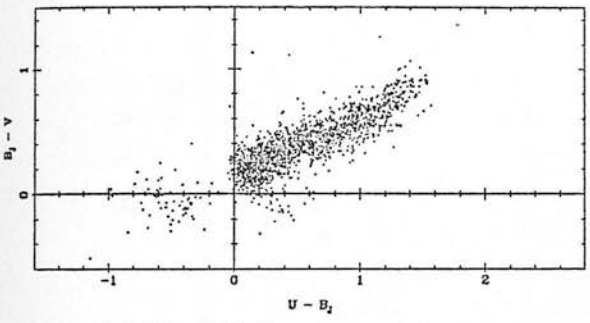

Fig 4.16i $18.5 < B_J < 19.0$

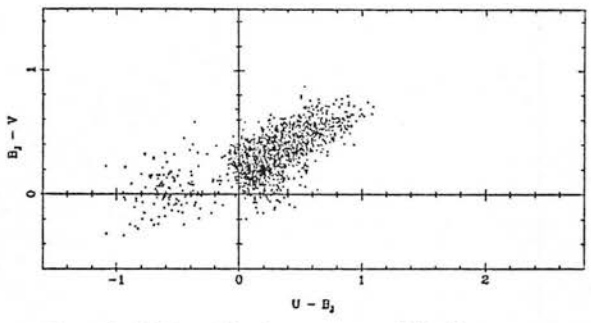

Fig 4.16j $19.0 < B_J < 19.5$

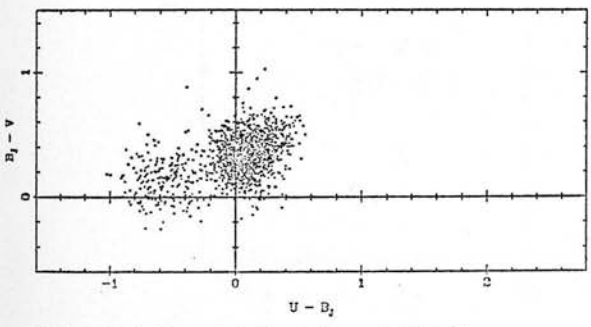

Fig 4.16k $19.5 < B_J < 20.0$

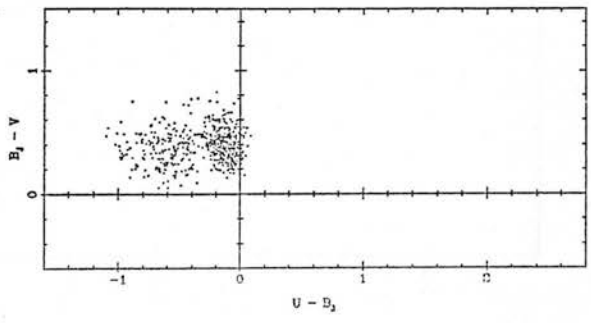

Fig 4.16l $20.0 < B_J < 20.5$

Fig 4.16 (continued).

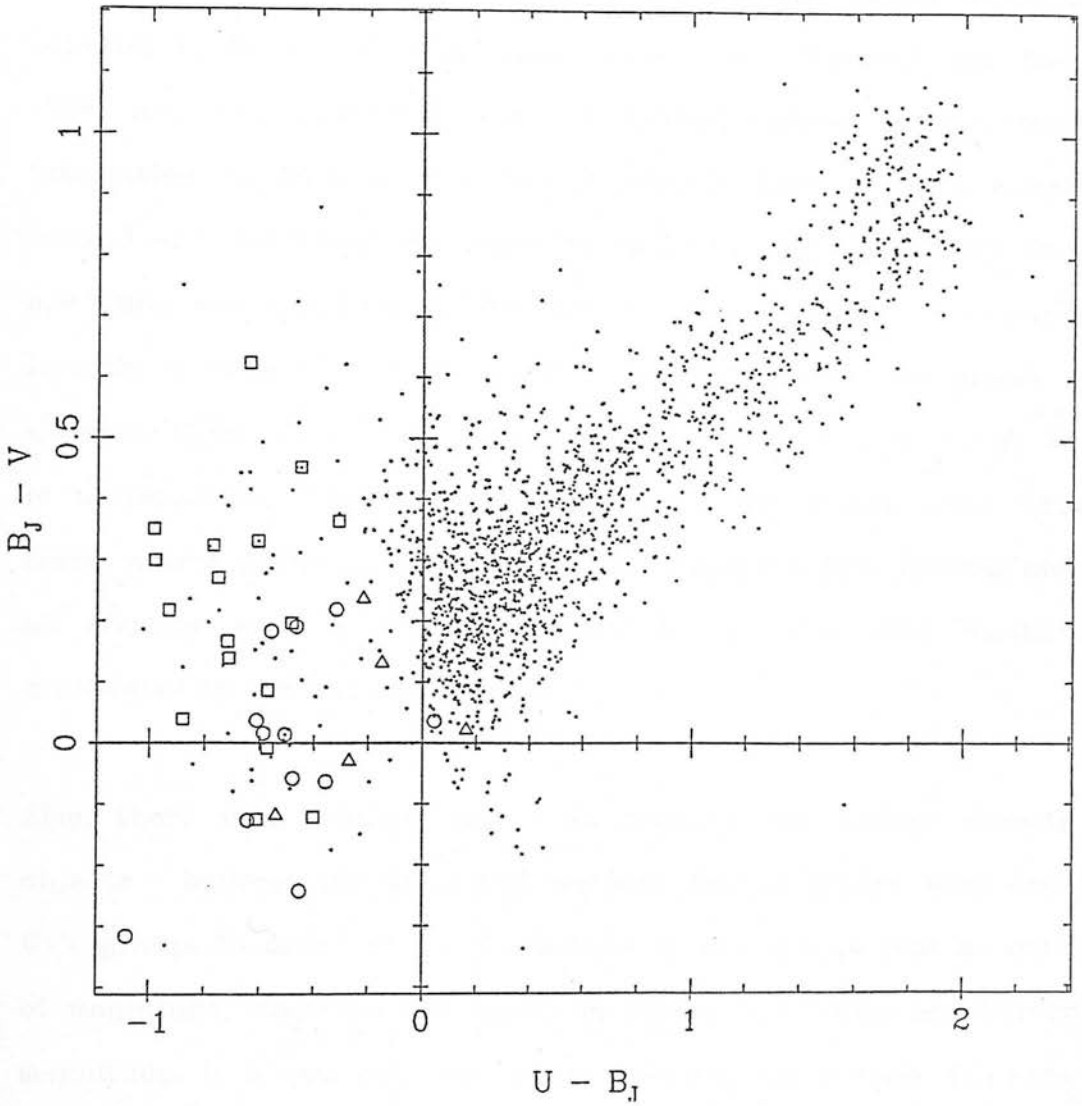

Fig 4.17 Two colour plot, $U - B_J$ vs. $B_J - V$. Data shown are one object in every 10 with magnitudes above the survey limit. Also plotted are quasars in the field which have slit spectroscopy. Open circles have $0 < z < 1$. Squares have $1 < z < 2$. Triangles have $z > 2$. Most objects fall in the UV excess regime, but this is not suprising because most surveys which have recieved spectroscopic attention in the field are in whole or in part search for UVX objects.

of the stellar main sequence (from Johnson, 1966) converted into Schmidt colours. Also marked are the typical positions of the major sources of contamination for most UVX surveys: the colours of those white dwarfs and subdwarfs taken from the PG survey which have Johnson U, B_J and V magnitudes (from Green, Schmidt and Liebert, 1986) and also converted into the Schmidt colour scheme. What is interesting to note is that the subdwarfs form a tight bunch at around -1.1, 0.3 whilst the white dwarfs, although less closely packed, are quite well confined at -0.5, 0.05. It may therefore be possible to identify a region at around -0.6, 0.4 where there are almost only quasars. Other interesting things to notice are that the $U - B_J \leq -0.4$ is unnecessarily harsh for this survey - the stellar locus objects finish almost entirely at $U - B_J = -0.25$. Applying this revised limit to all objects with $U - B_J$ information brings the total number of candidates in the survey to 1027.

Also, there is a distinct gap - an area of low surface density of objects - between the very high surface density stellar locus and the UVX group. In order to check whether or not this is just an artefact of magnitude, diagrams are shown in figure 4.16 which are binned in magnitude. It is still not clear where this gap comes from. Surveys by other authors do not show such a gap, but typically their photometry is also worse. One possibility is that it is caused by a non-linearity in the $U - B_J$ vs. stellar temperature relationship.

Figure 4.17 is also a plot of $U - B_J$ vs. $B_J - V$, this time showing only one in every ten objects from the survey (for the sake of clarity). Over-plotted are the objects known to be quasars, which have photometry - five known quasars in the field are not included: that

at $10^h40^m0.5^s$ +5°7'37" is seen on survey plates but is fainter than available photometry. The object at $10^h41^m31.3^s$ +3°30'36" which was rejected by the deblending software: the diffraction spike from a nearby bright star is blended with its image). In addition, two objects have no U magnitude (they are too faint) and a further one has no V magnitude. They could not therefore be included in figure 4.17.

Inspection of this figure shows that all but four of the known quasars are located by the UV excess survey, and of these four, three have redshifts ≥ 2.2. The fourth object has a strong emission line in the prism spectrum (which is why it was identified), with a redshift of $z = 0.213$. It has a $B_J \approx 17$, and from table 4.5 the error in $U - B_J \approx 0.16$. It is therefore about 1.8 σ inside the UV excess criterion, so its location could be the result of photometric error.

Figure 4.17 suggests that the cut should not just be a function of $U - B_J$, but also of $B_J - V$. If the UV excess survey is selected on these grounds (all of those objects in the polygon in figure 4.18, as well as all objects of $U - B_J \leq -0.25$, for those objects which have no V) then it takes the total number of UV excess objects to 1422, and also brings the total number of known quasars not located by the UV excess survey from four to two (it is this $B_J - V$ criterion which is referred to in column 7 of table 4.9).

Columns 2 to 4 of table 4.9 were compiled using number counts from Boyle, 1986. Boyle has number counts of all UV excess objects for a large number of small (0.7 sq. degree) fields, to faint magnitudes. For comparison, I have chosen star counts from two fields he denotes QSF (because they are at a similar galactic coordinate to field 927 - QSF is

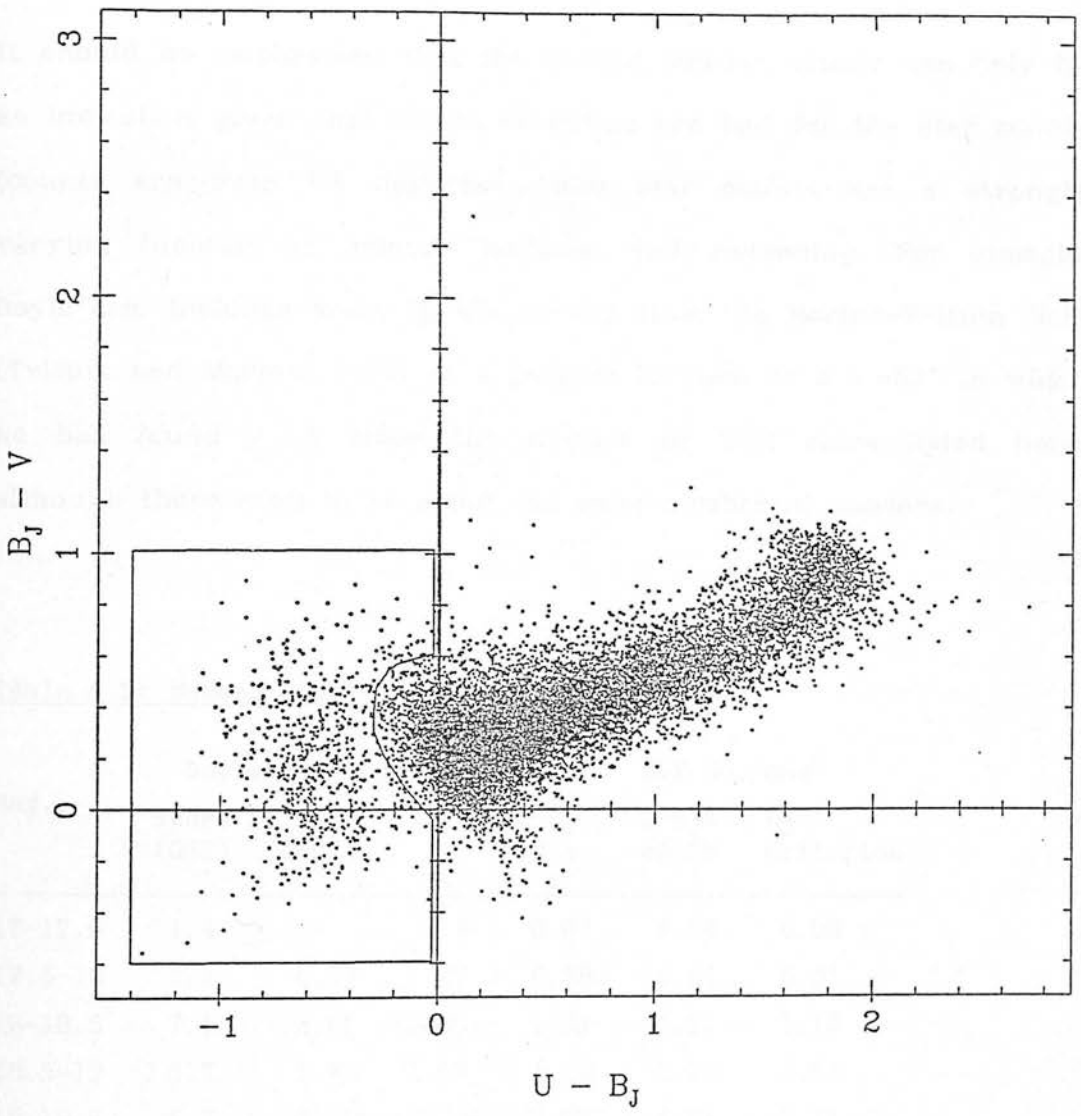

Fig 4.18 Two colour plot, $U - B_J$ vs. $B_J - V$. Data shown are all objects above the survey limit. Overplotted is the polygon used which defines the '$B_J - V$ criterion' reffered to in the text.

at b = -50°, while for F927 b = +52°). These star counts are then summed with the quasar counts (column 3) to give a total number/square degree in column 4.

It should be emphasised that the stellar number counts can only be an indication given that Boyles statistics are bad for the star counts (counts are over 1.4 degrees^2), and star counts are a strongly varying function of galactic latitude, and reddening. For example, Boyle also includes areas in his survey from the Morton-Tritton field (Tritton and Morton, 1984) at a galactic latitude of b = -52° in which he has found ≈ 1.5 times the number of UVX stars listed here, although there seem to be about the same number of quasars.

Table 4.9: Number counts of the UV excess survey.

Mag.	Boyle No./deg^2			UVX No./deg^2		
	Stars (QSF)	all QSO's	All	$U-B_J$ ≤0.4	$U-B_J$≤ ≤0.25	B_J-V criterion
17-17.5	1.4	-	1.4	0.04	0.04	0.08
17.5-18	7.1	0.17	7.27	0.38	0.51	0.51
18-18.5	7.1	0.56	7.66	1.01	1.01	1.14
18.5-19	5.7	1.83	7.53	1.69	2.32	2.53
19-19.5	5.7	5.24	10.94	3.97	4.81	5.11
19.5-20	2.9	7.38	10.28	7.56	9.63	10.47
20-20.5	11.4	11.43	22.83	14.4	16.89	24.79
20.5-21	11.4	11.43	22.83	7.68	7.69	14.53
21-21.5	-	-	-	0.21	0.21	0.42

In addition, Boyles' approach to the selection criterion was somewhat arbitrary: in some fields the limit is U - B = -0.4, while in others it is U - B = -0.3, and in others still it is U - B = -0.5. So close

agreement should not be looked for between say columns 4 and 6 - real comparison must wait for slit spectroscopy of the candidates.

4.8.2 The multicolour survey.

Few investigators have worked on the subject of selecting quasars from surveys in many colours, because it is only recently that the computer power and plate digitisation devices have allowed large quantities of data to be treated.

Those who have compiled multicolour surveys have not had the requirement that the survey must be combined with surveys from another source, as is the present case. As will be expanded upon below, this makes some demands of the candidate selection procedure. Examples of other multicolour surveys are Koo and Kron, (1982) and Koo, Kron and Cudworth (1986) both of whom simply select objects by eye from colour-colour diagrams which have non-stellar colours (effectively method 4 below).

The discovery of the first quasar at $z > 4$ was made by Warren *et al.* (1987). The object was discovered in a multicolour survey - they adopted a density calculation approach (method 2 below), but this particular object would have been identified by any selection method, as it is > 1 magnitude away from the stellar locus on their J - V vs. R - I plot.

The five magnitudes available to the survey can be used to generate four colours (U - B_J, B_J - V, V - R, and R - I) which can be thought

of as the coordinates of a four dimensional colour space. As has been seen in the preceeding sections, the locus of the stellar main sequence is fairly tightly confined in this colour-colour space. It should therefore be possible to identify all objects within the stellar locus, and so locate all objects with peculiar colours. Apart from the white dwarfs and subdwarfs already discussed, the only other faint objects with unusual colours are likely to be quasars. As has been mentioned, the problems for UV excess surveys arise when looking for quasars with $z > 2.2$. Given the large volume of colour-colour space available to quasars, and their predominately non-thermal energy generation, it is most unlikely that large numbers of higher redshift quasars will have stellar values in all colours. So a search in multi-colour space should go a long way towards eliminating the UV excess redshift bias, and generate a more complete survey than has hitherto been available.

A major source of difficulty for any photometric survey, and certainly for this one, arises from the fact that the number density of objects rises very steeply towards the magnitude cutoff. Therefore a large percentage of objects do not have a well defined magnitude in all wavebands. There are a total of 68532 stellar images, after the exclusion of all poor quality images, over 23.57 degrees^2. But only 15120 have well measured magnitudes in all bands, and thus can be included in the multicolour survey. This is why the survey is split into the UV excess part and the multicolour part - otherwise, large numbers of quasar candidates are lost, having no red colours. Very high redshift quasars may have these red colours, as indeed may other astrophysically interesting objects such as the brown dwarfs of Hawkins (1985). Be that as it may, it is not immediately possible to see

how to use these data to best effect, as they can have no part in the multicolour selection procedure. Consequently, there is a substantial wastage of information.

There is a slight difference in the total area of the multicolour survey from that of the UV excess survey. This is caused by the necessity to 'drill' around very bright stars. The IVn emulsion used for the I band is unbacked, because the backing used for other emulsions does not survive the hypersensitization process used for IVn. As a result, bright stars have a ring of light around them which is reflected off the back of the plate. Thus the COSMOS parameters of objects close to very bright stars are effected, and the objects must be discarded.

The most important question, as can be seen from figures 4.19 - 4.27 is on what basis to select objects. Virtually all methods of object selection that can be conceived contain some element of arbitrariness. It is important to remember this when trying to evaluate one method against another, because it is easy to form the impression that because one selection technique is more automatic than another, it is also less arbitrary. This may or may not actually be true.

Methods available for object selection are the following, with some of their advantages and disadvantages.

1) A line can be fitted to the stellar locus either on the basis of ones knowledge of stellar colours, or as a χ^2 minimization procedure. Objects can then be selected that are greater than a certain distance away from this line. This type of procedure has the advantage that it is likely to identify all the genuinely rare objects, it gives you some

sort of a 'criterion of rareness' in the distance away from the stellar locus (and so helps you to decide whether an object has been scattered out by photometric or other errors), and it is unaffected by the choice of coordinates. Disadvantages are that one must somehow locate the endpoints of the stellar distribution, which is likely to be an arbitrary process, and both density of the stars and errors vary along the locus, so the significance of the distance from the stellar locus is not obvious. Whether or not one uses a stellar locus derived from published material, errors in the stellar locus determination cause colour dependent systematic errors in candidate selection. From this point of view, the fitted locus is preferable.

2) A search of the density of colour space is possible, defining an object in a region of low enough density to be a 'good candidate'. Advantages of this method are that it is unaffected by the coordinate system, and has little systematic colour bias (further from the stellar locus). On the other hand, choice of the limiting density is somewhat arbitrary, and probably ultimately would depend on the amount of follow up slit spectroscopy available, or some other unrelated criterion. The density of stars varies with colour, so the survey would identify different percentages of contaminating stellar types. Whatever the choice of limiting density, the boundary to the stellar locus remains ill defined, as random errors produce small clusters and under-dense regions locally, close to the surface of the stellar locus. It is also hard to see how one can define a 'selected' and an 'unselected' volume, which one must do if one is to compare survey methods. It is possible that some of these difficulties could be overcome by smoothing the density distribution found, but at the cost of the resolution obtained (smoothing would have the same effect as poorer photometry).

3) A nearest neighbour search, although on the face of it is quite attractive, requires large numbers of passes through the dataset, and a large quantity of core memory. It is beyond the computing power of the R.O.E. STARLINK VAX 11/780 for a survey of this size, and would therefore require a large commitment of time to locate a more powerful machine, to transfer data and to write or adapt software. This method would have the additional disadvantage that it does not define regions of 'selected colour space', and so comparing surveys would be difficult.

4) The stellar locus can be defined by some interactive technique. Areas of equal density can be identified on colour colour plots, and objects within this locus on all two colour plots are then classed as stars. Advantages of this method are its extreme simplicity of implementation, it is very easy to see what is going on by using plots of the 2d cuts, and one can use the method to locate the candidates in the slitless spectrum surveys which lie irretrievably inside the stellar locus in the photometric survey, and so estimate completeness of the surveys and obtain sensible cross comparisons. The disadvantages are that the method is quite arbitrary: ones' eye is by no means an absolute judge of density, and worse the method is tied to the 2 dimensional cuts on which the limits of the stellar locus is drawn: there are in other words 'preferred directions'. This can alleviated to some degree by allowing the use of unusual colours such as U - V (= (U - B) + (B - V)). This is effectively the same as looking at the distribution from a different direction (ie. not parallel to a pair of axes). Photometric accuracy is not forfeited because the original magnitudes are available and allow calculation of these colours directly.

Although this last method is probably not the best - problems also include not yielding a 'value of candidate' parameter, such as a distance away from the stellar locus, as well as those mentioned above - this is one of the methods that has been adopted, because it was essential to be able to pick out which objects would not be identified from the other surveys. Figures 4.19 - 4.28 show a series of colour-colour plots of the photometric survey in which the stellar locus has been identified in this manner - by the interactive definition of the polygons drawn.

To reduce the effect of having 'preferred directions', polygons were taken quite close to the stellar locus. This process produced a list of 2316 objects, very many of which are lying on the surface of the stellar distribution, and are presumably stars. However, selection done in this way allows objects in other surveys to be assessed (chapter 5). With this smaller list another selection method can be applied: the nearest neighbour search. In order to use this search as effectively as possible, one can make various improvements to the non-stellar locus list.

Firstly, the list was paired with the UV excess list described in 4.8.1, and the objects in common were rejected (since they were already part of another candidate list). Next, it is highly unlikely that all of the remainder are quasars, and it would be desirable to be able to cut the candidate numbers down without affecting the completeness. This may be done by the use of physical information that is available about different classes of celestial objects. Thus if it is known that quasars are highly unlikely to inhabit a particular locality of multicolour space, or if there are likely to be substantial numbers of

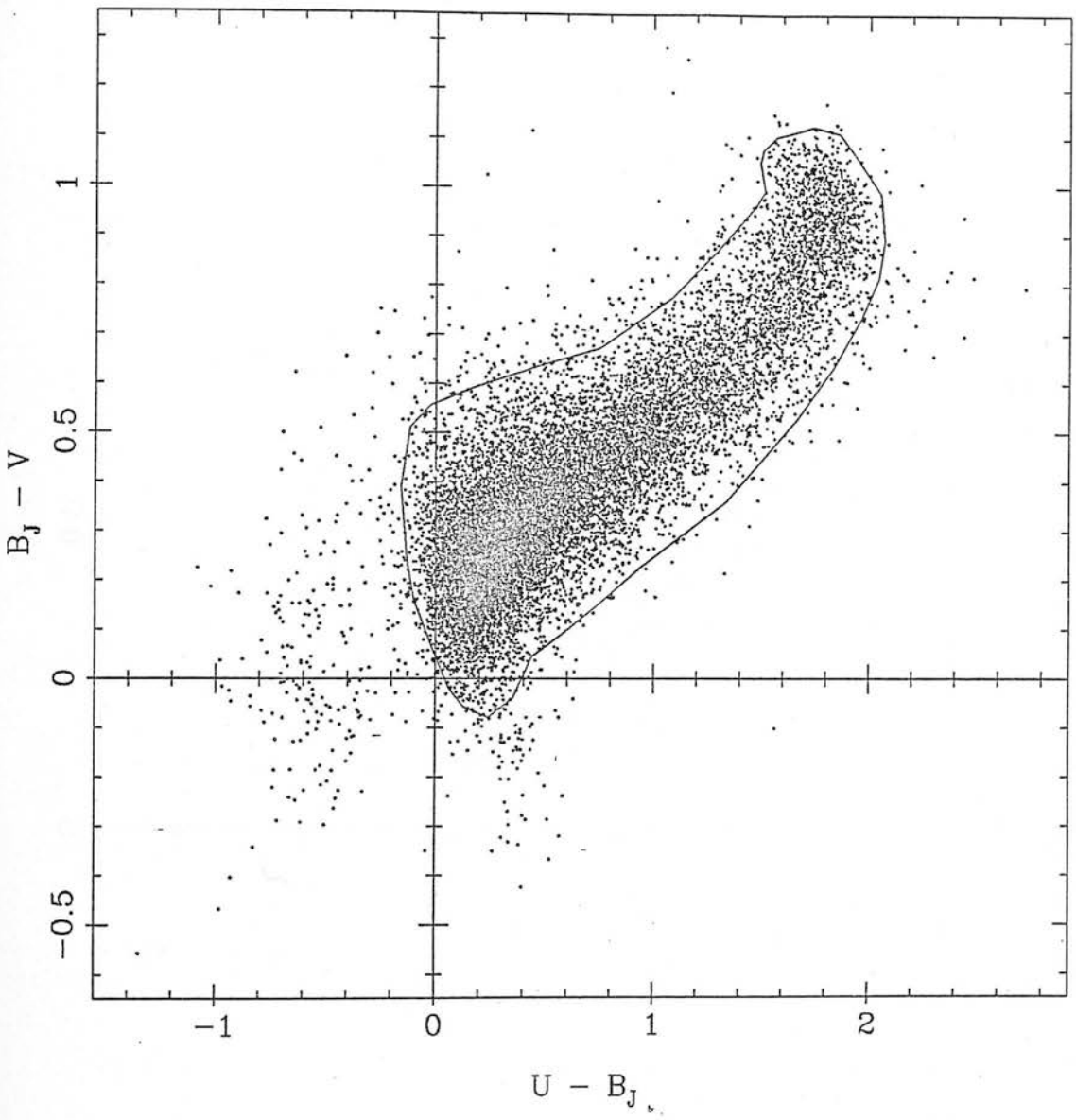

Fig 4.19 Diagram shows $U - B_J$ vs $B_J - V$ for all stellar objects in the photometric survey, except those with $B_J < 14.5$. Also plotted is the polygon which allows partial definition of the stellar locus.

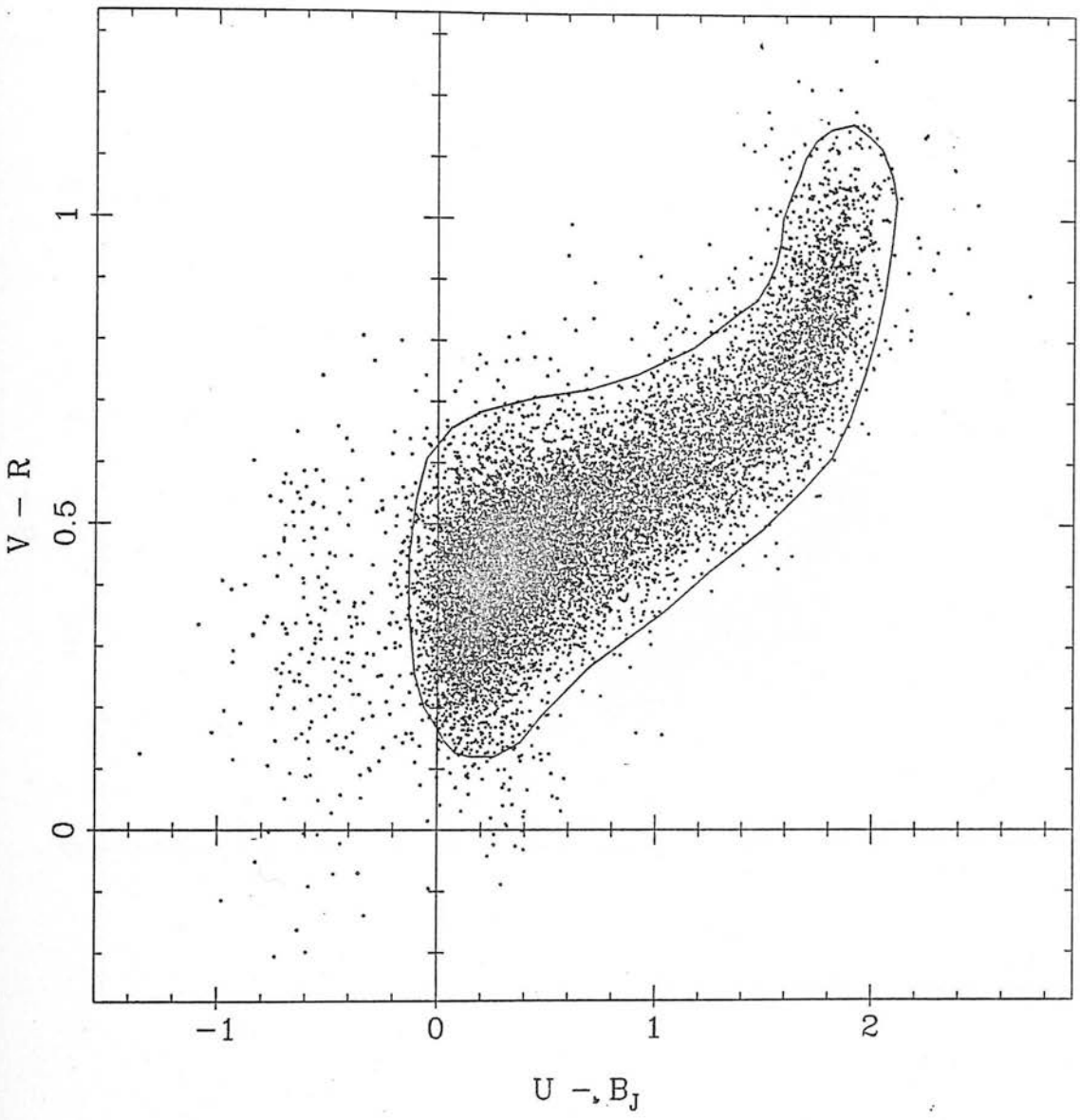

Fig 4.20 Diagram shows $U - B_J$ vs $V - R$ for all stellar objects in the photometric survey, except those with $B_J < 14.5$. Also plotted is the polygon which allows partial definition of the stellar locus.

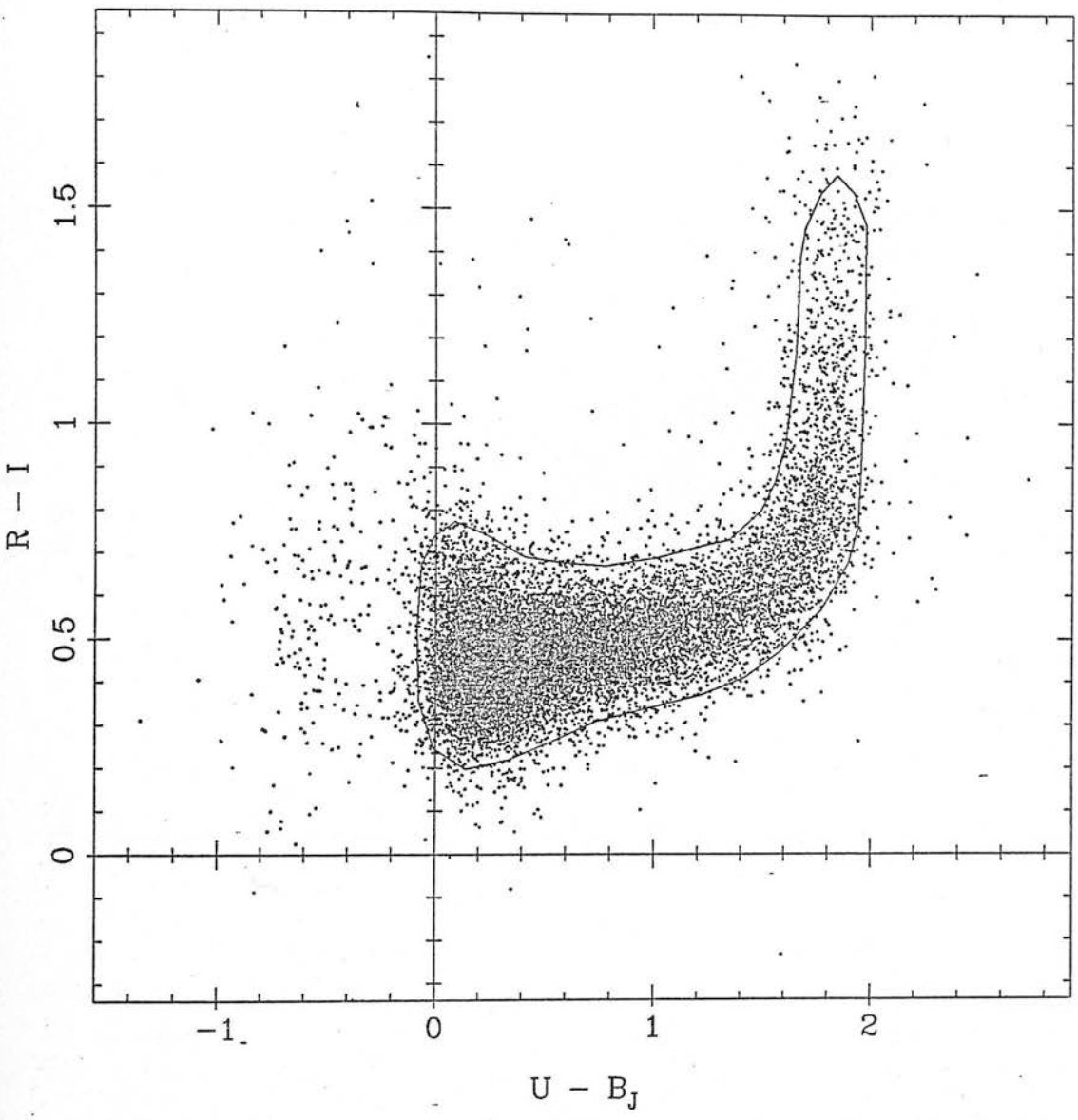

Fig 4.21 Diagram shows $U - B_J$ vs $R - I$ for all stellar objects in the photometric survey, except those with $B_J < 14.5$. Also plotted is the polygon which allows partial definition of the stellar locus.

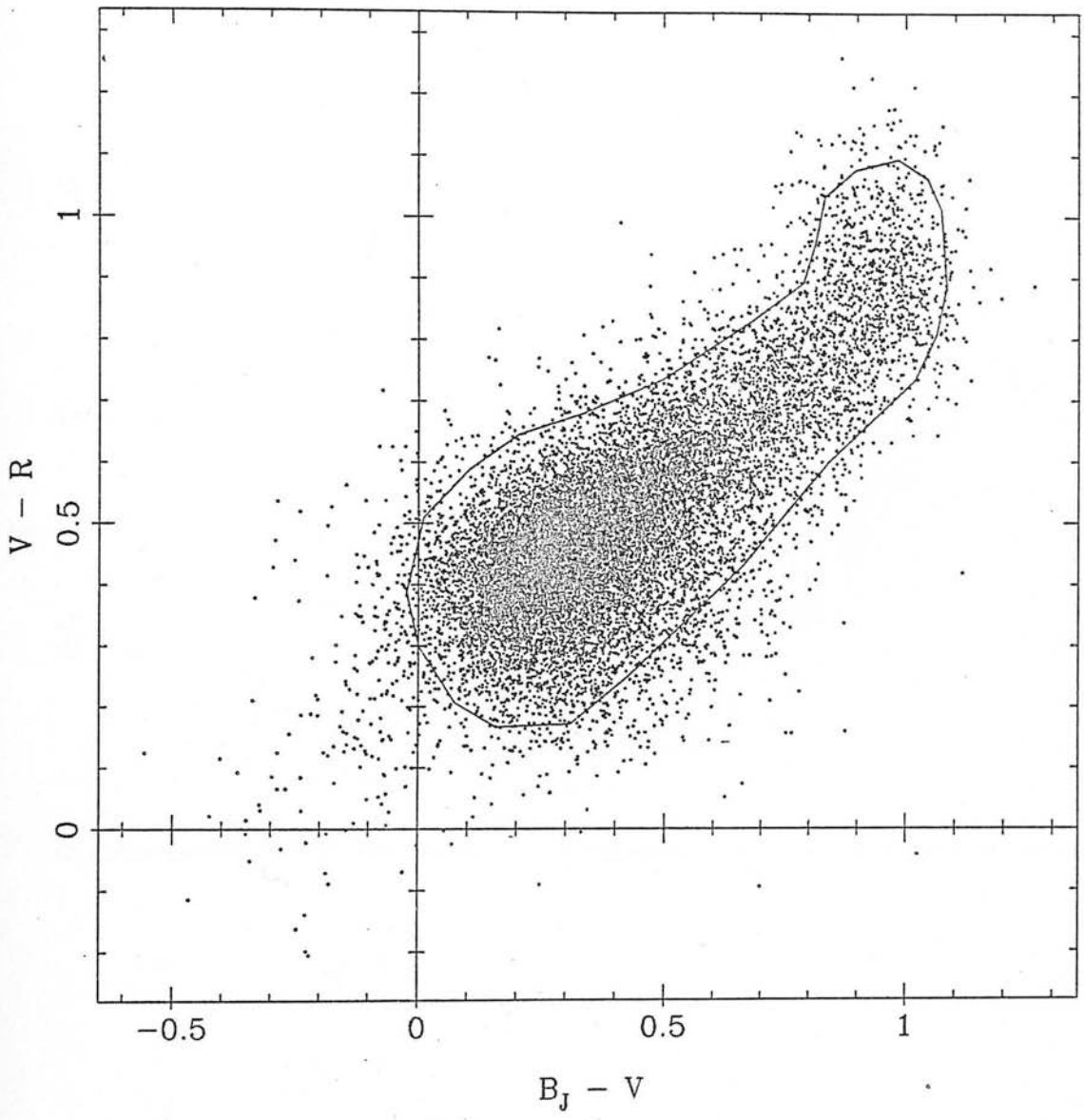

Fig 4.22 Diagram shows $B_J - V$ vs. $V - R$ for all stellar objects in the photometric survey, except those with $B_J < 14.5$. Also plotted is the polygon which allows partial definition of the stellar locus.

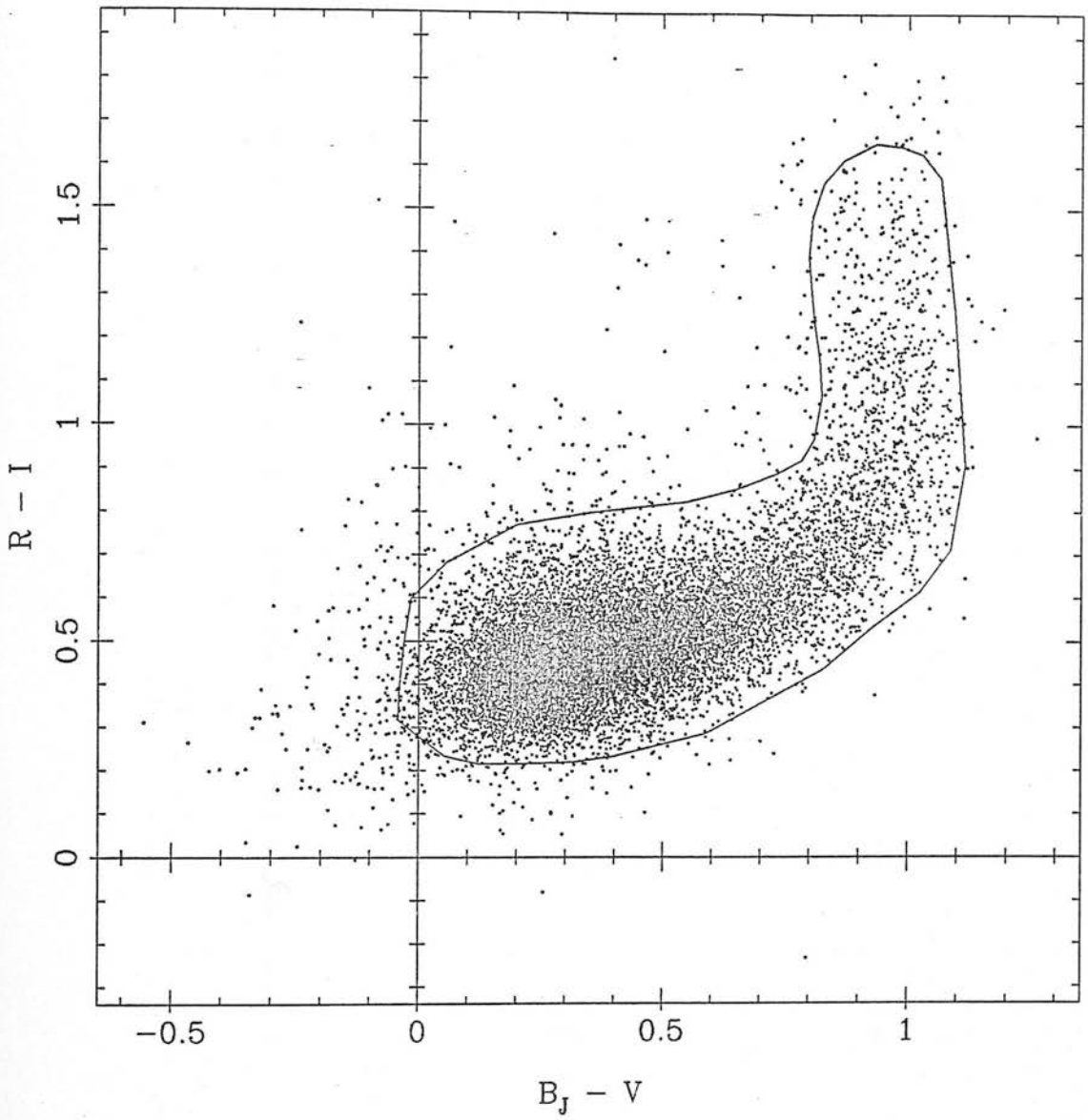

Fig 4.23 Diagram shows $B_J - V$ vs. R − I for all stellar objects in the photometric survey, except those with $B_J < 14.5$. Also plotted is the polygon which allows partial definition of the stellar locus.

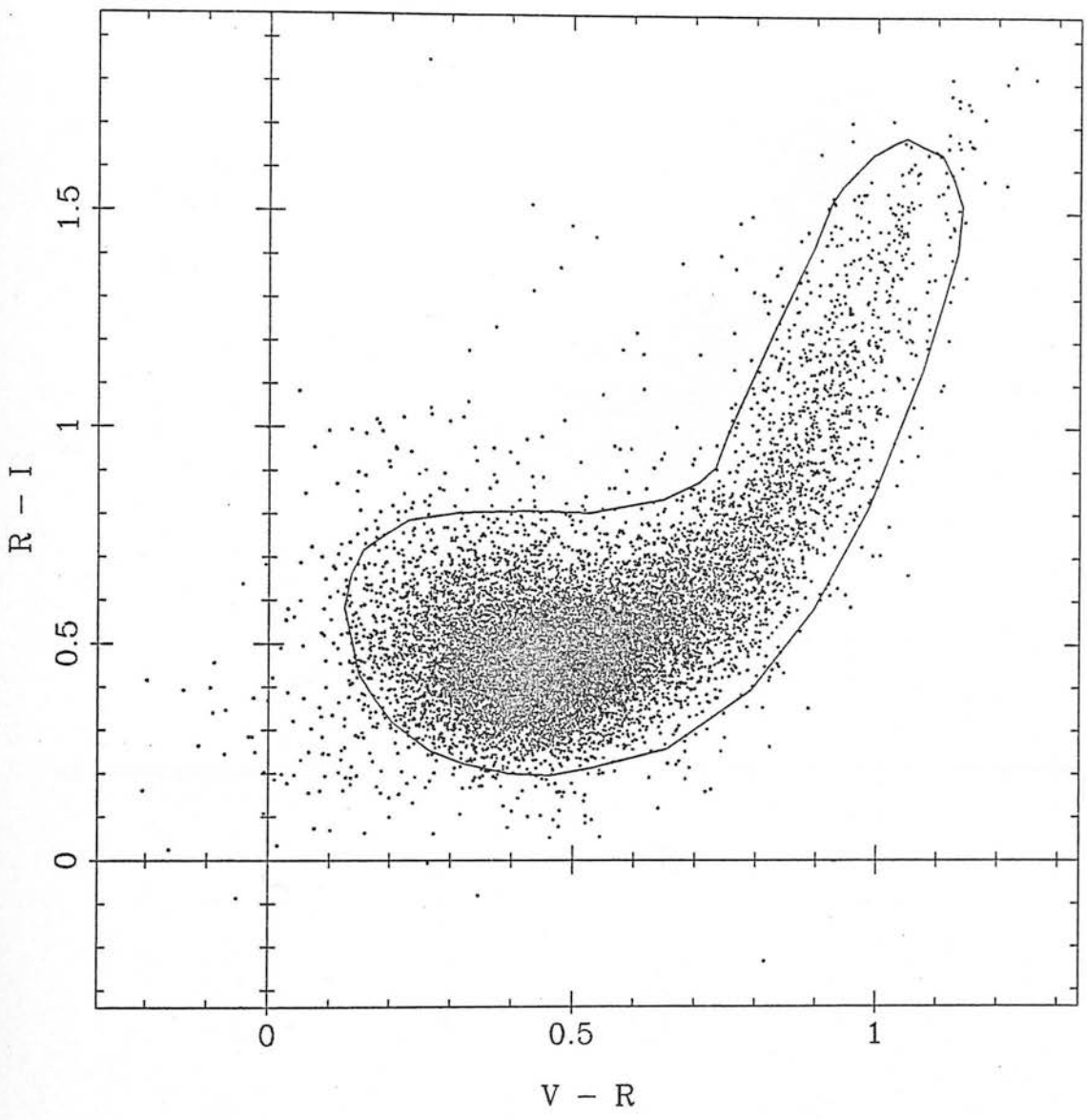

Fig 4.24 Diagram shows V − R vs. R − I for all stellar objects in the photometric survey, except those with $B_J < 14.5$. Also plotted is the polygon which allows partial definition of the stellar locus.

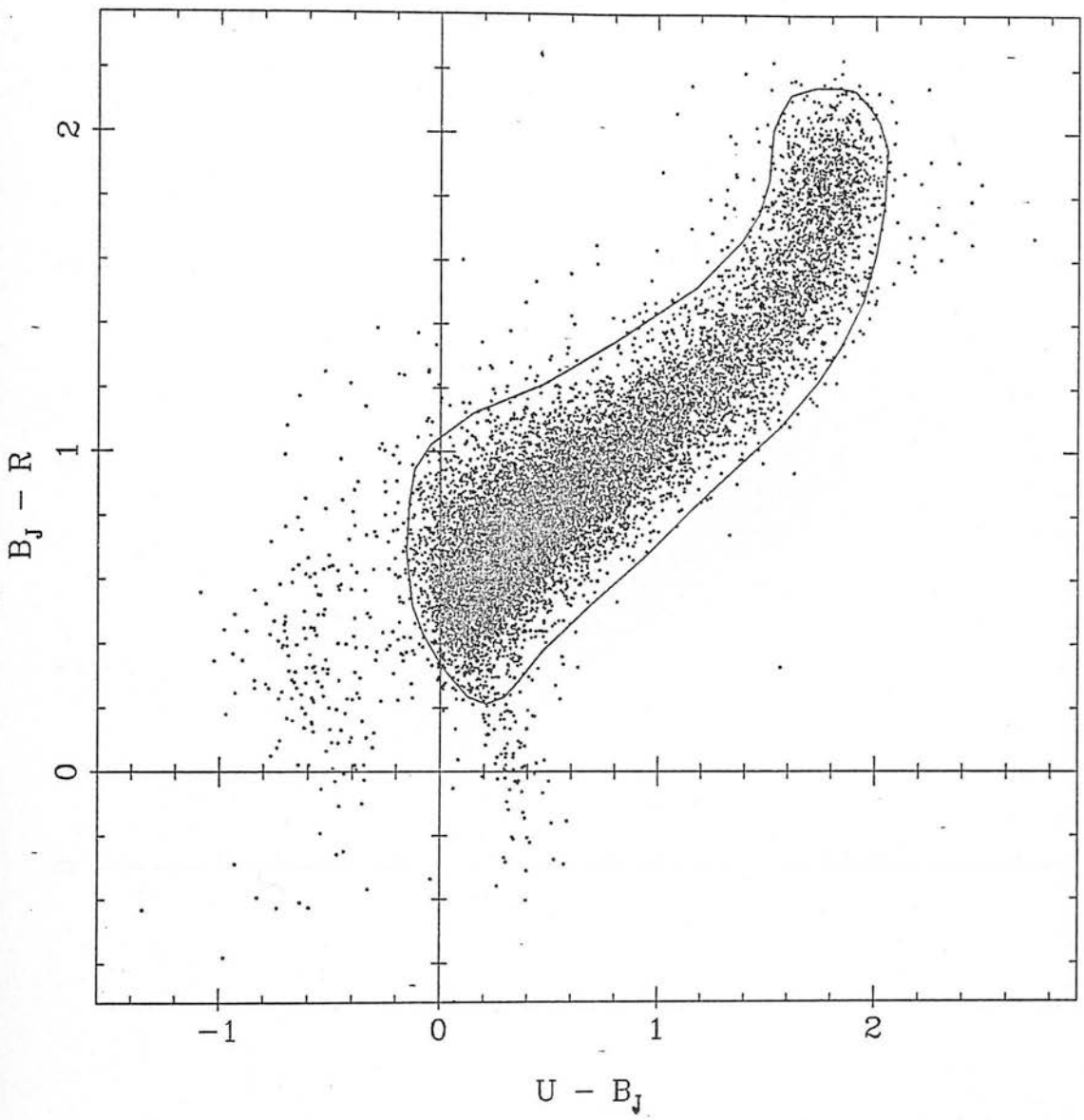

Fig 4.25 Diagram shows $U - B_J$ vs. $B_J - R$ for all stellar objects in the photometric survey, except those with $B_J < 14.5$. Also plotted is the polygon which allows partial definition of the stellar locus.

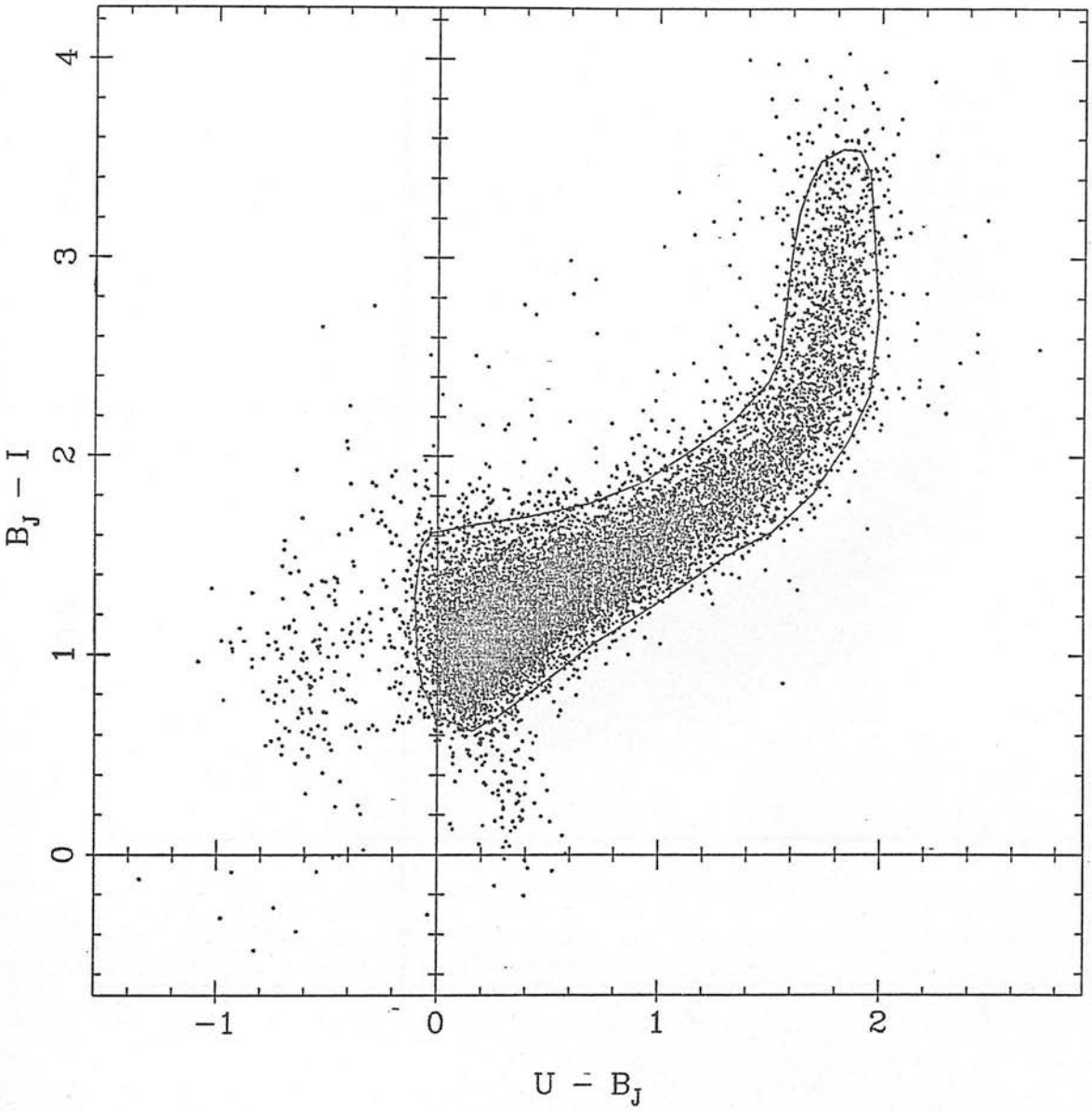

Fig 4.26 Diagram shows $U - B_J$ vs. $B_J - I$ for all stellar objects in the photometric survey, except those with $B_J < 14.5$. Also plotted is the polygon which allows partial definition of the stellar locus.

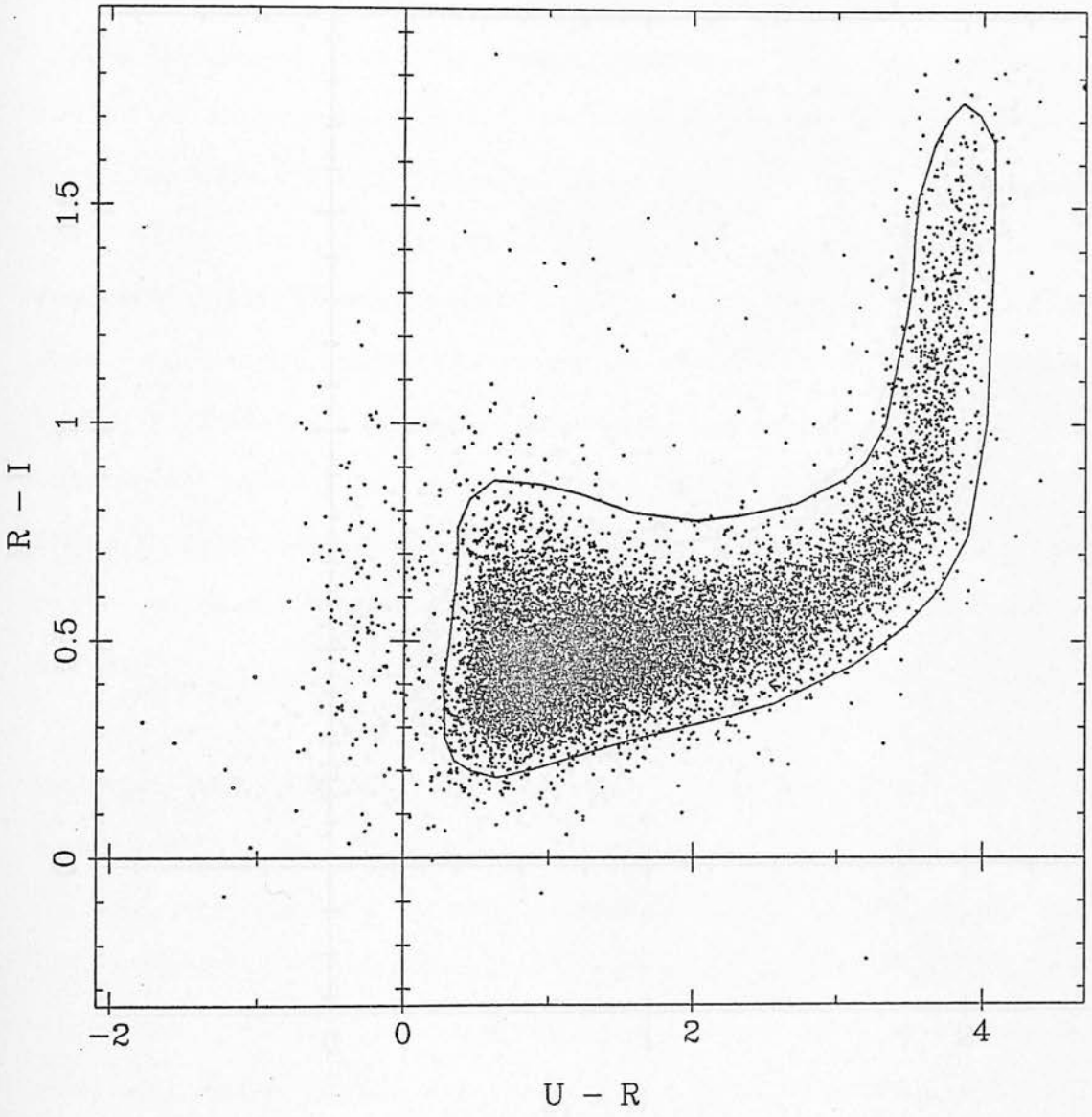

Fig 4.27 Diagram shows U - R vs. R - I for all stellar objects in the photometric survey, except those with $B_J < 14.5$. Also plotted is the polygon which allows partial definition of the stellar locus.

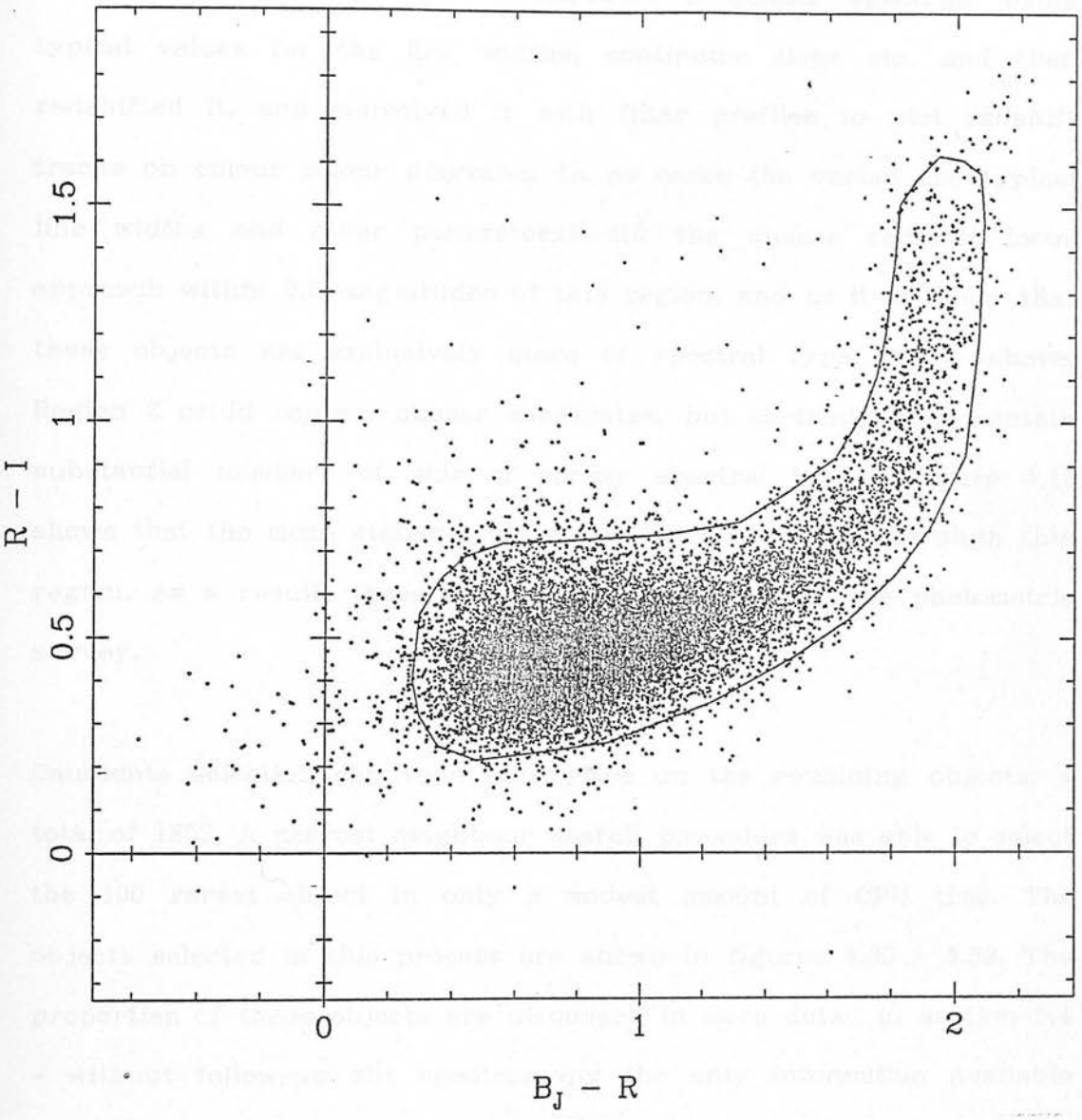

Fig 4.28 Diagram shows $B_J - R$ vs. $R - I$ for all stellar objects in the photometric survey, except those with $B_J < 14.5$. Also plotted is the polygon which allows partial definition of the stellar locus.

galactic stars, then this region has been excluded. For example, figure 4.29 defines two regions - region 1 has been excluded on the basis of extensive simulations carried out by Mitchell (1986, private communication) in which he constructed a quasar spectrum using typical values for the line widths, continuum slope etc. and then redshifted it, and convolved it with filter profiles to plot redshift tracks on colour colour diagrams. In no cases (he varied the typical line widths and other parameters) did the quasar redshift locus approach within 0.5 magnitudes of this region, and so it is likely that these objects are exclusively stars of spectral type M0 or above. Region 2 could contain quasar candidates, but certainly does contain substantial numbers of star of earlier spectral type - figure 4.15 shows that the mean stellar colours exit the stellar locus through this region. As a result, these objects are excluded from the photometric survey.

Candidate selection can then take place on the remaining objects: a total of 1852. A nearest neighbour search procedure was able to select the 100 rarest object in only a modest amount of CPU time. The objects selected in this process are shown in figures 4.30 - 4.33. The properties of these objects are discussed in more detail in section 5.4 - without follow-up slit spectroscopy the only information available regarding these objects is what they look like in other surveys.

4.9 Conclusions.

At the time of writing, it has been impossible to obtain slit

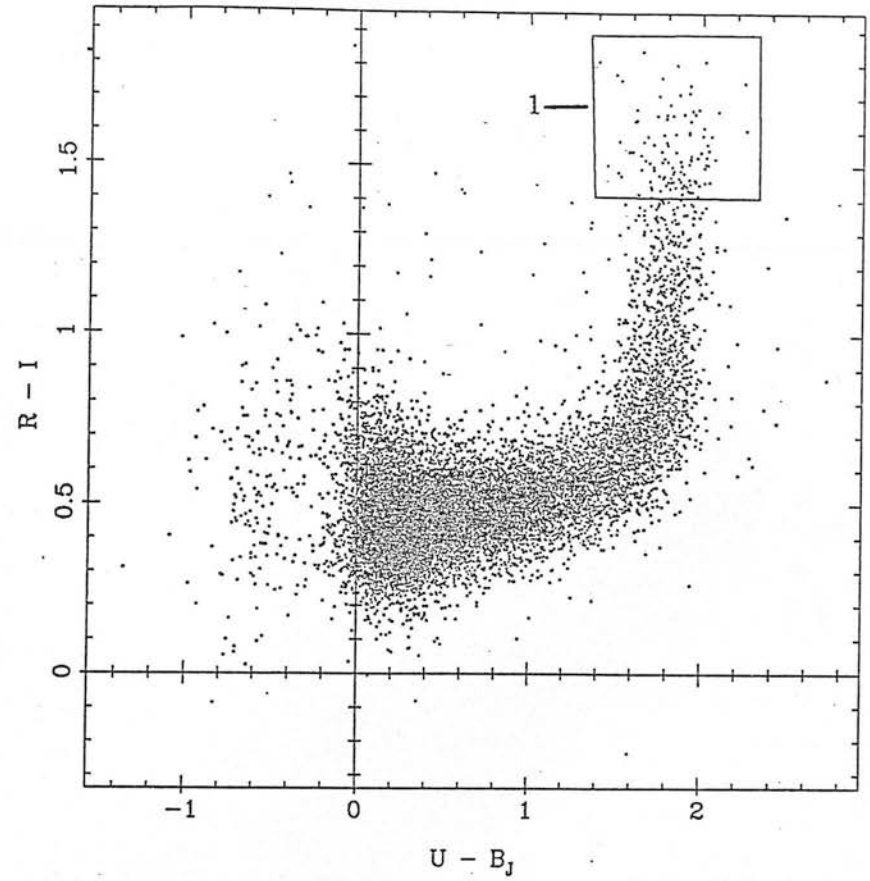

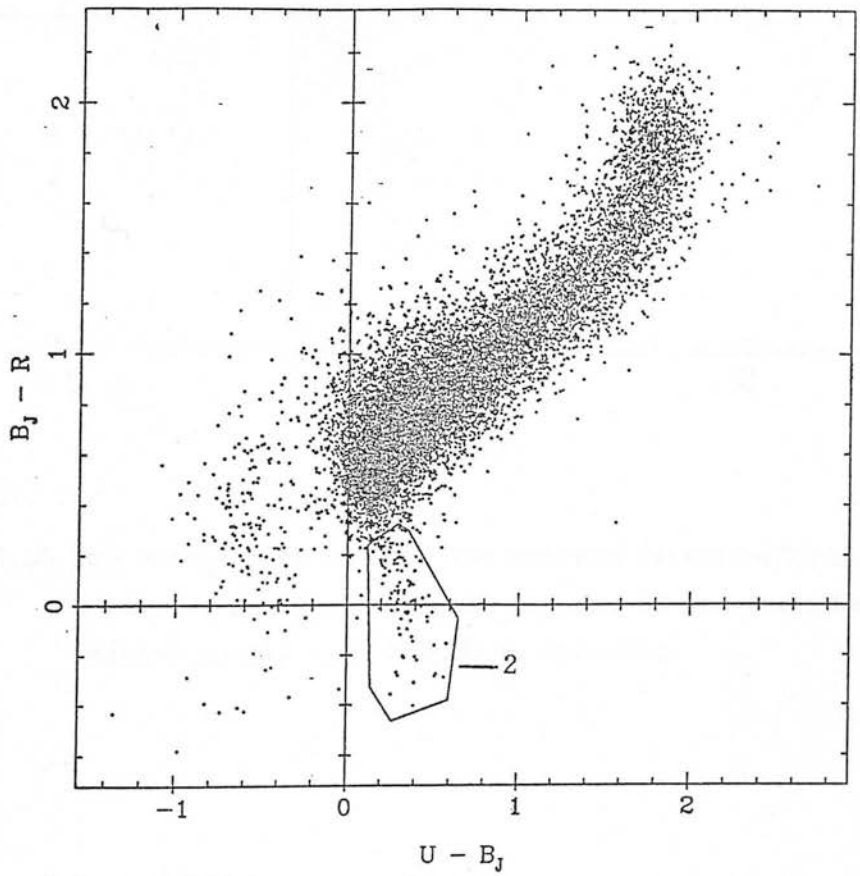

Fig 4.29 Two colour plots including regions of low density, therefore likely to identified in a nearest neighbour search, but unlikely to actually contain any quasars. The reasons for the definition of these regions is expanded in the text.

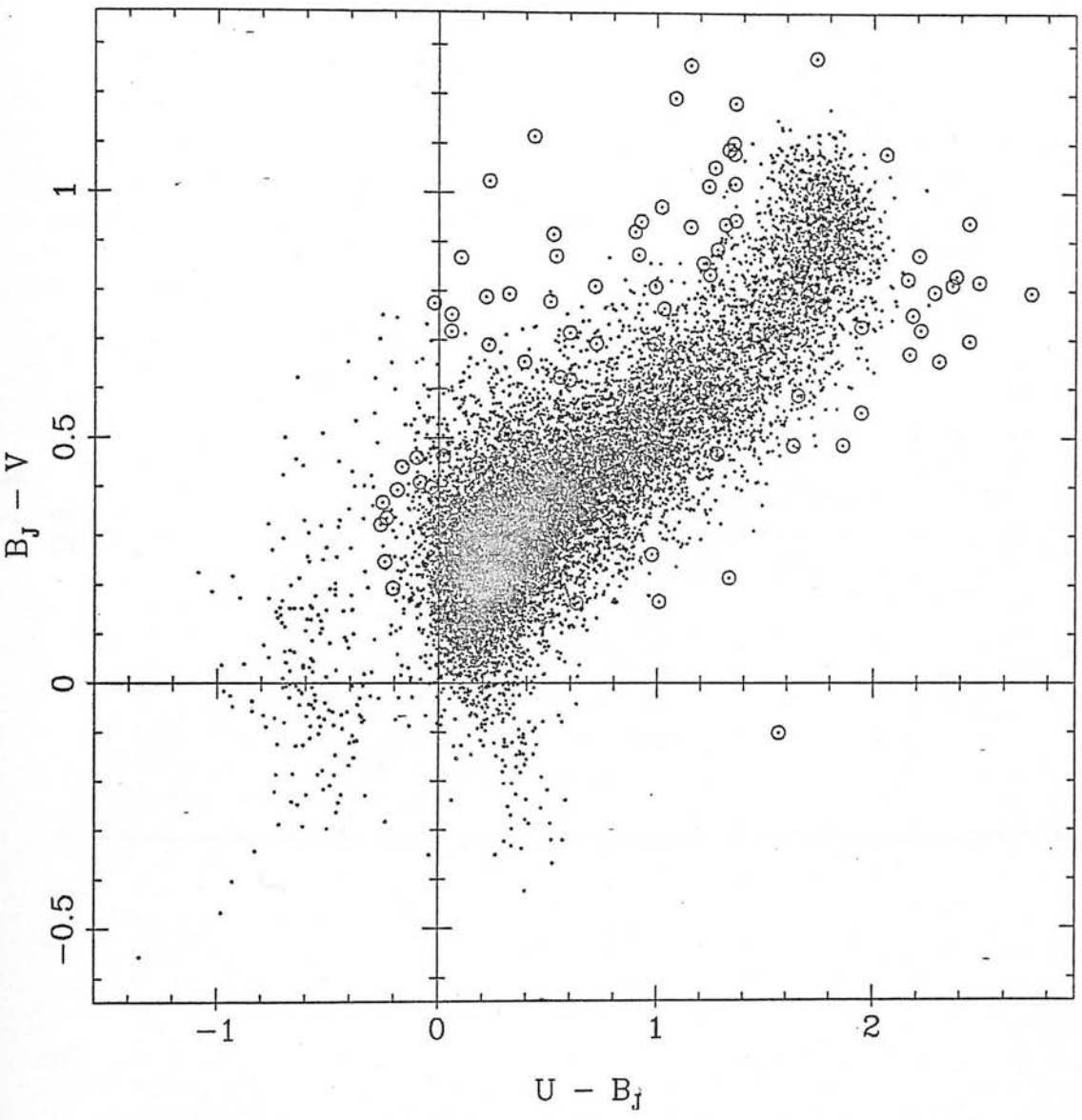

Fig 4.30 Two colour plot showing the hundred rarest objects, on a nearest neighbour search. Objects in the underdense regions in fig 4.29 have been excluded.

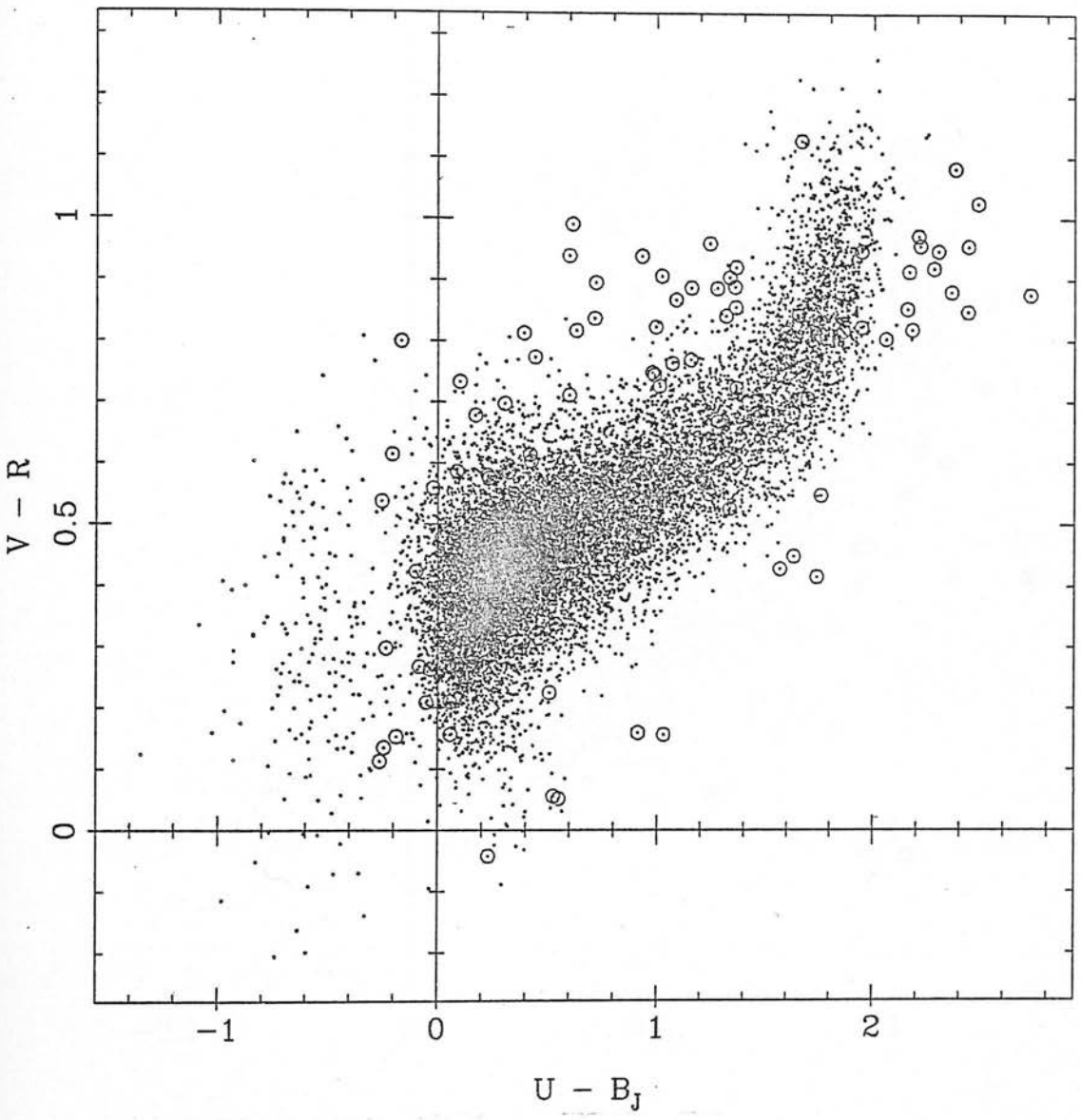

Fig 4.31 Two colour plot showing the hundred rarest objects. Some objects are clearly visible on the stellar locus. These actually lie above or below the locus in other dimensions.

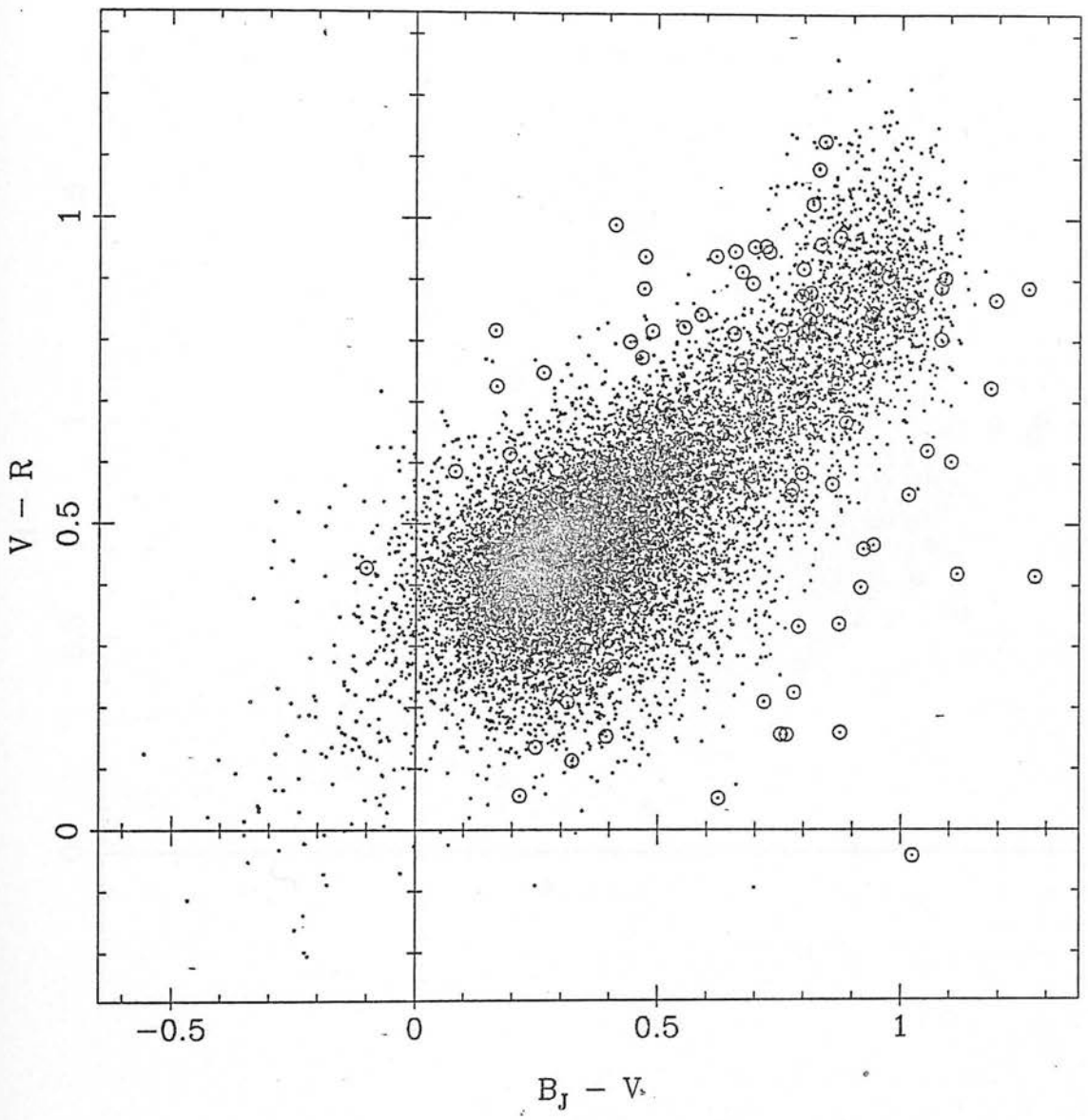

Fig 4.32 Two colour plot including the hundred rarest objects.

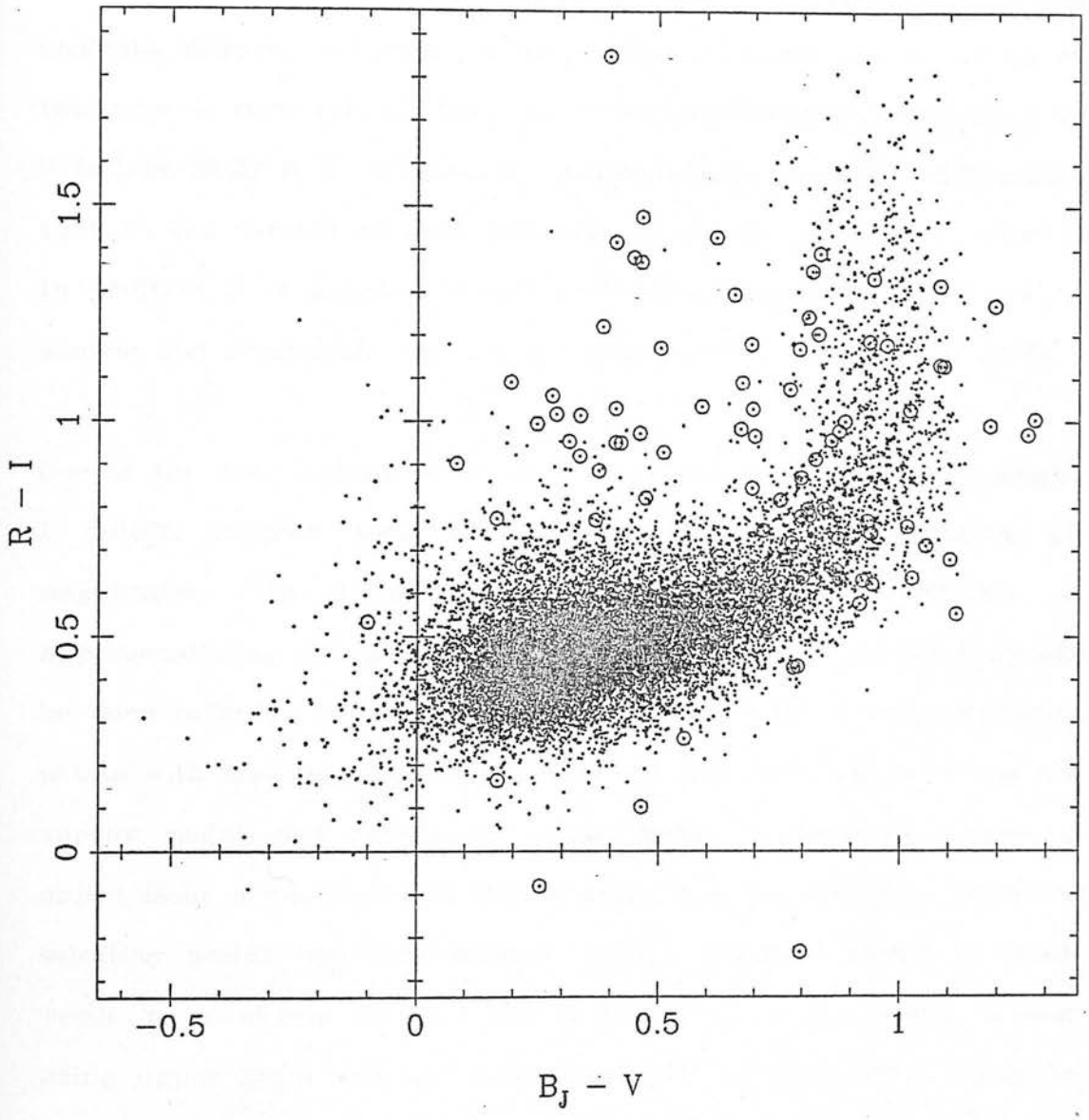

Fig 4.33 Two colour plot including the hundred rarest objects.

spectroscopy for many of the candidates. In addition, because there is so much less information available per candidate than in the low dispersion spectra, it is not possible to rank the candidates in any way. Thus it is not possible to give the survey a rigorous statistical analysis. However, informally it is possible to argue that a survey of this type is more reliable than the slitless spectrum surveys, because it is less likely to be effected by unquantifiable systematic difficulties such as the various redshift selection effects discussed in chapter 1. In addition it is possible to use properties of the other surveys to analyse the photometric survey, but this has been left to chapter 5.

One of the main limitations of the survey is the comparatively bright I cutoff, coupled with the requirement that objects have all magnitudes. The I plate limit it due to the difficulty of hypersensitizing IVn plates well. It is clear that further work should be done in order to use the information wasted by this survey (data points with less than five magnitudes). It may be possible to use the survey magnitudes cutoffs as bright limits in instances where an object lacks a magnitude. If this is done then the simplistic candidate selection modus operandi adopted in this chapter cannot be used. Trials have shown that attempting to obtain a meaningful answer using upper limits and two dimensional cuts is futile. What would be required is an 'intelligent' (in the sense of A.I.) evaluation procedure, which could use all of the information simultaneously in combination with information previously derived regarding the location of the stellar locus.

5. Relationships between surveys in the field.

One of the principle ideas behind this thesis is the generation of a quasar survey which attempts to deal with the selective incompleteness normally found in quasar surveys (discussed in section 1.3). In this chapter, a start is made toward that goal, by looking at what the relationships are between the surveys that have been collected in UK Schmidt field 927.

In order to achieve this, objects from other surveys (where possible) were located in the photometric survey in order that their properties in colour-colour space might be examined. Generally, once the catalogue is in the computer this is very easily done, because one can usually match their locations with sufficient precision for little or no confusion. Table 5.1 gives a list of the different surveys, and the limiting apparent magnitudes for each one. Section 1.3.4 has given an impression of the problems and inadequacies faced in trying to define these limits. They were defined by reference to histograms of the B_J magnitudes of objects - shown in figure 5.1. Thus many objects found are fainter than survey limits and must be discarded.

Section 5.1 is an examination of the eyeball prism survey technique, as exemplified by the He prism survey (discussed in section 2.1). Section 5.2 examines the automatic prism survey technique, divided by candidate selection method (emission line and UV excess - the AQD survey was discussed in section 2.2). Section 5.3 looks at the automatic grens survey of chapter 3 in the light of the photometric survey of chapter 4. Section 5.4 is a more detailed look at the

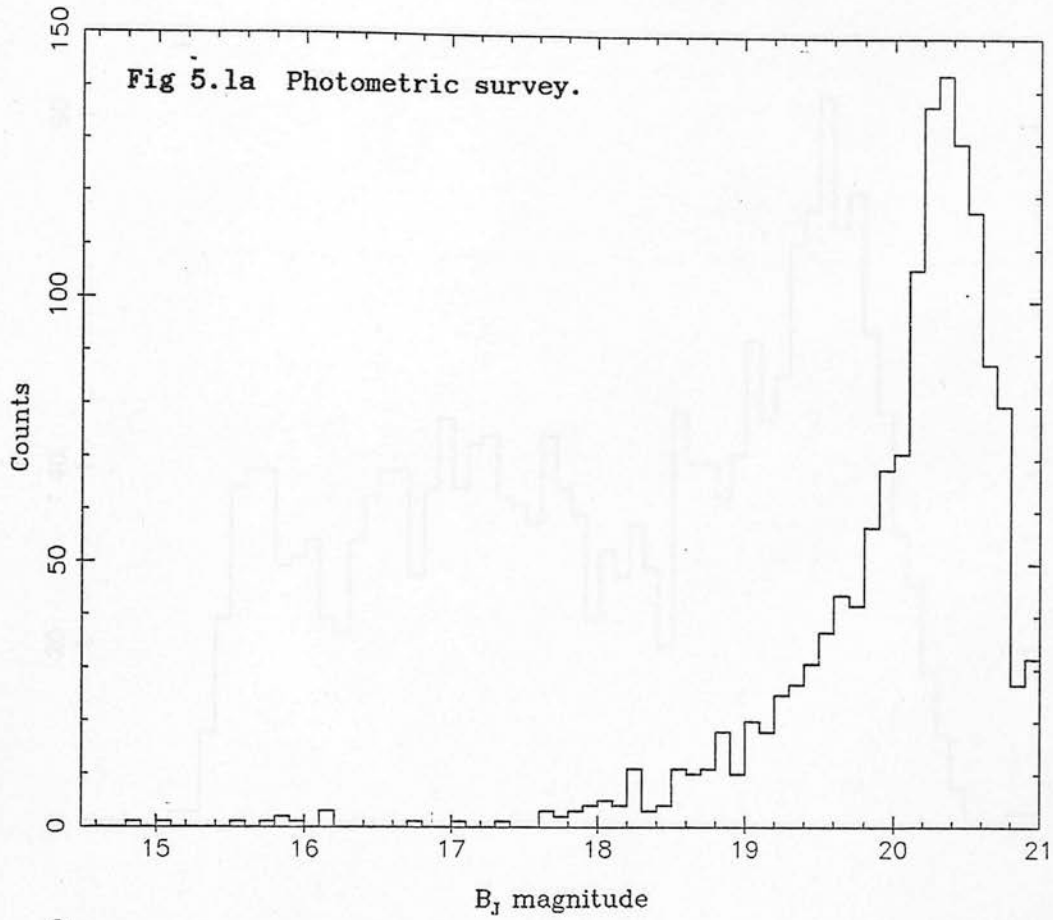

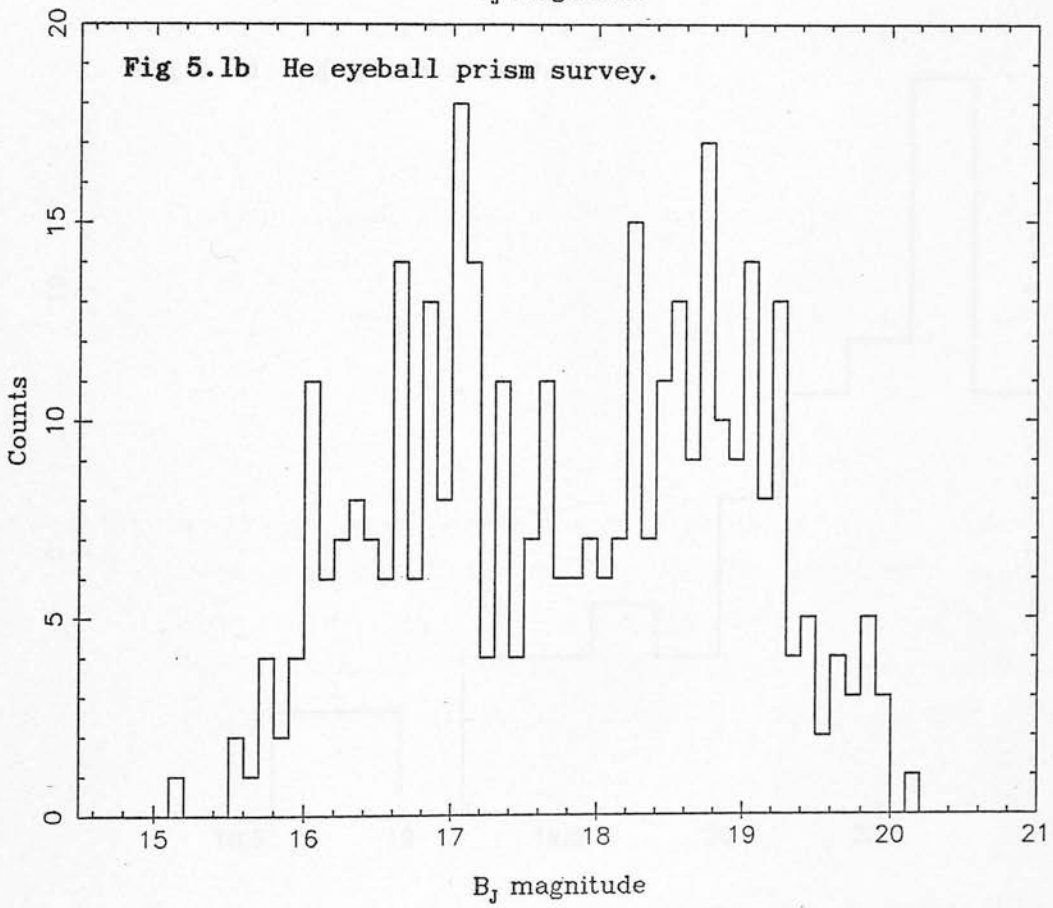

Fig 5.1 Number of candidates as a function of B_J magnitude for each survey considered.

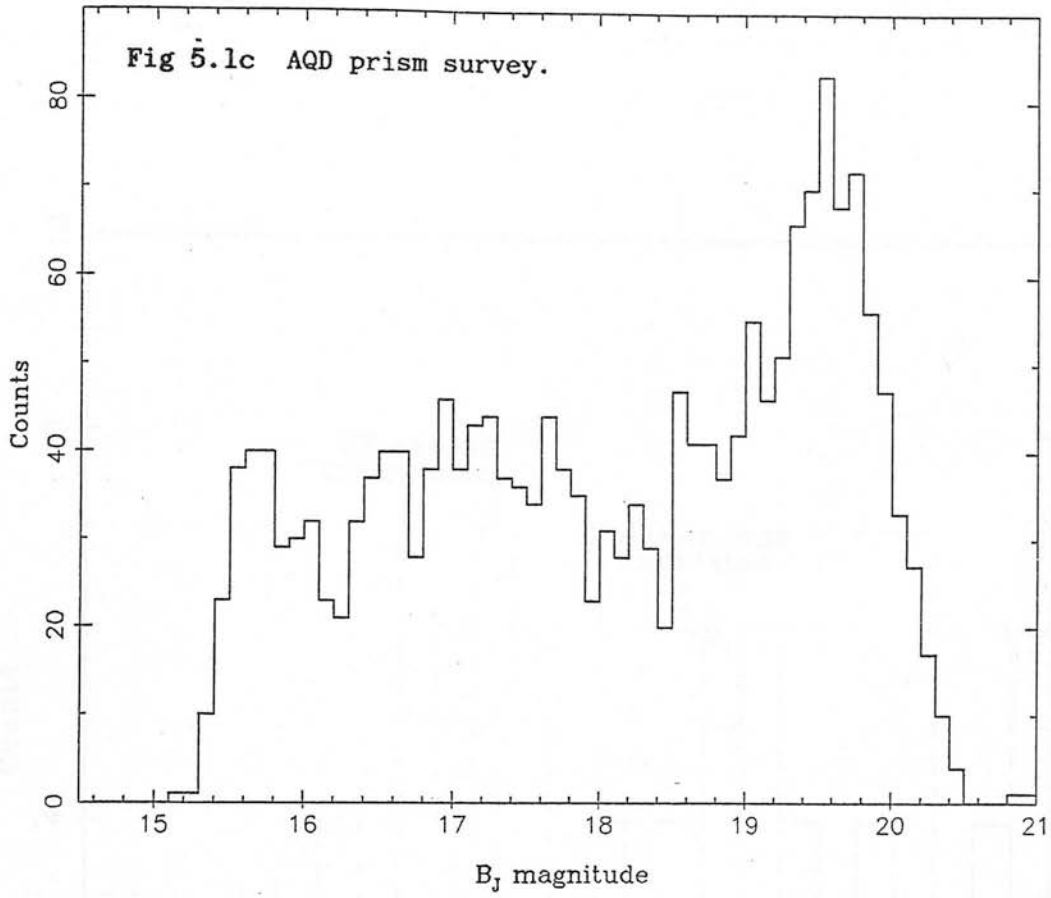

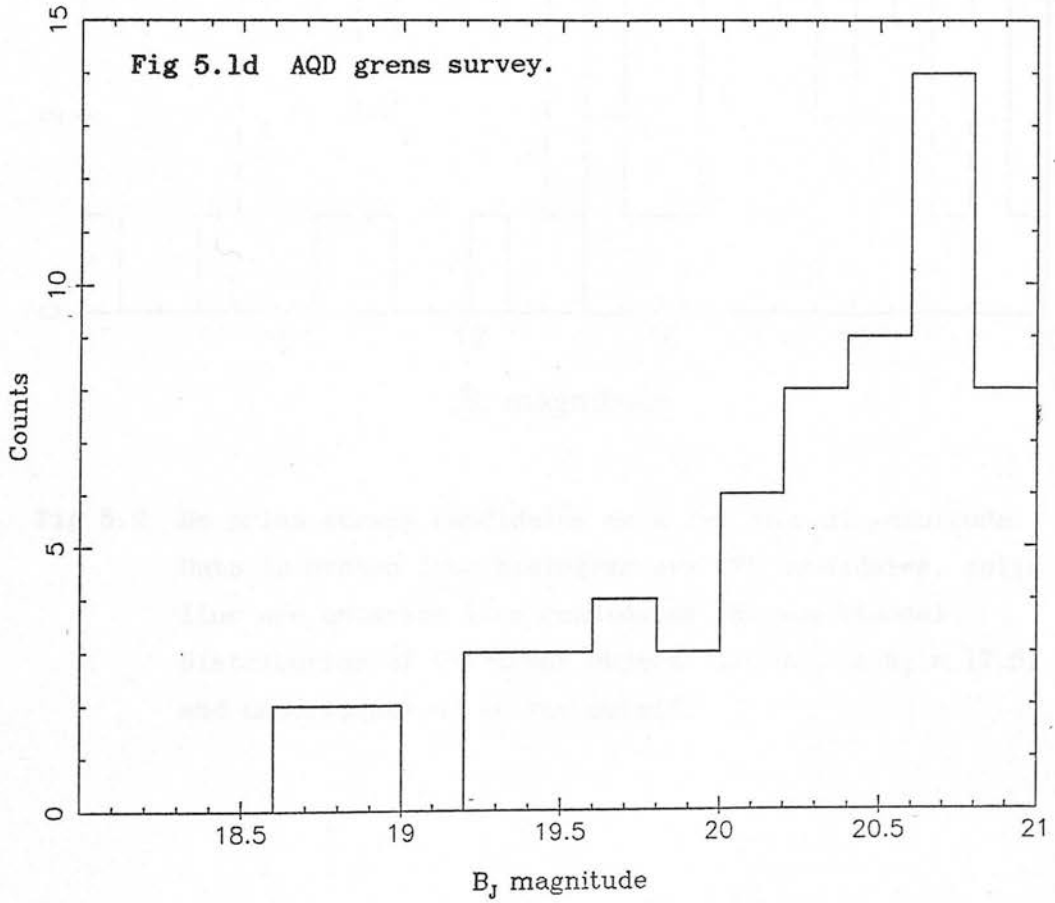

Fig 5.1 (continued).

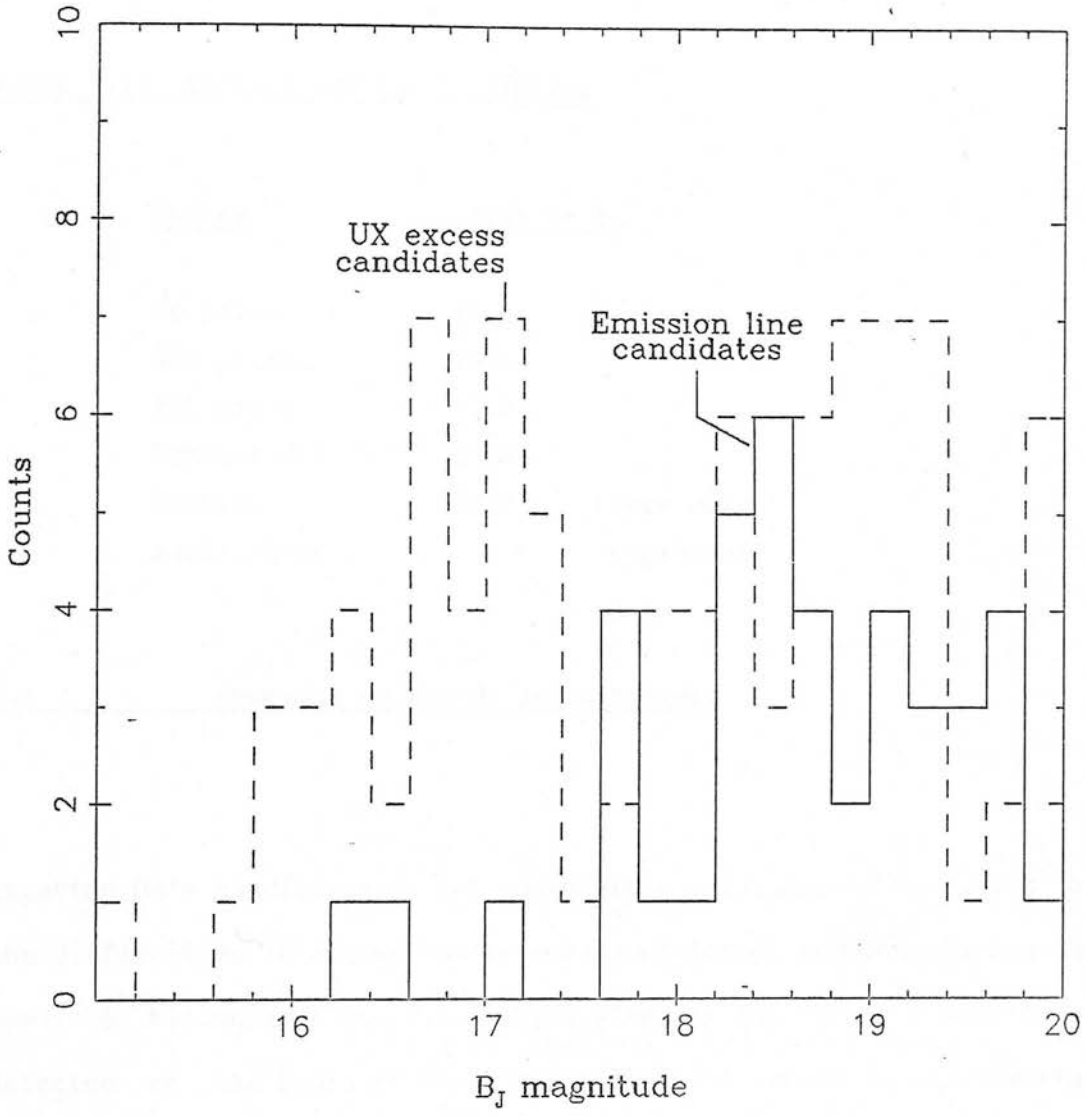

Fig 5.2 He prism survey candidates as a function of magnitude. Data in broken line histogram are UVX candidates, solid line are emission line candidates. Notice bimodal distribution of UV excess objects divided at $B_J \approx 17.5$, and uncertainty of survey cutoff.

photometric survey candidates with particular reference to objects in common with other surveys, and finally concluding remarks are made in section 5.5.

Table 5.1: Surveys and survey limits.

Survey	Limit in B_J	
He prism	19.4	
AQD prism	19.8	
AQD grens	> 20.8	
Schmidt UVX	20.8	
Schmidt multicolour	20.8	(very colour dependent)

5.1 Comments on the He prism survey.

Locating He's candidates in the photometric catalogue is revealing of the difficulties in attempting to construct large, complete surveys by eye. A histogram (fig. 5.2 - solid line) of the object magnitudes selected on the basis of their emission lines shows a substantial incompleteness at $B_J > 19$. This is despite the fact that some quasars are clearly quite readily identifiable at $B_J = 20$. A histogram of the UVX objects (fig. 5.2 - broken line), meanwhile, shows a strongly bimodal distribution, with a sharp decrease in quasar candidates at $B_J = 17.7$. The survey limit for the UVX candidates appears to be $B_J = 19.6$. The reason for this bimodality is presumably human error: It is easy to pick genuinely UVX objects which are bright, but many objects close to the plate limit appear to have long, flat continua and therefore to be UVX. This hypothesis can

be tested with the use of the photometric information - figure 5.3 shows a histogram of $U - B_J$ for these candidates, divided in magnitude at $B_J = 17.7$. This shows how difficult it is to pick the genuinely UVX objects from the prism plates by eye. The fainter ($B_J > 17.7$) group are more likely to be genuinely blue in $U - B_J$, but even so there are quite a large number around 0 in $U - B_J$. Almost all of the brighter $B_J < 17.7$ group are not blue in $U - B_J$. It is likely that they were picked out because the red end of the prism spectrum is quickly saturated at brighter magnitudes, and so the spectrum takes on a flatter appearance. This is also a problematic effect with the automatic survey - see figure 5.5.

5.1.1 Completeness of the He prism survey.

In order to obtain some insight into the difficulties endemic in eyeball searches, photometry of candidates is here compared with objects from Boyle (1986). The value of Boyles' work is that all of the objects have slit spectroscopic identifications. Values for the quasar number density are from Boyle (1987, private communication) while the ultraviolet excess galactic star counts are the 'QSF' fields from Boyle, (1986). Boyles' quasar number counts are an average of many widely separated ≈ 0.7 square degree fields, over a total of 8.74 square degrees. They are an extension in total area surveyed from Boyle (1986), but the number counts are essentially unchanged. The QSF field is chosen for galactic star counts, because this field is the closest in galactic latitude to field 927 (for QSF, $b \approx -51^\circ$, while for F927, $b = +52^\circ$). Number counts are presented in table 5.2. As was noted in chapter 4, these counts can be representative only, because

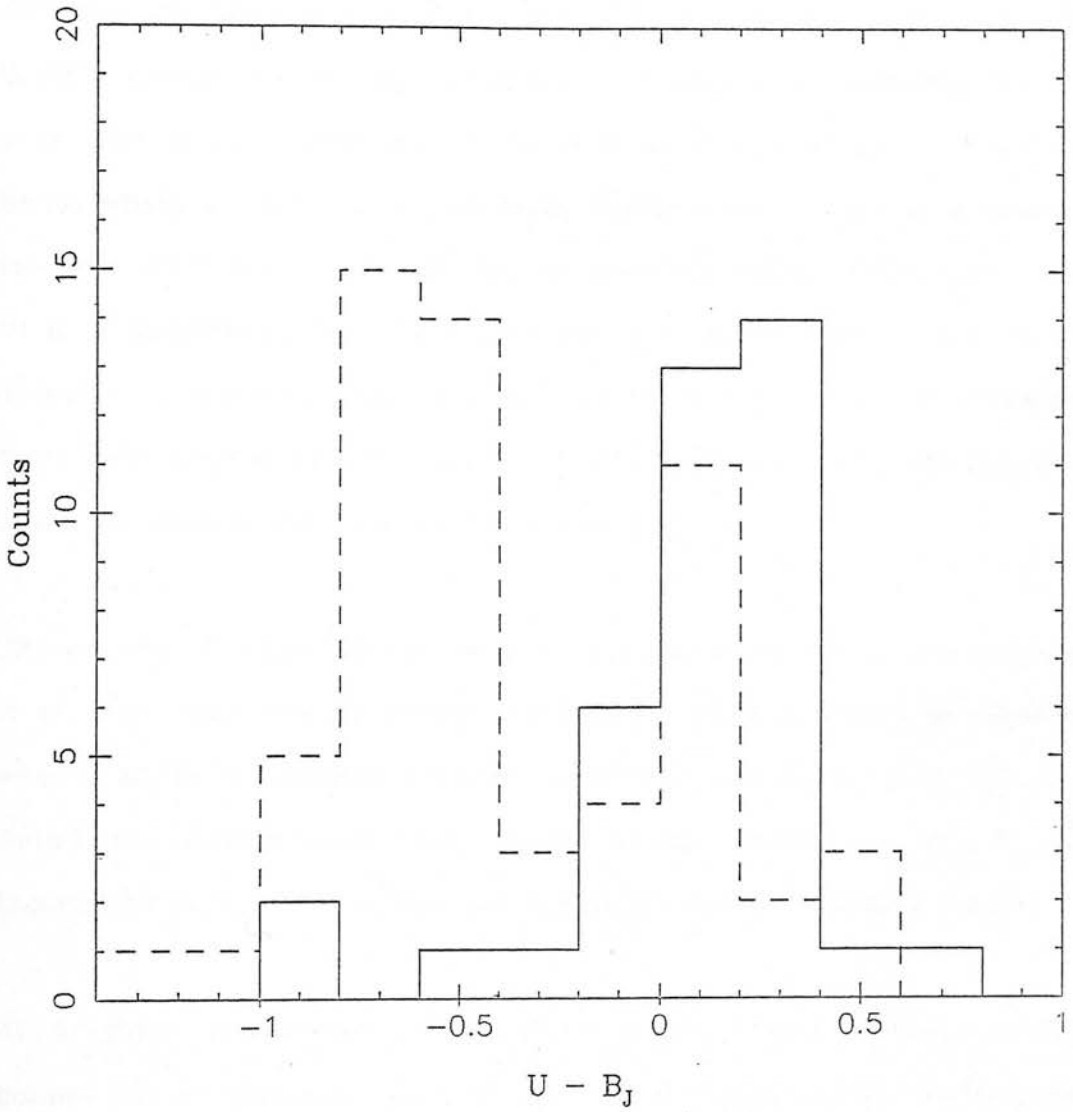

Fig 5.3 He prism survey candidates as a function of $U - B_J$. Data in solid line histogram are those objects which have $B_J < 17.5$. Data in broken line histogram are those objects which have $B_J > 17.5$.

i) statistics for Boyles' star counts are over two 0.7 square degree fields, so errors are likely to be large, ii) if a candidate displays an emission line in the prism spectrum, He will have classified it as an emission line candidate, and will not include it in the UVX count, iii) Boyle's quasar counts are sensitive to quasars of redshifts $z < 2.2$ only. The prism survey should be most sensitive in the $1.8 < z < 3.3$ band, where Ly-α is in the emulsion passband, iv) there is a possible intrinsic difference in counts due to differing galactic absorption, and v) it is possible to identify the broad band Balmer series lines in the objective prism spectrum of a hot white dwarf. He would therefore have been able to eliminate some UV excess objects on these grounds, since his search was exclusively for quasars.

The counts in table 5.2 can only be an indication, then, but even so it is clear that the He survey is missing large numbers of objects: even if all He candidates are considered (columns 4 and 5) and He has found no objects other than quasars, the survey is <u>still</u> $\approx$ 45% incomplete at $B_J = 18.75$ (the last whole bin before the plate limit).

At brighter magnitudes, the position is also very serious. Number counts for all classes of UVX object are dropping swiftly towards the brighter bin, and yet the counts for He remain virtually unchanged over three bins between $16.5 < B_J < 18.0$. So clearly He is locating other classes of galactic star which appear to have a UV excess (the problem is plainly in columns 2 and 3, the UV excess number counts).

The point made in chapter 4 is re-emphasised: the comparison with Boyles' numbers is not final or absolute in any way. Particularly, his

number counts for UVX stars are very unreliable (in so far as they are used as a basis for comparison with objects in another

Table 5.2: Number densities of He survey.

	UVX candidates		All cands.		Boyle 1986	
B_J	N(B)	N/deg^2	N(B)	N/deg^2	N_{QSO}/deg^2	N_{uvx}/deg^2
16.0 - 16.5	8	0.34	9	0.38	-	-
16.5 - 17.0	12	0.51	13	0.55	-	-
17.0 - 175.	12	0.51	13	0.55	-	1.4
17.5 - 18.0	7	0.30	12	0.51	0.17	7.1
18.0 - 18.5	11	0.46	18	0.77	0.56±0.25	7.1
18.5 - 19.0	15	0.64	26	1.11	1.83±0.49	5.7
19.0 - 19.5	15	0.64	24	1.02	5.24±0.79	5.7
19.5 - 20.0	8	0.34	14	0.60	7.38±0.85	2.9

part of the sky). This does not detract from the fact that the differences found are huge, even on a 'best possible case' assumption. Surveys of this type are clearly of very little value if the ultimate goal is to answer questions requiring a complete sample, especially since it is clear that objects lost are not lost at random. Such a survey may be used for programmes which do not require a complete sample, but only if it is realised that it is inefficient. The count rate at B = 16 is 0.0075 per degree^2 from Green, Schmidt and Liebert (1986), while He finds 0.38 objects per degree^2.

5.2 Comments on the AQD prism survey.

In this section, the AQD selected objects are examined in the same way as He objects were in section 5.1. First, photometry for them was obtained by matching astrometry for them in the photometric survey. Magnitude estimates from the direct plate, J9952, used in the AQD search are unreliable. This is because there is a strong background density variation across the plate, and because of its relatively long (100 minutes) exposure time, stellar objects are saturated only ≃ 2 magnitudes brighter than the plate limit. This plate was considered for inclusion in the photometric survey, but rejected on these grounds (it would have been very difficult to calibrate properly, and the background variations would have introduced colour field effects). However, positional information should not be in any way impaired, so it's use for the prism plate spectrum location is quite justified.

As a result, to make some assessment of the AQD survey, it had first to be paired with the photometric survey. This was done, and number counts of both the 'larger' and the 'good' AQD surveys are presented in table 5.3 (the differences between these categories are described in section 2.2), together with numbers from Boyle, (1986). As in section 5.1, Boyles quasar counts are from the whole survey, while his UV excess star counts come only from the QSF region. The only AQD objects not found in the photometric survey were those classified in that survey as galaxies. As Boyle also excludes galaxies from his survey, this should not make any difference to a comparison of number counts, although it is astrophysically arbitrary. The exclusion of galaxies is made necessary by the difficulty in calibrating them in

Table 5.3: Number densities of the AQD prism survey.

B_J	Larger				Good		Boyle	
	Emission		UVX					
	N(B)	N/dg^2	N(B)	N/dg^2	N(B)	N/dg^2	N/dg^2 qso's	N/deg^2 stars
15-15.5	17	0.72	23	0.97	3	0.13	-	-
15.5-16	113	4.77	85	3.59	7	0.29	-	-
16-16.5	132	5.57	18	0.76	8	0.34	-	-
16.5-17	192	8.11	2	0.08	7	0.29	-	-
17-17.5	198	8.36	2	0.08	2	0.08	-	1.4
17.5-18	171	7.22	8	0.34	8	0.34	0.17	7.1
18-18.5	132	5.57	19	0.80	10	0.42	0.56±.25	7.1
18.5-19	169	7.14	55	2.32	27	1.14	1.83±.49	5.7
19-19.5	189	7.98	138	5.83	55	2.32	5.24±.79	5.7
19.5-20	168	7.09	204	8.61	59	2.49	7.38±.85	2.9
20-20.5	57	2.41	50	2.11	22	0.93	11.43±1.34	11.4
20.5-21	-	-	2	0.08	-	-	11.43	11.4

the photographic data. The comparison of the AQD sample with Boyle's sample is not satisfactory, because the redshift limit of AQD should be $z = 3.4$ whereas Boyles sample is limited to $z = 2.2$. Previous spectroscopically confirmed emission line surveys, such as that of Osmer and Smith (1980) do not provide a particularly good basis for comparison either, because they are so dominated by Lyman-α detection.

5.2.1 The larger AQD sample.

Histograms of the distributions in magnitudes the larger AQD sample are presented in figure 5.4, distinguished by selection method. If an object was selected on grounds of both its emission lines and its UV

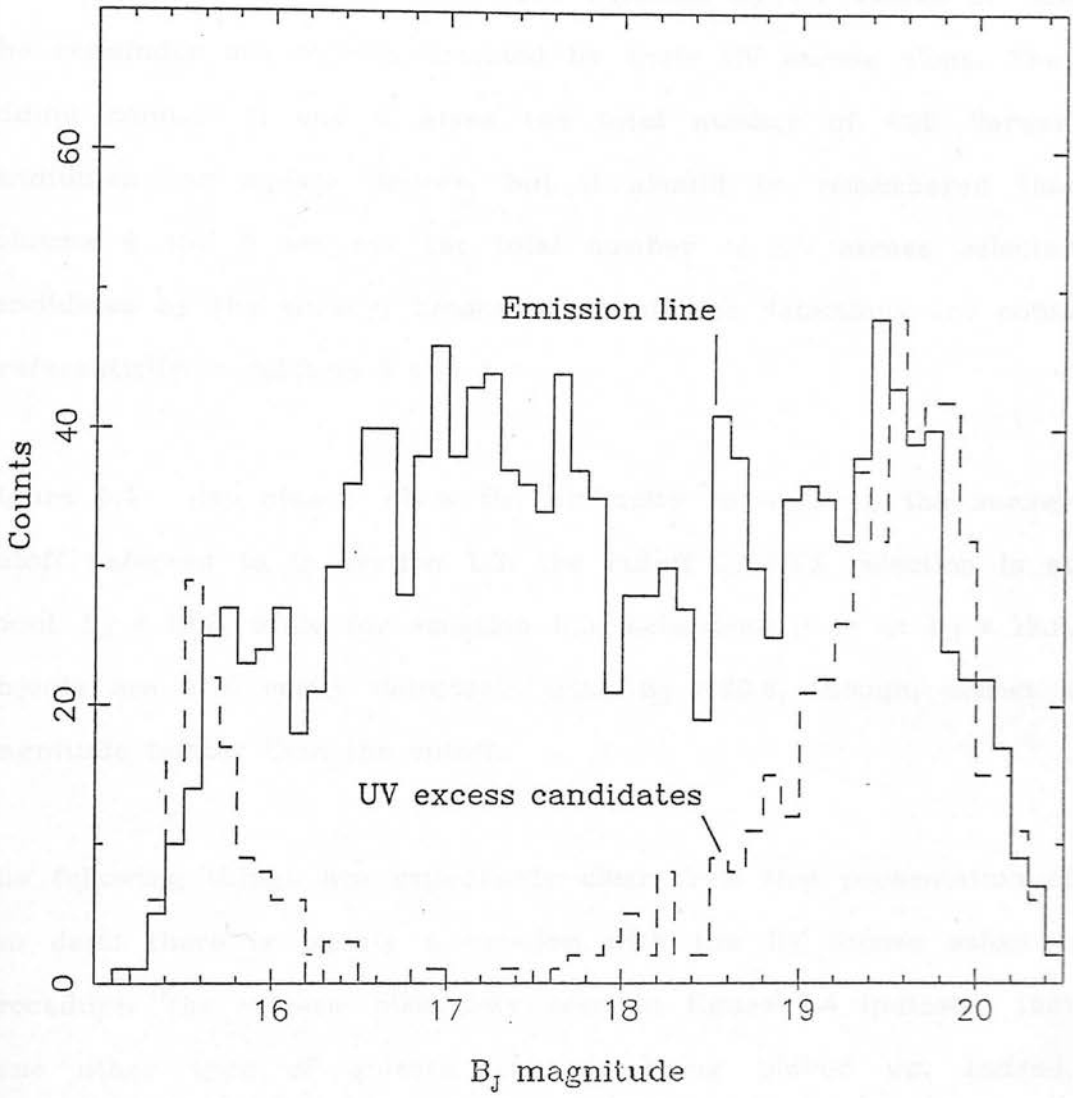

Fig 5.4 AQD prism survey candidates as a function of magnitude, and divided by selection method. Magnitudes are from photometric survey. Notice the extremely bimodal form of the UV excess histogram, and the virtually constant numbers of emission line candidates over ≈ 3 magnitudes.

excess, it is included in both the emission line and the UV excess diagrams. However, objects in table 5.3 are included only once, that is all objects are included in columns 2 and 3 if they were detected by an emission line, whether they were detected by UV excess or not. The remainder are objects detected by their UV excess alone. Thus adding columns 3 and 5 gives the total number of AQD 'larger' candidates per square degree, but it should be remembered that columns 4 and 5 are not the total number of UV excess selected candidates by the survey, because emission line detections are noted preferentially in columns 2 and 3.

Figure 5.4 also clearly show the difficulty in defining the survey cutoff referred to in section 1.3: the cutoff in UVX selection is at about $B_J \approx 19.7$, while for emission line selections it is at $B_J \approx 19.8$. Objects are still easily detectable until $B_J = 20.6$, though, almost a magnitude fainter than the cutoff.

The following things are immediately clear from this presentation of the data: there is plainly a problem with the UV excess selection procedure. The extreme bimodality seen in figure 5.4 indicates that some other type of galactic star is being picked up. Indeed, inspection of spectra of the objects in the bright bump of figure 5.4 (all UV excess objects with $B_J < 17.5$) shows that these are all objects which have saturated nearer the red end of the spectrum, and so the U / B_J ratio appears much more blue on the prism spectrum than it is in reality. Figure 5.5 shows a random selection of such objects - the emulsion cutoff is at the left end of the spectrum, and wavelength decreases towards the right. There are a total of 144 out of 620 UV excess candidates in this class, and they were rejected from the

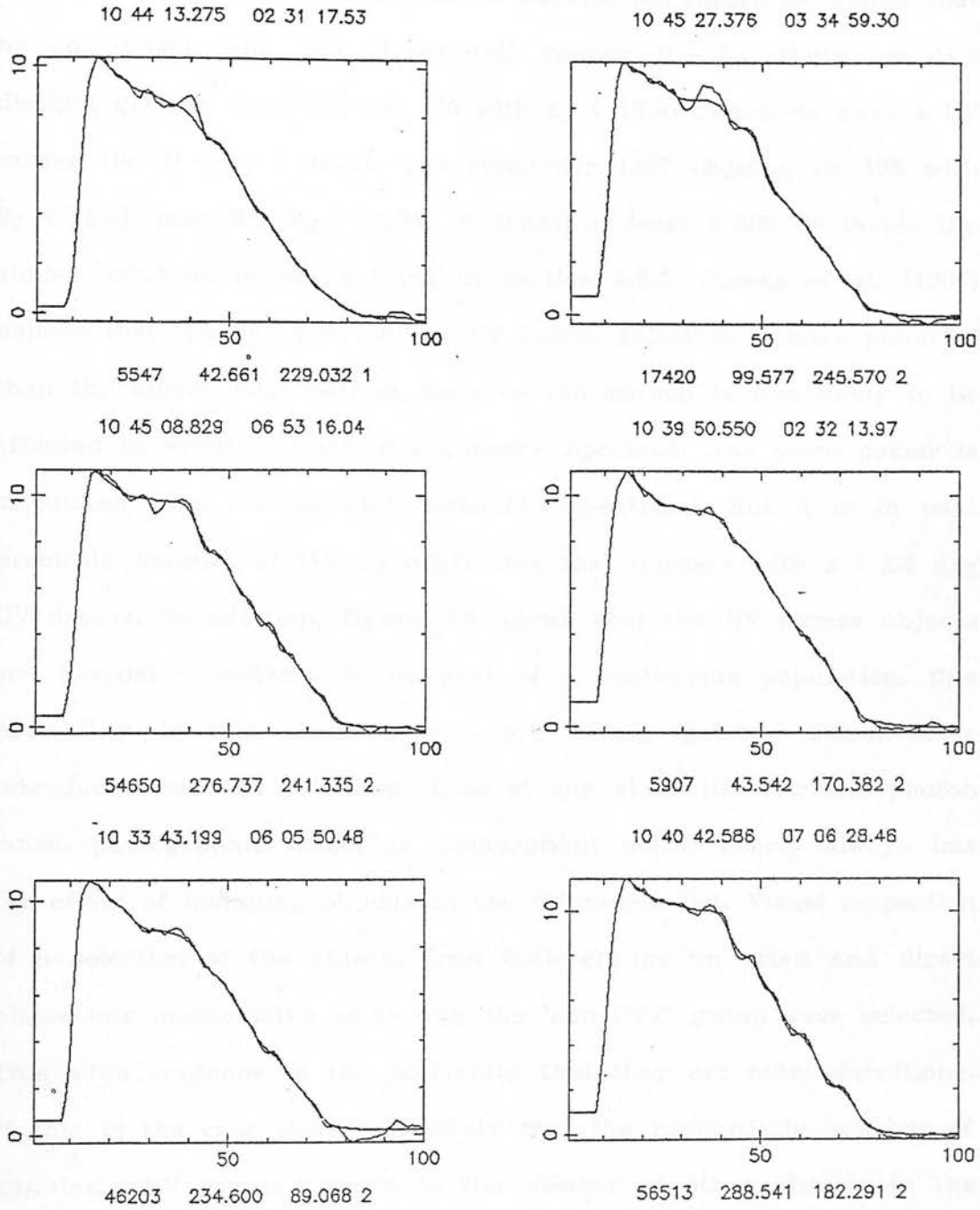

Fig 5.5 Selected prism plate AQD candidates from the bright part of the UV excess distribution. The emulsion cutoff is at the left end, and λ is decreasing to the right. All spectra are of a similar form, with the blue end cut off due to photographic saturation.

sample.

Considering the remaining UV excess candidates, figure 5.6 shows that by comparison with the photometric survey $U - B_J$, there are two distinct groups. Some 239 (or 175 with $B_J < 19.8$) genuinely have a UV excess (ie. $U - B_J < -0.25$). The remainder (237 objects, or 175 with $B_J < 19.8$) have $U - B_J > -0.25$. Of these, at least $\approx$ 50% lie inside the stellar locus as it was defined in section 4.8.2. Clowes *et al.* (1987) believe that the prism method of UV excess selection is more powerful than the direct plate method, because the method is less likely to be effected by emission lines in a quasars' spectrum (the prism colour is calculated from the objects' continuum spectrum). But it is in part precisely because of the Ly-α/NIV line that quasars with $z < 2.2$ <u>are</u> UV excess. In addition, figure 5.6 shows that the UV excess objects are bimodal - unlikely to be part of a continuous population. One possibility is that these objects are simply galactic stars. Noise introduced into the prism spectrum at any stage (ie. intrinsic photon noise, photographic noise, or measurement noise) nearly always has the effect of including objects in the UV excess list. Visual inspection of a selection of the objects from both groups on prism and direct plates was inconclusive as to why the 'non-UVX' group were selected. This adds credence to the possibility that they are noise detections. If this is the case then it is likely that the ratio of the number of genuinely UV excess objects to the number of other objects in the AQD UV excess list is a function of magnitude, since signal to noise in the spectrum is poorer at fainter magnitudes. Indeed, this does appear to be at least partially true, with no unsaturated objects in the AQD colour sample brighter than $B_J = 18.5$ having stellar colours, and then an increasing proportion have stellar colours until some 60%

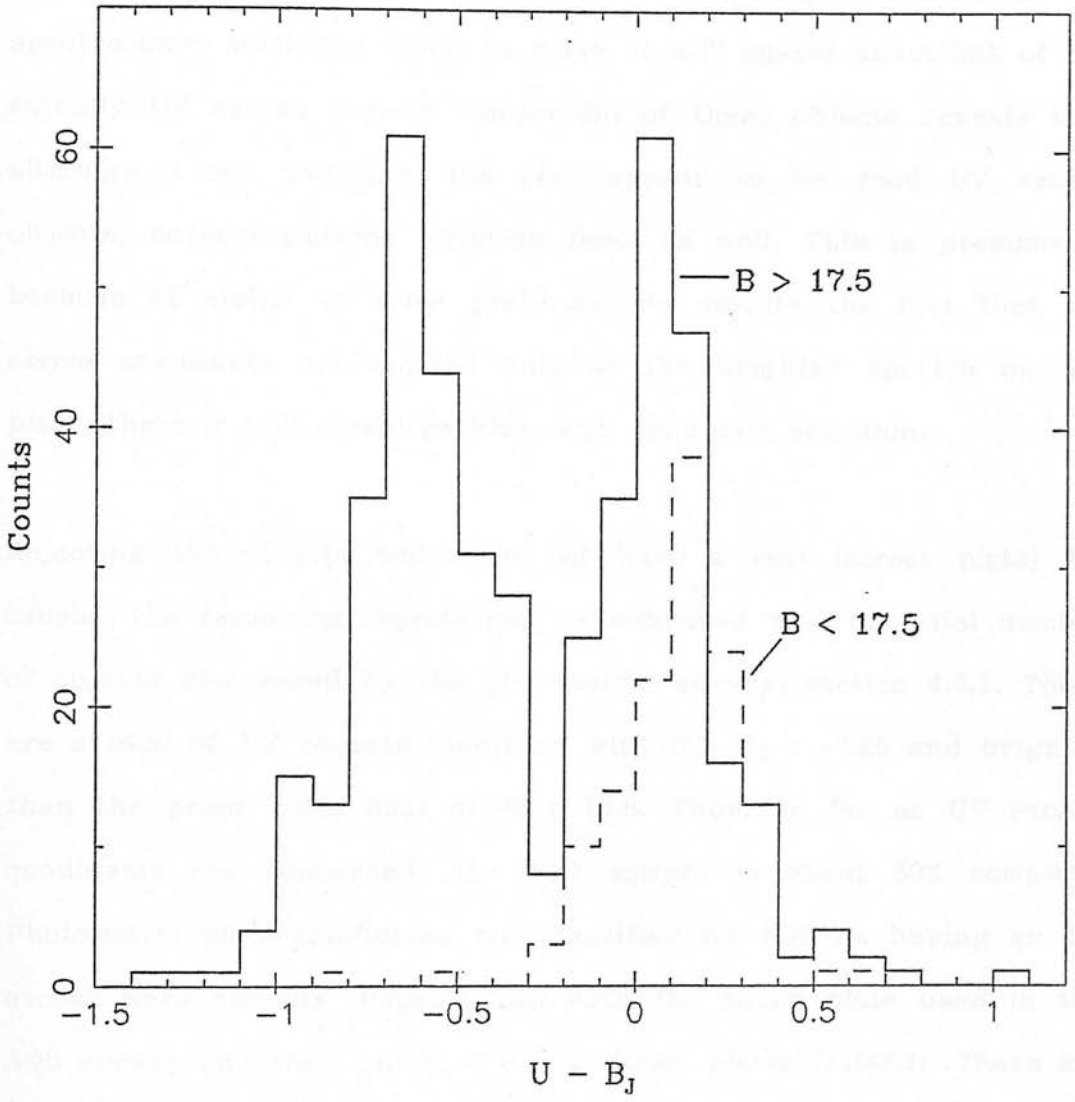

Fig 5.6 Histogram of AQD prism UV excess candidates. Data in solid line histogram are fainter, $B_J > 17.5$. Those in broken line histogram are brighter, $B_J < 17.5$. Objects in the solid line histogram were divided at $U - B_J = -0.25$ for visual inspection on the plates.

do at $B_J = 19.5$. However, there is a complicating factor, which is that 12 out of 39 UV excess photometric survey objects in the range $17.5 < B_J < 18.5$ are not found amongst the AQD survey. So although AQD does find some objects of peculiar very blue colours if the spectra have sufficient signal to noise, it still misses about 30% of the actually UV excess objects. Inspection of these objects reveals that although 4 are overlaps, the rest appear to be good UV excess objects, several showing emission lines as well. This is presumably because of signal to noise problems. So despite the fact that the above arguments are applied only to the brighter spectra on the plate, there is still a real problem with candidate selection.

Rejecting the objects which do not have a real (direct plate) UV excess, the remaining objects can be compared with the total number of objects discovered by the photometric survey, section 4.8.1. There are a total of 326 objects identified with $U - B_J < -0.25$ and brighter than the prism plate limit of $B_J = 19.8$. Thus, so far as UV excess candidates are concerned, the AQD sample is about 50% complete. Photometric plate candidates not identified by AQD as having an UV excess were visually inspected on both the prism plate used in the AQD survey and the deepest of the J direct plates (J10063). There are 151 objects not found by AQD, which one might expect to be, in the area. Of these, a few at least will be brighter than $B_J = 17.5$, but they must be included in the 'not located by AQD' class because they cannot be discriminated by AQD from other bright objects which have a saturated red end. In fact, extrapolation from Green, Schmidt and Liebert (1986) to this magnitude limit ($B_J = 17.5$) indicates only ≈ 3 objects are lost by AQD in this way. Results of this inspection are given in table 5.4.

Column 3 is the percentage of objects missed falling into each category, while column 4 is the percentage of all direct plate UVX objects falling into each category. There is no obvious reason for

Table 5.4: Inspection of UV excess candidates.

Prism category	No.	%	% of total
Overlap	52	34.4	15.9
UV excess	53	35.1	16.2
emission	46	30.5	14.1

the loss by AQD of rows labelled 'UV excess' and 'emission' (the latter meaning that an emission line was identified by eye in the prism spectrum, the spectrum showing an UV excess also). These objects have a large spread in $U - B_J$ (though always $U - B_J < -0.25$), and do not appear to have an unusual distribution in magnitude - they are not, for example, clustered in magnitude close to the prism survey cutoff. Thus there is every reason to expect them to be located by AQD on grounds of their UV excess.

The presence of a large group of candidates lost by AQD due to overlaps is less disturbing. Although it effects the total number counts and densities derived, it is statistically insignificant because the objects are lost at random.

Focusing now on the emission line objects, the question also arises as to the number missed by AQD. The visual inspection described above can be used to this end: objects which were not selected for their UV

excess may have been picked up by emission line detection. This comparison has the additional complicating factor that the redshift sensitivities are different for a UV excess candidate list and an emission line candidate list. However this should not effect the conclusions drawn here: the photometric UV excess list is simply used as a list containing a high proportion of interesting objects. Incidentally, I should make it clear at this point that if there is sufficient signal to noise in the spectrum it is possible to tell the difference by eye between absorption features which simulate emission lines in galactic stars and real emission lines.

The list inspected in table 5.4 was paired with the AQD emission line selections: this yielded a total of 16 objects, or only 35% of the emission lines found by eye. What is bizarre and interesting to note is that 6 of the AQD emission line objects actually number amongst the 'UV excess' class of table 5.4, rather than the 'emission' class. In other words, AQD has detected emission lines too faint for the eye to see, and yet has failed to detect lines which <u>are</u> clear to the eye. It should be noted that the visual inspection was undertaken <u>without</u> knowledge of which candidates AQD had identified by their lines, and a generally conservative approach was adopted when identifying lines.

Table 5.3 and figure 5.4 show that far too many emission line objects are located at bright magnitudes - in all bins up to $B_J \approx 18$, and so there is little point in directly comparing columns 3 and 8 of the table. A possible approach to this problem is to identify all those emission line candidates which have stellar colours. The unfortunate thing about doing this is that the survey then loses one of the greatest potential advantages of including a prism plate survey - that

of being able to recover those quasars lost to the photometric survey by dint of their stellar colours. Be that as it may, the prism survey emission line candidate list is plainly overwhelmed with stars, as it stands, and so objects with stellar colours were removed. That is to say, AQD emission line candidates

Table 5.5: Number densities after stellar colour removal.

B_J	Before removal		After removal		Boyle
	N(B)	N/dg^2	N(B)	N/dg^2	N/dg^2 qso's
15-15.5	17	0.72	-	-	-
15.5-16	113	4.77	16	0.68	-
16-16.5	132	5.57	16	0.68	-
16.5-17	192	8.11	22	0.93	-
17-17.5	198	8.36	31	1.31	-
17.5-18	171	7.22	38	1.61	0.17
18-18.5	132	5.57	38	1.61	0.56±.25
18.5-19	169	7.14	70	2.95	1.83±.49
19-19.5	189	7.98	119	5.03	5.24±.79
19.5-20	168	7.09	151	6.38	7.38±.85
20-20.5	57	2.41	50	2.41	11.43±1.34

which lay inside all of the polygons in figures 4.18 - 4.17 were excluded. Figure 5.7 shows number counts of emission line objects after the exclusion of stellar colour candidates, and table 5.5 shows the effect on number densities of removing objects with stellar colours. It is clear that this process has reduced the stellar contaminant to the survey, and brought the number counts into the realms of reasonableness. Once again it should be emphasised that the comparison with Boyle's number counts is not strictly 'fair' because of

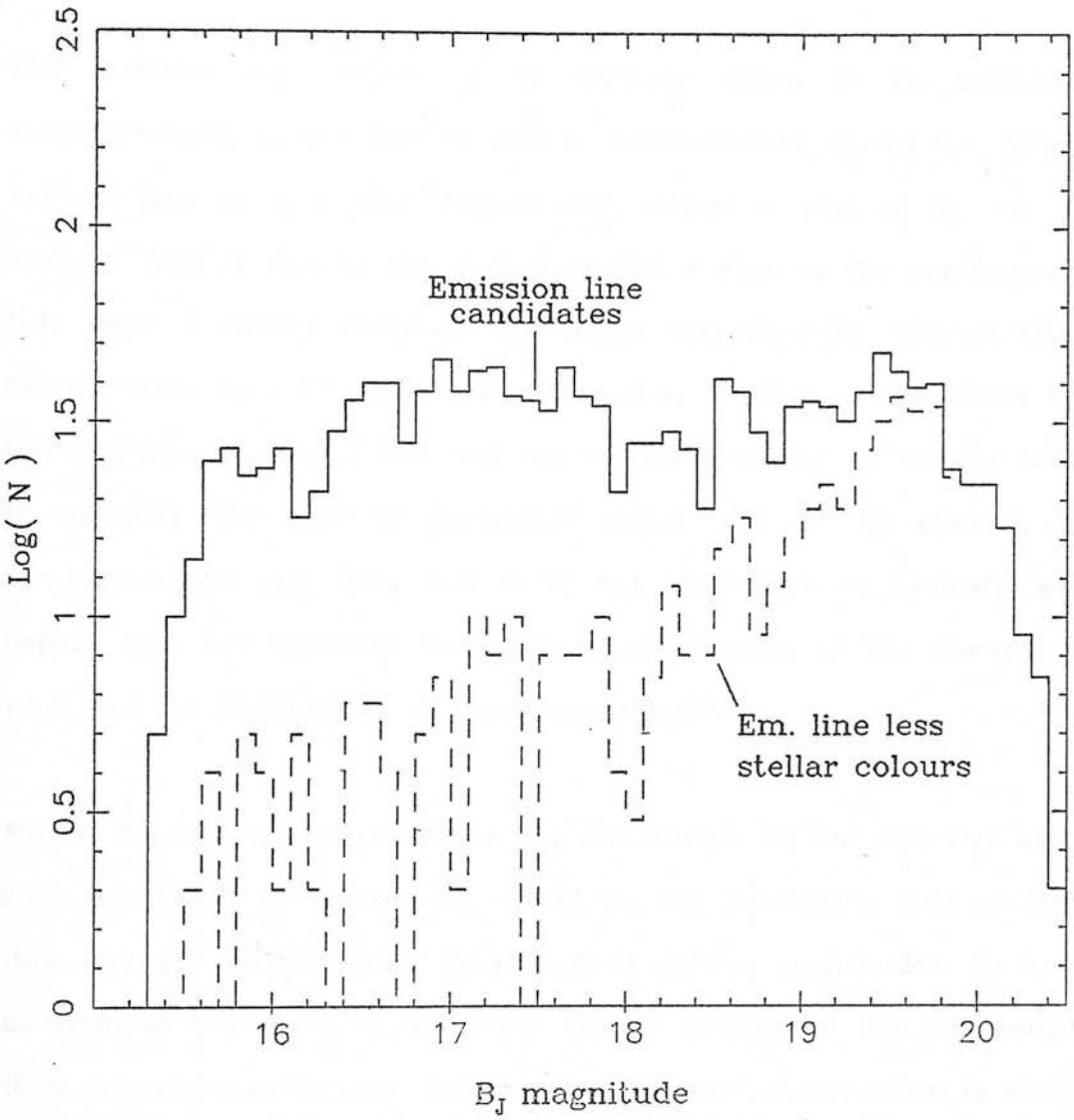

Fig 5.7 Log(number of candidates) as a function of magnitude for all AQD prism plate emission line candidates. The broken line are those objects remaining after the removal of objects which have stellar colours in the photometric survey.

the different redshift sensitivities of the survey methods. Never the less, Boyle is likely to be no more than 30% incomplete on the grounds of the redshift distribution in Hewitt and Burbidge, 1986.

The question also arises as to whether there is an increasing incompleteness, in the loss of weaker lined objects up to the nominal survey limit of $B_J \approx 19.8$. Figure 5.8 shows a plot of B_J vs. line energy (that is flux in the strongest line / flux in the continuum at this line) - clearly showing the effect described by Clowes (1981) fainter than $B_J = 17$. It is not clear what is to be done about this incompleteness: even if one had the values required by Clowes (1981) to quantify the area of parameter space lost to the survey, the candidates are <u>still</u> lost, and it is not clear how to identify what impact this will have on the ultimate conclusions of the survey (ie. what are the luminosities of the quasars lost?).

Figure 5.8 is a demonstration in the AQD sample of the selection effect first mentioned in section 1.3 - that is, the increasing loss of lower line strength emission line candidates at fainter magnitudes. In order to estimate how much of an effect this is having on the AQD sample, it is necessary to assume that the line strength distribution is similar at fainter magnitudes to the distribution at brighter magnitudes. It is then possible to make a least squares fit to the brighter line strength distribution, at a magnitude where one is confident that no candidates are being lost. This can then be scaled to what the distribution should be in the faint magnitude bin with the use of the stronger lined objects - the line strength distribution, deduced for bright objects, is fitted to the faint magnitude bin. This can be used to deduce how many objects are missed by integrating the fit to the

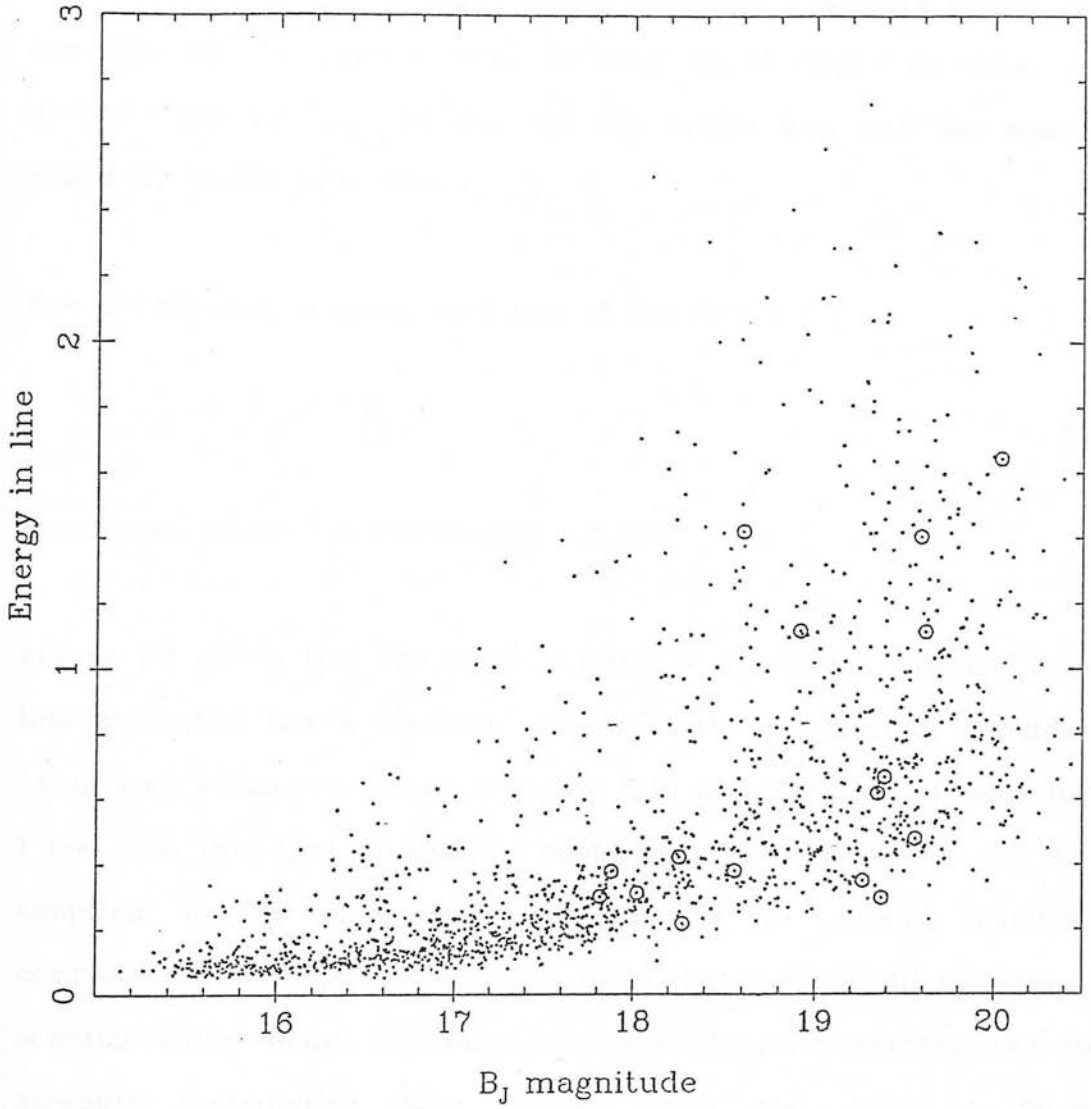

Fig 5.8 Energy in line as a function of magnitude for all objects detected by emission lines in the AQD prism survey. Objects circled are confirmed quasars in the field which were identified in the prism survey.

faint bin, and comparing with the number of objects actually found. A sensible lower line strength limit to the integration is the lowest line strength object found at any magnitude in the good sample. Figure 5.9 shows histograms from the bright bin, $16.4 < B_J < 17$ (solid lines) and one of the fainter bins (broken lines) $19.2 < B_J < 19.4$. Also included are the best fit line for the bright bin, and the same fit scaled up to the faint bin.

The distribution is steep, so a line of the form :

$$Y = \frac{a}{X^b}$$

was fitted, where a = 0.352 and b = 2.686.

Figure 5.9 shows that the large number of candidates selected at low line strengths has a dominant effect on the numbers of candidates being lost, which are shown in figure 5.10 as a function of magnitude. I feel that this type of analysis could easily be pushed too far. It is tempting to try and use these figures to give a candidate completeness estimate, but it is not clear that real, bright quasars are actually being found at lower line strengths, or whether the line strength distribution does actually stay the same at fainter magnitudes. Also, the large numbers of stars already shown to exist in the AQD sample are decreasing in number quite rapidly with increasing magnitude.

Attempts were also made to find an upper limit to the incompleteness by using the same procedure but with a linear fit to the stronger line strength candidates. This also was not successful, because a straight line is obviously the wrong parametric form to fit the line

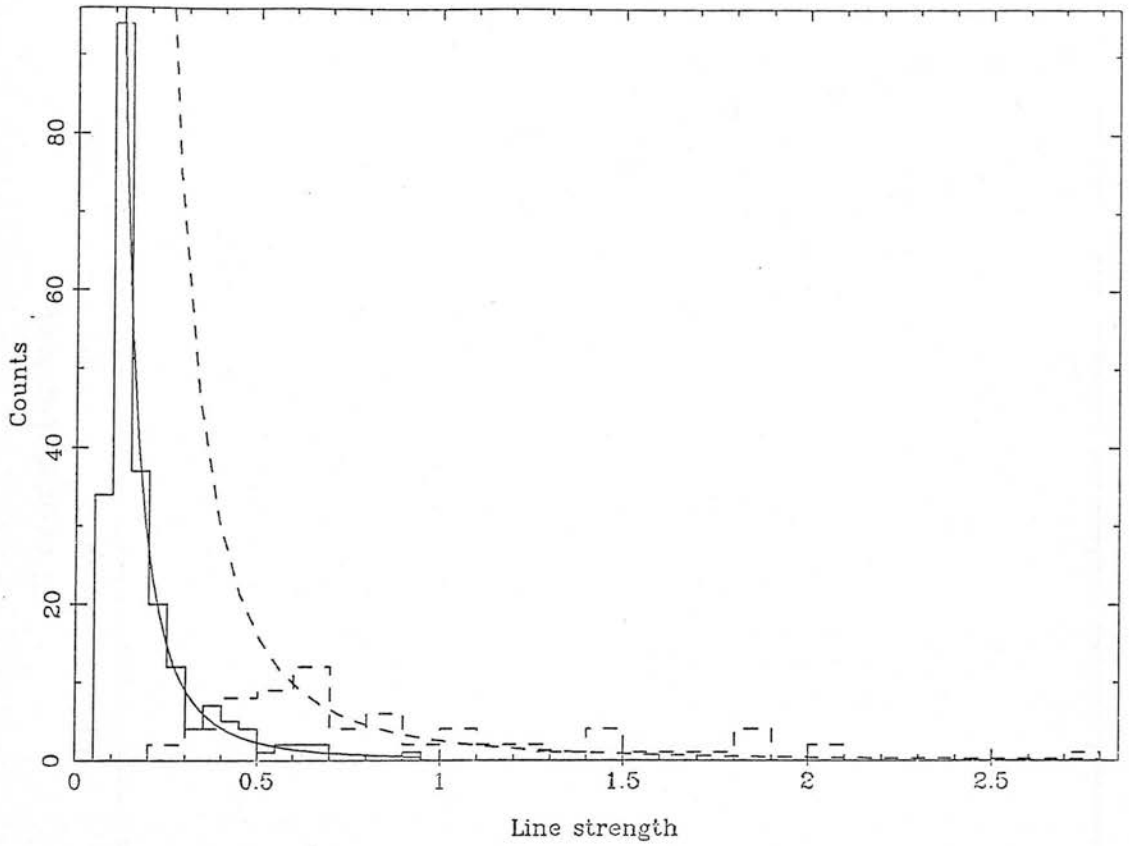

Fig 5.9 Solid histogram shows all emission line candidates with $16.4 < B_J < 17$. Broken histogram shows candidates which have $18.6 < B_J < 18.9$. Also included are the best fit line for the bright bin, and the same fit scaled up to give the least residual in the line strength region of $0.7 <$ l.s. < 2.1.

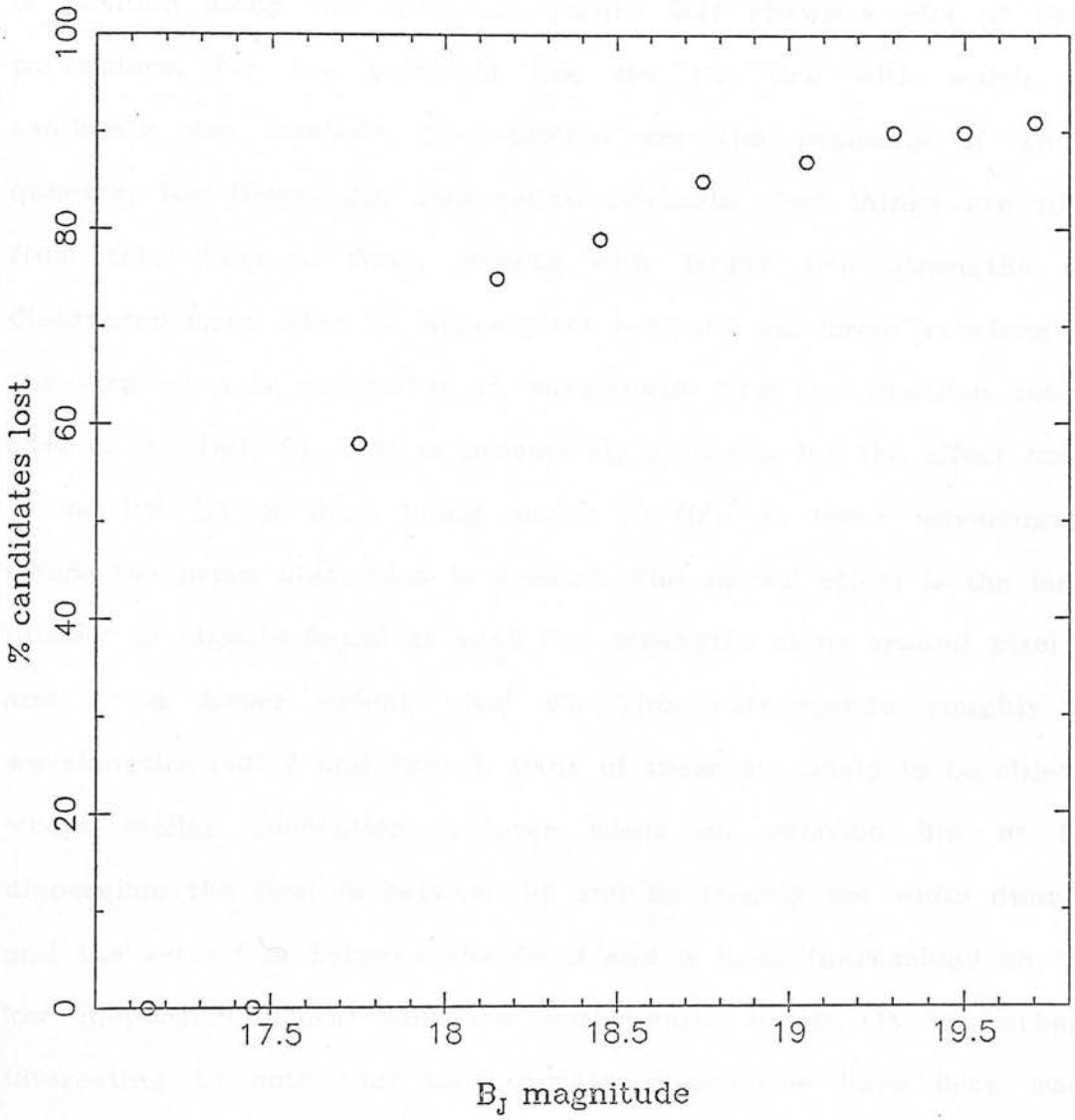

Fig 5.10 Percentage of candidates lost as a function of magnitude. Values were calculated using plots such as fig 5.9, and then integrating under the scaled up best fit line.

strength distribution.

It is also informative to look at emission line strength as a function of position along the spectrum. Figure 5.11 shows a plot of these parameters, for the principle line (ie. the line with which the candidate was located). Over-plotted are the positions of known quasars, for those with information available. Two things are plain from this diagram: first, objects with larger line strengths are discovered more often at larger pixel numbers (ie. lower wavelengths: the dispersion is decreasing in wavelength from the emulsion cutoff, 5380 Å, at pixel 20). This is presumably evidence for the effect noted in section 1.3 of lines being easier to find at lower wavelengths, where the prism dispersion is greater. The second effect is the large number of objects found at small line strengths at or around pixel 38 and to a lesser extent pixel 53. This corresponds roughly to wavelengths 4400 Å and 3890 Å. Many of these are likely to be objects where stellar absorption features mimic an emission line at low dispersion: the first is between Hβ and Hγ (mainly hot white dwarfs) and the second is between the Ca H and K lines (unresolved on the low dispersion prism) and the atmospheric cutoff. It is perhaps interesting to note that most quasar discoveries have been made within the larger of these groups.

Another possible method of obtaining an estimate of completeness relies on being able to independently locate a region of colour colour space which has no indigenous stellar population, ie. one is likely to find only quasars in this region, apart from objects with large photometric errors. This has been done, with limited success. Using the two colour plot shown in figure 4.12, over-plotted are average

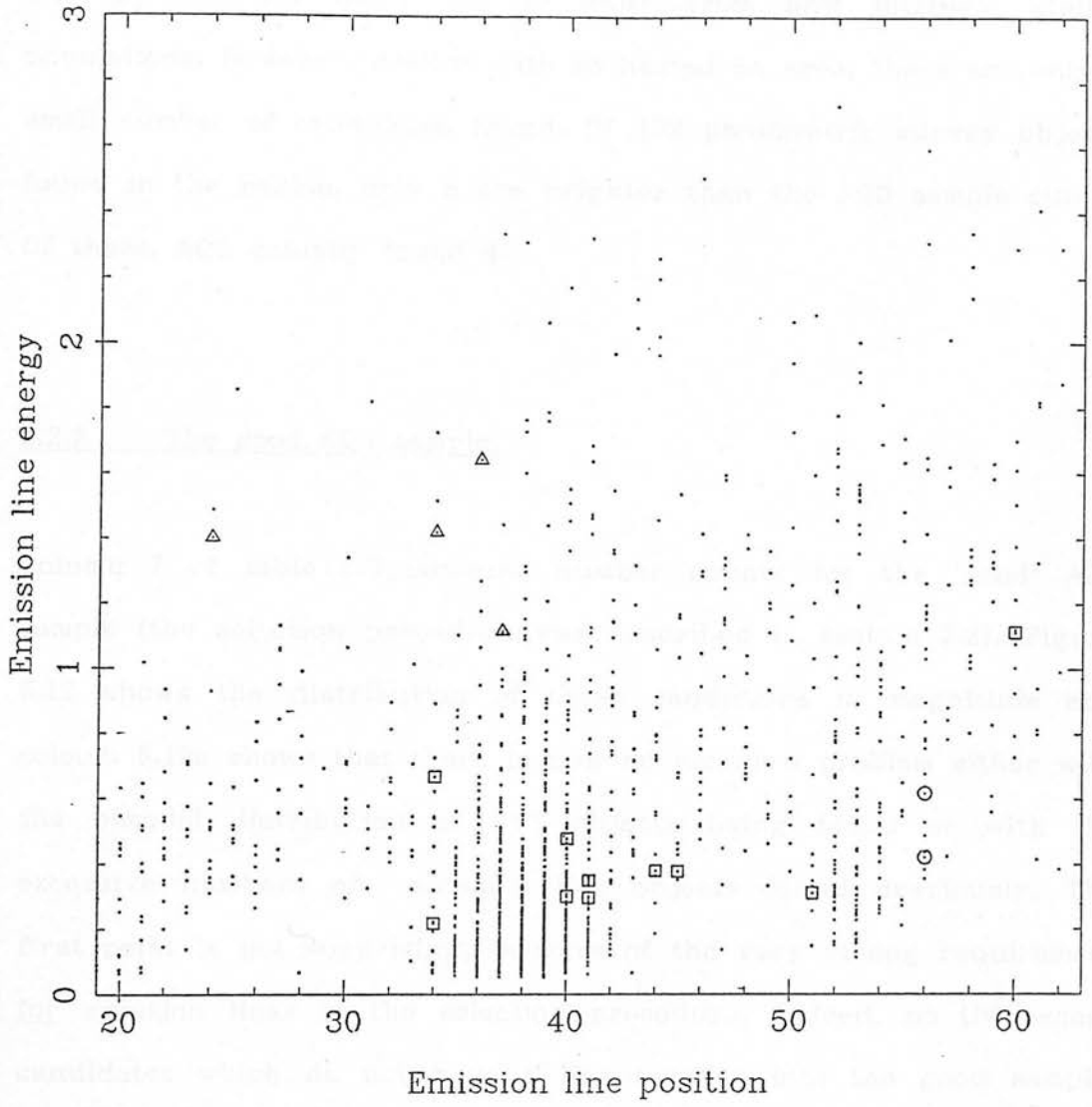

Fig 5.11 Emission line energy as a function of line position in pixels for all emission line candidates in the AQD prism survey. The emulsion cutoff is at pixel 10, and λ is decreasing towards higher pixel numbers. Symbols overplotted are confirmed quasars. Circles have $z < 1$, squares have $1 < z < 2$, and triangles have $z > 2$.

main sequence colours taken from Johnson (1966) and the locations of some of the white dwarfs and subdwarfs from Green, Schmidt and Liebert (1986). Thus an area can be chosen which has $U - B_J < -0.25$, and $B_J - V > 0.4$ which is far away from any intrinsic stellar populations. However, dealing with so limited an area, there are only a small number of candidates found. Of 132 photometric survey objects found in the region, only 8 are brighter than the AQD sample cutoff. Of these, AQD actually found 4.

5.2.2 The good AQD sample.

Column 7 of table 5.3 contains number counts for the 'good' AQD sample (the selection procedure was described in section 2.2). Figure 5.12 shows the distribution of these candidates in magnitude and colour. 5.12a shows that there is now no longer a problem either with the bimodal distribution of UVX objects being found or with the excessive numbers of emission line objects found previously. The first point is not surprising, because of the very strong requirement for emission lines in the selection procedure. Indeed, no UV excess candidates which do not have a line survive into the good sample. Thus, there is no UV excess column in table 5.3. The large number counts of bright objects are dealt with by the selection against stellar features. 5.12b shows the distribution in $U - B_J$ of all the good survey object which have this colour (182 out of 218).

Although the good survey can discover no new candidates (a serious problem, as discussed in section 5.2.1) it may be that nothing except junk has been eliminated, in going from the larger to the good

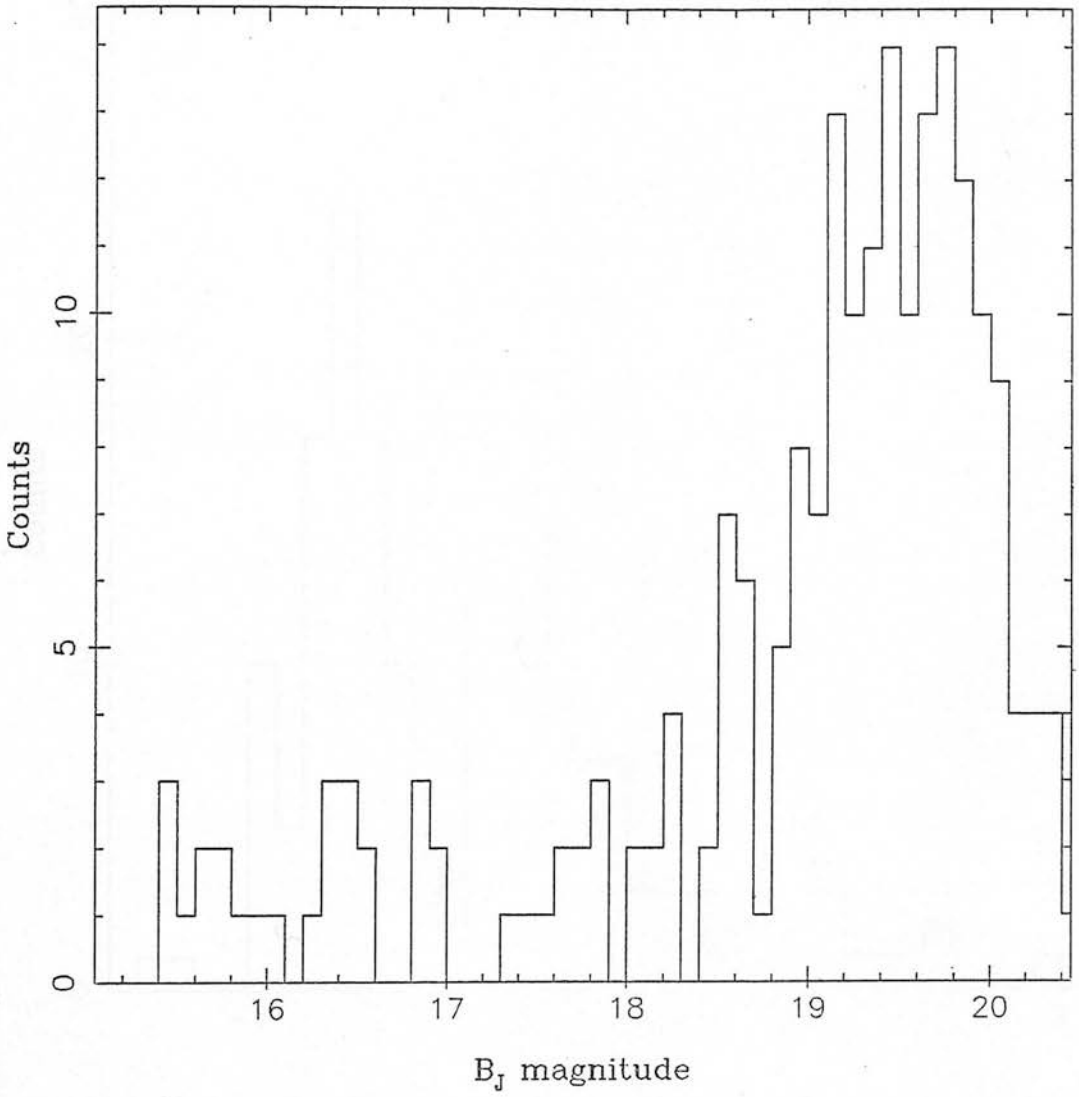

Fig 5.12a Histogram of the good AQD candidates, showing the number of candidats as a function of B_J magnitude.

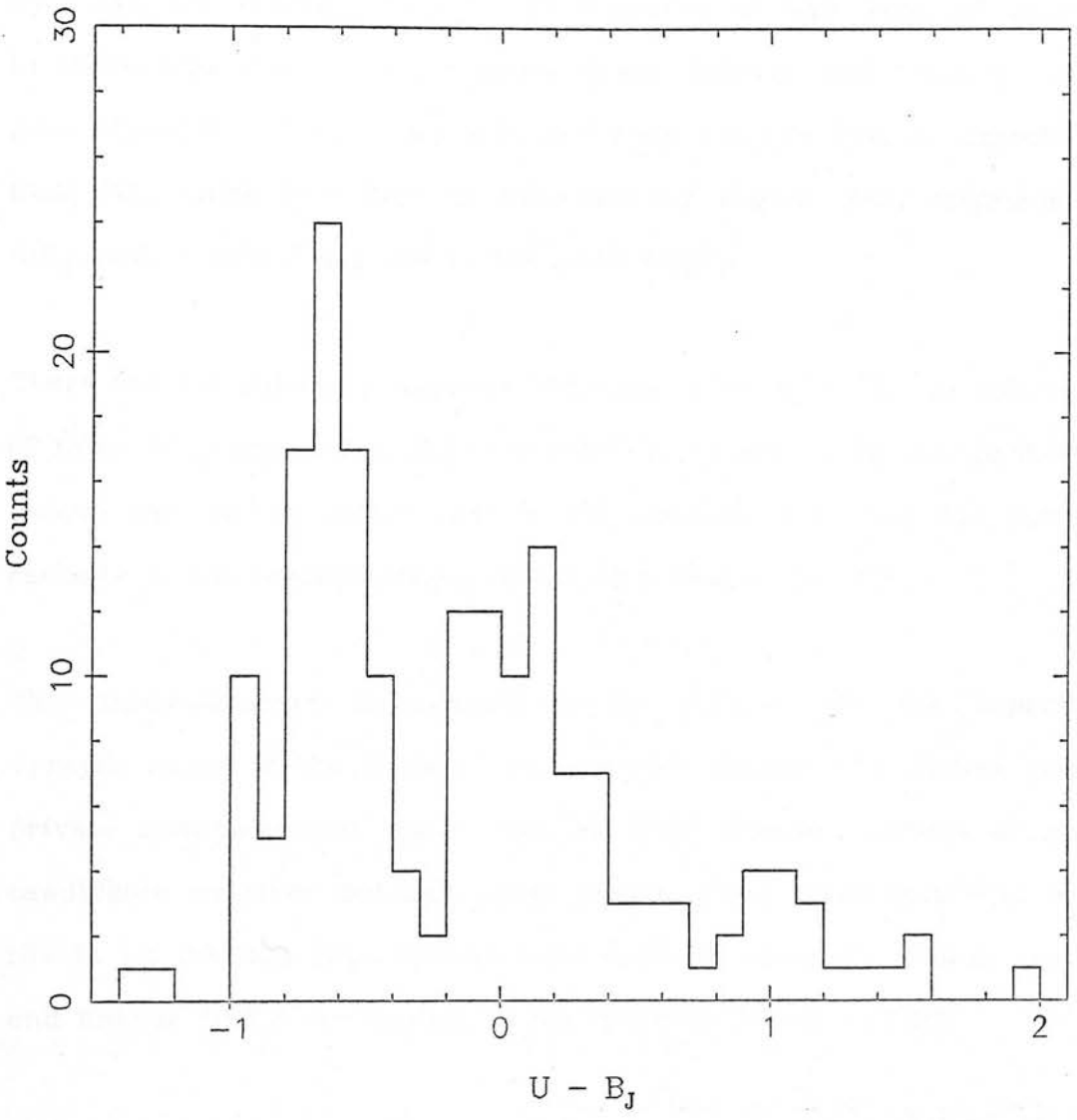

Fig 5.12b Histogram of the good AQD candidates, showing the number of candidates as a function of $U - B_J$ colour. Remember that there is a strong selection for emission line identification in the selection of the good objects.

sample. Thus it may be valuable in supplying a sample of very high probability candidates. This can be checked by looking at the survey completeness as defined by table 5.3. Magnitude bins brighter than $B_J = 16.5$ are ignored, because the numbers of AQD detected objects in these bins are still very large. Green Schmidt and Liebert (1986) give $N(B \leq 16.5) = 0.015$ / degree^2, and they actually find no objects in field 927, which is a part of their survey region. This compares to $N(B_J \leq 16.5) = 0.76$ / degree^2 in the good sample.

There are 4.3 objects / degree^2 between $17.0 < B_J < 19.5$ in column 7 of table 5.3, compared to 7.8 / degree^2 in column 8. So the good AQD sample can be no better than $\approx$ 50% complete (allowing for Boyles' estimate of the incompleteness of his own sample, ie. 10%).

This incompleteness is unlikely to be effected by the improved dynamic range of the COSMOS machine (see section 4.5). Clowes (1987, private communication) states that he finds similar numbers of good candidates on other Schmidt prism plates, which were measured with the 14 bit COSMOS data. Indeed total numbers given by Clowes, Iovino and Shaver (1987) are typical of the numbers found in F927.

The completeness estimate derived above has a major drawback: the comparison with Boyle's survey is inadequate. Boyle's survey is an average of many widely separated fields, and being a UV excess survey, it is limited to redshifts of $z < 2.2$. In addition, the completeness estimate ignores other parameters which are available for each slitless spectrum. Thus, the information advantage of having a low dispersion spectrum for each object is negated. So it would be preferable if one was able to make an estimate of completeness for the

AQD survey using other information in the field. Various approaches are possible.

Using the polygons obtained for the stellar locus definition in section 4.8 of the photometric survey, it is possible to locate all objects in the AQD sample which have genuinely stellar colours. This has been done, for the 'good' AQD sample. From a total of 218 objects which were located in the survey (other objects were ejected from the photometric survey on morphological grounds), some 21.1%, or 46 objects were found to lie irretrievably in the stellar locus of the photometric survey. Visual inspection of these objects on the prism plate led to the conclusion that 8.3%, or 18 objects have the spectrum of a G star (reference was made to Savage *et al.*, 1985, for all prism plate classification). 5.0% are remaining junk images (mainly overlaps badly classified by the software) and 7.8% are good quasar candidates. Figure 5.13 shows these good images superposed on a two colour diagram - they all lie at the blue end of the stellar distribution. These numbers are interesting because they confirm the statement of Clowes, Iovino and Shaver (1987) that $\approx$ 80% of the 'good' sample actually <u>are</u> quasars. Other objects in the survey are very much more likely to be genuine emission line locations (ie. basically quasars), because they have peculiar colours. They <u>cannot</u> be galactic stars (unless they are also at the $> 3\sigma$ end of the photometric errors), and they are very unlikely to be junk because overlapping does not effect the photometric survey to the same extent. Thus the only remaining potential source of additional rubbish after the exclusion of these 28 objects (the junk and G stars inside the stellar locus), are hot white dwarfs that have been mistaken for quasars.

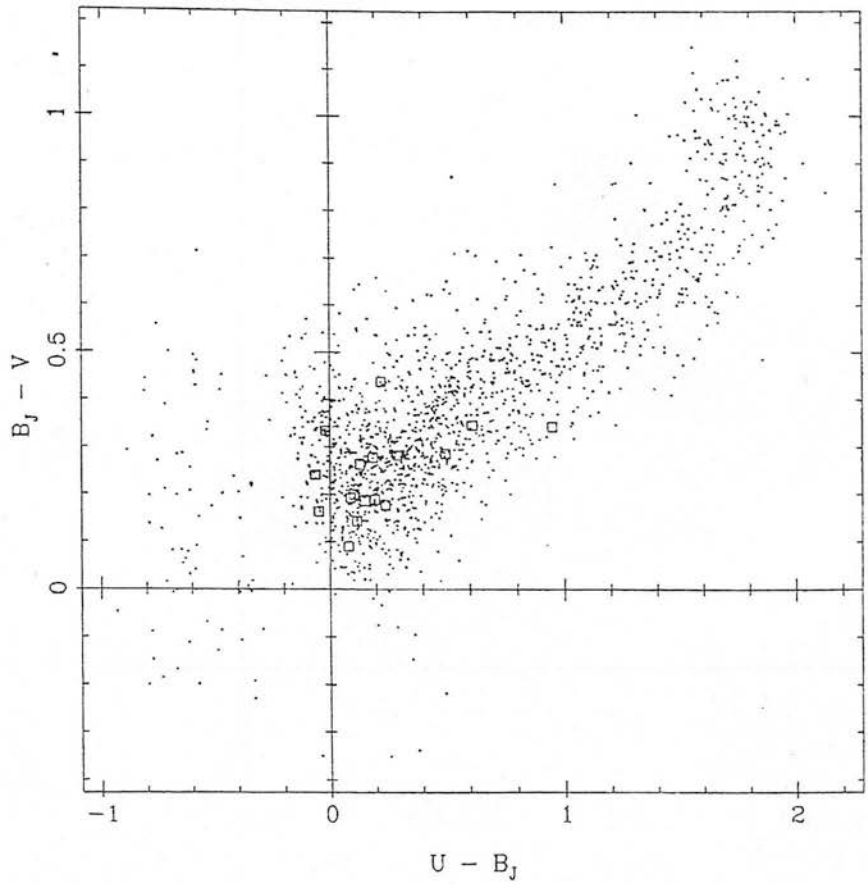

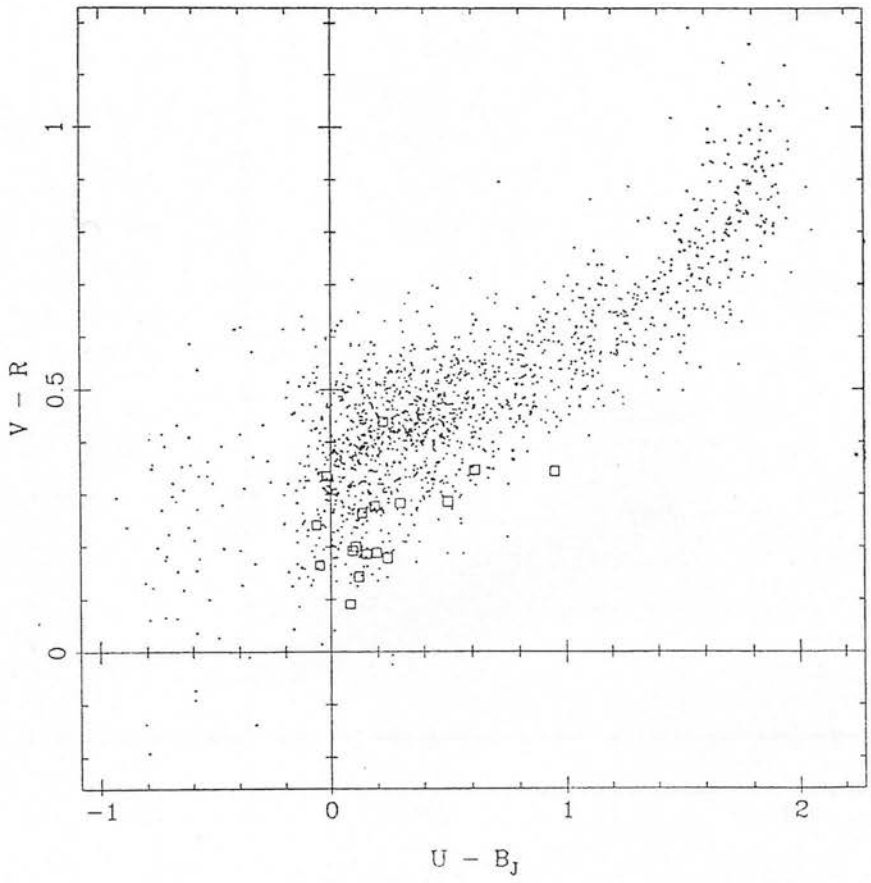

Fig 5.13 Two colour plots showing one in every ten of all objects in the photometric survey. The boxes plotted over are AQD survey objects which were identified as lying inside

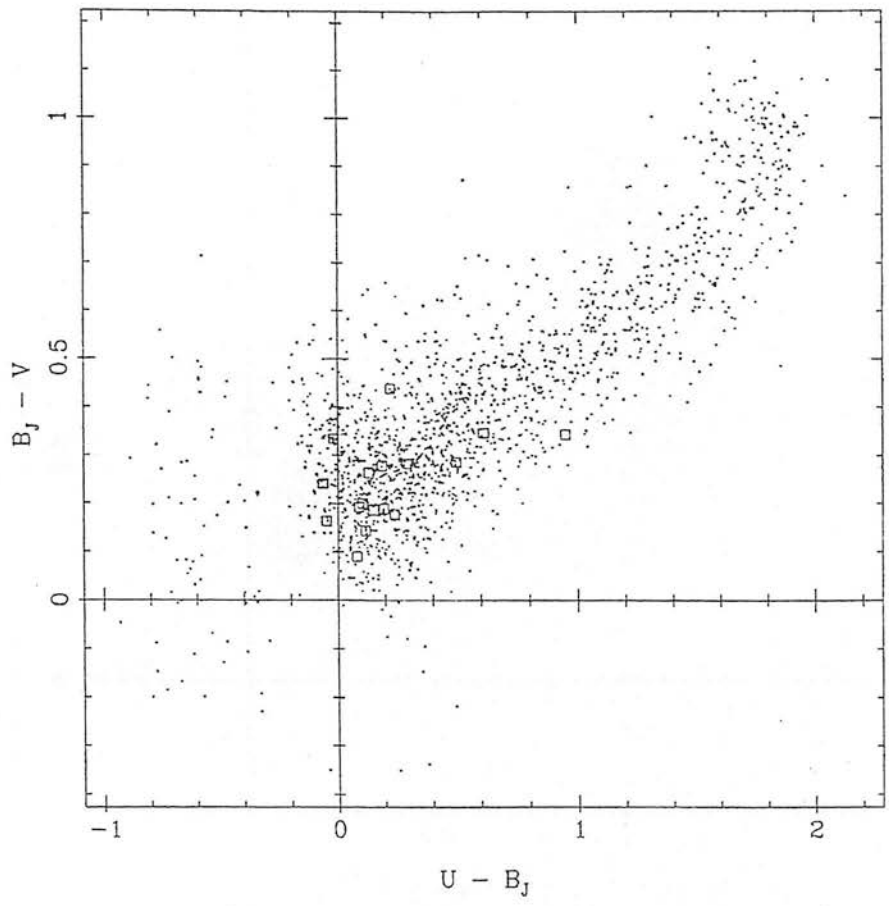

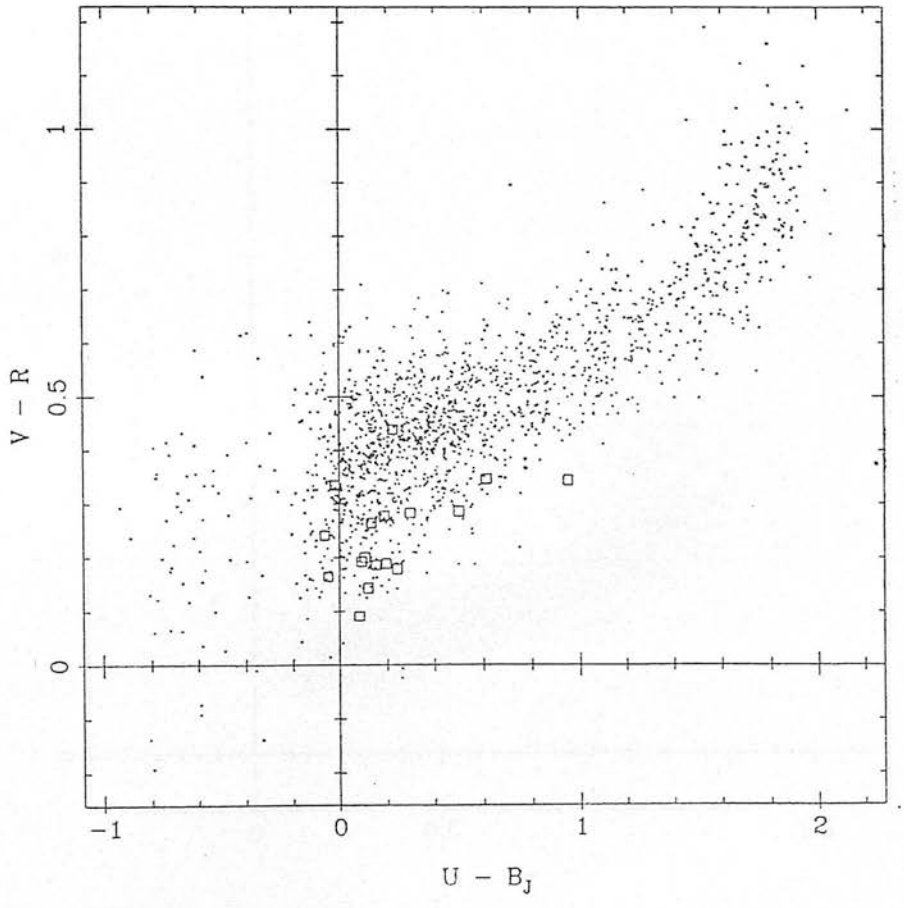

Fig 5.13 Two colour plots showing one in every ten of all objects in the photometric survey. The boxes plotted over are AQD survey objects which were identified as lying inside

Thus the remaining 189 AQD 'good' candidates have a very high probability of being quasars: ≈ 95%. They are not a representative sample, though, as the redshift sensitivity banding caused by the prism itself (shown in figure 5.11), as well as the candidate improvement procedure, still cannot be eliminated (described in sections 1.3 and 2.2). The only remaining contaminants in this group are as yet unidentified overlaps, amongst those objects not visually inspected, but presumably occurring at the same rate, and peculiar stellar types which can mimic an emission line at low dispersion, but have not so far been identified (as well as other genuinely extragalactic emission line objects which may appear stellar). Thus the percentage of overlaps in this group is 3.8%, the percentage of other objects remains unknown, but probably small.

5.3 A grens / photometric survey comparison.

One of the main difficulties that exists in attempting to compare the photometric and the grens survey is that without spectroscopy, comparison must be a statistical process. But the grens plate does not cover enough area for there to be very many objects on which to work. Out of 75 candidates in the grens survey, only 62 are bright enough to have a photometric survey counterpart of any sort. Only 7 have all five magnitudes, 17 have all except the I magnitude, and 23 have both a U and a B_J. Fortunately, the slit spectroscopy already obtained at ESO and described in chapter 3 has enabled fairly firm conclusions to be drawn.

This section is an attempt to use what information that there is in common between the surveys, in order if possible to check the conclusions drawn in chapter 3.

To this end, objects in the grens area of the UV excess and multicolour surveys were located, and visually inspected on the grens plate. Tables 5.6a and 5.6b give details of these inspections Fourteen of the UV excess candidates are also grens candidates, but the eye finds 3 emission line objects which are not found by AQD.

Tables 5.6a UV excess and 5.6b Multicolour candidates on the grens plate.

5.6a	Class	Number
	Featureless	10
	Overlaps	2
	Emission	11

5.6b	Class	Number
	Saturated	11
	Featureless	16
	Overlaps	2
	Emission	1

Two of the multi-colour objects are found in the grens survey - the two emission line objects in table 5.6b.

The conclusions from these numbers can only be very weak. It is hard to pick up spectral features by eye on grens plate spectra, because the dispersion is so low and it is easier to look at the broader wavelength range of the prism.

5.4 Multi-colour candidates.

The most interesting part of multi-colour space (in that it has so far remained largely unexplored) has so far been neglected. The selection of objects which are both positive in $U - B_J$, and also lying far from the stellar locus has been discussed in section 4.8.2. In this section these objects are considered in greater detail - with particular reference to their relationship to other surveys.

To recap, briefly, objects were first selected which are not a part of the UV excess survey, and which lie outside the stellar locus. A nearest neighbour search then identified a list of the 100 rarest objects, in that they lie the furthest from the stellar locus. This has the disadvantage that all magnitudes are required for the analysis. So a considerable amount of information is lost, particularly because the I magnitude limit is comparatively bright. Nevertheless, these objects do lie in unusual parts of multi-colour space, and so are of interest.

As a first step, they have been identified on the various plates available. Table 5.7 summarizes this visual inspection.

There follows an explanation of the classes in table 5.7, and their significance.

The 'too faint' class objects were too faint to identify or classify on prism plates UJ5846P and UJ5839P. There are relatively few of these, because of the I limit problem. None of these are blended (the next class), and so (photometric errors not withstanding) they represent a

Table 5.7: Inspection of rare U,B_J,V,R,I objects.

Class	No.	%	Number variable
Too faint	12	-	1
Blended	20	-	5
Stars	28	41.2	11
Overlaps	3	4.4	0
Emission line	20	29.4	5
Red	17	25.0	2

set of interesting objects.

The 'blended' class are objects which appear blended on the direct plates. COSMOS has a comparatively poor spatial resolution, because of the thresholded nature of the data. This defines the resolution limit. This has been alleviated somewhat with the introduction of deblending software (see section 4.7.5 for a description), but these are objects which have not been identified by the deblending process. They are very close together, and only just resolvable by eye.

The 'stars' class are likely to be galactic stars, from their appearance on the prism plate. This class includes all 9 objects in the candidate list which have $B_J < 15$. These bright objects are likely to be calibrated badly: on deeper plates the diffraction spikes are beginning to become visible for these objects. They have been calibrated badly, and so have peculiar colours. The remaining 19 objects in this class may either be genuinely variable stars or (more likely) they are objects with large photometric errors. Both of these ideas can be tested by returning to the originally calibrated magnitudes on each plate. Variables and large photometric errors

should show up as having a large scatter.

The 'overlaps' class are objects which have overlapped spectra on the prism plate, and so low dispersion spectral information is not available for them. As with other classes, these objects were identified after the removal of blended objects. Only one object is overlapped on both of the prism plates - the other 2 are too faint for classification on UJ5839P, the poorer of the two plates.

The 'emission line' class is self explanatory, as is the 'red' spectra class. These two still represent groups of interesting objects.

The column entitled 'numbers variable' in table 5.7 was generated by locating those objects in the list which have one or more plate magnitudes which varies by more than 3 x σ from the mean for that object in that band. σ's were calculated for all bands and magnitudes using binned plate data for all objects in a narrow magnitude range. As expected, objects which look like stars on the prism plates are more frequently found to be photometric errors than other types of objects.

Using this information, it is possible to draw up a list of best candidates from the photometric survey. These are objects with the following properties: Blends are excluded altogether. Objects which are too faint, overlapped or red are included unless they are very variable on one or more plate. Stars are included unless they are very variable or are brighter than $B_J = 15$, and emission line objects are included whether or not they are variable. This is because quasars can be intrinsically variable, and the fact that they show an

emission line on the prism plate is of course in their favour. This produces a total of 58 good candidates. Pairing this set of 100 rare objects with the full AQD catalogue yields only 4 objects in common. None of these survive the selection procedure to remain in the good multi-colour list. One is fainter than the prism survey cutoff (but was excluded anyway on grounds of variability) the second is a blend on the direct plate. The third is overlapped on the AQD prism plate, and the final object was excluded on grounds of variability.

6. Conclusion.

The ultimate goal of this thesis was to obtain a quasar survey free from selection effects. The construction of this survey is left to section 6.1, and its discussion is found in section 6.2. The first part of this chapter reviews interesting points that have been raised through the comparison of surveys in a single field. Finally, I will give what I believe to be the main recommendations for future work based on the findings of this thesis, in section 6.3.

The eyeball prism search was done by one of the most experienced prism plate workers in the world. It is therefore of the highest possible quality, for such a survey. As seen in section 5.1, though, by examination of the prism candidates actual magnitudes and colours in the photometric survey it has become apparent that the eye is not good at making quantitative estimates of spectral colours. At bright magnitudes, even where spectra are unsaturated, too many spectra are identified as having an UV excess for a reasonable programme of follow up slit spectroscopy. At the same time, at fainter magnitudes the eye misses large numbers of very blue objects. As regards emission line location, the eye is clearly quite reliable at looking for objects brighter than about B_J = 18.5, but once again spectra with poorer signal to noise often go unnoticed. In addition, the eyeball emission line detection suffers from the same redshift dependent selection effects as the automatic prism survey - they are intrinsic to the survey instrument, rather than the search technique.

Thus if other search methods are possible, it does not seem

reasonable to use the eyeball prism plate colour search method for any purpose at all. In the only magnitude regime where the method is likely to be complete, the eye identifies a large number of very blue objects which are not actually blue. Since one already has a significant job identifying actual quasars from galactic stellar types which have an UV excess, adding more is a simple waste of slit spectroscopy.

The automatic prism plate survey was compared in detail to the photometric survey in section 5.2. As was seen there, problems in the selection of objects by colour are similar to those encountered in the eyeball search. AQD also locates a fairly large number of brighter stars, because of the saturation of the red end of the spectrum. Evidently the eye is capable of identifying these, because they are not seen in large numbers in the He survey. In addition, though, a large proportion of the fainter colour candidates in the AQD survey actually have stellar colours. This is simply because of poor signal to noise in the fainter spectra ($B_J > 18.5$). In summary, the colour selection works well amongst unsaturated spectra of good signal to noise ($17 < B_J < 18.5$).

The emission line selection procedure has not overcome the redshift sensitivity variations caused by the use of a non-linear dispersion element (the prism), coupled with the confusion of certain stellar types appearing to have emission lines at low dispersion and varying intrinsic line strengths. In addition there are a substantial number of objects on the plate which appear to have an emission line to the eye but which are not selected as AQD candidates, and also remaining overlaps which are spuriously included in the sample. Once again,

most of these problems are largely caused by poor signal to noise, and so disappear amongst brighter objects. In particular, it is clear that the faint objects lost due to poor signal to noise are not lost at random.

Amongst objects with a reasonably good signal to noise it should be possible to identify the stars which emulate emission lines with the use of cross correlation with the slit spectrum of a known star of the appropriate type, after it has been rebinned to the prism dispersion and convolved with the emulsion and atmospheric sensitivity profiles. In the context of this survey, colour information from the direct plates can be used to eliminate these stars (see section 6.1).

Clearly, the method developed by Clowes (described in section 2.2 and by Clowes, Iovino and Shaver, 1987) to select high probability candidates from the AQD survey cannot overcome the inherent problems of looking for candidates amongst spectra of low signal to noise. The objects have already been lost from the survey, and the high probability procedure finds no new objects.

Thus a programme to generate a complete quasar sample using prism plate material should above all not seek a survey limit where the spectral signal to noise is poor, even though some quasars are readily identifiable at fainter magnitudes. Objects then identified using a colour criterion and a line criterion (in order to eliminate the UV excess galactic stars) or better by the line criterion and cross correlation with the contaminating galactic stars would be both largely complete and relatively free from contaminating objects. Sources of incompleteness would then be overlaps, which could be dealt with

using two cross dispersed plates, and the very occasional bright quasars. The disadvantage of the former method (colour and line) is that it is redshift limited to $z < 2.2$ because of the reliance on colour selection. It's advantage, on the other hand, is that no additional slit spectroscopy is required until the follow up redshift identification.

It was not possible to examine the grens survey of chapter 3 in the same way as the AQD survey - there is not enough in common either in magnitude or in spatial extent to draw conclusions regarding the grens on the basis of the colours objects have in the photometric survey. Fortunately there was an independent source from which conclusions could be drawn. Slit spectroscopic confirmation and follow up of about 1/3 of the candidates allows one to make conclusions regarding the whole survey, and thus the surveying instrument. The conclusions of chapter 3 was that the survey is complete for $18 < B_J < 21$ and $z < 3.3$. It is possible to make this statement because there is no redshift sensitivity function caused by a non-linear dispersion element, and so narrow lines discovered at any point between $3800A < \lambda < 5380Å$. The survey should incorporate a method for eliminating stars whose spectra can emulate emission lines at low dispersion, and also cross dispersed plates are more important for the grens than for the prism because despite the larger plate scale, the large quantity of scattered light from the grens causes significant portions of the plate to be obscured. It is not clear how much effect the reduced signal to noise of spectra at $B_J = 21$ has on the survey - just as with the prism plates there may be spectra lost due to this. But whatever effect it has, it is not convolved with redshift as on the prism. In addition, the identification of narrow line objects at $B_J = 20.8$ (see chapter 3) is encouraging. Thus it is

reasonable to suppose that one can go fully 1.5 magnitudes fainter using the grens than possible with the prism, and still remain complete for objects with $z < 3.3$.

The final survey to be considered here is the photometric survey itself. This was discussed at some length in section 5.4, as well as being the subject of chapter 4. The only source of additional information which can be brought to bear on the survey is what the candidates look like on the prism plates (if they are bright enough to be seen at all on the prism plates) and how the individual plate measurements behave, compared to typical errors at that magnitude. The qualities of the survey divide quite neatly into a set of positives and negatives, which are all that are discussed here.

On the positive side, firstly the survey goes some 1.5 magnitudes fainter than the prism. Secondly, overlaps are not a problem as they are on the prism plates. As seen in chapter 5, numbers of candidates lost due to overlapping are not insignificant, and though they do not constitute a selection effect because objects are lost at random they are a source of incompleteness. Thirdly the selection effects are nothing like as complex as the redshift sensitivity banding seen on the prism. Fourthly, good quality direct plates are much easier to obtain than good quality prism plates. This is because the quality of prism plates is much more sensitive to seeing, whereas poorer seeing generally only reduces the plate limit of a direct plate. Finally, the data obtained from direct plates is much easier to handle - it is not as bulky - as the data from prism plates. In a situation in which computer resources are not abundant, this can unfortunately be of considerable importance.

On the other, negative side of the photometric survey are the following points. Firstly, many high quality plates are required in each band. Although this is offset somewhat by the fact noted above that they are easier than prism plates to obtain, it can still be a trying and arduous task. Secondly, the survey is hampered by the relatively poor quality of the I band. The IVn emulsion used for this band is difficult to hypersensitize, and as a result the plate limit is typically 1.5 magnitudes brighter than the neighbouring R band. In addition, the background is typically not smooth, and the hypersensitizer used can leave scars in the emulsion if not carefully applied. Finally, star/galaxy separation on morphological grounds breaks down at fainter magnitudes (see section 4.7.4). Amongst other things, this means that the survey cannot also be used for galactic astronomy, for example in scale height measurements of different stellar types.

As was noticed, in chapter 5, the area of greatest overlap between candidates selected by AQD and those selected by the photometric survey is amongst the UV excess objects, but even here it is poor. Some of the reasons for this are clear: others less so. If the multicolour method is actually to overcome the redshift $z < 2.2$ problem of previous colour surveys then it should be finding objects in the $2.2 < z < 3.4$ range which are also found by AQD emission line detection.

One obvious problem is the signal to noise problem seen in chapter 5. Most of the peculiar colour objects are either very faint or unidentified on the prism plate. Meanwhile AQD identifies large numbers of galactic stars because of poor signal to noise in their

spectra. Whether or not this is ultimately the explanation must await further work, in particular a slit spectroscopy programme designed to probe different regions of unusual colour space.

6.1 Construction of the final survey.

From what has been learnt in chapter 5, is should be possible to combine surveys of different types in such a way as to generate the best possible final survey. In particular, the redshift regime of $z > 2.2$ must be covered, since it is at these redshifts that the UV excess surveys become inadequate. It had been hoped to examine colour space in order to learn enough to select candidates directly from the photometric survey. This has not been done, at the present, because slit spectroscopy is required to discriminate between quasars and other exotic objects.

The first part of the sample is drawn from the 'larger' AQD survey, in order to locate higher redshift objects, because as has been shown, the 'good' AQD survey introduces new selection effects. Also, as has been discussed in chapter 5, there is little point in attempting to push the prism survey to the magnitude suggested by the plate cutoff, because signal to noise difficulties in the spectrum give progressive and substantial losses of candidates with increasing magnitudes.

The AQD emission line candidates were therefore limited to $17 < B_J < 19$. The bright limit of $B_J = 17$ is useful since there are

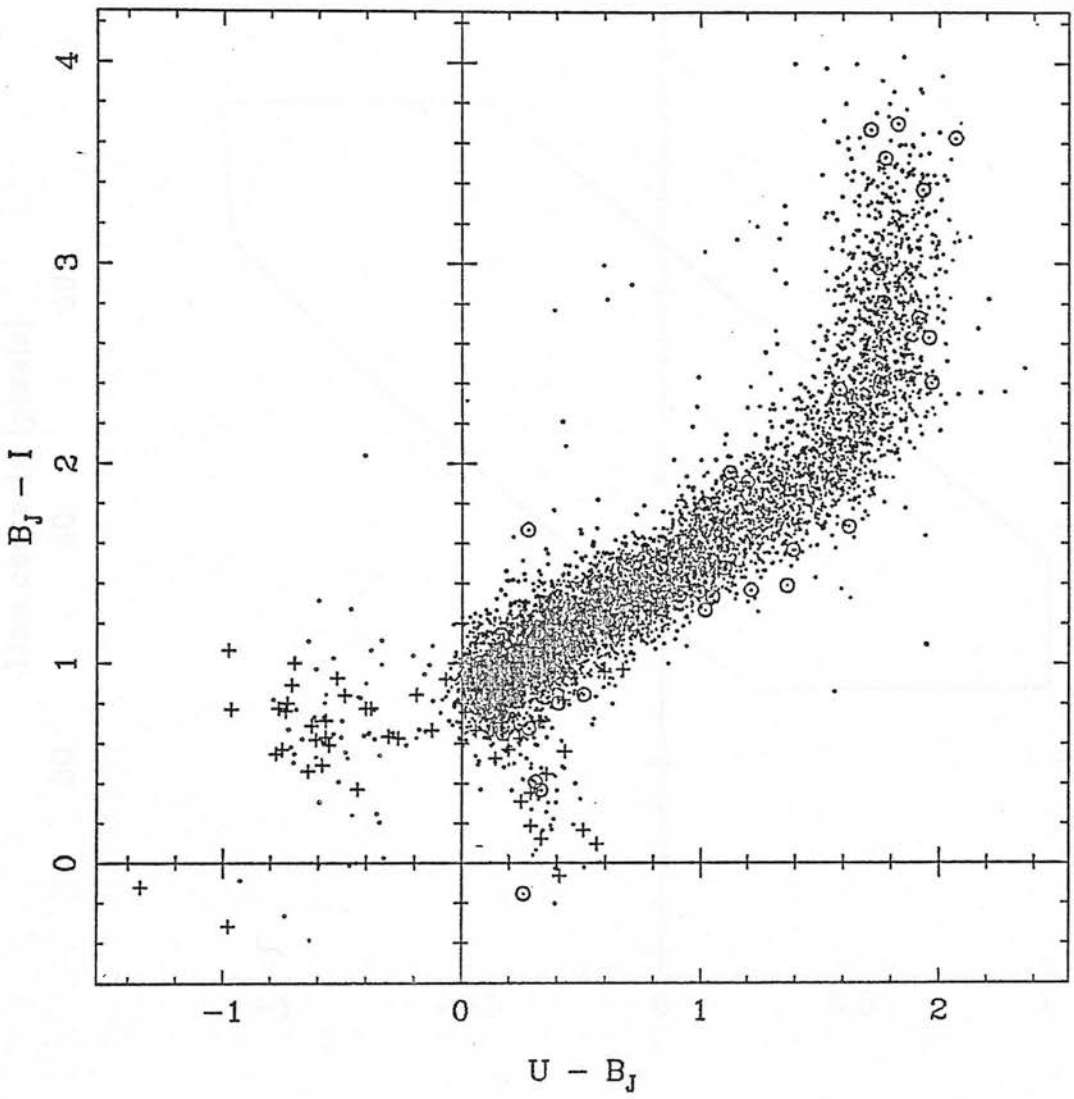

Fig 6.1 $U - B_J$ versus $B_J - I$ for all stellar objects which have $17 < B_J < 19$. Overplotted are objects which appear to have emission lines under visual inspection (plus signs) and those rejected (circles).

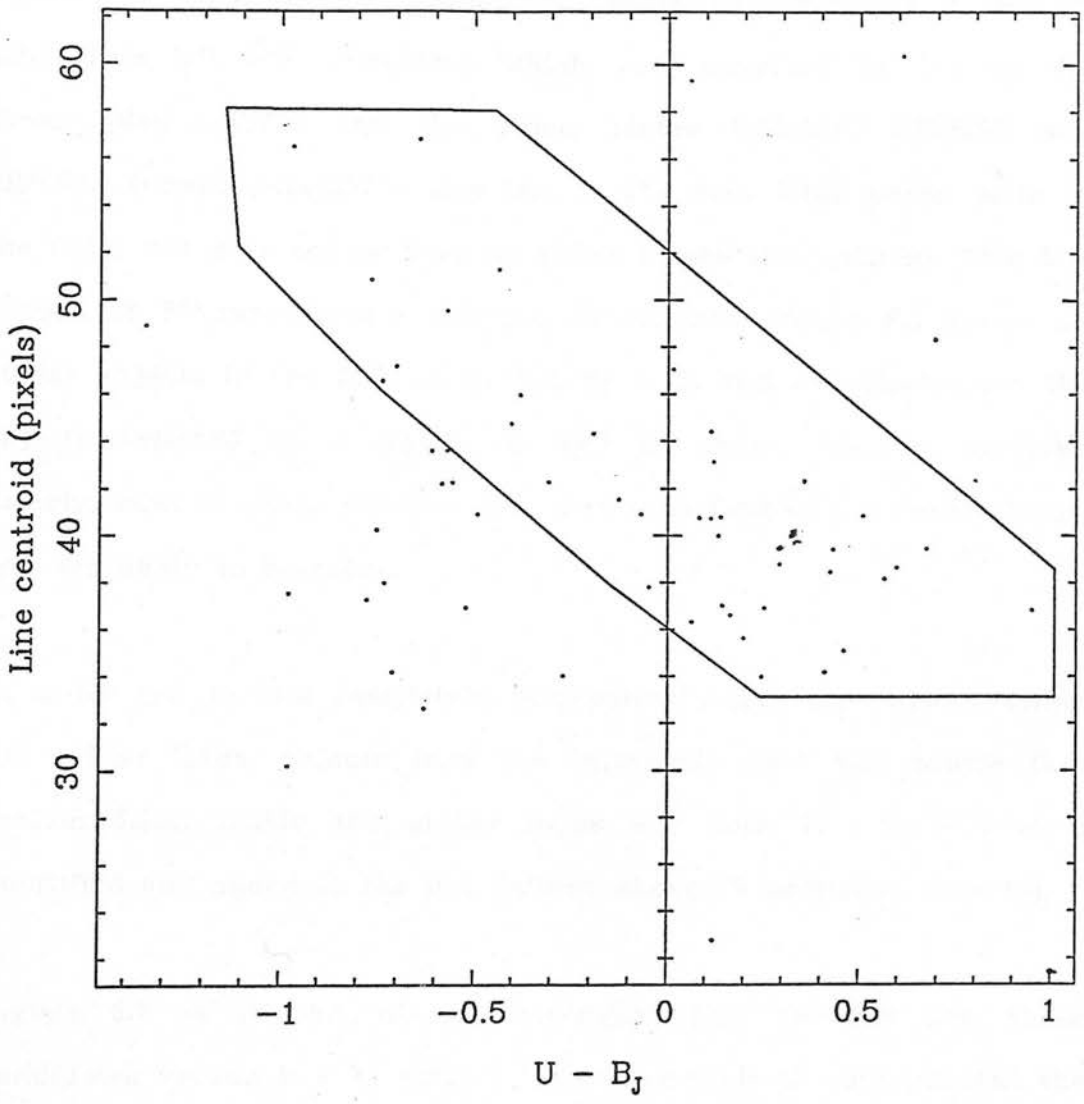

Fig 6.2 Line centroid as a function of $U - B_J$ colour. The significance of the polygon is elucidated in the text.

likely to be very few quasars lost, but large numbers of white dwarfs and other stars with peculiar colours will be rejected. Next, objects inside the stellar locus were removed, in order to eliminate the vast number of stars that dominate this sample, as discussed in section 5.2.1. This left 105 candidates, which were examined by eye on the direct plate J10715 and the prism plates UJ5846P, UJ5839P and VR7563Q (where possible - this last is the best IIIaF prism plate in the field, but it is not as deep as either of the IIIaJ plates). This left a total of 55 candidates satisfying all criteria. Figure 6.1 shows all stellar objects in the field with $17 < B_J < 19$, and overplotted are the objects selected (plus signs) as well as those rejected (circles). Clearly, most of those rejected are on the surface of the stellar locus, and are likely to be stars.

In order not to lose completely information regarding objects within the stellar locus, objects from the improved, good AQD sample (see section 5.2.2) inside the stellar locus and with $17 < B_J < 19$ were identified and added to the list defined above (5 additional objects).

Figure 6.2 is a plot of the strongest line centroid for these candidates versus $U - B_J$ colour. It is reasonable to suppose that the progression of objects contained within the polygon are objects whose Lyman-α has been identified. If this is done, then a quasar with a redshift of 2.3 has a $U - B_J \approx -0.25$. The identification of these lines allows redshifts to be estimated for the objects within the polygon.

Next, objects from the UV excess catalogue of section 4.8.1, which have $17 < B_J < 19$ were chosen (101 candidates). These were paired with objects which had already been selected above (27 objects had

already been located) and the remainder were inspected on the direct and prism plates. In addition, direct plate magnitudes were examined for evidence of 'variability', either genuine of caused by measurement error. Only 4 objects could be rejected on a synthesis of these criteria - once again, the most conservative choice must be taken at each stage, to retain completeness.

The UV excess candidates were added to the emission line objects already found, to give a final sample of 130 candidates. Details of these objects, including redshifts where they could be measured, are given in the appendix. In addition, figures 6.3 and 6.4 show the survey distribution with magnitude and colour. Table 6.1 gives number counts for the survey.

Table 6.1: Number counts for the final survey.

Magnitude	Number	No./deg^2
17 - 17.5	3	0.13
17.5 - 18	23	0.98
18 - 18.5	35	1.48
18.5 - 19	69	2.93

6.2 Examination of the final survey.

The survey should be complete for all redshifts $z < 3.4$, where Lyman-α drops off the edge of the IIIaJ / prism wavelength band. Having said that, some 16% of objects with $2.2 < z < 3.4$ will be lost at

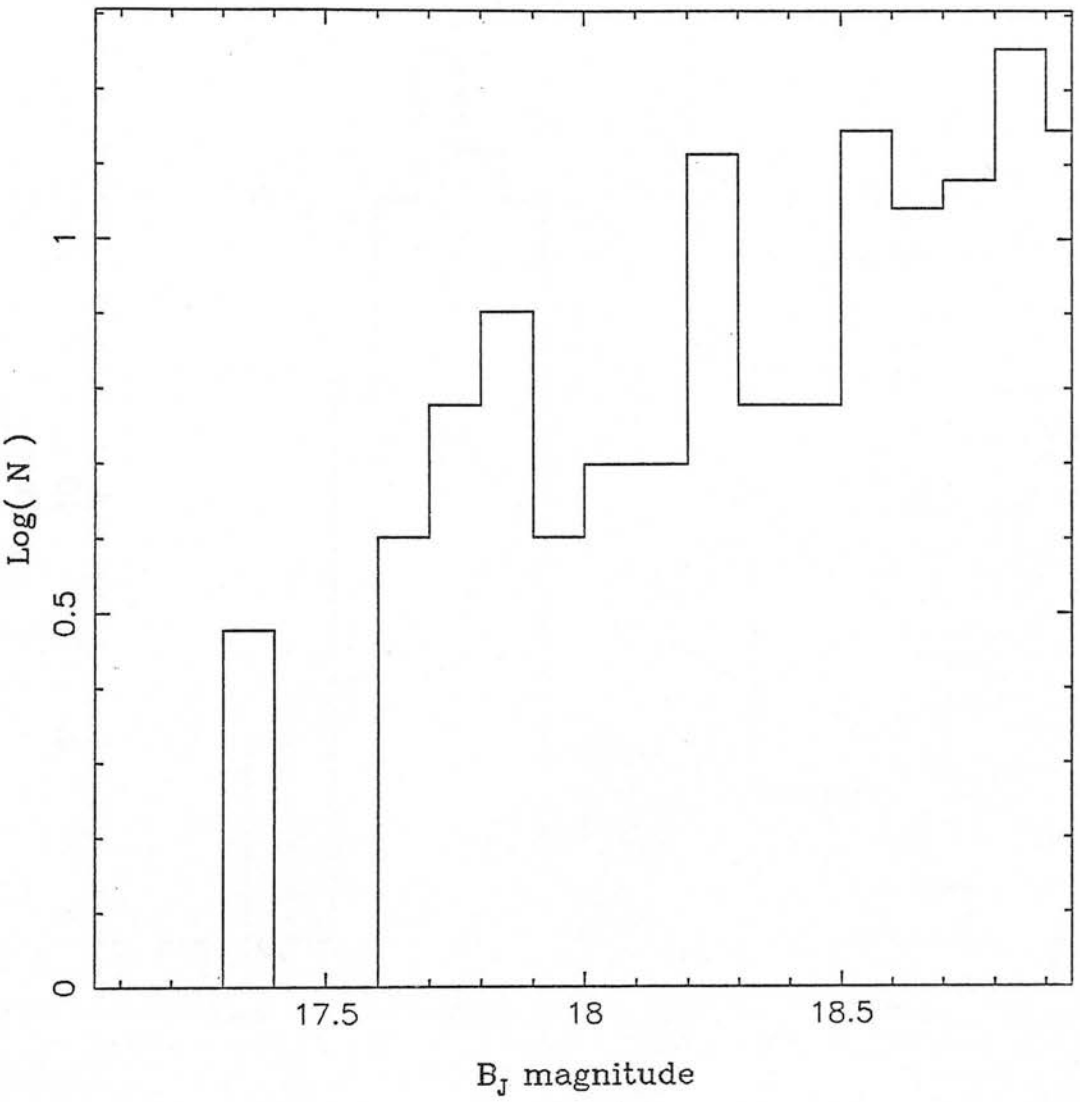

Fig 6.3 Log(number) as a function of B_J for the final survey.

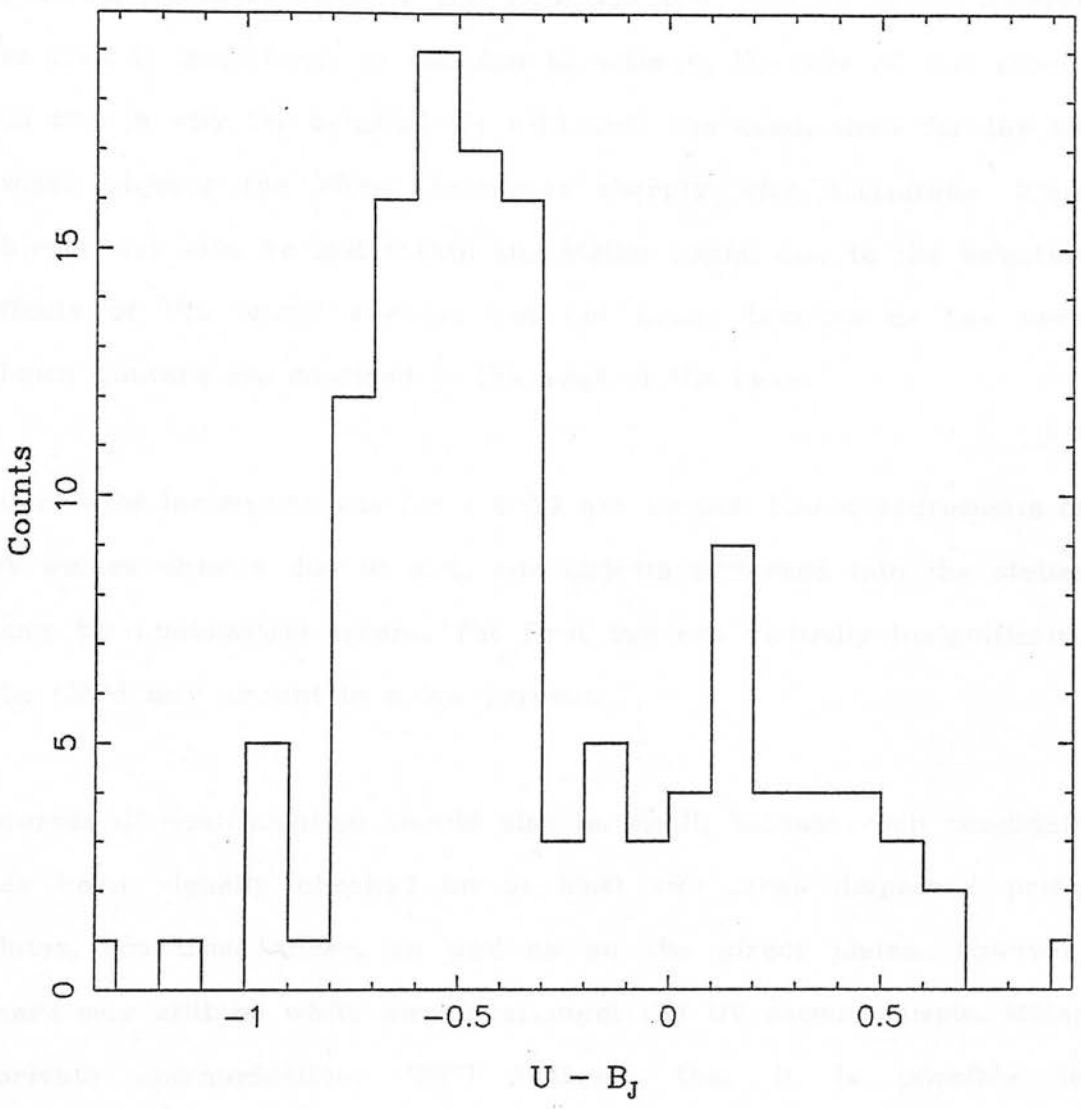

Fig 6.4 Number as a function of $U - B_J$ colour.

random due to overlaps on the prism plate, since this is the only method of coverage of this redshift regime. In addition, there may be a progressive loss of objects with increasing magnitude due to poorer spectrum signal to noise, in the same way that AQD UV excess objects are lost. It is difficult to see how to estimate the size of this effect, but this is why the brighter $B_J = 19$ limit was used, since for the UV excess objects the effect increases sharply with magnitude. Some objects may also be lost within the stellar locus, due to the selection effects of the 'good' survey, but not many, because as has been shown quasars are confined to the edge of the locus.

Sources of incompleteness for $z < 2.2$ are blends, bad measurements of UV excess objects due to dirt, and objects scattered into the stellar locus by photometric errors. The first two are virtually insignificant. The third may amount to a few percent.

Sources of contamination should also be small, because each candidate has been visually checked on at least two cross dispersed prism plates, sometimes three, as well as on the direct plates. However, there may still be white dwarfs amongst the UV excess sample. Miller (private communication, 1987) believes that it is possible to discriminate against these using the $U - B_J$ versus $B_J - I$ diagram (figure 6.1).

If the conclusions above regarding completeness are indeed correct, then the survey should certainly contain all of the quasars in the field. It has already been established (in section 5.2.2) that a very high probability quasar list can be made from the 'good' AQD sample. Pairing this list with the final survey, yields a total of 27 pairs, and

8 objects in the AQD good sample not contained in the final survey. Inspection of these 8 revealed that 4 objects were originally included, but were rejected because of a stellar appearance, and the other 4 were caused by emulsion blemishes in the spectrum.

Having said this, it is not clear why the progression seen in figure 6.2 does not continue. Few objects are found with line centroids less than pixel 32, and none are seen where the line could correspond to Lyman-α. It is not likely that this is caused by the diminishing prism dispersion - figure 5.11 indicates that candidates <u>are</u> found with lines in this region. One other explanation is that this reflects a real lack of quasars with redshifts $z > 2.7$, or that higher redshift quasars are all fainter. I am not sufficiently confident of the redshift estimation procedure to put great value in these conclusions.

The good AQD sample and the emission line identifications in the medium survey are drawn from the same source, so it is perhaps not suprising that all good AQD objects are found by the medium survey, except for junk. What is more interesting is that all of the previously known quasars in the field, in this magnitude range were identified again by the medium survey.

6.3 Future work.

Only the most direct next steps from this thesis are discussed here. Plainly, the final objective is a new quasar survey for which follow up slit spectroscopy must be obtained for the objects identified here,

and then specific questions can be addressed such as the luminosity function of quasars.

A general point is now made about all of the surveys. All of the surveys presented here made use of the simplest algorithms possible to do the job. The use of more complex data search and processing algorithms holds great potential, and should be investigated. For example, a search procedure to identify objects with peculiar colours from fewer than the total number of magnitudes, in some way that objects found can be tied to the rest of the survey. Also, a cross correlation procedure could be developed, to identify objects of specific types in the low dispersion spectra. This would help to cut down contamination of samples produced from the low dispersion plates. Another idea would be to work on procedures to identify closer blends on direct plates. The deblending described in section 4.7.5 approaches the problem, but there may be some geometrical criterion which can identify closer lying blends. The problem with such ideas is that although they are easy enough to imagine, and even to implement on a computer, what one is actually doing to the data must be checked at every stage in order to have confidence in the results and understand its effects on the survey. For example the procedure to identify galactic stars described in section 2.2 is of marginal benefits: although it certainly identifies the stars, it also introduces new selection effects against quasars of particular redshifts. This usually requires (at the very least) some additional spectroscopy to be done.

The final survey of sections 6.1 and 6.2 is clearly the place to start a programme of slit spectroscopy. The properties of the survey have

been examined in some detail, resulting in the conclusion that it is the first quasar survey to overcome the $z = 2.2$ barrier, while still retaining a high level of completeness for lower redshift objects. In addition, the large amount of information available for each candidate ensures that the survey is free from large numbers of contaminating objects, so little time spent on slit spectroscopy is likely to be wasted on spurious objects.

6.4 Evolution of quasars.

What can be said using the surveys of this work with regard to the evolution of quasars?

Other complete optically selected samples are exclusively based on UV excess surveys (apart from the very recent unpublished work by Hewitt *et al.* 1987), and so it is with these that the present survey must be compared. Thus one is not comparing like with like for two reasons:

a) UV excess surveys can only identify quasars with $z < 2.2$, and

b) the present survey contains contaminants, most notably blue galactic stars included in the ultraviolet part of the Schmidt survey. Since there are relatively more of these contaminants at brighter magnitudes, the slope of a derived number magnitude relationship is likely to be reduced. This is because of the large number of objects added by the UV excess criterion. Nevertheless, a best fit to the Schmidt survey data of this work to the $\log N(<B) = a + b.B$ relation gives $b = 1.0 \pm 0.2$. Comparable complete surveys over the same magnitude range have been Boyle *et al.* (1987), who finds $b = 1.1 \pm 0.05$ for $18 < B < 19.5$ and Marshall *et al.* (1984) who finds $b = 1.0 \pm 0.1$.

In a Euclidian universe with no evolution, one would expect to find $b = 0.6$ (see for example Longair, 1978). In a Freidmann universe, one cannot predict a value of b for no evolution without some knowledge of z and Ω except to say that $b < b_{euc}$. For example figure 16 of

Longair 1978 which shows the z dependence of the slope for a particular object class, normalized to the Euclidian value. At no redshift or value of Ω do the source counts go above b = 0.6.

The consistently high value of b found in these surveys demonstrates the existence of cosmological evolution (ie. quasars were more frequent, or they had higher absolute luminosities in the past), despite the differences between the surveys.

Figure 6.5 gives integral surface density counts for these surveys, including other recent complete surveys, both brighter and fainter. Although it is true that one should really use differential number counts, to preserve the statistical independence of the points, integral counts are given here to provide comparison with earlier authors. Error bars marked on this plot are just N Poissonian values. These errors have been marked on points from the survey of this work, but it should be remembered that these are just lower limits because the number of contaminants is an unknown function of magnitude (except for the point at B = 20.5, which is based on the spectroscopically confirmed grens survey).

Various interesting points are seen on this plot. These are taken survey by survey, and compared with the values from this work: firstly, the brighter survey of Mitchell, Warnock and Usher (1984). The best fit line to this survey has a slope of b = 0.67 ± 0.07, not quite as steep as the fainter and more recent surveys. The likely explanation for this is that the Mitchell, Warnock and Usher survey was compiled by eyeball, and so is subject to loss of objects at

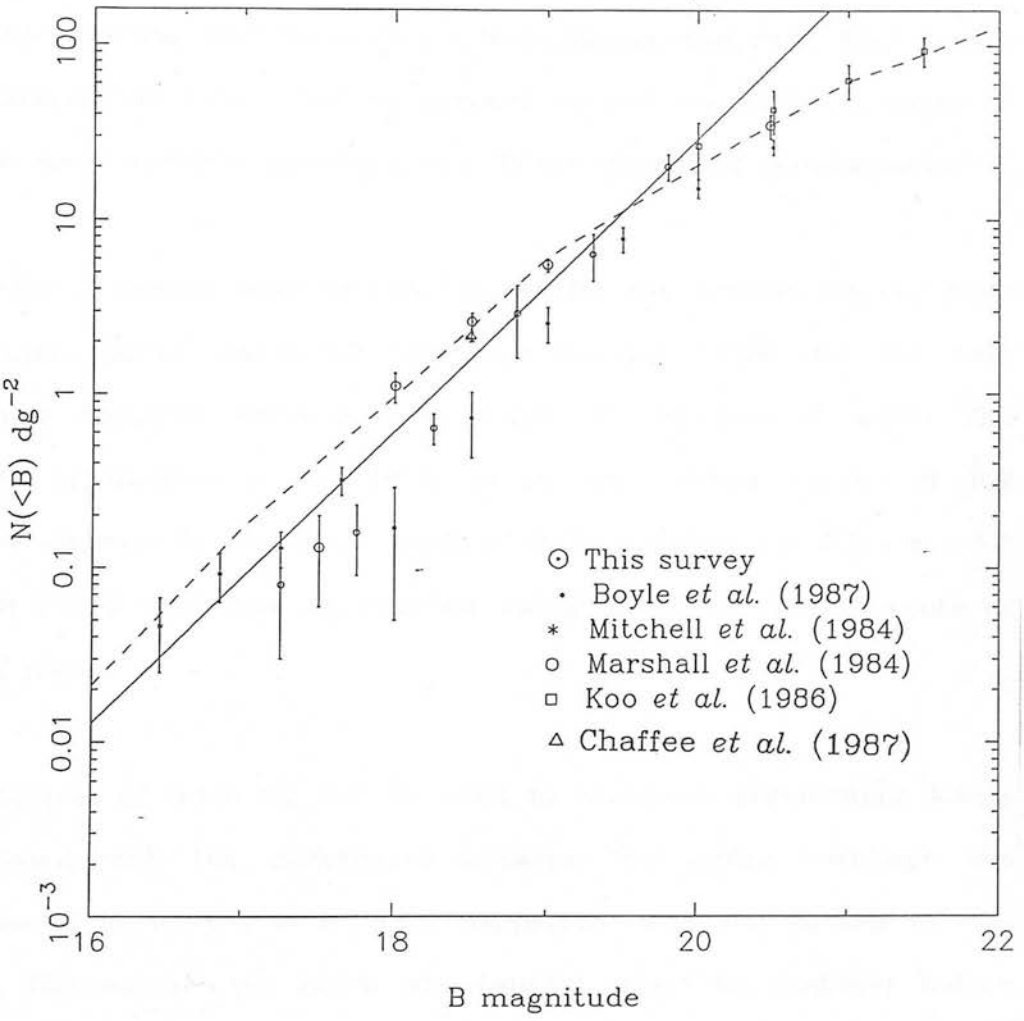
N(<B) dg^{-2}
100
10
1
0.1
0.01
10^{-3}
16
18
20
22
B magnitude
⊙ This survey
· Boyle *et al.* (1987)
* Mitchell *et al.* (1984)
○ Marshall *et al.* (1984)
□ Koo *et al.* (1986)
△ Chaffee *et al.* (1987)

Figure 6.5

magnitudes brighter than the plate limit.

As has already been stated, best fit slopes for the surveys covering the intermediate magnitude range have almost the same high value. However, actual values for the present survey are larger, because of 1) increased redshift coverage, and 2) the remaining contaminants.

In order to assess whether the figures for the present survey have predictive power, table 6.2 assembles density values for the best available complete surveys, with those of the present work. The survey of Chaffee *et al.* (1987) is an unpublished survey of 102 square degrees in the Virgo cluster. It is complete for $0.2 < z < 3.3$ and $B < 18.5$, and was constructed using automatic measurements of prism plates.

The figures of table 6.2 can be used to construct significance levels associated with the differences between the tables. Although the Chaffee *et al.* survey is directly comparable with the survey in this work, figures for the Boyle *et al.*survey must be modified before comparison can be made. Boyle (1986) estimates that the survey is 10% incomplete for $z < 2.2$, and Chaffee *et al.* find that $\approx$ 20% of their quasars are in the range $2.2 < z < 3.3$. So before a comparison can be made, Boyles figures must be revised upwards by 30%. This is a very crude estimate, since no account can be taken of the redshift - magnitude dependence.

Thus at $B = 18.5$, there is a factor of 1.23 ± 0.17 between the Chaffee *et al.* survey and the present work. This is significant at the 1.3σ

level. At the same magnitude, there is a factor of 2.5 ± 1.1 between the Boyle *et al.* survey and the present work. This is significant at the 1.4σ level. Thus although the differences in figure 6.5 look interesting, they are at best of marginal significance.

To pursue the matter a little further, this implies that at B = 18.5 there are between 20% and 60% too many counts in this survey. The extra numbers are mostly the UV excess survey contaminants, the metal poor subdwarfs and white dwarfs. Fluctuations in the numbers of these objects are large - as seen in section 4.8.1, Boyle (1986) has found that the proportion of UV excess quasars to other UV excess objects varies at least between 20% and 35% at the same galactic latitude, at B = 18.5.

Table 6.2. Number densities.

B	This work N(<B)	Boyle *et al.* (1987)	Chaffee *et al.* (1987)
17.5	0.13 ± 0.07		
18	1.11 ± 0.22	0.17	
18.5	2.59 ± 0.33	0.73 ± 0.25	2.1 ± 0.13
19	5.52 ± 0.49	2.56 ± 0.55	

There may be some evidence to indicate that the Boyle *et al.* survey is in fact less complete than they beleive, as again at B = 18.5 there is a factor of 2.2 ± 0.82 difference between the Boyle figure and that

of Chaffee *et al.* However, this also is of marginal significance at the 1.5σ level.

The Koo *et al.* (1986) and the fainter part of the Boyle *et al.* (1987) surface density figures have a significantly different slope: for Koo *et al.*, the slope $b = 0.35 \pm 0.01$.

This change in slope has been identified by Boyle *et al.* (1987) with a discontinuity in the quasar luminosity function, rather than with a change in the rate of evolution. They used spectroscopy on all objects in the survey to construct a series of luminosity functions at different redshifts. They parameterize the quasar luminosity function using two power laws, with a 'knee' where they meet. This feature allows an accurate definition of the evolution function, out to a redshift of $z = 2.2$, which they conclude has

$$L(z) = L(z=0).(1+z)^{3.7\pm0.3}$$

where $L(z)$ is the luminosity function as a function of z, and $L(z=0)$ is the luminosity function for $z = 0$.

Also marked on figure 6.5 are lines derived by Braccessi *et al.* (1980) from their evolution models. The solid line is their predicted pure density evolution, while the broken line is their predicted pure luminosity relationship, similar to the evolution derived by Boyle *et al.* (1987). Both of these are for $z < 2.2$. Thus it is possible to firmly rule out pure density evolution, since at magnitudes fainter than $B = 20$, number counts fall away very rapidly from those expected in a pure density evolution environment.

The point at B = 20.5 provided in this work by the grens survey has a slightly different interpretation. It has been shifted to the left on the diagram by 0.02 magnitudes to reduce confusion in this area. It is based on spectroscopic observations of the grens survey (discussed in chapter 3). As a result, it can be assigned a more meaningful error bar than for the Schmidt data, as it is not subject to the contamination problems affecting the other points in this survey. On the other hand, the point is based on a small number of objects (7 quasars, of which none have $z > 2.2$) over a small area.

What can this survey be expected to provide? As has been seen, one of the main tools for the understanding of the quasar process is the luminosity function, and mapping its evolution with cosmological epoch. To date, this has only been possible using samples restricted in redshift, which have shown a continuous power law increase in the luminosity function towards earlier epochs.

The quasar evolution model derived so far cannot be the whole answer, because at some epoch in the universe quasars must have formed. Boyle *et al.* (1987) have only been able to say that quasar densities increase indefinitely with increasing redshift, up to $z = 2.2$. Searches for higher redshift quasars (such as that of Osmer, 1982) show that they are rare objects at redshifts $z > 3.4$.

If spectroscopy were available for this survey, then, it would be possible to map the downturn in the evolution of the quasar luminosity function, and so to identify the epoch of quasar formation.

The main area of good statistics in the present survey are at B = 18.5, so spectroscopy would identify the high redshift luminosity function at higher luminosity, unless the analysis of more grens data were also undertaken to improve statistics in this part of the survey.

It has been suggested that the turn on of visible Ly α emission may not actually coincide with the epoch of quasar formation - it is possible that young quasars have weak emission lines or were shrouded by dust (Hazard *et al.*, 1984). This possibility could be tested in the present survey, since it would mean that the broad absorption line phenomenon seen in the spectra of some quasars is epoch dependent. If this were actually to be the case, the only way to identify the actual onset of quasar activity would be to construct non-optical surveys, such as more sensitive IR or X-ray surveys than are available at present.

The physical interpretation of what has been discovered so far falls into two main categories: either quasars are very long lived (ie. the evolution seen is reflecting the evolution of individual quasars), or else that this parameterization represents the evolution in average luminosity for many generations of short-lived objects.

The search for evidence to constrain the evolution and its consequences at high redshift has been hampered by observational uncertainties at lower redshifts. This is because observers expectations of what they would find at high redshift is determined by the evolution law that is used, which must be based on low redshift data. Thus if density evolution is extended to high redshift,

large numbers of quasars are expected. When few are found, this appears to be a highly significant result.

Now that the problem has been largely resolved, by Boyle *et al.* (1987) the observational search for a cutoff at higher redshift can begin in earnest. It is clear that there is great potential in machine based multicolour searches and a better understanding of the properties of colour space is urgent if surveys are to push fainter than the B = 19 available to the Schmidt prism. Either this or a more extensive grens survey is needed incorporating the suggestions of chapter 3 to follow the 'knee' in the luminosity function discussed above.

The identification of the quasar cutoff is interesting in its own right, because it will tell us more about how quasars work. It may also ultimately provide constraints on theories of galaxy formation. If the quasar cutoff is produced by a reduction in the quasar birthrate, then the formation of structure in the universe and the cutoff are linked. The trigger can either be the formation of clusters (if quasars are triggered by galaxy interactions) or the galaxies themselves. In either case, the best probe available will be the detailed examination of the structure and environment of high redshift quasars.

Boyle, B.J., Fong, R., Shanks, T., & Peterson, B.A. *Mon. Not. R. astr. Soc.* (1987) 227 717

Braccessi, A., Zitelli, V., Bonoli, F., & Formaggini, L. *Astron. Astrophys.* (1980) 85 80

Chaffee, F.H., Foltz, C.B., Hewett, P.C., MacAlpine, G.M., Turnshek D.A., Weymann, R.J., & Anderson, S.F. poster paper 170th AAS meeting (1987)

Hazard, C., Morton, D.C., Terlevich, R., McMahon, R. *Astrophys. J.* (1984) 282 33

Longair, M.S. in *"Observational Cosmology"* (1978) eds. Maeder, A., Martinet, L., & Tammann, G.

Marshall, H.L., Avni, Y., Braccessi, A., Huchra, J.P., Tananbaum, H., Zamorani, G., Zitelli, V. *Astrophys. J.* (1984) 283 50

Mitchell, K.J., Warnock, A., & Usher, P.D. *Astrophys. J.* (1984) 287 L3

Osmer, P.S. *Astrophys. J.* (1982) 253 28

Appendix. The $17 < B_J < 19$ survey.

ID	RA (1950)	Dec	B_J	$U-B_J$	B_J-V	V-R	R-I	S	Z
1	10 30 58.3	5 12 47.8	18.86	-0.18	0.08	0.29		3	
2	10 31 3.3	2 48 6.6	18.62	-0.38	-0.15	0.16	0.77	1	2.4
3	10 31 10.7	5 52 7.4	18.87	-0.52	-0.18	0.53	0.58	1	
4	10 31 25.4	3 41 26.4	18.91	-0.05	0.16	0.37	0.44	2	2.6
5	10 31 30.3	5 46 37.2	18.41	-0.43	0.09	0.13	0.60	3	
6	10 31 55.0	5 51 19.6	19.00	0.08	0.09	0.34	0.39	2	2.5
7	10 31 55.7	2 40 59.6	18.71	-0.29	0.09	0.29	0.27	3	
8	10 31 57.4	7 23 29.8	18.46	-0.98	-0.20	-0.09		3	
9	10 32 5.6	7 2 52.6	18.98	-0.38	-0.12	0.37	0.82	3	
10	10 32 7.6	6 52 5.4	18.79	-0.41	-0.06	0.15	0.54	3	
11	10 32 26.0	2 45 39.5	18.13	-1.35	-0.56	0.12	0.31	1	
12	10 32 29.6	6 17 14.6	18.74	-0.47	0.19	0.39	0.69	3	0.245
13	10 32 33.5	6 18 27.0	18.59	-0.54	-0.10	0.05	1.08	3	
14	10 32 49.4	3 7 34.0	17.89	0.14	0.01	0.52	0.15	1	2.5
15	10 32 56.6	6 7 31.0	18.85	-0.68	0.04	0.06		3	
16	10 32 57.1	2 35 59.7	18.08	-0.78	-0.09	0.35	0.29	1	
17	10 32 58.2	6 54 44.5	18.52	-0.69	0.12	0.05	0.60	3	
18	10 33 25.5	5 49 30.1	18.65	-0.31	-0.03	0.10	0.56	1	2.5
19	10 33 30.2	4 8 9.3	18.82	-0.61	0.03	0.59	0.35	3	
20	10 33 32.2	7 10 19.2	18.25	-0.10	-0.22			3	
21	10 33 40.5	3 34 49.6	18.56	-0.57	-0.01	0.45	0.19	1	1.513
22	10 33 41.4	6 58 38.7	18.61	-0.60	-0.07	0.09	0.28	3	
23	10 33 50.4	5 10 10.0	18.28	-0.56	-0.02	0.31	0.31	1	
24	10 33 56.2	4 12 41.2	18.81	-0.58	0.25	-0.09	0.34	3	
25	10 34 0.3	7 25 24.3	18.74	-0.44	-0.22	0.12		3	
26	10 34 3.7	3 5 35.6	17.73	-0.58	-0.04	0.27	0.26	1	
27	10 34 7.6	6 35 59.2	18.43	-0.44	-0.06	0.06	0.37	1	2.2
28	10 34 11.4	3 17 22.1	18.72	-0.70	-0.01	0.48	0.08	3	
29	10 34 14.7	6 30 45.8	18.10	-0.63	-0.25	-0.16	0.02	3	
30	10 34 16.0	2 33 54.6	18.31	0.25	-0.12	0.15	0.28	1	2.6
31	10 34 22.2	4 27 57.1	18.89	-0.62	-0.02	0.16	0.59	3	
32	10 34 26.8	3 42 21.3	18.40	-0.68	-0.36	-0.06		3	
33	10 34 34.6	2 36 28.3	18.72	-0.34	0.40	0.34	0.26	3	
34	10 34 39.9	4 5 4.1	18.89	-0.67	-0.17	0.06		3	
35	10 34 55.3	7 5 27.8	17.84	0.60	0.26	0.29	0.41	1	2.6
36	10 34 58.4	4 8 6.7	17.84	-0.34	-0.08	0.05	0.23	3	
37	10 35 4.0	4 5 21.8	18.66	-0.58	0.13	0.09	0.58	3	
38	10 35 12.9	4 18 17.7	17.82	-0.75	0.27	0.20	0.10	1	1.085
39	10 35 14.0	5 35 5.0	18.51	-0.36	-0.03	-0.07	0.35	3	
40	10 35 15.4	6 46 16.8	18.39	0.42	0.27	0.27	0.28	1	2.6
41	10 35 17.0	2 29 28.5	18.10	-0.07	0.36	0.25	0.31	1	2.5
42	10 35 17.9	7 14 12.1	18.59	-0.39	-0.11	0.13	0.63	3	
43	10 35 21.6	4 5 59.1	18.80	-0.19	-0.07	0.30	0.62	1	2.4
44	10 35 54.8	6 24 49.3	17.66	-0.73	-0.19	0.41	0.57	1	

45	10 36 17.2	3 16 35.6	18.73	0.11	0.21	0.13	0.65	1	2.5
46	10 36 47.5	3 33 24.2	18.99	-0.49	-0.13	0.08		3	
47	10 36 56.0	3 15 39.9	18.33	0.11	0.25	0.16	0.36	1	2.4
48	10 36 57.5	6 20 16.9	18.14	-0.98	-0.47	-0.11	0.26	1	
49	10 37 0.7	5 17 54.8	17.78	0.51	-0.29	0.12	0.33	1	2.5
50	10 37 13.5	2 46 58.7	18.32	-0.64	-0.01	0.65	0.47	3	
51	10 37 15.7	6 49 2.3	18.90	-0.77	0.17	0.54	0.05	1	2.2
52	10 37 31.1	6 40 49.9	18.22	-0.18	-0.03	0.40	0.30	3	
53	10 37 37.4	4 27 18.9	17.85	0.41	-0.29	0.07	0.16	1	2.7
54	10 37 39.7	5 20 2.7	18.26	-0.44	-0.23	-0.02	0.25	3	
55	10 37 49.1	5 53 26.8	18.80	-0.33	-0.18	-0.04		3	
56	10 37 52.8	3 27 54.9	18.54	-0.60	0.11	0.56	0.65	3	
57	10 38 0.2	4 48 30.8	17.40	0.61	0.35	0.53	0.35	2	
58	10 38 11.0	2 42 41.7	18.21	-0.67	0.07	0.09	0.46	3	
59	10 38 30.2	2 29 33.0	18.86	-0.24	-0.28	0.23	0.64	3	
60	10 38 35.1	5 53 24.6	18.52	0.12	0.22	0.16	0.47	1	
61	10 38 38.8	3 58 52.3	18.66	-0.79	0.08	0.45	0.29	3	
62	10 38 38.8	4 6 20.5	18.87	-0.51	0.01	0.19	0.43	3	0.928
63	10 38 48.6	4 10 31.5	18.02	-0.57	0.09	0.53	0.09	1	1.41
64	10 39 1.8	6 1 35.4	17.60	0.20	0.04	0.23	0.30	1	2.7
65	10 39 19.4	6 28 39.9	18.88	-0.54	-0.07	0.33	0.38	3	
66	10 39 34.6	7 11 40.2	17.78	0.29	-0.18	-0.09	0.46	1	2.6
67	10 39 49.3	3 0 48.1	18.05	-0.47	-0.19	-0.07	0.24	3	
68	10 39 50.3	4 11 21.3	18.36	-0.57	0.02	0.29	0.53	3	
69	10 40 13.8	3 49 37.9	17.39	-0.93	-0.40	0.11	0.20	3	
70	10 40 29.7	5 41 37.8	18.73	0.25	0.11	0.02	0.49	1	2.8
71	10 40 31.8	3 57 5.9	18.08	-0.61	0.04	0.38	0.29	3	0.854
72	10 40 46.2	3 22 13.7	17.78	-0.74	-0.22	-0.21	0.16	3	
73	10 40 48.1	4 38 2.4	18.92	0.16	0.02	0.24	0.77	1	2.33
74	10 40 50.9	5 41 4.8	18.98	0.01	0.15	0.04	0.56	1	2.3
75	10 41 18.8	6 12 16.1	18.87	-0.35	-0.07	0.09	0.52	3	
76	10 41 22.2	4 54 9.8	18.60	-0.27	-0.03	0.25	0.40	1	2.41
77	10 41 22.4	6 19 7.8	18.90	-0.34	-0.08	0.18	1.01	3	
78	10 41 36.9	2 30 21.3	17.91	-0.49	0.08	0.26	0.50	1	
79	10 41 40.9	5 57 7.1	18.20	0.12	0.14	0.27	0.41	2	2.4
80	10 41 49.7	6 48 52.0	18.67	-0.49	-0.21	0.22	0.55	3	
81	10 41 54.4	5 34 43.9	17.66	-0.39	0.15	0.33	0.17	3	
82	10 41 55.2	7 24 29.0	17.60	-0.46	-0.26	0.15	0.35	3	
83	10 42 2.4	2 57 58.8	18.55	-0.74	-0.07	0.15	0.68	1	2.4
84	10 42 7.4	5 13 31.9	18.67	0.06	0.20	0.17	0.49	1	2.7
85	10 42 9.7	7 22 39.8	17.98	-0.52	-0.22	0.28	0.34	3	
86	10 42 24.7	5 39 56.6	18.84	0.95	0.34	0.56	0.48	2	2.6
87	10 42 32.0	3 26 0.3	18.96	-0.50	-0.24	0.11		3	
88	10 42 43.0	5 40 43.8	18.65	-0.48	-0.06	0.03	0.55	3	
89	10 42 50.5	6 26 22.5	17.77	0.14	0.02	0.24	0.27	1	2.6
90	10 43 16.5	6 40 24.6	17.88	-0.61	-0.13	0.40	0.34	1	1.507
91	10 43 24.2	6 32 21.4	18.85	-0.13	0.01	0.37	0.71	3	
92	10 43 37.3	3 52 12.4	18.95	-0.40	-0.12	0.35	0.67	3	1.48

93	10 43 39.2	5 11 12.1	18.80	-1.15	-0.52	-0.08		3	
94	10 43 39.2	7 17 38.2	18.57	0.13	0.16	0.18	0.34	1	2.5
95	10 43 41.0	4 35 21.3	18.54	0.43	-0.14	0.14	0.57	1	2.6
96	10 44 2.5	2 34 13.5	18.89	-0.37	-0.04	0.34	0.33	3	
97	10 44 3.2	7 26 34.8	17.95	-0.61	-0.29	0.47	0.35	3	
98	10 44 4.6	2 42 43.6	17.38	0.29	-0.16	0.17	0.34	1	2.6
99	10 44 7.3	2 47 19.4	18.60	-0.63	-0.01	0.25	0.45	1	
100	10 44 9.1	2 58 24.5	18.77	-0.43	-0.09	0.27	0.65	3	
101	10 44 20.8	5 57 39.7	18.28	-0.71	0.14	0.26	0.49	1	1.223
102	10 44 35.1	3 44 46.6	18.22	-0.71	0.17	0.27	0.06	3	
103	10 44 37.9	5 40 31.7	18.47	0.46	0.46	0.25	0.42	1	2.7
104	10 44 40.4	6 7 49.4	18.26	-0.64	-0.13	0.15	0.44	1	0.888
105	10 44 49.2	2 40 41.8	18.03	-0.58	0.03	0.12	0.45	3	
106	10 45 2.5	5 56 44.9	18.27	-0.60	-0.23	-0.20	0.42	3	
107	10 45 4.1	3 29 43.6	18.98	-0.34	-0.08	-0.07		3	
108	10 45 9.8	3 59 54.0	18.28	-0.13	0.01	0.22	0.43	1	2.5
109	10 45 24.5	6 18 3.1	17.62	0.67	0.24	0.29	0.44	1	2.6
110	10 45 27.6	5 42 12.9	17.95	-0.33	-0.23	-0.14	0.39	3	
111	10 45 32.1	3 10 21.7	18.91	-0.84	-0.31	0.03		3	
112	10 45 33.0	2 36 29.6	18.70	-0.98	0.04	0.41	0.62	1	
113	10 46 0.5	2 46 43.7	18.28	0.36	-0.15	0.24	0.35	1	2.5
114	10 46 1.5	3 50 9.8	18.52	-0.41	0.07	0.50	1.47	3	
115	10 46 1.7	3 24 4.0	18.99	-0.58	-0.11	0.34	0.50	3	
116	10 46 4.3	5 51 42.9	18.66	-0.97	-0.02	0.19	0.59	1	2.1
117	10 46 19.3	5 24 40.3	17.77	0.57	-0.32	0.03	0.39	1	2.6
118	10 46 33.2	5 51 53.4	18.59	-0.50	-0.30	0.43	0.58	3	
119	10 46 42.8	3 10 36.2	18.56	-0.40	-0.17	0.27	0.67	1	2.4
120	10 46 48.6	6 1 37.7	18.47	0.33	-0.30	0.09	0.33	1	2.6
121	10 47 6.4	3 15 43.0	18.81	-0.37	-0.12	0.35	0.53	3	
122	10 47 46.7	7 2 16.1	18.28	-0.72	-0.29	0.54	0.33	3	
123	10 48 2.3	7 19 16.0	18.20	0.06	-0.01	0.27	0.40	1	
124	10 48 30.8	3 23 16.6	17.82	0.32	0.09	0.34	0.28	1	2.5
125	10 48 39.8	5 26 16.2	18.84	-0.69	-0.27	-0.11		3	
126	10 48 43.5	7 21 0.9	18.74	-0.59	0.04			3	
127	10 48 51.9	3 21 33.4	18.88	-0.70	0.01	0.47	0.52	1	2.3
128	10 49 6.1	5 53 2.1	17.83	0.33	0.02	0.33	0.36	1	2.5
129	10 49 9.6	4 24 24.3	18.94	-0.32	-0.20	0.25		3	
130	10 49 17.0	3 34 38.8	18.31	-0.41	-0.27	0.26		3	

Notes. 1) The column labelled 'S' gives the source of the object. S = 1 indicates an AQD main survey object. S = 2 indicates an AQD good survey object photometrically within the stellar locus. S = 3 indicates a UV excess survey object.

2) Column 'Z' if not underlined is redshift estimate based on the line centroid of the strongest line, for AQD objects where there is evidence to suggest that the line is Lyman-α. If the figure is underlined, it is a redshift from previous slit spectroscopy.

References.

Beichman, C.A., Soifer, B.T., Helou, G., Chester, T.J., Neugebaur, G., Gillet, F.C., Low, F.J. (1980) *Astrophys. J.* 308 L1

Bessell, M.S. (1979) *Publ. Astron. Soc. Pac.* 91 589

Blair, M., & Gilmore, G. (1982) *Publ. Astron. Soc. Pac.* 94 742

Boroson, T.A., Oke, J.B., & Green, R.F. (1982) *Astrophys. J.* 263 32

Boroson, T.A. & Oke, J.B. (1984) *Astrophys. J.* 281 535

Boroson, T.A., Persson, S.E. & Oke, J.B. (1985) *Astrophys. J.* 293 120

Borra, E.F., Edwards, G., Petrucci, F., Beauchemin, M., Brousseau, D., Grondin, L., Beaulieu, A. (1987) preprint

Boyle, B.J. (1986) Ph. D. thesis, Univ. of Durham

Boyle, B.J., Shanks, T., Fong, R. & Clowes, R.G. (1985) *Mon. Not. R. astr. Soc.* 216 623

Boyle, B.J., Fong, R., Shanks, T., & Peterson, B.A. (1986) *Mon. Not. R. astr. Soc.* submitted.

Buzzoni, B., Delabre, B., Dekker, H., D'Odorico, S., Enard, D., Focardi, P., Gustafsson, B., Nees, W., Panreau, J., & Reiss, R., (1984) *ESO messenger* 34

Cannon, R.D., Dawe, J.A., Morgan, D.H., Savage, A., & Smith, M.G. (1982) *Proc. Astron. Soc. Aust.* 4 (4) 468

Cheney, J.E., & Rowan-Robinson, M. (1980) *Mon. Not. R. astr. Soc.* 195 497

Clowes, R.G. (1981) *Mon. Not. R. astr. Soc.* 197 731

Clowes, R.G. (1984) in "*Astronomy with Schmidt type telescopes, IAU symp. 78*", p. 107, ed. Capaccioli, M., D. Reidel, Dordrecht

Clowes, R.G., Cooke, J.A., & Beard, S.M. (1983) *Mon. Not. R. astr.*

Soc. 207 99

Clowes, R.G., Emerson, D., Smith, M. G., Wallace, P. T., Cannon, R.D., Savage, A., & Boksenberg, A. (1980) *Mon. Not. R. astr. Soc.* 193 415

Clowes, R.G., Iovino, A., & Shaver, P. (1987) *Mon. Not. R. astr. Soc.* in press

Clowes, R.G., & Savage, A. (1983) *Mon. Not. R. astr. Soc.* 204 365

Condon, J.J. (1984) *Astrophys. J.* 287 461

Condon, J.J., O'Dell, S.L. Puschell, J.J., & Stein, W.A. (1981) *Astrophys. J.* 246 624

Cousins, A.W.J. (1980a) *Mon. Not. R. astr. Soc. South Africa* 39 80

Cousins, A.W.J. (1980b) *S. A. Astrophys. Obs. Criculars* 1 234

Cristiani, S. (1986) in "*Structure & Evolution of Active Galactic Nuclei*", p. 81 eds. Giuricin, G., *et al.* D. Reidel, Dordrecht

Dunlop, J.S., Downes, A.J.B., Peacock, J.A., Savage, A., Lilly, S.J., Watson, F.G., & Longair, M.S. (1986) *Nature* 319 564

Fouere, J.C., Lelievre, G., Lemonnier, J.P., Salmon, D.A., Odgers, G.J., & Richardson, E.H. (1982) *Optica Acta* 29 383

Formiggini, L., Zitelli, V., Bonoli, F., & Bracessi, A. (1980) *Astron. Astrophys. Suppl. Ser.* 39 129

Fried, J.W. (1986) in "*Structure & Evolution of Active Galactic Nuclei*" p. 309, eds. Giuricin, G. *et al.* D. Reidel, Dordrecht

Furenlid, I. (1978) in proc. ESO workshop "*Modern techniques in Astronomical Photography*", p. 153, eds. West, R.M., & Heudier, J.L.

Gehren, T., Fried, J., Wehinger, P.A., & Wyckoff, S. (1984) *Astrophys. J.* 278 11

Gioia, I.M., Maccaro, T., Schild, R.E., Stocke, J.J., Liebert, J.W., Danziger, I.M., Kunth, D., & Lub, J. (1984) *Astrophys. J.* 283

Graham, J.A. (1982) *Publ. Astron. Soc. Pac.* 94 244

Greenstein, J.L. & Oke, J.B. (1970) *Publ. Astron. Soc. Pac.* 82 898

Green, R.F., Schmidt, M., & Liebert, J. (1986) *Astrophys. J. Suppl. Ser.* 61 305

Hawkins, M.R.S.H. (1986) *Mon. Not. R. astr. Soc.* 219 417

Hazard, C., & McMahon, R. (1985) *Nature* 314 238

Hazard, C., Morton, D.C., McMahon, R.G., Sargent, W.L., Terlevich, R. (1986) *Mon. Not. R. astr. Soc.* 223 87

He, X.-T., Cannon, R.D., Peacock, J.A., Smith, M.G., & Oke, J.B. (1984) *Mon. Not. R. astr. Soc.* 433 211

Heckman, T.M., Bothun, G.D., Balick, B. & Smith, E.P. (1984) *Astron. J.* 89 958

Heckman, T.M., Smith, E.P., Baum, S.A., van Breugal, W.J.M., Miley, G.K., Illingworth, G.D., Bothun, G.D., & Balick, B. (1986) *Astrophys. J.* 311 526

Hewett, P.C. (1983) Ph. D. thesis, Univ. of Edinburgh

Hewett, P.C., Irwin, M.J., Bunclarck, P., Bridgeland, M.T., Kibblewhite, E.J., He, X.-T., & Smith, M.G. (1985) *Mon. Not. R. astr. Soc.* 213 971

Hewitt, A., & Burbidge, G. (1986) *Astrophys. J. Suppl. Ser.* 63 1

Hickson, P., & Hutchings, J.B. (1987) *Astrophys. J.* 312 518

Hoag, A.A., & Schroeder, D.J. (1970) *Publ. Astron. Soc. Pac.* 82 1141

Hutchings, J., & Campbell, B. (1983) *Nature* 303 584

Hutchings, J., Crampton, D., Campbell, B., (1984) *Astrophys. J.* 280 41

Hutchings, J., Crampton, D., Campbell, B., Duncan, D., & Glendenning, B., (1984) *Astrophys. J. Suppl. Ser.* 55 319

Iben, I. (1967) *Ann. Rev. Astron. Astrophys.* 5 571

Iriarte, B., & Charira, E. (1957) *Bol. Obs. Tonantzintla y Tacubaya* 16 36

Johnson, H.L. & Morgan, W.W. (1953) *Astrophys. J.* 117 313

Johnson, H.L. (1966) *Ann. Rev. Astron. Astrophys.* 4 193

Kibblewhite, E.J., Bridgeland, M.T., Bunclark, P., & Irwin, M.J. (1983) in proc. of *"Astronomical Microdensitometry Conference"* p. 277, ed. Klinglesmith, D.A.

Koo, D.C., & Kron, R.G. (1982) *Astron. Astrophys.* 105 107

Koo, D.C., Kron, R.G., & Cudworth, K.M. (1986) *Publ. Astron. Soc. Pac.* 98 285

Kron, R.G. (1980) *Astrophys. J. Suppl. Ser.* 43 305

Landolt, A.U. (1983) *Astrophys. J.* 88 439

Lynds, R. & Wills, D. (1972) *Astrophys. J.* 172 531

Lynds, R. & Petrosian, V. (1972) *Astrophys. J.* 175 591

MacGillivray, H.T., Stobie, R.S. (1984) *Vistas in Astron.* 27 433

Malkan, M. (1984) *Astropys. J.* 287 555

Margon, B., Downes, R.A., & Chanan G.A. (1985) *Astrophys. J. Suppl. Ser.* 59 23

Marshall, H.L. (1985) *Astrophys. J.* 299 109

Nandy, K., Reddish, V.C., Tritton, K.P., Cooke, J.A., & Emerson, D. (1977) *Mon. Not. R. astr. Soc.* 178 63P

Neugebaur, G., Miley, G.K., Soifer, B.T., & Clegg, P.E. (1980) *Astrophys. J.* 308 815

Oke, J.B. (1974) *Astrophys. J. Suppl. Ser.* 27 21

Osmer, P.S. (1980) *Astrophys. J.* 247 762

Osmer, P.S., & Smith, M.G. (1980) *Astrophys. J. Suppl. Ser.* 42 333

Osterbrock, D.E., (1984) *Quar. J. R. astr. Soc.* 25 1

Peacock, J.A. (1983) in *"Quasars & Gravitational Lenses"* p.86, proc of International Astrophysical Colloquium, 24th, Liege

Peacock, J.A., Miller, L., Longair,M.S. (1986) *Mon. Not. R. astr. Soc.* 218 265

Prestage, R.M. (1985) Ph.D. thesis, Univ. of Edinburgh

Pritchet, C., & Van den Bergh, S. (1977) *Astrophys. J. Suppl. Ser.* 34 101

Richardson, E.H. (1979) *Can. J. Phys.* 57 1365

Richer, H.B., & Fahlman, G.G. (1986) *Astrophys. J.* 304 273

Sandage, A. (1965) *Astrophys. J.* 141 1560

Sandage, A., & Luyten, W.J. (1967) *Astrophys. J.* 148 767

Sandage, A. & Veron P. (1965) *Astrophys. J.* 142 412

Sargent, W.J.W., Young, P.J., Boksenberg, A., & Tytler, D. (1980) *Astrophys. J. Suppl. Ser.* 42 41

Savage, A. (1978) Ph. D. thesis, Univ. of Sussex

Savage, A., Waldron, D.J., Fretwell, M., Morgan, D.H., Tritton, S.B., Cannon, R.D., Bruck, M.T., Beard, S.M., & Palmer J.B. (1985) *U. K. S. T. Objective Prism Handbook.*

Schmidt, M. (1963) *Nature* 197 1040

Schmidt, M. (1970) *Astrophys. J.* 162 371

Schmidt, M. (1986) in *"Structure & Evolution of Active Galactic Nuclei"* p.3 eds. Giuricin, G. *et al.* D. Reidel, Dordrecht

Schmidt, M., & Green, R.F. (1983) *Astrophys. J.* 269 352

Schmidt, M., Schneider, D.P., Gunn, J.E. (1987) *Astrophys. J.* 316 L1

Shanks, T., Fong, R. & Boyle, B.J. (1983) *Nature* 303 156

Smith, M.G. (1978) *Vistas in Astron.* 22 321

Smith, M.G. (1981) in "*Investigating the Universe*" p. 151 ed. Kahn, F.D. D. Reidel, Dordrecht

Smith, M.G. (1984) in "*Quasars & Gravitational Lenses*", p. 4 proc. of International Astrophysical Colloquium, 24th, Liege

Stockton, A., & MacKenty, J.W. (1987) *Astrophys. J.* 316 584

Stobie, R.S. (1986) *Pattern Recognition Lett.* 4 317

Stobie, R.S., Sagar, R., & Gilmore, G. (1985) *Astron. Astrophys. Suppl. Ser.* 60 503

Stritmatter, P.A., (1969) *Ann. Rev. Astron. Astrophys.* 7 665

Tritton, K.P., & Morton, D.C. (1984) *Mon. Not. R. astr. Soc.* 209 429

United Kingdom Schmidt Telescope Handbook (1983)

van de Kamp, P. (1971) *Ann. Rev. Astron. Astrophys.* 9 103

Wampler, E.J., & Ponz, D. (1985) *Astrophys. J.* 298 448

Warren, S.J., Hewett, P.C., Irwin, M.J., McMahon, R.G., Bridgeland, M.T., Bunclark, P.S., & Kibblewhite E.J. (1987) *Nature* 325 131

Weedman, D.W. (1986) in *"Structure and Evolution of Active Galactic Nuclei"* p.215 eds. Giuricin, G. *et al.* D Reidel, Dordrecht

Wildey, R.L., Burbidge, E.M., Sandage, A.R., & Burbidge, G.R. (1962) *Astrophys. J.* 135 94

Wills, D., & Lynds, R. (1978) *Astrophys. J. Suppl. Ser.* 36 317

Windhorst, R.A., Miley, G.K., Owen, F.N., Kron, R.G. & Koo, D.C., (1985) *Astrophys. J.* 289 494